UNIVERSITEIT VAN PRETORIA
UNIVERSITY OF PRETORIA
YUNIBESITHI YA PRETORIA
Denkleiers • Leading Minds • Dikgopolo tša Dihlalefi

Investigations into the use of a novel graphene wool sampler for organic air pollutants

By

Yvonne C. Mason

Submitted in partial fulfilment of the requirements for the degree

Master of Chemistry

In the Faculty of Natural & Agricultural Sciences

University of Pretoria

Pretoria

April 2020

Supervisor: Prof P.B.C. Forbes

Declaration

I, Yvonne Caroline Mason, declare that the dissertation, which I hereby submit for the degree Master of Chemistry at the University of Pretoria, is my own work and has not previously been submitted by me for a degree at this or any other tertiary institution.

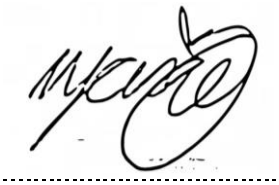

Signature: Yvonne C. Mason

14 July 2020

Date

Summary

With increasing concerns regarding the adverse health effects caused by trace levels of organic air pollutants, it has become ever more desirable to develop air samplers with superior capacities and sensitivities to target a wide range of gaseous trace analytes. Although carbon-based samplers are well known and widely used in the field of active air sampling, the novel GW sampler, presented in this study, has the potential to provide users with a reusable carbon-based sampler, which can be synthesized and assembled easily in-house, with a large sampling capacity due to the substantial surface area graphene has been reported to intrinsically possess.

Selected fundamental laboratory-based studies were undertaken to investigate the strengths and weaknesses of a novel graphene wool (GW) sampler as an active air sampler for gaseous volatile organic compounds (VOCs) and semi-volatile organic compounds (SVOCs). In selected studies, the GW sampler was comparatively evaluated to a quartz wool (QW) sampler, made in a similar fashion to the GW sampler, to determine the impact that the graphene layers grown on the QW substrate had on various sampler properties. The GW sampler was also compared to a polydimethylsiloxane (PDMS) sampler, which has historically been used in a wide range of air monitoring studies.

The hygroscopicity of a sorbent is pertinent to know before sampling, as water has shown to compete for active sites in hydrophilic sorbents, thereby decreasing the sampling capacity of a sampler and increasing risk of premature breakthrough of target analytes during sampling. It was shown that the GW adsorbed < 0.5% (m/m) water at 42 - 70% humidity, whilst at > 80% humidity ± 50% water was retained on the GW sampler by mass. The hygroscopicity of the GW sampler was compared to QW and PDMS samplers in humidity ranges > 90%, where it was found that the polar QW retained the most water whilst the non-polar PDMS sampler retained the least. Therefore, since the GW showed negligible adsorption of water at humidity ranges < 80%, it was shown that water retention will not be a problem when using the GW sampler under typical ambient conditions.

The back-pressure incurred by the GW sampler was compared to that incurred by the QW and PDMS samplers at set flow rates. The back-pressures associated with the GW and QW samplers were found to be far higher and more unstable at flow rates > 400 $mL.min^{-1}$, as compared to the back-pressures recorded for the PDMS samplers at equivalent flow rates. This may be primarily attributed to the GW and QW samplers

having a packed fibrous sorbent structure resulting in a higher back-pressure, which would be more susceptible to instability as compared to the PDMS samplers, which consists of an open-tubular structure. The back-pressure incurred by the GW and QW samplers was observed to be stable at a flow rate of 400 $mL.min^{-1}$, whilst the back-pressure incurred by the PDMS sampler was found to be stable at 500 $mL.min^{-1}$. Although it is recommended to sample at a flow rate of 200 - 250 $mL.min^{-1}$ by Manura (2019) and the International Organisation for Standardization (2001 and 1991), this result is positive as the GW sampler has shown low flow resistance.

The application of both the plunger assisted solvent extraction (PASE) (Munyeza et al. 2018) and thermal desorption (TD) extraction methods were evaluated to determine the optimal extraction method for the GW sampler when targeting SVOC analytes such as polycyclic aromatic hydrocarbons (PAHs). PASE is cheaper than TD and allows for multiple analyses per sample, but has the disadvantage of diluting the sample which reduces sensitivity. The initial PASE study showed that the first extraction was ineffective in extracting the PAH analytes with hexane, as the bulk of the analytes were only extracted in the second and third successive extractions. An overestimation of the extracted PAHs was observed, which could be attributed to solvent losses. The second PASE study involved an 8 hr hexane soak of the GW in the sampler prior to PASE, which proved to be a promising procedure which should be investigated further, as the PAHs were effectively extracted in the first extract.

TD of the GW sampler resulted in good extraction efficiencies for the lighter PAHs such as naphthalene (97% recovery) however, the extraction efficiency was observed to decrease as the molecular mass of the PAHs increased. An example of which is the 1.8% recovery of dibenz[a,h]anthracene from the GW sampler. This result indicates that the larger molecules are more susceptible to being irreversibly adsorbed onto the GW and therefore should not be targeted when using the GW sampler. It may thus be advantageous to optimise PASE, whilst exploring solvents used such as CS_2 and acetonitrile, for PAH extraction from GW samplers.

Intra- and inter- sampler variability studies involved the spiking of VOCs and SVOCs (hydrocarbons (HCs) and PAHs) onto fresh GW samplers with subsequent TD-GCxGC-TOF-MS analysis. It was found that VOCs with higher $LogK_{ow}$ values had lower variability in the peak areas recorded as compared to compounds with lower $LogK_{ow}$ values. This may be due to the more non-polar compounds adsorbing with greater

reproducibly onto the GW sorbent. The C_8 - C_{20} HCs showed increasing % RSDs (2.8 - 55%) with increasing molecular masses for the intra-sampler study, as expected from the previous TD study, whilst the inter-sampler study showed overall higher % RSDs (35 - 76%). The analysis of inter-sampler variability of thermally desorbing the PAHs from the GW sampler reflected % RSDs of approximately twice that of the intra-sampler analysis. This was likely due to non-uniformity of the graphene layers in the GW material, which was confirmed by transmission electron microscopy (TEM) images of the material, in which it was shown that fibres from the same GW batch did not possess uniform graphene layering growth on the QW substrate. The inconsistency in the uniformity of the graphene layers may thus be the primary cause of discrepancies observed between different GW samplers.

Sampler retention volumes (RVs) were investigated for GW, PDMS and QW samplers for nine analytes with varying boiling points (BPs) and polarities using a GC-FID system, in which the GC column was replaced with the sampler of interest. This study was undertaken to better understand the RV trends exhibited by the GW sampler as opposed to the QW and PDMS samplers. It was found that GW had superior RVs for three of the nine analytes, all polar, as compared to the other two samplers. This was contrary to initial assumptions that the GW sampler would show a greater retention of non-polar compounds. This trend is likely attributed to exposed QW fibres in the GW, which would innately exhibit a higher affinity for polar compounds. The low RVs (ranging between 29 $mL.g^{-1}$ sorbent for hexane to 563 $mL.g^{-1}$ sorbent for cyclohexanone) for the GW sampler may be attributed to inconsistencies in packing of the GW resulting in channelling taking place with localised saturation of adsorbent sites. Therefore, optimisation of the packing of the GW sorbent is required.

Following the laboratory-based studies, the application of the GW sampler was tested for sampling the combustion emissions from three different fuel sources using a combustion aerosol standard (CAST). Emissions were simultaneously sampled onto GW, PDMS and commercial activated charcoal tube samplers. The GW and PDMS samplers were directly thermally desorbed and analysed by GC-MS whilst analytes sampled onto the activated charcoal were extracted with CS_2 prior to GC-MS analysis. Rapeseed oil methyl ester (RME) and gas-to-liquid (GTL) fuels were found to be better fuel alternatives to diesel (B0) due to lower VOC and SVOC emissions. In terms of the performance of the samplers during this sampling campaign, the activated charcoal was found to be ineffective as it showed high background noise and required liquid extraction, which

diluted the sample to below the limit of detection (LOD) of the GC-MS. The results from the TD of the PDMS samples reflected relatively higher concentrations of the targeted VOC and SVOCs as compared to the GW sampler, however TD of the GW samplers showed that the target analytes were quantified with lower % RSDs than for the PDMS sampler, particularly for the HCs. Lighter HCs, such as octane and nonane, were only effectively sampled by means of the GW sampler. These results indicate that the GW sampler may be used to target trace concentrations of lighter non-polar analytes.

Overall, it was found in this study that the GW sampler requires further optimisation prior to widespread application. However, the GW sampler is seen to be a promising candidate as an active air sampler for VOCs and lighter SVOCs.

Acknowledgements

I would like to express my sincere gratitude to the following people and institutions:

I'd like to thank my greatest supporter, harshest critic and love of my life, my husband, Richard Mason, for his continued love and support shown every step of the way.

I wish to express my heartfelt appreciation to my supervisor, Professor Patricia B.C. Forbes, for her enthusiasm, support, encouragement and most of all, for her patience.

I'd like to thank my colleagues Madelien Woodling, Chiedza Munyeza, Sifiso Nsibande, Niel Malan and Loreley Cairns. Yvette Naudé is thanked for her patience, her constant willingness to assist, guide and advise on matters regarding chromatographic instrumentation and techniques used in this study. Gratitude is also extended to David Masemula, for his assistance with the gas and the liquid nitrogen and for building the PDMS samplers used in this study. Thanks to Nico van Vuuren for assisting with manufacture of the stands and plungers.

The financial assistance of the National Research Foundation (NRF) towards this research is hereby acknowledged (Grant No. 105807). Opinions expressed and conclusions arrived at, are those of the author and are not necessarily to be attributed to the NRF. Thank you to my colleague, Genna-Leigh Schoonraad, from the University of Pretoria (UP) and Jürgen Orasche, Christoph Bisig, Gert Jakobi and Ralf Zimmerman from the Comprehensive Molecular Analytics (CMA), Helmholtz Zentrum Munich, Germany, for their support and assistance during the CAST generator sampling campaign. Gratitude is further extended to the ASG Analytik-Service for providing the fuels for the CAST campaign.

Research Outputs

Oral presentation:

"Investigations into the use of a novel graphene wool sampler for organic air pollutants" - presented on the 26th of September, at the 2019 Chromatography Postgraduate Student Workshop, held at the University of Johannesburg.

Journal articles:

Yvonne C. Mason, Genna-Leigh Schoonraad, Jürgen Orasche, Christoph Bisig, Gert Jakobi, Ralf Zimmermann & Patricia B.C. Forbes. **2020**. Comparative sampling of gas phase volatile and semi-volatile organic fuel emissions from a combustion aerosol standard system. *Environmental Technology and Innovation*, 19, 100945, 1-12, DOI: 10.1016/j.eti.2020.100945.

Genna-Leigh Schoonraad, Yvonne Mason, George C. Dragan & Patricia Forbes. A novel graphene wool gas adsorbent for volatile and semi volatile organic compounds, *ACS Applied Materials & Interfaces*, in preparation.

Note: Excerpts of these journal papers have been included in the CAST and sampler tube retention volume sections of this dissertation, whilst the full published paper is included in Appendix J.

Table of Contents

List of Figures

List of Tables

List of abbreviations and acronyms

ACGIH	American Conference of Governmental Industrial Hygienists
ANOVA	analysis of variance
APCVD	atmospheric pressure chemical vapour deposition
AQA	Air Quality Act
AQMD	South Coast Air Quality Management District
ASE	accelerated solvent extraction
AVOC	anthropogenic volatile organic compound
BOVOC	biogenic oxygenated volatile organic compounds
BP	boiling point
BTEX	benzene, toluene, ethylbenzene and xylene
BV	breakthrough volume
BVOC	biogenic volatile organic compound
CAS	Chemical Abstracts Service
CAST	combustion aerosol standard
CEES	chloroethyl ethyl sulphide
CIS	cooled injection system
CMS	carbon molecular sieve
CNS	central nervous system
CNT	carbon nanotube
COHb-emia	carboxyhemoglobinemia
CVD	chemical vapour deposition
DDT	dichlorodiphenyltrichloroethane
$_dH_2O$	deionized water
DMMP	dimethyl methyl phosphonate
DMS	dimethyl sulphide
DNPH	2,4-dinitrophenylhydrazine
DNT	dinitrotoluene
DV	dead volume
ECD	electron capture detection
EGDMA	ethylene glycol dimethacrylate
EGPE	equilibrium gum-phase extraction
EU	European Union
FET	field effect transistors
FID	flame ionization detector
FLD	fluorescence detection
FPD	flame photometric detector
GAW	Global Atmosphere Watch
GC	gas chromatography
GCxGC-TOF-MS	comprehensive two-dimensional gas chromatography coupled to time of flight mass spectrometry
GO	graphene oxide
GPE	gum phase extraction

GS	graphene sponge
GW	graphene wool
HFC	hydrofluorocarbon
HPLC	high performance liquid chromatography
IC	ion chromatography
i.d.	inner diameter
IMPROVE	Interagency Monitoring of Protected Visual Environments
IMS	ion mobility spectroscopy
IS	internal standard
LVOC	low volatility organic compound
MA	methacrylic acid
MAE	microwave assisted extraction
mg.Nm^{-3}	milligram per cubic meter of air, at 25 °C and 1 atm pressure
MM	molecular mass
MS	mass spectrometry
N	number of experimental repeats
NASA	National Aeronautics and Space Administration
NMHC	nonmethane hydrocarbon
NMVOC	nonmethane volatile organic compound
NO_x	nitrogen oxides; includes NO, NO_2 and N_2O
NTD	needle trap device
NTP	normal temperature and pressure
NVOC	non-volatile organic compound
OTT	open tubular trapping
PAH	polycyclic aromatic hydrocarbon
PAN	peroxyacetyl nitrate
PASE	plunger assisted solvent extraction
PBB	polybrominated biphenyl
PCB	polychlorinated biphenyl
PDMS	polydimethylsiloxane
PEG	polyethylene glycol
PFCs	perfluorocarbon
PM	particulate matter
ppm	parts per million
PPr	polypyrene
Q ion	quantification ion
QW	quartz wool
RGO	reduced graphene oxide
RSD	relative standard deviation
RT	retention time
RV	retention volume
SA	South Africa
SAW	surface acoustic wave
SBV	specific breakthrough volume

SEM	scanning electron microscopy
S/N	signal to background noise ratio
SOA	secondary organic aerosol
SO_x	sulphurous compounds, includes SO_2 and SO_3
SPDE	solid-phase dynamic extraction
SPE	solid-phase extraction
SPME	solid-phase microextraction
STEL	short-term exposure limit
SVOC	semi-volatile organic compound
SWNT	single-walled carbon nanotube
TD	thermal desorption
TDS	thermal desorption system
TEM	transmission electron microscopy
TGA	thermogravimetric analysis
TLV	threshold limit value
TWA	time-weighted average
UE	ultrasonic extraction
UK	United Kingdom
URT	upper respiratory tract
US	United States of America
US EPA	United States Environmental Protection Agency
UV	ultraviolet detection
VOC	volatile organic compound
VVOC	very volatile organic compound
Wa	weight of adsorbent resin
WHO	World Health Organisation
WMO	World Meteorological Organisation
XPS	x-ray photoelectron spectroscopy

Chapter 1: Introduction

This chapter serves to highlight current global air pollution issues and provide an outline of how the research conducted in this study aims to improve on existing methods and techniques for the sampling of gaseous volatile organic compounds (VOCs) and semi-volatile organic compounds (SVOCs) by means of investigating a novel graphene wool (GW) sampler.

1.1 Problem Statement

Air pollution in developing countries has made international headlines in recent years as it has been reported to kill more people than AIDs, malaria, breast cancer or tuberculosis (Rohde and Muller, 2015; World Health Organisation, 2014; O'Keefe, 2013; Yang et al., 2013; World Health Organisation 2012). Globalisation has given developing countries, such as China, a chance to become amongst some of the fastest growing economies (Cheremukhim et al., 2015) consequently, it is no coincidence that these counties then report exponential increases in air pollution. An example is that 92% of the population of China has been reported to be exposed to unhealthy air, and 46% of these people are exposed to pollution above the highest threshold of the United States Environmental Protection Agency (US EPA) and is thus deemed to be "hazardous", as quantified by standards set out by the US EPA (Rohde & Muller, 2015). Concerning levels of air pollution are however not limited to developing countries. With 91% of the world's population living in locations exceeding the World Health Organisation (WHO) guideline limits for air pollutants, an estimated 4.2 million deaths every year are attributed to human exposure to outdoor air pollution (World Health Organisation, 2019).

Environmental concerns such as the depleting ozone-layer, caused by air pollution, have been addressed by international treaties such as the Vienna Convention as well as the Montreal Protocol and its Amendments. These protocols have required developing countries, such as South Africa (SA), to phase out specified chemicals by 2010 (Department of Environmental Affairs, 2018). SA further acknowledges and supports the right to have an "environment protected, for the benefit of present and future generations, through reasonable legislative and other measures" as stated in Section 24 of the Bill of Rights contained within the Constitution of SA (1996). The South African government is hence constitutionally pressured to research and standardize air quality monitoring and

management as stated in Air Quality Act (AQA) (Act No. 39 of 2004) (National Environment Management, 2017).

While AQA No. 39 (2004) introduced local air quality management plans, the 2017 National Framework for Air Quality Management in South Africa contains limited information concerning the limit values of individual volatile organic compounds (VOCs) as well as semi-volatile organic compounds (SVOCs) such as saturated straight chain (C_8 - C_{20}) hydrocarbons (HCs) and the polycyclic aromatic hydrocarbons (PAHs), which are compounds of growing concern. There is, however, existing legislation that provides limit values for groups of compounds emitted from certain industries such as PAHs from char, charcoal and black carbon production (0.1 $mg.Nm^{-3}$), VOCs produced from primary aluminium production (40 $mg.Nm^{-3}$) and total VOCs from vapour recovery/destruction units of industries storing and handling petroleum products (150 $mg.Nm^{-3}$) (Department of Environmental Affairs, 2015). Although the ambient limit value of benzene was already set in 2009 (5 $\mu g.m^{-3}$/ 1.6 ppb) (Department of Environmental Affairs, 2009), a draft of the "Regulations for Hazardous Chemical Agents" has been published by the South African government, which can act as a guideline for standard limit values of many individual VOCs in occupational settings until it has been enacted (Department of Labour, 2018).

Some VOCs and SVOCs are emitted from natural sources however, due to the industrialisation of cities worldwide, urban expansions into otherwise rural areas have typically resulted in an increase in the volume and toxicity of VOCs and SVOCs released into the ambient atmosphere. Primary pollutants, including VOCs and SVOCs, are produced directly by a source and are emitted into the atmosphere. In addition to the direct effects these pollutants may have on human health and the environment, primary pollutants may undergo photochemical reactions to form secondary pollutants. A photochemical reaction is catalysed by the absorption of energy in the form of light by a molecule, which in turn, forms a transient excited state followed by the formation of secondary pollutants (Longworth et al., 2018). These secondary VOCs and SVOCs may then accumulate to form harmful photochemical smog as shown in Figure 1.1.

The sampling of trace concentrations of hazardous gaseous compounds, which include VOCs and SVOCs, has become ever more critical with an increasing number of studies linking various adverse environmental and human health effects to ambient air pollution (Landrigan et al., 2019; Goldemberg et al., 2018; Landrigan et al., 2018; Yan et al., 2018). VOCs and SVOCs have been noted to potentially cause the enhancement of respiratory,

cardiovascular, infectious and allergic diseases through contact with the skin or through inhalation (Raza, et al., 2018; Bernstein et al., 2004; Finlayson-Pitts & Pitts Jr, 1999; Finlayson-Pitts & Pitts, 1997). VOCs and SVOCs have the potential to be carcinogenic (Helen et al., 2020; Lerner et al., 2018; Hemminki & Pershagen, 1994), and cause reproductive complications, as well as birth defects (Bhatt, 2000). Many SVOCs have also been reported to be endocrine-disrupting in nature which implies that they have the ability to mimic or block endogenous hormones (Xu & Zhang, 2011).

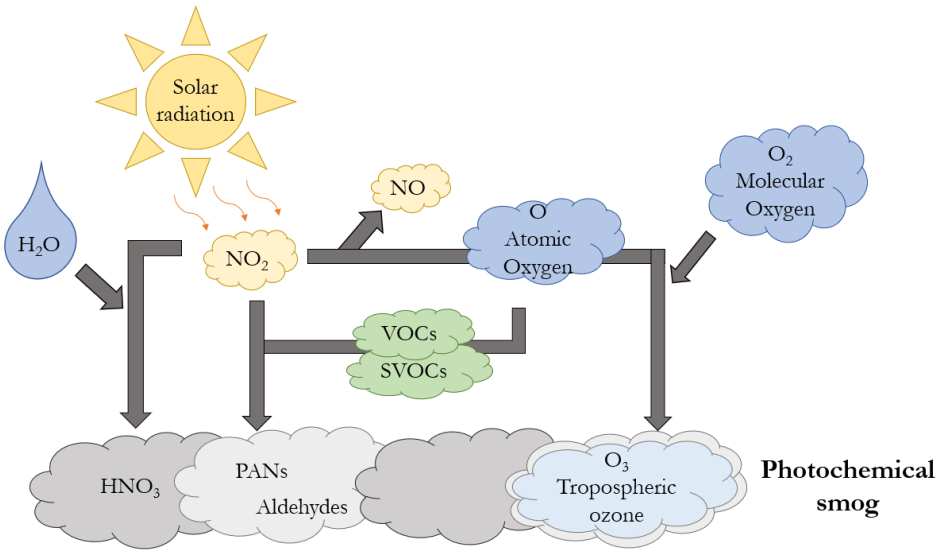

Figure 1.1: Photochemical smog formation; sunlight reacts with NO_2 which then interacts with other molecules in the air to form smog. ***Source:*** *Adapted from Afework et al. (2019) and Finlayson-Pitts & Pitts (1997).* ***Abbreviations: PAN****; peroxyacetyl nitrate.*

The use of carbon-based air samplers is not a novel concept in the field of environmental air monitoring, however the use of graphene in this field is gaining popularity due to many of its innate properties. An example of which is the ability of every atom of this material to interact with any other atom(s) with which it comes into contact due to the planar 2D structure of graphene (Basu & Bhattacharyya, 2012; Schedin et al., 2007), either via weak van der Waals interactions or strong covalent bonding (Yuan & Shi, 2013). Graphene has been calculated to have an impressive theoretical specific surface area of 2630 m^2g^{-1} (Züttel et al., 2004), which is far above the 1000 m^2g^{-1} required of a "strong" sorbent (US Environmental Protection Agency, 1999). Owing to the ultrahigh surface area which graphene possesses in combination with its non-polar nature, Schoonraad and Forbes developed a means to synthesize graphene in a way which allows facile use thereof as an adsorbent in an active air sampler, called a graphene wool (GW) sampler, as later shown in Figure 2.8 of Section 2.3.2

(Schoonraad et al., 2020; Schoonraad & Forbes, 2019a and 2019b). These samplers have been optimised to contain ± 120 mg of the GW spanning a length of 60 mm in a 178 mm long glass tube.

Currently VOCs are typically sampled onto commercially available retaining media such as Carbotrap, Carbosieve™S-III or Tenax®, which are carbon- and polymer-based sorbents respectively. SVOCs are commonly sampled onto the same retaining media as the VOCs in addition to retaining media such as polydimethylsiloxane (PDMS), a polymeric organosilicone material. Multi-channel PDMS traps consist of 22 parallel PDMS tubes housed in a 178 mm long glass tube which are prepared in-house with the same dimensions as the GW sampler (Munyeza et al., 2018; Forbes & Rohwer, 2009; Ortner & Rohwer, 1996). SVOCs have also been sampled onto a triglyceride material known as triolein (Nollet & Lambropoulou, 2017), which may be embedded into semipermeable membranes for passive sampling applications (Tang et al., 2012). Other commercial samplers used for VOC and SVOC applications include Spherocarb®, Carboxen™ 1000 and Anasorb® CMS series sorbents. Samplers such as Tenax®, Carbopack™/trap C and Anasorb® GCB2 are considered to be "weak samplers" by the US EPA as their surface areas are less than 50 m^2g^{-1} (US Environmental Protection Agency, 1999).

1.2 The aim and objectives of the study

This study was undertaken to investigate the capability of the novel GW sampler to sample gaseous VOCs and SVOCs through selected fundamental laboratory-based studies in comparison to quartz wool (QW) and PDMS samplers. The PDMS sampler was chosen as it has been used in a wide range of studies to date. The QW sampler, with an identical set-up as the GW sampler, was investigated as a means by which to determine the impact of the graphene layers grown on the QW substrate. Once the more fundamental laboratory-based studies were complete, fuel combustion emissions from three different fuels were sampled simultaneously onto GW, PDMS and commercial activated charcoal samplers from a combustion aerosol standard (CAST) generator.

This study focused on the sampling of gaseous VOCs, including benzene, toluene, ethylbenzenes and xylenes (BTEX), halogenated organic compounds, such as chlorinated alkanes and benzenes, along with other species of VOCs - which included various aromatic species. In addition to VOCs, this study investigated the capabilities of the GW sampler to sample gaseous SVOCs, specifically PAHs, and C_8 - C_{20} n-alkanes, also known as saturated straight chain hydrocarbons (HCs).

Objectives relating to the fundamental laboratory-based studies of the GW sampler:

i. To conduct hygroscopicity studies for the GW sampler as compared to the QW and PDMS samplers.
ii. To determine the variability in back-pressure between different GW, QW and PDMS samplers at selected flow rates over a sampling period.
iii. To compare the plunger assisted solvent extraction (PASE) and thermal desorption (TD) extraction methods to determine the optimal extraction method for the GW sampler when targeting PAH analytes.
iv. To examine the intra- and inter-sampler variability of thermally desorbing selected VOCs and SVOCs from GW samplers.
v. To determine the retention volumes (RVs) of the GW sampler as compared to the QW and PDMS samplers for representative analytes with a range of boiling points (BPs) and polarities.

Objectives relating to the case study: Application of the GW sampler:

i. To use a CAST generator as a stable source of trace levels of targeted gaseous VOCs and SVOCs in the form of combustion emissions from diesel (B0), gas-to-liquid (GTL) and rapeseed oil methyl ester (RME) fuels, in order to comparatively evaluate the performance of the novel GW, multi-channel PDMS and commercial activated charcoal samplers.

1.3 Justification for the study

With numerous studies linking the increasing concentrations of ambient VOCs and SVOCs to potential negative health effects, it has become ever more critical to develop improved means to sample and quantify the emission of these trace pollutants. To sample trace concentrations, a sorbent with a large surface area, i.e. a large capacity to sample analytes, is desirable. This study aims to investigate a promising sampler, namely the GW sampler, which has been synthesized on a QW substrate (Schoonraad et al., 2020). Besides the large surface area graphene innately possesses (Züttel et al., 2004), an additional potential benefit of the GW sampler is that it can be easily made in-house utilising atmospheric pressure chemical vapour deposition (APCVD), and has been found to possess a large sampling capacity for octane, dodecane and hexadecane (Schoonraad et al., 2020, prepared for submission to *ACS Applied Materials & Interfaces*).

Many authors have demonstrated that graphene is an attractive gas sensor material (Wang et al., 2014; Sitko et al., 2013; Yuan & Shi, 2013; Hwang et al., 2012), making GW a promising candidate as an adsorbent in active air samplers for gaseous VOCs and SVOCs. The GW sampler is expected to have a high capacity due to the large surface area of graphene, thereby allowing for the pre-concentration of trace target analytes. Due to the non-polar nature of graphene, it is hypothesized that the GW sampler will show a greater affinity for non-polar compounds and therefore better adsorb these compounds as compared to polar compounds of similar molecular masses (MMs). The GW sampler may then be further optimised based on how the graphene is grown on QW (which is polar), to better control the uniformity of the graphene layers which may in turn allow for the targeting of both polar and non-polar analytes, depending on the layering and distribution of the graphene on the QW substrate.

1.4 Dissertation outline

This dissertation encompasses selected fundamental laboratory-based studies that aim to investigate properties of the novel GW sampler as developed by Schoonraad et al. (2020), as well as to ascertain the capability of the GW sampler to sample VOCs and SVOCs. To do so, Chapter 2 firstly provides a background to VOCs and SVOCs, as these compound classes were targeted in this study. An evaluation of other gaseous samplers for these target analytes that are currently employed, along with a motivation as to why the GW sampler is a good candidate for active air sampling are provided. The analytical techniques and procedures employed in the fundamental laboratory-based studies are detailed in Chapter 3, together with background to the case study that involved a CAST generator to compare the performance of the GW sampler. The results of the studies carried out are detailed and discussed in Chapter 4. The final chapter summarises the results and draws conclusions from this study, and provides recommendations for future work. The Appendices include supplementary data such as tables detailing the compounds investigated in this study, calibration curves and certificates of analysis.

Chapter 2: Literature Review

In this chapter, the general sources and impacts of gaseous VOCs and SVOCs are addressed, along with the legal limits in this regard. The gaseous VOCs and SVOCs selected for investigation in this study are then expanded on. Furthermore, this chapter provides a comparative review of selected commercial VOC and SVOC air samplers with their associated advantages and disadvantages. Theoretical background on graphene is then given to explain why the GW sampler is a potentially strong candidate for sampling gaseous VOCs and SVOCs. The theory related to experiments undertaken in this study are described so as to provide background. Relevant extraction techniques and methods of analysis are then reviewed, with the final section addressing the theoretical background to the CAST generator.

2.1 Volatile Organic Compounds and Semi-Volatile Organic Compounds

Due to the number of compounds falling under the umbrella terms of "volatile organic compounds (VOCs)" and "semi-volatile organic compounds (SVOCs)", an array of subclasses has been defined to aid in further grouping these organic compounds. These include; biogenic VOCs (BVOCs), biogenic oxygenated VOCs (BOVOCs), anthropogenic VOCs (AVOCs), nonmethane hydrocarbons (NMHC) and nonmethane VOCs (NMVOCs) along with a list of others (Kesselmeier & Staudt, 1999).

The NMVOCs subclass is, for example, comprised of a large variety of compounds that promote the formation of atmospheric oxidants (Hobbs et al., 2004) such as ozone (O_3) and peroxyacetyl nitrate (PAN). PAN is known to kill plants (Taylor, 1969) and has been found to be mutagenic whilst also causing an array of adverse effects in humans ranging from mild side effects, such as eye irritation from short-term exposure (Manahan, 2017), to more concerning conditions such as emphysema and chronic bronchitis from long-term exposure to the analyte (Vyskocil, et al., 1998). The chemical structure of PAN is shown in Figure 2.1. PAN is one of the many secondary organic pollutants which form part of photochemical smog, as shown in Figure 1.1 in Chapter 1. The formation and the impact of photochemical smog, which is comprised of a complex mixture of primary and secondary organic pollutants, has been described in Section 1.1 and will be further addressed in Section 2.1.1.

Figure 2.1 primarily serves to illustrate how VOCs may be alternatively classified according to their chemical composition. Of the VOC analytes shown in Figure 2.1, this study will focus on PAHs, such as pyrene and anthracene, and halogen containing compounds, such

as trichloroethene, in addition to other compounds. However, due to the vapor pressure of PAHs, such as pyrene and anthracene, this group of compounds is able to readily transition between the gaseous and particulate phases. Therefore, PAHs, as well as C_8 - C_{20} HCs, have been classified as SVOCs in this study.

VOC class	Example	
	Name	Structure
Aliphatic	Formaldehyde	
	Acetone	
Cyclic	Cyclohexane	
	Cyclohexanone	
Aromatic	Benzene	
	Toluene	
Polycyclic aromatic	Pyrene	
	Anthracene	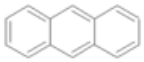
Nitrogen containing	Acetonitrile	
	Peroxyacetyl nitrate	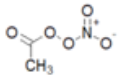
Halogen containing	Trichloroethylene	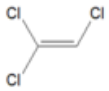
	Tetrachloromethane	

Figure 2.1: Classification of VOCs according to their chemical composition. ***Source:*** *Adapted from Vandenbroucke (2015).*

Since the regulations for limit values of many of the target analytes used in this study have not been enacted in South Africa, the limit values for both the VOCs and SVOCs as set by agencies such as the WHO, the US EPA and the American Conference of Governmental Industrial Hygienists (ACGIH), were referred to in this study and can be found in Tables A1 - A3 in Appendix A. These tables are further elaborated on in Section 2.1.2. The US EPA defines VOCs as "organic compounds composed of carbon, excluding a couple of carbon-based molecules such as carbon monoxide, carbon dioxide, carbonic acid, metallic carbides

or carbonates and ammonium carbonate, which participate in atmospheric photochemical reactions, except those designated by US EPA as having negligible photochemical activity" (US Environmental Protection Agency, 2017). In more generalized terms, VOCs may be defined as chemically reactive carbon-containing compounds of low molecular weights and high vapor pressures (Pennerman et al., 2016).

Organic pollutant classifications, as stated by the WHO for indoor air, consist of three broad categories based on BP ranges and are namely; very volatile organic compounds (VVOCs), VOCs and SVOCs. Table 2.1 provides examples of compounds classified under these categories whereas the specific VOCs and SVOCs included in the laboratory-based studies are listed in Tables B1 - B3 in Appendix B.

Table 2.1: Classification of organic pollutants. ***Source:*** *Adapted from United States Enivronmental Protection Agency (2017) and World Health Organisation (1986).*

Description	Abbreviation	BP Range (°C)	Example Analytes
Very volatile organic compounds	VVOC	< 0 to 50 - 100	Propane, butane and methyl chloride
Volatile organic compounds	VOC	50 - 100 to 240 - 260	Formaldehyde, toluene, acetone, ethanol, 2-propanol and hexanal
Semi-volatile organic compounds	SVOC	240 - 260 to 380 - 400	PAHs, pesticides (DDT, plasticizers, phthalates), fire retardants (PCBs, PBBs)

Abbreviations: ***DDT****; dichlorodiphenyltrichloroethane,* ***PBB****; polybrominated biphenyl,* ***PCB****; polychlorinated biphenyl.*

2.1.1 Sources of VOCs and SVOCs

Air pollution may be viewed as a complex mixture of gaseous compounds and particulate matter (PM) that may either be of natural or anthropogenic origin. These compounds are free to interact with one another and undergo various tropospheric chemical reactions, of which, photochemical smog forming reactions are an example (Section 1.1). These reactions add to the generation of secondary organic aerosols (SOAs) and greenhouse gases (Kesselmeier & Staudt, 1999) which may, in turn, impact the environment, as well as human health.

The formation of SOA from oxidation reactions were found to be dominated by classes of VOCs and SVOCs (Kroll & Seinfeld, 2008). Due to the high vapour pressure of VOCs, these compounds typically remain in the gaseous phase, whilst SVOCs partition between the gaseous and particle phases. SVOCs thus have the potential to undergo deposition only to

partition back into the atmosphere at a later stage pending the reactivity and half-life of the analyte (Figure 2.2).

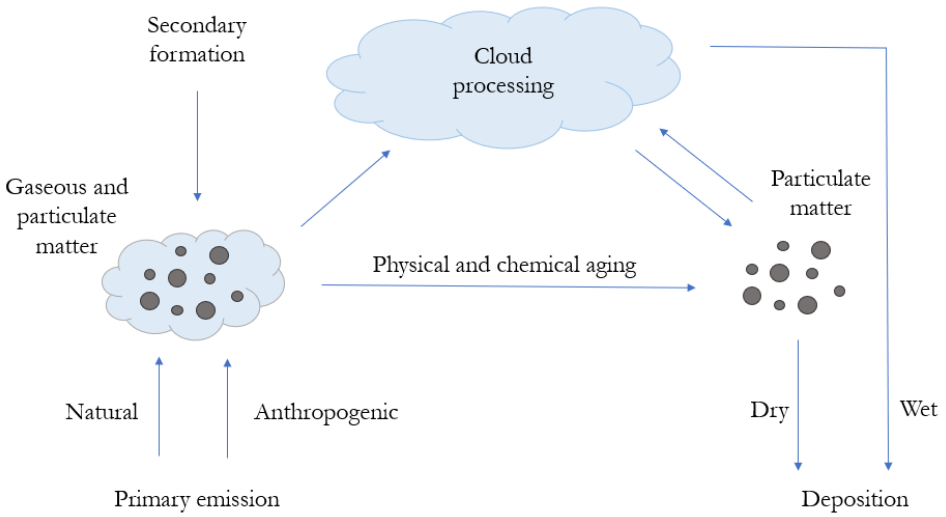

Figure 2.2: Atmospheric cycling of aerosols. ***Source:*** *Adapted from Pöschl (2005).*

Research has reported higher indoor air concentrations of VOCs and SVOCs than what has been reported for outdoor air (Chin et al., 2013; Barro et al., 2009). This is concerning as the US EPA has reported that the average American spends 90% of their day indoors (US Environmental Protection Agency, 2018), which is supported by other studies reporting adults spend an average of 21 hrs/day indoors, while children spend an average of 17 - 19 hrs/day indoors (Mercier et al., 2011). Therefore, since the general public will spend most of their lives indoors, it is of interest to better inform them of emission sources of indoor VOCs and SVOCs so as to allow them to be cognisant of the health effects which these analytes may cause. Specific health effects will be further elaborated on in Section 2.1.2.

The following is a small but representative list of everyday household products that release VOCs and SVOCs; paints, wood preservatives, aerosol sprays, cleaning supplies, disinfectants, pesticides, air fresheners, stored fuels and automotive products. Other sources of VOCs and SVOCs include the dry cleaning of clothing, building materials, furnishings, glues, adhesives and many other solvents; especially in industry. Figure 2.3 a) serves to summarise major anthropogenic contributors to VOCs in ambient outdoor air, whilst Figure 2.3 b) summarises the aforementioned sources of VOCs and SVOCs to ambient indoor air pollution.

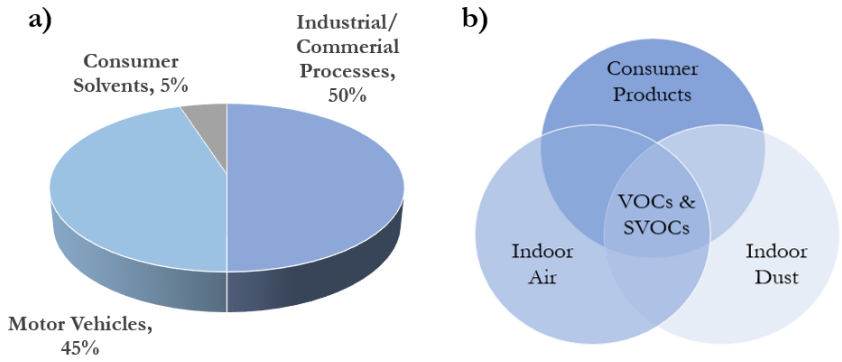

Figure 2.3: Summary of **a)** anthropogenic sources of VOCs estimated in 2018 and **b)** contributors to indoor VOCs and SVOCs. ***Source:*** *Adapted from National Aeronautics and Space Administration (2018) and Lucattini et al. (2018), respectively.*

It is well known that cities in developing countries, such as China, have poor air quality as a result of anthropogenic pollution generated from the expansion of local industries. The air quality is further worsened by transport emissions and household consumer products used by the country with an estimated population of 1.43 billion people (World Population Review, 2019), which accounts for ± 19% of the current world population whilst occupying only ± 2% of the surface area of Earth. Figure 2.4 shows the mass fractions of individual VOC and SVOC species which contribute to SOA formation for China in 2010.

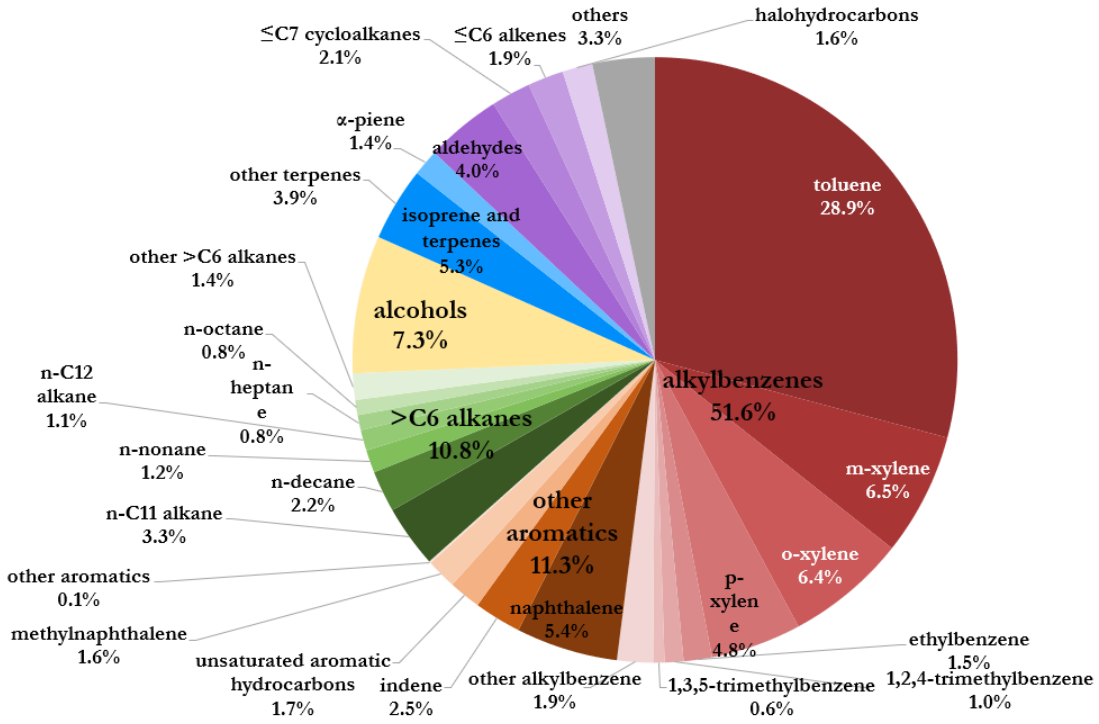

Figure 2.4: Contributors to SOA formation of major VOC groups and individual VOC species in China in 2010. **Source***: Adapted from Wu e al. (2017).*

In 2010, it was estimated that in China, alkylbenzenes were the greatest contributors to SOA formation at 51.6% (Figure 2.4). For individual VOCs shown in Figure 2.4, the top five species which contributed the most to the SOA are toluene (28.9%), m-xylene (6.5%), o-xylene (6.4%), naphthalene (5.4%) and p-xylene (4.8%) (Wu et al., 2017). SOA compounds, such as toluene along with the xylene isomers, were further calculated to contribute 15 - 44% to the total SOA formation in Hong Kong in 2013 (Wang et al., 2013). The ambient atmospheres of cities are made up of hundreds of VOCs, with each of them having their own reaction rates, mechanisms and lifetimes (Olumayede, 2014). Hence, the relative contribution of individual VOCs to photochemical tropospheric ozone formation varies from one compound to another. The World Meteorological Organization (WMO) states that VOC measurements are particularly challenging due to the number of molecules that fall under this category. The Global Atmosphere Watch (GAW) workshop, held in Geneva, Switzerland in 2006, proposed the fifteen molecules shown in Table 2.2 be monitored as representative VOCs.

Table 2.2: Fifteen VOCs proposed as representative molecules to provide information on many anthropogenic processes along with their lifetimes. ***Source:*** *Adapted from World Meteorological Organization (2017).* ***Abbreviations: DMS****; dimethyl sulphide,* ***OH****; hydroxyl radical.*

Analyte	Lifetime	Information provided by chosen analyte
Ethane	2 - 4 months	Mixed, mainly anthropogenic sources; tracer for methane sources; trends in global OH; impact of Cl atom chemistry
Propane	3 weeks	Mixed, mainly anthropogenic sources; tracer for methane; trends in global OH
Acetylene	3 weeks	Tracer for vehicular emissions and biomass burning; air mass age
Isoprene	1 -2 hours	Biogenic emissions; source of formaldehyde; ozone precursor; emissions sensitive to environmental conditions/ climate
Terpenes	1 hour	Aerosol precursor
DMS	1 day	Aerosol precursor; tracer for marine emissions/ productivity
Formaldehyde	2 hours - 2 days	Indicator of isoprene oxidation; satellite validation
Acetonitrile	0.4 - 1 year	Biomass burning tracer
Methanol	2 weeks	Oxidation product; biogenic emissions
Ethanol	1 week	Oxidation product; biofuel tracer
Acetone	1 month	Oxidation product; source of free radicals
Benzene	1 week	Tracer for combustion processes
Toluene	2 days	Aerosol precursor
Iso/n-butane	2 - 3 days	Air mass age/ OH concentration
Iso-/n-pentane	2 - 3 days	Impact of NO_3 chemistry

Molecules listed in Table 2.2 were chosen for their ease of measurement, as well as for their usefulness in providing information on many processes such as emissions from defined sources, long-range transport and chemical loss processes (World Meteorological Organization, 2017). Routinely measuring a set number of molecules allows for a greater global correlation of data whilst the additional monitoring of other hazardous compound concentrations will only benefit researchers by expanding the holistic understanding of ambient air pollution.

In addition to the active monitoring of selected analytes through targeted sampling and analysis, it is useful to include the utilisation of surface ozone readings as an indication of areas dense with the emission of various VOCs and SVOCs along with other highly reactive species (World Meteorological Organization, 2017). These surface ozone calculations are useful due to the high concentrations of tropospheric ozone being generated from highly industrialised areas releasing a large volume of VOCs and SVOCs into the atmosphere.

2.1.2 Effects of VOCs and SVOCs on human health and the environment

Air pollution has various mechanisms by which it can negatively affect human health and the environment. In addition to the gases which can cause direct harm to the general health of the exposed population, there are gases that indirectly negatively impact people by means of altering the ecosystems and climatic conditions which humans and other organisms rely on. One way in which these analytes affect the climate is through a phenomenon known as 'climate forcing'. Climate forcing may be defined as an imposed perturbation of the energy balance of the Earth (National Research Council, 2001). An example of which are NMVOCs that accumulate in the atmosphere and absorb infrared radiation, which would have otherwise escaped back into space, thereby resulting in the warming of the Earth's atmosphere.

With an ever-growing population, the harmful VOC and SVOC emissions released into the troposphere have exponentially grown, due to expansions of both the industrial and transport sectors worldwide. These anthropogenic sources of air pollutants have added to the natural sources of VOC and SVOCs, which has subsequently resulted in enhanced temperature inversions. Temperature inversions cause harmful and toxic gases to be trapped in the troposphere and thereby, further concentrate photochemical smog close to the Earth's surface; this phenomenon is often seen in urban areas during the winter mornings.

In addition to worsening outdoor air quality, supporting literature has highlighted that the concentrations of many VOCs are consistently higher indoors than outdoors, due to the number of sources of VOCs emitted by a wide array of products in homes and buildings, as previously listed in Section 2.1.1 (Tang et al., 2016; Barro et al., 2009; Jia et al., 2008; World Health Organisation, 1989). As the concentration of VOCs and SVOCs rises indoors, the likelihood of sensory effects increases. The most notable side effects that first result from exposure to VOCs above the recommended safety levels are eye and respiratory tract irritations. Additionally, people have reported experiencing headaches, dizziness, visual disorders and memory impairment soon after exposure to particular classes of organic compounds (Yu & Kim, 2010; Pöschl, 2005). For further details on the potentially hazardous side effects resulting from the exposure to the specific analytes used in this study, refer to Tables A1 - A3 in Appendix A.

Tables in Appendix A also list the available associated time-weighted averages (TWA), short-term exposure limits (STEL) and threshold limit values® (TLV®), compiled from various sources for each of the listed organic compound; of which the main source is the ACGIH (ACGIH, 2012). The TWA is the average exposure reported over a specified period of 1, 3, 8 or 24 hr. The TWA has been reported on the basis of approximately 8 hr in Tables A1 - A3 in Appendix A i.e. a standard working day. The STEL for many compounds is still unavailable, however, for compounds for which this information is available, it describes the acceptable average exposure over a short term, generally being 15 min. The TLVs® refer to "airborne concentrations of chemical substances and represent conditions under which it is believed that nearly all workers may be repeatedly exposed" (ACGIH, 2012). The "TLV® Basis", found in Tables A1 - A3 in Appendix A, lists the adverse effect(s) upon which the TLV® is based. TLVs® are expressed in ppm or $mg.m^{-3}$ and can be interchangeably converted using Equation (Eq) 1.

$$\text{TLV in ppm} = \frac{(TLV\ in\ mg.m^{-3})(24.45)}{(molecular\ weight\ of\ substance\ in\ g\ )} \qquad \text{... Eq 1}$$

In Equation 1, note that 24.45 is equal to the molar volume of air in litres at normal temperature and pressure (NTP) conditions.

2.1.3 Legal limits of VOCs and SVOCs

In terms of indoor air quality, there exists an overlap between consumer and occupational exposure (Nørgaard et al., 2014). To protect the general public, concentrations of hazardous chemicals present in the ambient air may need to be more stringently enforced, in which case, major industrial area emissions may be better monitored and controlled, alternatively, limits may be placed on the maximum tolerable concentration in the goods and products from which they originate. In some cases, these limits are in terms of total VOCs and not the specific compounds which are present. For example, total VOC may be defined as the sum of all peaks which elute in a particular retention window of a GC chromatogram using a specific GC column (Berglund et al., 1997). In other cases, specific limits are set for individual compounds. Different regions and different industrial areas have their own regulations, limits and corresponding test methods. There exists no globally agreed de facto limits or definitions and hence the analyst needs to be very clear on which specification they are testing against if they are to report something as non-compliant. For example, there are official standards for paint but they vary depending on where in the world you are. In the UK, for paint tins to claim "low-VOC", they need to contain less than 80 $g.L^{-1}$ of VOCs as the paint is governed by the British Coatings Federation. However, if one was to live in California, then the South Coast Air Quality Management District (AQMD) rules would apply and a "low-VOC" status on a paint tin would mean that it contains less than 50 $g.L^{-1}$ of VOCs (Points, 2019).

The most current National Framework for Air Quality Management in SA was published on the 26th of October 2018 (Department of Environmental Affairs, 2018). This framework is however lacking on information regarding gaseous organic analytes, as it focuses on NO_2, SO_2, ozone, PM_{10}, $PM_{2.5}$ and CO. Therefore, for individual limits of VOCs and SVOCs, the limits set by the US EPA and ACGIH for individual analytes can be utilised as the benchmark until the regulations for hazardous chemical agents in SA has been made part of legislation (Government of SA, 2018). These limits are listed in Tables A1 - A3 in the Appendix and have been previously described in Section 2.1.2.

2.1.4 VOCs and SVOCs investigated in this study

The VOCs and SVOCs selected for investigation in this study were chosen for various reasons. Firstly, in broad terms, organic compounds were chosen as the initial target compounds for the investigation of the applications of the newly developed GW sampler;

which will be addressed in Section 2.3. This is due to graphene showing a high affinity for organic analytes in past studies (Ge et al., 2015; Yuan & Shi, 2013), and it was therefore logical to start testing the capabilities of this material to sample organic compounds through an adsorption mechanism.

Section 2.1.1 listed fifteen representative VOC molecules which were chosen to be routinely measured in the background atmosphere (World Meteorological Organisation, 2017). Of these fifteen molecules, benzene and toluene were part of the VOC mixture purchased for use in this study. More specifically, this 60 analyte VOC mixture was dominated by halocarbons which have regained popularity amongst researchers due to their potential side effects. An example of which is trichlorofluoromethane, which has not only been reported to cause cardiac sentitization but also depletes the ozone layer of the atmosphere (Lin et al., 2019; ACGIH, 2012). Additionally, these halocarbons, along with other VOCs in the purchased mixture, were used to expand the range of this research and test the ability of the novel sorbent to adsorb these compounds. The chemical structures of the selected VOCs may be found in Table B1a in Appendix B.

The SVOCs selected as target analytes were PAHs and HCs, whose chemical structures are shown in Table B2 and Table B3a in Appendix B, respectively. Keith (2015) detailed the origins of the US EPA list of 16 priority PAH pollutants in a review wherein the author explained that 7 of the PAHs were selected primarily due to the availability of analytical standards (Keith, 2015). Additionally, three of the PAHs were chosen due to being suspected carcinogens in water supplies, the others were selected as they were commonly obtained in coal and tar or were chemical intermediates in the production of dyes and other fine chemicals. Due to the range of sources from which these compounds are emitted, a PAH mix was chosen for this study, containing most of the US EPA 16 priority PAH pollutants.

A class of HCs, known as n-alkanes (C_8 - C_{20}), were added to the scope of this research to gauge the performance of the GW sampler when sampling straight chain alkanes, which are typical analytes emitted from the industrial and transportation sectors.

2.2 Sorbents currently used to sample VOCs and SVOCs

Air sampling of gaseous analytes may be achieved by means of either absorption or adsorption, whilst the technique of condensation sampling may be used for vapor-phase pollutants. The difference in principles between the absorptive sampling of analytes, such as how PDMS retains analytes, and adsorptive sampling of analytes, such as how graphene

retains analytes, is illustrated by Figure 2.5. Adsorbents, such as graphene, may be classified into three groups; inorganic materials, carbon-based and organic polymers. The carbon-based sampler grouping may be further subdivided into three additional sub-groupings: activated carbon, carbon molecular sieves (CMS) and the graphitized or porous carbon variety. When considering which air sampler will meet the needs of the application, the chemical composition of the target compounds and that of the sampling medium needs to be understood, to exploit the advantages of any new or existing samplers and enhance their interactions with the desired analytes.

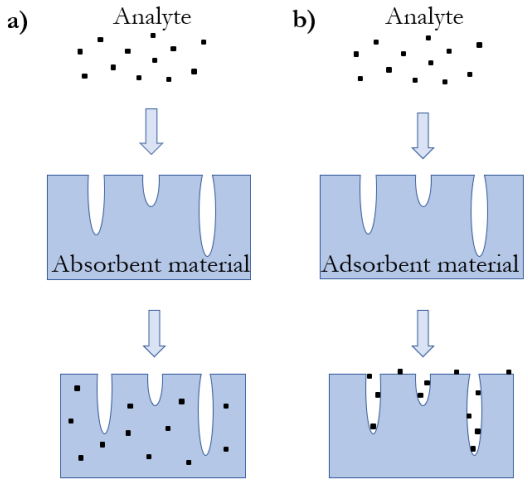

Figure 2.5: The difference between **a)** absorption and **b)** adsorption by a material.

Additional properties of interest include the hygroscopicity and relative chemical reactivity of the sampler. The sampler needs to have a high enough affinity for the analyte of interest so as to 'capture' the analyte by means of absorption or adsorption, but not so strong that desorption or extraction of the analytes from the sorbent after sampling is problematic. It is desirable for a good sampler to contain a stable, pure sorbent so as to have little background noise during analysis. It is also desirable for a good sampler to be as inert as possible so as to not facilitate the catalysis of reactions and formation of artifacts. These factors were taken into account when designing the scope of the experimental section of this study to facilitate the investigation of the novel GW air sampler.

As introduced in Chapter 1, VOCs are typically sampled onto retaining media such as Carbotrap, Carbosieve™S-III and Tenax® which are respectively, carbon- and polymer-based samplers. SVOCs are commonly sampled onto the same retaining media as the VOCs along with retaining media, such as PDMS, a polymeric organosilicon, and a triglyceride known as triolein (Nollet & Lambropoulou, 2017). Table 2.3 lists common VOC and SVOC

samplers used today, along with their analyte volatility ranges, maximum temperatures the sorbent should be exposed to, surface area and example target analytes.

Table 2.3: A list of available VOC samplers along with recommended target analytes for which they are used and the analyte volatility range (AVR) and the specific surface areas (SSAs) of the sorbents. ***Source:*** *Adapted from US Environmental Protection Agency (1999) and Woolfenden (2010). (-) indicates that information on the relative strength of a sampler was unavailable.*

Sample Tube Sorbent	Approx. AVR & relative strength	Max. Temp (°C)	SSA ($m^2.g^{-1}$)	Target analytes
Carbosieve SIII*® Carboxen 1000*® Anasorb® CMS*	-60 to 80 °C Very strong	> 450	800	Ultra VOCs such as hydrocarbons (C_2 - C_5), volatile haloforms and freons.
Carbotrap C® CarbopackC® Anasorb® GCB2	n-C_8 to n-C_{20} Weak	> 400	12	Alkyl benzenes and aliphatics ranging in volatility from C_{12} - C_{20}
Carbotrap® CarbopackB® Anasorb® GCB1	n-C_4 to n-C_{14} Weak/Medium	> 400	100	Wide range of VOCs, including ketones, alcohols, aldehydes (BP > 75 °C) and all non-polar compounds within volatility range
Chromosorb 106	50 to 200 °C Medium	225	750	For low-boiling hydrocarbons, benzene, labile compounds and VOCs
Chromosorb® 102	50 to 200 °C Medium	250	350	For a wide range of VOCs incl. oxygenated compounds and chlorine-containing pesticides
Coconut Charcoal* (rarely used)	-80 to 50 °C	> 400	> 1 000	Broad range of primarily non-polar compounds
Porapak N	50 to 150 °C / n-C_5 to n-C_8 Medium	180	300	Volatile nitriles; acrylonitrile, acetonitrile and propionitrile. Also, pyridine, volatile alcohols from EtOH, MEK, etc.
Porapak Q	50 to 200 °C / n-C_5 to n-C_{12} Medium	250	550	A wide range of VOCs including oxygenated compounds
Spherocarb*	-30 to 150 °C/ n-C_3 to n-C_8	> 400	1 200	VVOC such as VCM, ethylene oxide, CS, and CHCl. Volatile polars e.g. MeOH, EtOH and acetone.
Tenax GR	100 to 400 °C/ n-C_7 to n-C_{30}	350	35	Alkyl benzenes, vapor phase PAHs and PCBs and as above for Tenax TA
Tenax® TA	100 to 400 °C/ n-C7 to n-C_{26}	350	35	Aromatics except benzene, non-polar components (BP > 100 °C) and less

			volatile polar components (BP > 150 °C)
Zeolite Molecular Sieve 13X**	-60 to 80 °C Very strong	> 400	1,3-butadiene and nitrous oxide.

**These sorbents exhibit some water retention, **Significantly hydrophilic*

When selecting an appropriate sampler, it is also important to be aware of the limitations of the specific sampler of interest. Table 2.4 lists some of the limitations associated with common samplers.

Table 2.4: Limitations of several sorbents. ***Source:*** *Adapted from US Environmental Protection Agency (1989).*

Charcoal	· High surface area causes artifact formation during sampling · High background contamination if using TD · High affinity for water · High catalytic activity · Incomplete sample recovery · Impurities in solvent extraction may be high · Solvent extraction causes dilution of sample
CMS	· Solvent extraction required · Desorption efficiency decreases with BP > 100 °C
XAD - 2	· Questionable thermal stability · Compounds below C_7 lost/ breakthrough extensive · Solvent extraction causes dilution of sample
Silica Gel	· High affinity for water · Thermal breakdown thus not compatible to TD
Tenax®	· Poor desorption of highly polar compounds (e.g. alcohols) · Possibly retains O_2 which leads to sample oxidation · Limited to some volatile compounds · High benzene background · Low breakthrough volume for some organics

Abbreviations: CMS*; carbon molecular sieves,* ***TD****; thermal desorption.*

With most forms of sampling and analysis, trade-offs need to be made when it comes to the strengths and limitations of the available techniques. There are, however, limitations that are very important in terms of GC analysis, such as if a sampler has a strong affinity for water. A hydrophilic sampler, for example, would be unsuitable to sample target analytes in humid sampling conditions as the water will not only have the potential to displace target analytes on the sorbents but also provide challenges in analysis. It is therefore crucial to understand

the limitations associated with each sampler, as well as the capabilities of individual laboratories regarding available equipment to decide how the intended sampler will be analysed before purchasing it.

2.3 Graphene as an alternative adsorbent to other carbon-based samplers

This section will detail the history and uses of graphene, as well as state why this material has a potential use as an adsorbent in an active sampler in sampling trace concentrations of gaseous organic analytes in air.

2.3.1 History and uses

Although the credit for the discovery of graphene went to Geim and Novoselov in 2004, this is not to say that graphene was a novel concept, as graphene has been noted to have already been theoretically explored as early as the 1940's and its existence was subsequently confirmed in the 1960's (Brownson et al., 2012). Since the discovery of graphene in 2004, its ability to act as a gas sensor and sampler has been investigated; owing to piqued interest in its intrinsic sensitivity which has been attributed to the high quality 2D crystal lattice structure that results from how the carbon atoms bond in the material (Yuan & Shi, 2013; Schedin et al., 2007). This material has since found a place in industries such as electronics, clothing, rubber manufacturing and drug delivery (Sadasivuni et al., 2015; Yang et al., 2015).

Graphene is a carbon-based material just like charcoal, graphite and diamond. The difference between these structures lies in the way in which the carbon atoms are bonded together, giving each of the materials their own unique shapes and properties as is shown in Figure 2.6. Due to the 2D structure of graphene, every atom of the structure has the capability of interacting with any molecule with which it comes into contact (Basu & Bhattacharyya, 2012), via interactions ranging from weak van der Waals interactions to strong covalent bonding (Yuan & Shi, 2013).

Graphene possesses the most resemblance to graphite however it does not contain a structural z-dimension. That is to say, whereas graphite, fullerenes and diamonds take on a 3-D structure, monolayered graphene adopts a 2-D structure. This similarity had a role in graphene's discovery in 2004, whereby Geim and Novoselov used the "Scotch™ tape method" to pull carbon layers from a block of graphite using subsequent pieces of Scotch™ tape until a single layer of pure graphene remained on the tape (Novoselov et al., 2004).

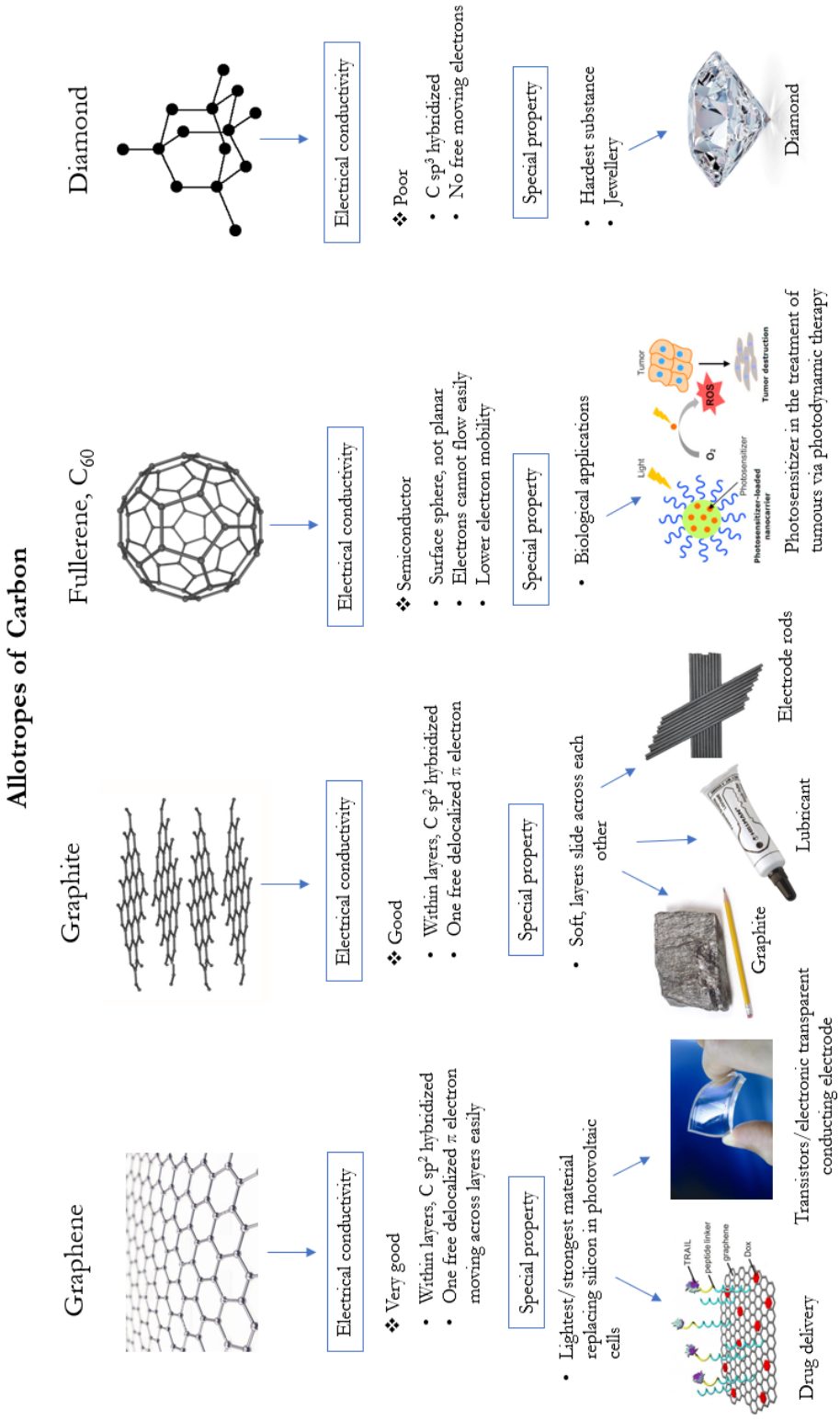

Figure 2.6: Brief summary of the electrical conductivity, special properties and uses of graphene as compared to diamond, graphite and fullerene. ***Source:*** *Adapted from Kok (2014).*

Regarding the way in which the carbon atoms of graphene bond, the structure is sp^2 hybridized with four electrons present in each of the outer shells of the carbon atoms. Three

of these electrons fall into the plane and share electrons with neighbouring carbon atoms to form equivalent bonds. These bonds, which occur through the σ orbitals, shown in Figure 2.7, are what give graphene the flexibility, strength and mechanical properties it possesses. These properties have made this light-weight material an ideal candidate to incorporate into spaceships, as it performs well at extreme temperatures (Graphene Flagship, 2020). The fourth electron in the graphene structure is unbonded, and according to Heisenberg's uncertainty principle, may be present in either of the π orbitals. The fourth electron is responsible for the heat carrying, electrical charge and the transparency of the material (Fogelström, 2014).

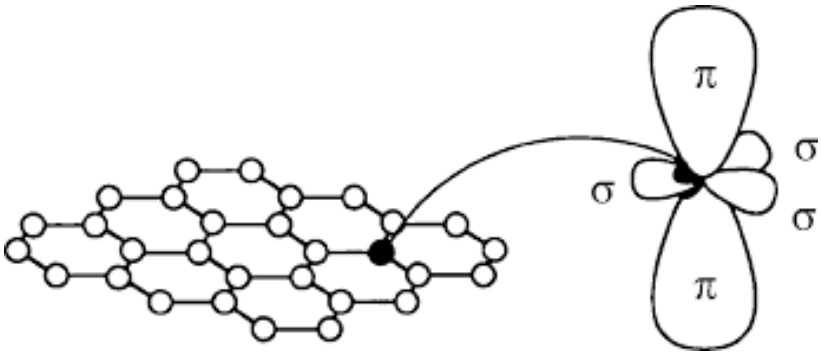

Figure 2.7: The carbon atomic σ and π orbitals in the sp^2 honeycomb lattice of graphene. ***Source:*** *Jorio et al. (2011).*

Due to the previously stated innate 2D structure of graphene, it has a high theoretical specific surface area of 2630 m^2g^{-1} (Züttel et al., 2004), which exceeds the 1000 m^2g^{-1} required of a "strong" sorbent (US Environmental Protection Agency, 1999). In particular, graphene oxide adsorbents have become a popular topic of research in the field of gas detection. In 2012, a review was published which summarised the different sensor parameters of various devices based on graphene and reduced graphene oxide (RGO), which can be found in Table 2.5 (Basu & Bhattacharyya, 2012). Table 2.5, for example, lists a graphene oxide/polypyrene (GO/PPr) composite-based sensor for the detection of 'organic vapours' (Zhang et al., 2012). This polymer composite was however only investigated for its sensitivity towards toluene and has the possibility of being tested for its capability of adsorbing other VOCs in the future. Table 2.5 shows the wide range of target gaseous analytes as well as detection limits obtained (from 38.8 ppt for the detection of oxygen to 10 ppm for the detection of ammonia) using graphene-based materials in sensing applications. Suitable applications of these materials would vary due to the differences in detection limits.

Table 2.5: Comparison of detection limits of various graphene-based gas sensors. ***Source:*** *Adapted from Yuan & Shi (2013) and Kuila et al. (2011).*

Graphene material	Type of sensors	Target gas	LOD	Response time	Ref.
Thermally RGO	p-type semiconductor	NO_2	2 ppm	-	(Lu, et al., 2009)
Hydrazine RGO	-	NO_2, NH_3, DNT	< 5ppm (NO_2 and NH_3), 28ppb DNT	-	(Fowler et al., 2009)
CNT	-	NO_2, NH_3,	2 ppm	< 600s	(Kong et al., 2000)
CNT	-	NO_2, nitrotoluene	44 ppb, 262ppb	< 600s	(Li et al., 2003)
CNT	-	NH_3,	10 ppm	~100s	(Suehiro et al., 2003)
CNT	-	NO_2	5 - 100 ppb	~600s	(Valentini et al., 2004)
Mechanically exfoliated G	-	NH_3, CO, ethanol	1 ppb	-	(Schedin et al., 2007)
SWNT	-	HCN	4000 ppb	-	(Robinson et al., 2008)
	-	CEES	0.5 ppb	-	
	-	DMMP	0.1 ppb	-	
	-	DNT	0.1 ppb	-	
RGO	-	HCN	70 ppb	-	(Robinson et al., 2008)
	-	CEES	0.5 ppb	-	
	-	DMMP	5 ppb	-	
	-	DNT	0.1 ppb	-	
Mechanically exfoliated G	Hall geometry	NO_2	1 molecule	6 s	(Schedin et al., 2007)
Mechanically exfoliated G	Chemiresistor	CO_2	-	8 s	-
CVD grown G	Chemiresistor	N_2O	103 ppt	Few min	(Chen et al., 2012)
		O_2	38.8 ppt	Few min	
		SO_2	67.4 ppt	Few min	
		NO	158 ppt	5 min	
Epitaxial grown G	Chemiresistor	NO_2	-	5 min	(Nomani et al., 2010)
RGO	Chemiresistor	DMMP	-	18 min	(Hu et al., 2012)
RGO	SAW	H_2	-	~1 min	(Arsat et al., 2009)
		CO	-	~1 min	
Chemically modified G	Chemiresistor	NO_2	3.6 ppm	5 min	(Yuan et al., 2013)
Porous G	FET	NO_2	15 ppb	5 - 7 min	(Han et al., 2011)
		NH_3	160 ppb	-	
G/PPr	Chemiresistor	Toluene	-	Tens of s	(Zhang et al., 2012)
G/ZnO	Chemiresistor	Ethanol	-	-	(Yi et al., 2011)

G/SnO_2	Chemiresistor	H_2S	-	5 s	(Zhang et al., 2011)
G/Pd	Chemiresistor	NO	-	4 min	(Li et al., 2011)

Abbreviations: ***CEES****; chloroethylethyl sulphide,* ***CNT****; carbon nanotube,* ***DMMP****; methylphosphonate,* ***DNT****; dinitrotoluene,* ***FET****; field-effect transistor,* ***G****; graphene,* ***HCN****; hydrogen cyanide,* ***ppb****; parts per billion,* ***ppm****; parts per million,* ***RGO****; reduced graphene oxide,* ***SAW****; sound acoustic wave,* ***SWNT****; single-walled carbon nanotube.*

The sensitivity of the graphene-based gas sensors is potentially excellent, with sensitivities the ppm range, such as for ammonia using carbon nanotubes (CNTs), to ppb levels, such as for nitrogen dioxide using CNTs. Other studies on gas sensors involving reducing graphene oxides (Deng et al., 2012) have been published, although few have focused on the detection of VOC analytes.

2.3.2 Graphene wool as an adsorbent

Due to the ultrahigh specific surface area of graphene (noted in Section 2.3.1) in combination with its non-polar nature, Schoonraad and Forbes developed a means to synthesize graphene in a way which allows facile use thereof as an adsorbent in an active air sampler, called a graphene wool (GW) sampler, as shown in Figure 2.8 (Schoonraad et al. 2020; Schoonraad & Forbes, 2019a & 2019b). These samplers typically consist of ± 120 mg of the graphene wool material spanning 60 mm of a 178 mm long glass tube, i.d. of 4 mm and o.d. of 6 mm, which is held in place by two screens; the first screen is positioned 2 cm from the end of the glass tube. This configuration is compatible with a commercial thermal desorption system.

Figure 2.8: Graphene wool (GW) sampler showing the GW of 60 mm bed length housed in a glass tube.

2.3.3 Synthesis of Graphene Wool

The GW was prepared using the optimised method published by Schoonraad et al. (2020). Commercially available 9 - 30 μm coarse quartz wool (QW) (Arcos Organics, Industrial Analytical, SA) was used as a substrate for the growth of graphene by atmospheric pressure chemical vapour deposition (APCVD) (Figure 2.9).

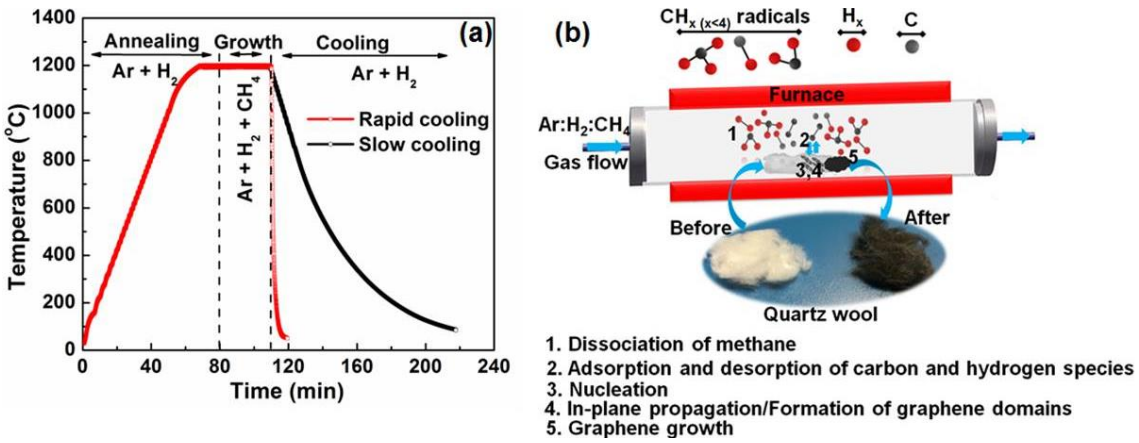

Figure 2.9: a) Temperature profile of the CVD process as measured by a series of thermocouples and **b)** schematic of the non-catalytic direct growth of graphene on the quartz wool substrate. ***Source:*** *Schoonraad et al. (2020).*

The deposited graphitic carbon takes the shape of the quartz wool substrate by covering the surface of each fibre (Figure 2.10) and it was not necessary to remove the substrate, thus the term 'graphene wool (GW)' in this study infers graphene coated on QW (Schoonraad et al., 2020). Once the GW was synthesized as described by Schoonraad et al. (2020), transmission electron microscopy (TEM) images were taken which showed the multi-layered growth of graphene on the QW substrate (Figure 2.10).

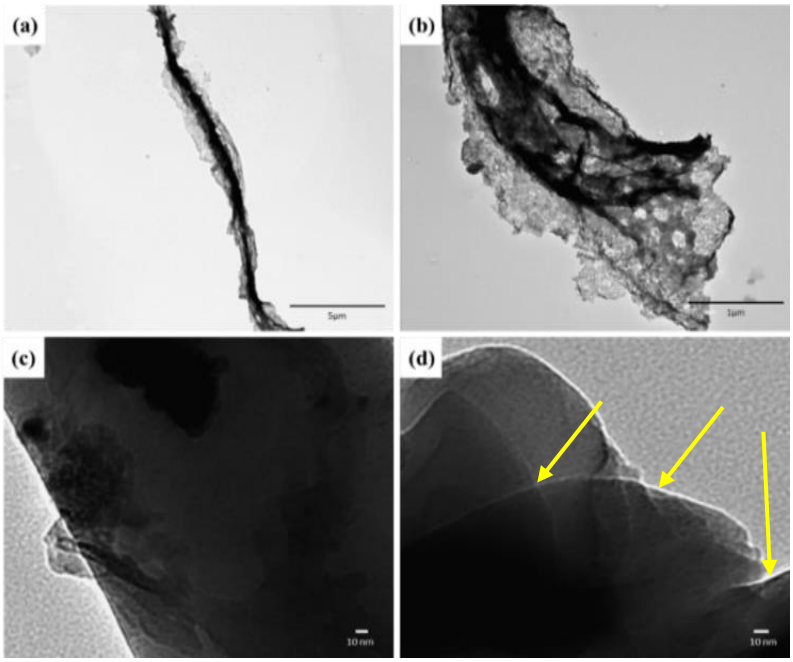

Figure 2.10: TEM images of the graphene wool grown under optimised experimental conditions. ***Source:*** *Schoonraad et al. (2020).*

2.4 Characterisation of sorbents used for VOC and SVOC sampling and the analysis thereof

Before samplers containing a novel sorbent are commercialised, the basic characteristics and abilities of the sampler are examined to better inform the user of their associated strengths and weaknesses. These characteristics included the hygroscopicity of the GW and how it compares to that of other materials. Secondly, the theory of back-pressure is addressed. After which, extraction techniques are explored; namely thermal desorption (TD) and the novel PASE method introduced by Munyeza et al. (2018). A background to common techniques and instrumentation utilised in air sampler analysis then precedes a review of the determination of breakthrough volumes (BVs) for selected analytes with low BP ranges. Lastly, the CAST generator has been described so as to provide a basis as to why it was chosen as a means to compare the performances of the GW, PDMS and activated charcoal samplers.

2.4.1 Hygroscopicity

As determined by Ho et al. (2017), high humidity in an air sample can influence the breakthrough behaviour of sampler sorbents, thereby resulting in a low collection efficiency. Therefore, when investigating a novel sorbent to sample analytes of interest, it is crucial to perform hygroscopicity studies to determine the affinity for water the sorbent exhibits. As shown by Figure 2.11, the maximum water vapor content of the air depends on temperature. Humidity may be reported in two ways; as relative or absolute humidity. Relative humidity is defined as "the ratio of moisture in air as compared to the maximum amount of moisture the air can hold", which is dependent on the air temperature whilst absolute humidity is defined as "the actual amount of water vapor in a specified volume of air" (AcuRite, 2017; Harper, 1992). Relative humidity is reported in this study.

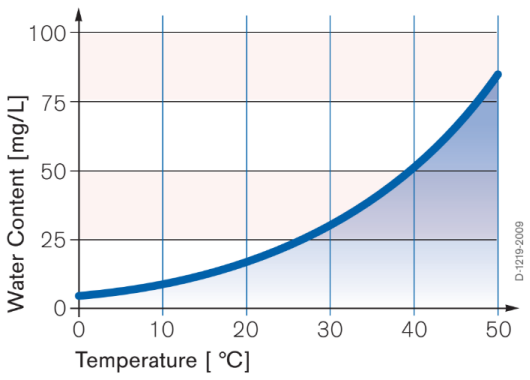

Figure 2.11: Maximum water content versus temperature. ***Source:*** *Lübeck (2015).*

Water has been found to be amongst the compounds adsorbed by graphene due to the electronic properties thereof even though graphene is theoretically non-polar (Melios et al., 2018). Additionally, since graphene may not be uniformly layered on the QW in GW, there may be exposed areas of QW which would possess a higher affinity to interact with the water due to hydrogen bonding, which would take place between the exposed oxygen atoms of the QW interacting and the hydrogen atoms of the water molecules as shown in Figure 2.12.

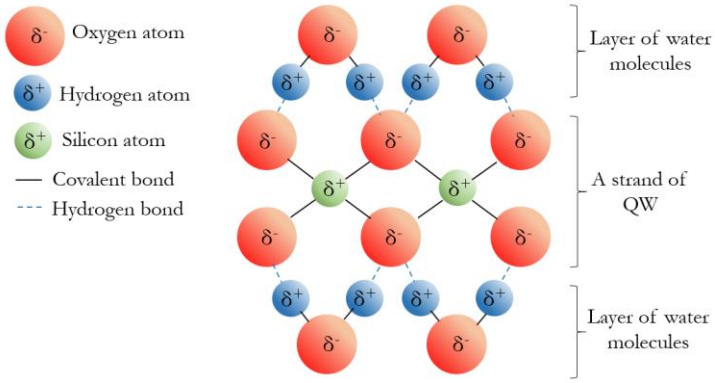

Figure 2.12: Bonding between QW fibres and the water molecules.

Since it is established that graphene adsorbs water (Melios et al., 2018) and QW has an affinity to interact with water molecules, literature was further consulted to better understand the potential implications of this on the sampling of organic compounds using GW in environments containing a high-water content. A study conducted by Weingartner et al. (1997), showed that wetted carbon aggregates collapsed into a more compact structure, which may imply a decrease in the surface area of the GW for the adsorption of VOCs and SVOCs in conditions of high ambient humidity if this phenomenon also occurs with GW. Zhao et al. (2012), however, reported that graphene in the form of a graphene sponge (GS) was used to remove organic substances, such as chloroform, ethylene glycol, diesel oil, vegetable oil, acetic esters, n-heptane and ethanol from water (Zhao et al., 2012). This implies that the application of the GW sampler for sampling gaseous VOCs and SVOCs in humid conditions should be possible, as both polar and non-polar organic compounds were adsorbed even when the graphene was fully submerged in a water. Indeed, it has been recently shown that GW can be successfully employed as an adsorbent to remove PAHs from water (Adeola and Forbes, 2020). Peters and Bakkeren (1994) also noted that water molecules may be adsorbed by graphene but are displaced by larger organic molecules that possess a higher affinity for the graphene than that of water. Therefore, it is hypothesized that humidity should not pose a significant complication in the sampling of VOCs and SVOCs, even if GW exhibits an affinity to water.

2.4.2 Back-pressure of samplers and sampling flow rate

Whilst using an active air sampler, it is favourable to have a constant flow of air through the sampler to ensure a steady and stable stream of target analytes are being sampled onto the sorbent in a reliable manner for target analysis. Inconsistencies in the back-pressure may cause sudden pressure build ups in the active air samplers during sampling, which could lead to premature breakthrough of analytes taking place, and therefore it is also desirable to maintain a steady back-pressure during sampling. For this study, the term 'back-pressure' will refer to pressure opposed to the desired flow of gases in a confined space, such as an air sampler (Hales, 2018; Kumar, 2015). Depending on the type of pump selected to perform air sampling, the user can set a constant flow rate, whereby the pump maintains the set flow rate as the back-pressure across the sampler changes during the sampling event. Alternatively, in constant pressure mode, the flow rate will vary as restrictions occur during the sampling event, depending on the structure of the sorbent through which the air passes as well as particle loading of the air sample. Samplers which contain packed sorbent beds will typically exhibit higher and more irregular back-pressures due to restricted air flow as compared to sorbents with an open tubular structure, which would in turn not allow for small portable personal sampling pumps to be used.

It has been reported in literature that for glass tube with an i.d. of 4.0 mm, the sampling flow rate should not exceed 250 $mL.min^{-1}$ (Manura, 2019) whilst in two of the air sampling methods published by the International Organization for Standardization (ISO), namely ISO 16200-1 (2001) and ISO 9487 (1991), it has been stated that the maximum sampling flow rate should not exceed 200 $mL.min^{-1}$. There are however reports of the successful sampling of analytes using a flow rate of 500 $mL.min^{-1}$, for example when using a PDMS sampler (Munyeza et al., 2019; Geldenhuys et al., 2015), therefore this is a parameter that will be further investigated in this study to determine which flow rate results in a desirably steady back-pressure in GW samplers.

2.4.3 Extraction techniques

In past years, solvent-based extraction methods such as Soxhlet were very popular amongst scientists, however, the Soxhlet method requires a relatively large quantity of hazardous and flammable organic solvent (such as 50 - 500 mL) to reflux for a long period of time (from 8 - 48 hrs) (Munyeza et al., 2019). The extract then needs to be concentrated, thereby adding to the environmental impact thereof, which is a fundamental contradiction to the goals of

an environmental researcher. Table 2.6 lists the advantages and disadvantages associated with selected popular extraction techniques described in literature. TDS and PASE are seen to be the most time efficient and use the smallest volumes of solvents. Figure 2.13 illustrates the popularity of various extraction techniques used to extract PAHs bound on sampling media, with Soxhlet and ultrasonic extractions being the most popular, as documented by Munyeza et al. (2019). Note that reflux is different to a Soxhlet extraction as normal refluxing apparatus consists simply of a flask and a cooling system above whilst Soxhlet would typically consist of a more complicated set-up.

Table 2.6: Advantages and disadvantages associated with various extraction techniques, which apply to VOC and SVOC samplers.

Extraction technique	VOCs	SVOCs	Advantages	Disadvantages	Reference
TDS	✓	✓	• Most environmentally friendly technique – no solvent use. • Reduced extraction time (~12 min).	• Expensive – once off expense to purchase • Additional expenses to run; liquid N_2 needed for CIS.	(Munyeza et al., 2018)
PASE	U	✓	• High extraction efficiency for PAH analysis from a PDMS sampler. • Quick (< 2 min). • Cost effective. • Allows for reanalysis of sample extracts.	• Low volume of solvent required; 1 - 2 mL.	(Munyeza et al., 2018)
Reflux	✓	✓	• Extracts desired analytes of interest.	• Takes a long time; 45 min – 5 hr • High temperatures required; 100 °C • Low efficiency	(Dhanani et al., 2017; Qu et al., 2009; Zhang et al., 2006; Pan et al., 2003)
Soxhlet extraction	✓	✓	• Repeated extraction with fresh solvent minimizing solvent effects.	• Takes a long time; 8 – 48 hr. • Large amount of hazardous and flammable liquid organic solvent; 50 – 500 mL. • Low efficiency.	(Munyeza et al., 2018; Azwanida, 2015; Qu et al., 2009; Zhang et al., 2006)
UE	✓	✓	• Run at low temperatures.	• Takes a long time; 30 - 90 min. • Large amount of solvent; 50 mL. • Low efficiency.	(Qu et al., 2009; Kim et al., 2007; Zhang et al., 2006; Pan et al., 2003)

MAE	✓	✓	· Higher recovery as compared to Soxhlet at temperatures of 124 -140 °C.	· Reduced extraction time; 10 min. · Large amount of solvent; 50 mL. · Analytes may be degraded · Cost of equipment	(Arias et al., 2009; Qu et al., 2009; Kim et al., 2007; Zhang et al., 2006)
ASE	U	✓	· Found to effective in extraction of environmental samples. · Temperature and pressure control	· Takes a long time; > 60 min · Critically dependent on the type of solvent · Cost of equipment	(Azwanida, 2015)

Abbreviations: ***ASE****; accelerated solvent extraction,* ***MAE****; microwave assisted extraction,* ***PASE****; plunger assisted solvent extraction,* ***TDS****; thermal desorption system,* ***UE****; ultrasonic extraction,* ***U****; unknown.*

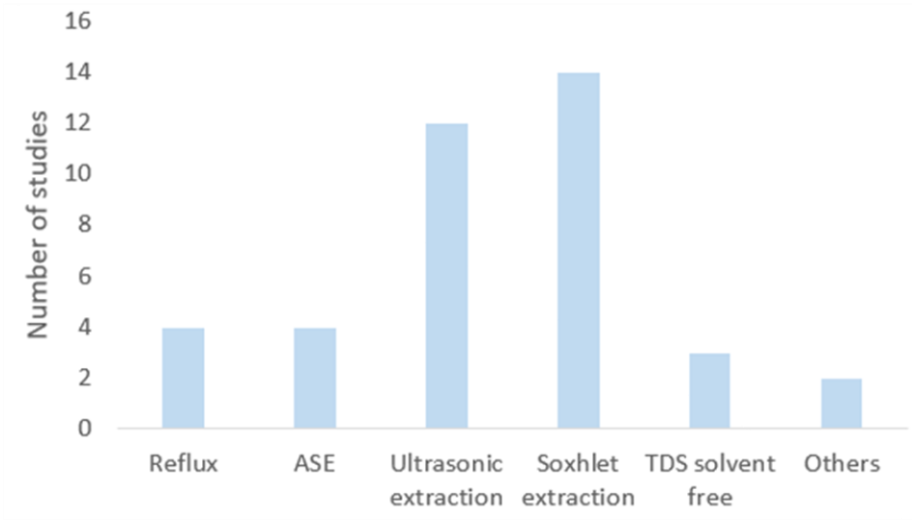

Figure 2.13: Commonly employed extraction methods used to extract PAHs bound on sampling media. ***Source:*** *Adapted from Munyeza et al. (2019).*

Thermal desorption (TD), as defined by the US EPA Compendium Method TO-17, is defined as "the use of heat and a flow of inert (carrier) gas to extract volatiles from a solid or liquid matrix directly into the carrier gas and transfer them to downstream system elements such as the analytical column of a GC. No solvent is required" (US Environmental Protection Agency, 1999). In this study, focus will be drawn to the applicability of TD as a means by which to extract VOCs and SVOCs from the novel GW sampler using TD-GCxGC-TOF-MS, the components of which are shown in Figure 2.14.

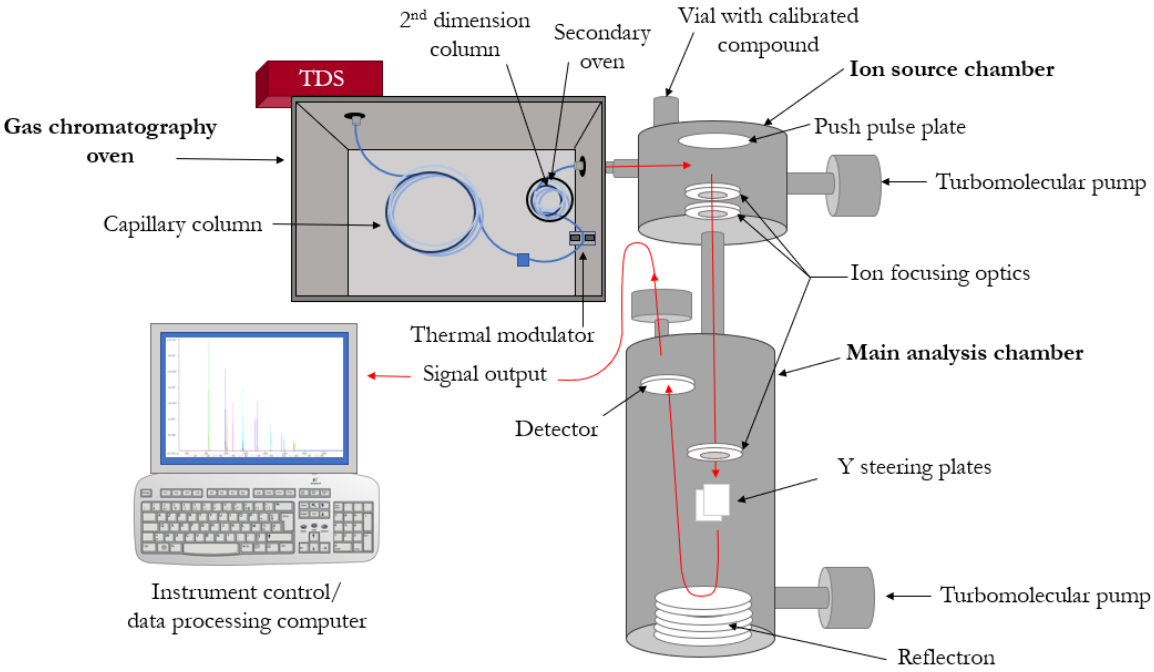

Figure 2.14: Schematic of TD-GCxGC-TOF-MS. ***Source:*** *Adapted from Eiserbeck et al. (2014).*

The efficiency of TD of the GW sampler will be compared to a recently developed method known as plunger assisted solvent extraction (PASE), which is quick and uses as little as 2 mL of solvent per sampler extraction (Munyeza et al., 2018). The set-up of PASE for a silicone rubber trap is shown in Figure 2.15, which has been optimised and then applied to the GW sampler in this study. Both TD and PASE extraction methods are considered eco-friendly due to the use of no solvent for TD and little solvent for PASE, as compared to other solvent-based extractions, such as Soxhlet.

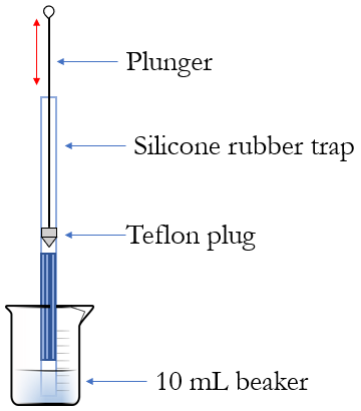

Figure 2.15: The plunger assisted solvent extraction (PASE) set-up for a PDMS sampler. ***Source:*** *Adapted from Munyeza et al. (2018).*

For the analysis of samples acquired using a GW sampler, it is important to consider analyte-sorbent interactions so as to apply extraction techniques in the most effective manner possible. For example, if the graphene layers of the GW are not uniformly grown on the QW, in that there are areas where multiple layers of graphene are present, this may cause heavier non-polar analytes to adsorb with a higher affinity than smaller non-polar analytes which in turn, may require harsher desorption conditions, such as higher TD temperatures, to desorb all the target analytes from the sorbent.

2.4.4 Analytical methods

According to the US EPA, detection limits for atmospheric monitoring at ppb and sub-ppb levels vary depending on several key factors including the minimum artifact levels (which are desirable to be < 10% of the masses of analytes collected during air monitoring), GC detector selection and the volume of air sampled. In order to sample at low concentrations, it is desirable to have low artifact levels; typical artifact levels for 0.6 cm o.d. tubes of 8.9 cm length range from 0.01 ng and 0.1 ng for carbonaceous sorbents and Tenax®, respectively (US Environmental Protection Agency, 1999).

Once an air sample has been collected onto a sampler, the analytes require extraction and subsequent analysis. There are various means to analyse air samples as shown by Table C1 in Appendix C. Amongst the most popular techniques is the use of gas-chromatography (GC) coupled to either mass spectrometry (MS) or flame ionization detection (FID), which will also be used in this study.

Before analysis can take place, the limit of detection (LOD) and limit of quantification (LOQ) must be calculated as shown in Equations 2 and 3 using the lowest standard concentration analysed. In Equations 2 and 3, S/N is the signal to background noise ratio, as calculated by the instrument.

$$LOD = \frac{\text{Standard Concentration (ppm)} \times 3}{S/N} \quad \ldots \text{Eq 2}$$

$$LOQ = \frac{\text{Standard Concentration (ppm)} \times 10}{S/N} \quad \ldots \text{Eq 3}$$

2.4.5 Analyte retention volumes

Of the various techniques available to sample gaseous organic vapours, the use of a sorbent tube is common. The sorbent tube may be seen as a type of chromatographic column (Peters & Bakkeren, 1994) whereby the sorbent is then the stationary phase whilst the air stream is the mobile phase which carries analytes of interest and allows the interaction of the gaseous analytes with the sorbent.

The US EPA defines retention volume (RV) in the Compendium Method TO-17 as the "volume of carrier gas required to move an analyte vapor plug through the short-packed column which is the sorbent tube." (US Environmental Protection Agency, 1999). Alternatively, RV has been more simply defined as the "volume of air required to elute the band maximum" (Zaranski & Bidleman, 1987). Breakthrough volume (BV) has been defined as the "volume of vapour in air that can be passed through the sorbent tube before concentrations of eluting vapour reaches 5% of applied test concentration" (Peters & Bakkeren, 1994). The specific breakthrough volume (SBV) is defined in terms of the concentration or mass of an analyte (Züttel et al., 2004); which are unknown in a real-case scenario until sampling and quantification of the anlatye has taken place. Figge et al. (1987) has defined SBV as the volume of gas that causes an analyte to migrate through an adsorbent bed of 1 gram, at a specific temperature. BVs and RVs are dependent on factors such as vapour concentration, temperature, humidity, interferences, flow rate and sorbent bed geometry (Harper, 1992 and 1993).

The individual analyte SBV for a sampler is an important piece of information to be aware of before quantitative sampling can take place. This information will tell the user if the sampler being used is able to quantitatively sample a specific analyte of interest or if the analyte will simply flow through the sampler without retention and thereby result in inadequate pre-concentration above LOQ levels. Also, if the analyte is indeed retained, this information will inform the user of the maximum sampling volume before breakthrough and loss of the analyte occurs, at a certain temperature and pressure.

For the determination of the BV of an air sampler, there are two techniques available; the elution and frontal techniques as shown by Figure 2.16. Of these two methods, Zaranski and Bidleman (1987) have stated that it is experimentally easier to investigate adsorbents using the elution rather than the frontal technique. Therefore, although both methods will be reviewed in this section, for the purpose of this study, the elution technique was used to

preliminarily investigate the chromatographic RVs for the GW, QW and PDMS samplers as shown in Figure 2.18 and later elaborated in Section 3.6 of Chapter 3.

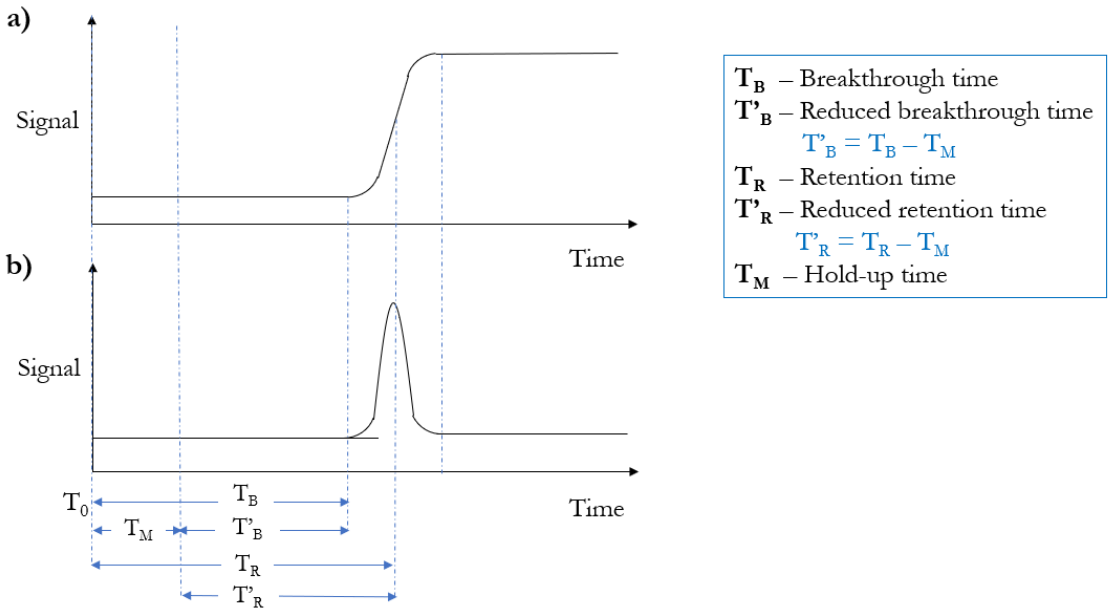

Figure 2.16: a) Chromatographic techniques, namely the frontal technique and **b)** elution technique used for the determination of the SBV and/or RV. ***Source:*** *Adapted from Dettmer (2002).*

Under real conditions using the frontal technique, the RV (termed V_R in Figure 2.17) may be inferred from the breakthrough curve as it corresponds to half the maximum analyte concentration (Bielicka-Daszkiewicz & Voelkel, 2009) as seen in Figure 2.17.

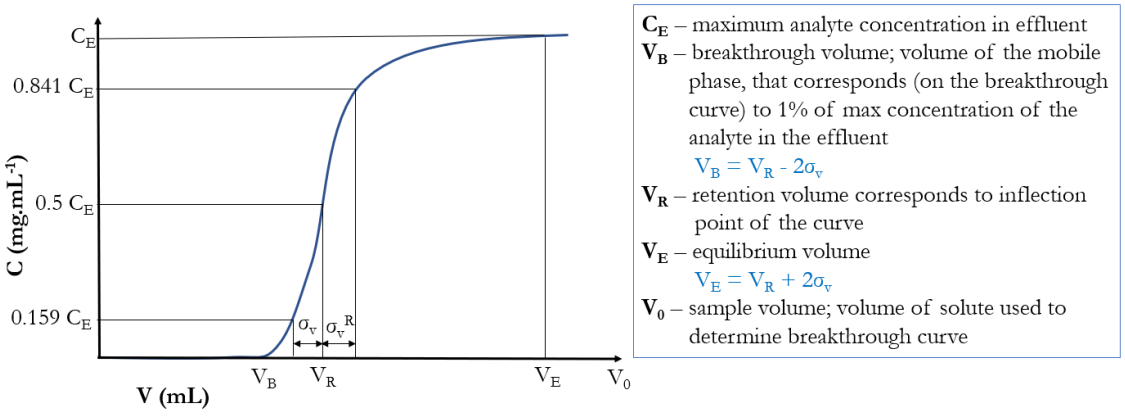

Figure 2.17: Breakthrough curve. ***Source:*** *Adapted from Bielicka-Daszkiewicz & Voelkel, (2009).*

The BV, which is the volume of sample which has to flow through the sorbent in order to obtain a 95 - 99% retention, may be calculated from $V_B = V_R - 2\sigma_V$ whereby σ_V and σ^R_V are

the standard deviations of the derivative curve determined graphically from the breakthrough curve; these values correspond to 0.159 and 0.841 of the maximum concentration of the analyte in the effluent (C_E) when using the frontal technique (Bielicka-Daszkiewicz & Voelkel, 2009). Other relevant equations relating to various parameters of interest such as plate number, retention factor, etc. have been further derived and compiled by Bielicka-Daszkiewicz and Voelkel (2009).

Whilst the frontal technique has been found to be desirable by some authors, the performance of the two methods has been compared and have shown good agreement for low boiling analytes (Mastrogiacomo et al., 1995; Bertoni et al., 1981). Since this study focused on VOCs and SVOCs, the application of either method is relevant and the elution method has been chosen. Dettmer and Engewald (2002) stated that the elution technique is based on the assumption that that the analyte is present at infinite dilution and the breakthrough is only caused by a migration of the analyte through the adsorbent bed similar to gas-solid chromatography using packed columns. According to Manura (2019), the term BV has in the past also been referred to as RV and therefore Equation 4, in Figure 2.18, may be utilized in the determination of the RV for a selected sorbent for individual target analytes.

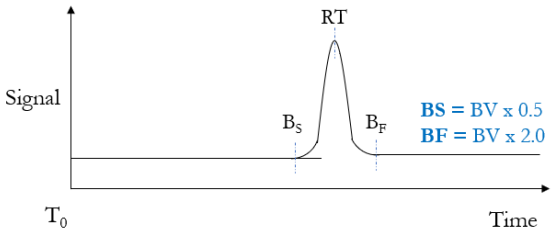

$$BV = \frac{(RT\ x\ Flow) - DV}{Wa\ x\ 1000\ mL.L^{-1}} \quad \ldots \text{Eq 4}$$

BS – Safe sample volume
BF – complete sample elution volume
BV – Breakthrough volume ($L.g^{-1}$)
RT – Retention time of analyte (min)
Flow – Carrier gas flow ($mL.min^{-1}$)
DV – Dead volume (mL)
Wa – Weight of sorbent resin (g)
1000 mL/L – Conversion factor to convert data from $mL.g^{-1}$ to $L.g^{-1}$

Figure 2.18: Breakthrough calculation theory. ***Source:*** *Adapted from Manura (2019).*

The use of Equation 4 to calculate RV rather than BV is further supported by refering back to the definitions of RV and BV, whereby RV is related to the band maximum (as is used by Equation 4), whereas BV is closer related to the value at which the effluent concentration of the analyte reaches 5% of the inlet concentration (Harper, 1992). Therefore, to calculate percent BV, Equation 5 may be used in the case whereby a downstream (secondary) sorbent

$$BV\ (\%) = \frac{S}{S + P} \times 100 \quad \ldots \text{Eq 5}$$

S - Concentration found on secondary (2°) bed
P - Concentration found on primary (1°) bed

may be analysed for concentrations of analytes sampled and be comparitively evaluated to the upstream (primary) sorbent.

2.4.6 The CAST system

The term 'aerosol' may be defined simply as a suspension of particles in the atmosphere (Collins, 2019) and as such, unlike gases, aerosols cannot be stored due to the interaction between the aerosol particles leading to processes such as coagulation and sedimentation. These processes result in a decreased number of particles and surface area whilst the mean particle diameter in the aerosol increases. To solve this difficulty, standard particles needed to be produced instantaneously in a continuous process of reliable reproducibility (Kasper, 2009) within a regulated aerosol generator. It is from this need that the combustion aerosol standard (CAST), as shown in Figure 2.19, was created by Dr Lianpeng Jing. In this study, trace levels of VOCs simultaneously generated by a CAST system were sampled using the GW sampler as well as PDMS and charcoal samplers for comparison.

The principle of the CAST generator is based on laminar propane co-flow diffusion flame. Due to the heat produced at the flame front, pyrolysis occurs. There are no particles found outside the flame in the combustion region, however, soot particles are formed when the combustion process is quenched by rapid cooling or with inert "quenching" gases. The quenching gas is added to prohibit further combustion processes from taking place in the subsequent particle stream. In addition to stabilizing the soot particles, the process of quenching inhibits condensation in the particle stream under ambient air conditions. This particle stream is subsequently diluted by supplying compressed air to it (Jing, 2009; Kasper, 2009).

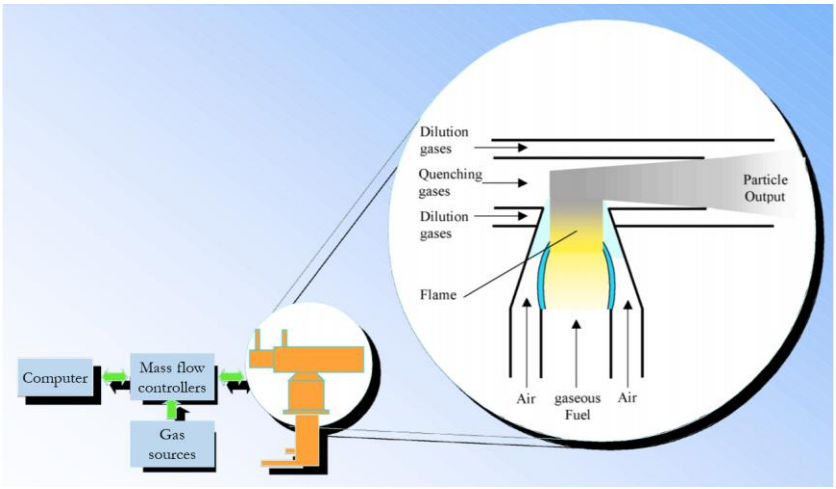

Figure 2.19: Principle of CAST. ***Source:*** *Adapted from Jing (2002).*

It is beneficial to note that select parameters and variables, shown in Table 2.7, can be varied in the CAST; for example, the size of the particles can be decreased by manually moving the quenching gas lower and therefore closer to the combustion zone. Note that high volumes of gas flow will produce a high flame which will yield smaller particles whilst the reverse also holds true, low volumes of gas flow will lead to the generation of larger particle sizes. Caution needs to be taken when changing the conditions of the CAST as these alterations will change the combustion pattern, as well as the particle properties and limit the stability and repeatability of particle generation (Kasper, 2009).

Table 2.7: Parameters and variables involved in CAST.

Parameters and Variables in CAST	Description	Source
Influencing Parameters	• Gas flows of fuel and oxidation gas: variable particle size range of 30 - 200 nm	(Kasper, 2009)
Constant Parameters	• Quenching gas (Nitrogen or ambient air) • Dilution air (Compressed or ambient air) • Fuel gas type (of user's choice but must be oil free and purity > 99.0%)	(Jing, 2002)
Variables	• Flow rates of fuel gas, oxidation air for flame and N_2 in fuel • Quench position on diffusion flame	(Jing, 2002)

Chapter 3: Methods

The individual studies detailed in this chapter are described according to the chemicals, standards, instrumentation and analytical methods used. This is followed by the procedures employed in each study.

3.1 Assembly of the samplers

3.1.1 The synthesis and assembly of the GW samplers

For all studies, the graphene wool (GW) sorbent was synthesized onto a commercially available 9 - 30 µm coarse QW substrate (Acros, Industrial Analytical, SA) in-house according to previously optimised conditions (Schoonraad et al., 2020). For the assembly of the GW samplers, ± 120 mg of GW was weighed out using a calibrated Sartorius Entris analytical balance and packed into 178 mm long glass tubes (i.d. 4 mm, o.d. 6 mm, Listco, SA), for the relevant studies, whilst maintaining a bed length of 60 mm (equivalent to the thermal desorption (TD) zone of a Gerstel 3 TDS). The percent relative standard deviation (%RSD) of the sorbent masses for the assembly of the GW samplers for this work was 5.0%. The GW sorbent was held in place by means of stainless-steel screens (Merck, SA); which were designed for Gerstel TD tubes of the same inner diameter (i.d.). The GW samplers were conditioned at 300 °C for 8 hrs using hydrogen (≥ 99.999% purity, AFROX, SA) with a gas flow of 100 mL.min^{-1} using a Gerstel TC 2 Tube Conditioner (Chemetrix, SA). After the samplers were conditioned, they were capped with quartz glass rods which were held in place by Teflon sleeves as shown in Figure 2.8 in Chapter 2.

3.1.2 The assembly of the QW samplers

The same commercially available 9 - 30 µm coarse QW substrate (Acros, Industrial Analytical, SA), described in Section 3.1.1, was used as the sorbent in this sampler type. The sampler was assembled, conditioned and capped identically to the GW sampler described in Section 3.1.1.

3.1.3 The assembly of the PDMS samplers

The PDMS samplers were prepared based on the method described by Ortner and Rohwer (1996). Each trap consisted of 22 parallel PDMS tubes (55 mm long, 0.3 mm i.d., 0.6 mm o.d., Sil-Tec, Technical Products, Georgia, US) in a 178 mm long glass tube (6 mm o.d., 4 mm i.d., Listco, SA). The PDMS traps were conditioned prior to use at 280 °C for 16 hrs using hydrogen (≥ 99.999% purity, AFROX, SA) with a gas flow of 100 mL.min^{-1} using a

Gerstel TC 2 Tube Conditioner. The PDMS samplers were capped identically to samplers described in Sections 3.1.1.

3.2 Hygroscopicity studies

The aim of the hygroscopicity studies was to firstly investigate the effect that the graphene layers grown on the QW substrate had on the natural affinity for water that QW exhibits in a saturated environment as explained in Section 2.4.1 and further shown in Figure 2.12. Secondly, this study aimed to determine the water retention of the GW sampler under ambient humidity (48 - 72%), followed by investigations into the water retention of the GW sampler in simulated humidity ranges >75%, as compared to QW and PDMS samplers.

In the first study, the GW was placed in an empty SPE cartridge and flushed with a set volume of deionized water ($_dH_2O$) which was deemed sufficient to saturate the material. It is of value to note that although the water retention of GW in a compressed state was investigated in a water-saturated environment, the GW sorbent will be exposed to water in the form of fine aerosols during air sampling i.e. humidity and not liquid i.e. rain. The ambient conditions during air sampling should be clear of rain as during rainfall, tens to hundreds of small aerosols and analytes adhere to the surface of each raindrop before making contact with the ground. This natural phenomenon is known to clear the air of pollutants including gaseous organic compounds (Chu, 2015). Therefore, to simulate a more realistic sampling environment at various humidity levels for the GW sampler, a humidity chamber study was subsequently conducted. In the humidity chamber study, the GW samplers sampled air at differing ambient humidity ranges, and the uptake of water by the GW sampler during sampling was evaluated by means of analytically measuring the mass of the sampler before and after the sampling events.

3.2.1 Consumables and instrumentation used

For the first part of the hygroscopicity study, the empty SPE tubes and frits (all from ANPEL Laboratory Technologies, Shanghai) were purchased from Stargate Scientific, SA for the assembly of the cartridges. A pump (model: DOA-P504A-BNGAST, US) was utilised to draw vacuum into the SPE manifold (Waters, Massachusetts, US). The deionized water ($_dH_2O$) used in this study was generated using an in-house Millipore Direct-Q® 3 UV system (Molsheim, France).

For the second part of the hygroscopicity study, a fish tank (450 mm x 220 mm x 300 mm, Lifestyle Pet Hyper, SA) was utilised as a humidity chamber. To generate the aerosols which

would simulate set ambient humidity ranges > 75%, an aquarium mist maker (M-12L, Sobo, China) was utilised. The mist maker was placed in a deep circular petri-dish (110 mm i.d., 115 mm o.d., 64 mm height) and was sufficiently submerged in the same $_dH_2O$ used in the first part of the hygroscopicity studies. A make-shift splash guard was placed above the petri-dish to allow the generated aerosols to flow out the top of the petri-dish as a fine mist whilst not allowing larger water droplets generated to directly splash out and compromise the study. Aluminium stands were made in-house to hold the samplers at the same height at which the humidity monitor (Monitor de la Humedad, AcuRite) recorded the ambient air reading. Teflon tubing was firstly utilised to connect the end of the samplers to the inlet of a glass condenser, which prevented water from entering the Gilian® GilAir® Plus Air Sampling Pumps (Sensidyne®, US). The Teflon tubing was then further used to connect the outlet of the condenser to the pump.

3.2.2 Procedure for the SPE-based study

A SPE set-up was used to test the water uptake of the compressed GW material in a fully saturated environment, as compared to its QW substrate. To assemble the cartridges for this study, individual base and top frits and ± 50 mg of GW or QW were weighed before being subsequently assembled in duplicate cartridges, A and B. As a control, two separate cartridges containing only pre-weighed base and top frits were assembled into duplicate cartridges, C and D. The method is schematically illustrated for GW or QW in Figure 3.1.

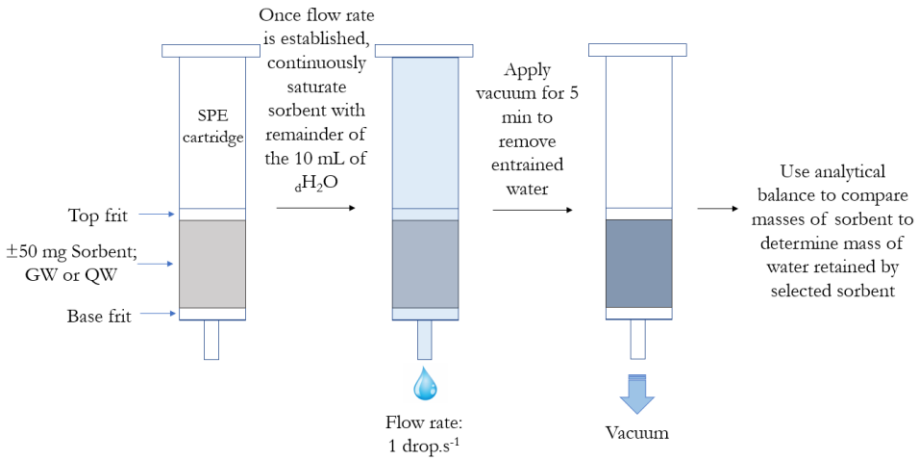

Figure 3.1: Schematic summary of the protocol used for the SPE-based hygroscopicity study of the GW sorbent and QW substrate.

To begin, the first cartridge, cartridge A, was placed into the SPE manifold. The pump was then switched on to create a vacuum in the manifold, with the tap of the manifold in which

the cartridge was positioned closed. A volume of 1 mL of the total 10 mL $_{d}H_2O$ was initially added to fill the cartridge. The tap of the cartridge was then opened and once a flow rate of 1 drop.s^{-1} was established, the water level of the cartridge was continuously maintained with the remainder of the 10 mL of $_{d}H_2O$ to ensure the GW was fully saturated until the full 10 mL volume of $_{d}H_2O$ had passed through the GW.

Once the 10 mL of $_{d}H_2O$ had passed through the cartridge, the tap was fully opened and the remainder of the entrained water was drained from either the GW or the QW with the use of the created vacuum in the manifold for 5 min. The cartridge was then weighed and the subsequent cartridge runs were conducted in an identical manner, using the same position on the manifold. The total adsorbed water was calculated for each cartridge using Equations 6 to 12. The (A) and (B), in Equations 6 and 7, referred to the duplicate cartridges containing GW/QW whilst (C) and (D), in Equations 9 and 10, refer to the duplicate control cartridges, which did not contain any of the sorbent materials.

$$\text{Post } {}_{d}H_2O\ (A) - \text{Pre } {}_{d}H_2O\ (A) = T_{\text{water ads. (A)}} \quad \ldots \text{Eq 6}$$

$$\text{Post } {}_{d}H_2O\ (B) - \text{Pre } {}_{d}H_2O\ (B) = T_{\text{water ads. (B)}} \quad \ldots \text{Eq 7}$$

$$\frac{\text{Eq 6} + \text{Eq 7}}{2} = T_{\text{water ads. by GW/QW+frits}} \quad \ldots \text{Eq 8}$$

$$\text{Post } {}_{d}H_2O\ (C) - \text{Pre } {}_{d}H_2O\ (C) = T_{\text{frits ads. (C)}} \quad \ldots \text{Eq 9}$$

$$\text{Post } {}_{d}H_2O\ (D) - \text{Pre } {}_{d}H_2O\ (D) = T_{\text{frits ads. (D)}} \quad \ldots \text{Eq 10}$$

$$\frac{\text{Eq 9} + \text{Eq 10}}{2} = T_{\text{ave water ads. by frits}} \quad \ldots \text{Eq 11}$$

$$\text{Eq 8 -E11} = T_{\text{water GW/QW ads.}} \quad \ldots \text{Eq 12}$$

3.2.3 Chamber hygroscopicity study

The second part of the hygroscopicity study was conducted inside a humidity chamber which was assembled in-house as shown in Figure 3.2. The samplers were placed on stainless-steel stands at an appropriate sampling height relative to the humidity monitor to acquire accurate humidity readings for the height at which the samplers were drawing air. The sampling events which took place at three set humidity ranges, between 48 - 72%, occurred with the lid of the humidity chamber removed. The lid was removed to obtain an environment that would be of constant desired humidity with no air flow affects which may have otherwise caused variations in the humidity during sampling events. The mist generator was switched off to sample the ambient laboratory humidity between 48 - 72%. For sampling events which

occurred at humidity ranges > 75%, the mist generator was used inside the chamber with the lid on (as in Figure 3.2 a)), so as to simulate a more humid environment than what was typically experienced in the laboratory.

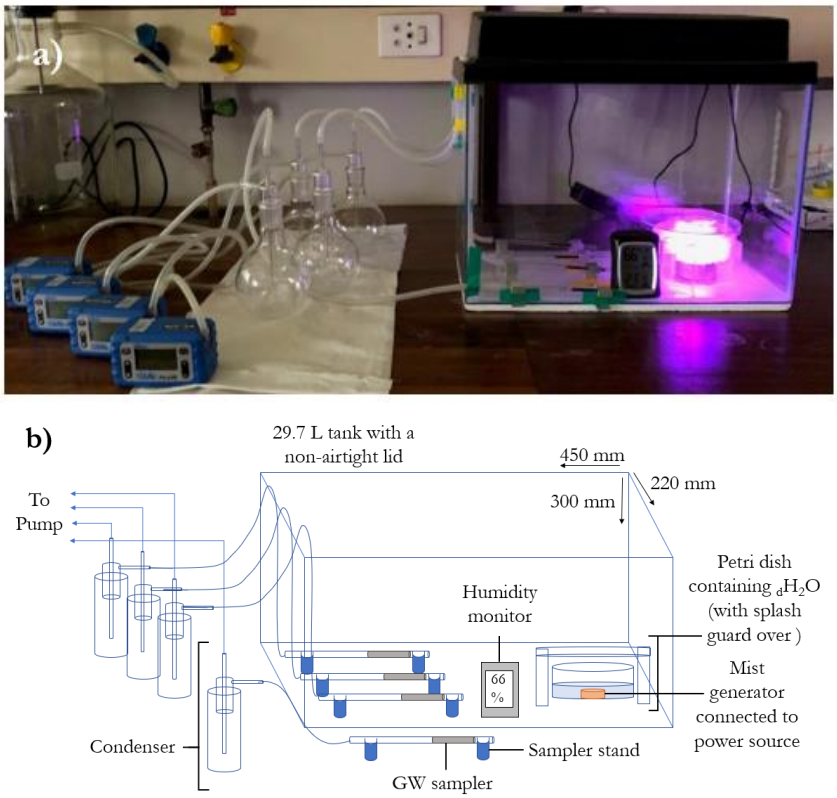

Figure 3.2: a) Experimental set-up for the determination of humidity uptake on GW samplers inside the chamber and **b)** schematic of experimental set-up.

Each sampling event took place for 10 min at a set sampling flow rate of 500 mL.min^{-1}. Each sampler thereby sampled ± 5 L of air inside the chamber at the established humidity ranges. An additional sampler was used concurrently to the samplers inside the chamber, which was attached to the outside of the chamber, so as to provide further surety to the results obtained from the three samplers inside the chamber for humidity ranges 48 - 72%. The GW samplers were weighed before and after the sampling events to acquire the accurate mass difference of the samplers and obtain the gross uptake of moisture.

Additionally, randomly chosen samplers of each of the types of sampler (GW, QW and PDMS) were placed inside the humidity chamber. The lid was placed on the chamber, as shown in Figure 3.2 a), and the aquarium mist maker was switched on. The sampling events were started when the humidity monitor showed the ambient humidity at the sampling height was > 90%. The humidified air inside the humidity chamber was then sampled at 500 mL.min^{-1} for 10 min. Once the sampling period was concluded, the samplers were removed

from the tank and the outside walls of the samplers were dried with a paper towel. The excess entrained water was removed by flicking the water out of the tubes by hand, five times from each end of the samplers, and cotton swabs (Copan, Brescia, Italy) were then used to remove the excess water on the inside of the sampler tubes before subsequent mass measurements of the samplers took place.

3.3 Back-pressure study

High back-pressures are undesirable for air samplers as it is not compatible with the use of small portable personal sampling pumps. This is primarily due to high back-pressures reducing the battery life of pumps significantly and resulting in possible pump failures during sampling events which subsequently leads to inaccuracies in the reported data. It is noted that back-pressures are generally higher and more unstable at higher flow rates therefore, the change in back-pressure of a sampler during a sampling event may be used as an indication of the consistency in the air flow rate during sampling, as described in Chapter 2. Once a flow rate corresponding to a steady back-pressure was observed, the reproducibility of the assembly of the GW samplers was investigated by comparing inter-sampler flow rate consistency at the selected suitable flow rates. Each sampler was tested in triplicate and the consistency of these samplers were evaluated accordingly.

3.3.1 Sampler assembly and instrumentation used

The tested samplers were assembled according to Sections 3.1.1 - 3.1.3. These samplers were connected by Teflon tubing to Gilian® GilAir® Plus Air Sampling Pumps (Sensidyne®, US), which were operated at 500 mL.min^{-1} for 10 min.

3.3.2 Procedure for the back-pressure consistency study

To observe and record the resulting back-pressure from drawing air through the optimised GW sorbent bed at set flow rates, a GW sampler was randomly selected from a batch of newly assembled GW samplers as per Section 3.1.1. The change in back-pressure of this GW sampler (N=1) was then recorded in 10 s intervals from the resultant back-pressures displayed on the pumps, in real-time, at four different flow rates set on the pump (in constant flow mode), namely 200, 300, 400 and 500 mL.min^{-1}, for a sampling period of 10 min. Once a flow rate was observed for which the back-pressure was deemed to be sufficiently consistent, the flow rates of two additional GW samplers were observed and recorded, every 10 s for 10 min, at the set flow rate. This allowed for an investigation into the reproducibility

of the GW samplers which were built in-house (*N*=3). Once completed, the same procedure was applied to three, randomly selected, QW and PDMS samplers for comparison (*N*=3).

3.4 Extraction techniques: A) PASE versus B) TD

Whilst TD is commonly known to be an effective form of desorbing many target analytes from various sorbents, solvent-based extraction techniques have several associated advantages. Although liquid extractions dilute the samples, they have the advantage of allowing for multiple injections of a given sample. The samples can then be stored (time dependent on half-life and reactivity of analytes present in the sample), which allows for possible comparative analyses on different analytical instruments against other liquid samples. Solvent extraction is sometimes preferred over TD if analytes strongly adsorb onto the sorbent and thereby require harsher extraction conditions, for which TD is inadequate. Additionally, for laboratories located in developing countries with limited funding, the thermal desorption system (TDS) is an additional expense which may be avoided through solvent-based extractions. The fast and low solvent use PASE method which Munyeza et al. (2018) developed was detailed in Chapter 2 and was previously optimised for PDMS. Therefore, the application of PASE to the GW sampler required investigation and optimisation.

A: PASE

3.4.1 Chemicals, standards and instrumentation used

For this section of the study, PAHs, detailed in Table B2 in Appendix B, were used as a representative class of compounds for SVOCs whilst VOCs were excluded as it was decided that their vapor pressures were too high to reproducibly undergo the PASE method; in that volatilisation losses would be too high. The PASE plunger was made in-house using a stainless-steel rod with a Teflon tip which screwed onto the tip of the stainless-steel rod. For PASE, 10 mL polytop vials were utilised with polymer lids instead of 10 mL beakers used by Munyeza et al. (2018). Once the PASE was completed, the extracts were immediately transferred into sealed 5 mL amber GC vials (Stargate Scientific, SA) and stored at 5 °C until analysis within 24 hrs.

3.4.2 GCxGC-TOF-MS analyses

Offline analysis of the GW samplers was performed by a LECO Pegasus 4D GCxGC-TOF-MS (LECO, St. Joseph, MI, US) that was equipped with an Agilent Technologies 7890 GC

(Palo Alto, CA, US), a quad jet dual-stage modulator and a secondary oven. Data acquisition and processing was executed by ChromaTOF software version 4.0 (LECO Corp., St. Joseph, MI). Synthetic air was used for the hot jets and liquid N_2 was used to cool nitrogen gas, generated by a Peak Scientific Nitrogen Generator, for the cold jets with an AMI Model 186 liquid level controller to maintain sufficient levels. The GC column set consisted of a Restek Rxi-1MS nonpolar phase 100% dimethyl polysiloxane (30 m, 0.25 mm i.d., 0.25 µm df) as the first dimension (1D) and a Rxi-17Sil MS, midpolar 50% diphenyl/50% dimethyl polysiloxane (0.79 m, 0.25 mm i.d., 0.25 µm df) as the second dimension (2D) (both columns from Restek Corporation, U.S.A.).

3.4.3 Analytical method for the liquid injection of SVOCs using GCxGC-TOF-MS

A 1 µL volume of the PASE sample extracts were directly injected in duplicate into the GCxGC-TOF-MS system, described in Section 3.4.2, by splitless inlet. The front inlet temperature was maintained at 250 °C throughout the run. The front inlet septum purge flow was set to 3 $mL.min^{-1}$. Helium was used as the carrier gas with a flow rate of 1.40 $mL.min^{-1}$. The oven started at 40 °C with a hold time of 5 min and was then ramped to 315 °C at 5 $°C.min^{-1}$ and then held for 15 min. The transfer line temperature was set to 300 °C. The mass spectrometry method was set to scan from m/z 50 - 300 with an electron energy of -70 eV and an ion source temperature of 230 °C.

3.4.4 Quality control for analysis of liquid injections using GCxGC-TOF-MS

After injecting the first liquid extract, an instrumental blank was subsequently run and no carryover of the target analytes was observed, therefore no procedural blanks were used between analysis whilst a daily system and solvent blank was used to ensure no contamination took place during sample analysis. The performance of the instrument was monitored daily through leak checks and tuning of the mass detector.

3.4.5 PASE with hexane

For the determination of the percent extraction efficiency of PASE to extract PAHs from the GW samplers, the initial solvent (hexane) extraction volume was decreased from 1 mL per PASE extraction, as detailed by Munyeza et al., (2018) for PDMS samplers, to 0.75 mL per PASE extraction for GW samplers so as to further concentrate the extracts. It was found that less solvent could be used for GW samplers as compared to PDMS samplers due to the packed structure of the GW sorbent as compared to the open tubular structure of the PDMS sorbent. This is beneficial as it reduced the amount of extract dilution. Figure 3.3 illustrates

how PASE, when applied to a PDMS sampler by Munyeza et al., (2018) (Figure 3.3 a)), was optimised for the GW sampler by using the same solvent, i.e. hexane, at a lower volume (Figure 3.3 b)). It was desirable to use polytops with lids that fit securely and made it more efficient for taking them on and off between weighing and PASE steps, as compared to the beaker covered with Parafilm used by Munyeza et al. (2018). All of the polytops mentioned in this section were sealed with lids during weighing steps on a Sartorius analytical balance (Sarto Mass Services CC) so as to minimise solvent losses in the form of solvent evaporation.

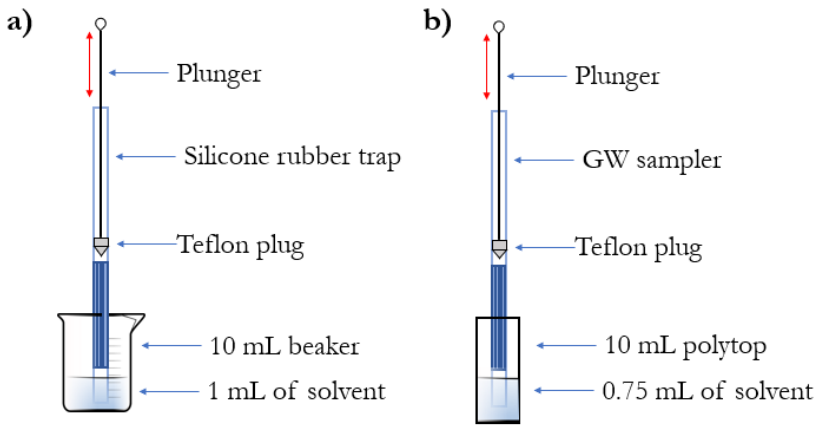

Figure 3.3: a) The original set-up of PASE by Munyeza et al. (2018) with **b)** the optimised solvent volume for the GW sampler.

Once each of the GW samplers were conditioned as detailed in Section 3.1.1. A 5 µL volume of a 2 000 ng.µL^{-1} mixed PAH standard (Table B2 in Appendix B) was spiked onto the GW sampler (giving a total mass of 10 000 ng of each PAH spiked onto the GW sampler). Samplers were reused at the start of the optimisation trials however it was noted that carry over occurred when the GW samplers were spiked with 10 000 ng of PAHs. Therefore, fresh GW samplers needed to be utilised when determining the percent extraction efficiency of PASE for PAHs spiked onto the GW samplers.

Once spiked with 5 µL of the mixed 2 000 ppm PAH standard, the GW sampler was capped and left to equilibrate for 10 min before sequentially plunging the sampler 10 times with three 0.75 mL hexane aliquots in 10 mL polytops. The three aliquots resulted in three separate PASE extracts from the same sampler which were subsequently pipetted into separate 5 mL amber vials and refrigerated at 5 °C until analysis occurred within 24 hrs by means of GCxGC-TOF-MS. LODs and LOQs were calculated using Equations 2 and 3.

$$LOD = \frac{\text{Standard Concentration (ppm)} \times 3}{S/N} \quad \ldots \text{Eq 2}$$

$$LOQ = \frac{\text{Standard Concentration (ppm)} \times 10}{S/N} \quad \ldots \text{Eq 3}$$

3.4.6 Analysis of the PASE extracts

To determine the ng extracted in each of the relevant PASE extracts, the chromatographic peak areas of duplicate injections from one extract analysis were averaged for each analyte. The concentrations, in $ng.\mu L^{-1}$, of each analyte were then calculated from the established calibration curves and subsequently multiplied by the corresponding extract volumes (µL). The 5-point instrument calibration curves, ranging from 0 to 12 ppm (N=3) for each target analyte, were established for the PASE extracts by injecting 1 µL of the standard solutions diluted to desired concentrations (Section D in Appendix D). The volume of solvent in the vials, after PASE, was calculated by means of the mass difference of the empty polytop and that of the polytop vial containing solvent after PASE, in conjunction with the literature value of the density of hexane. This resulted in the quantification of each extract in terms of providing insight into the total mass, in ng, of PAHs extracted by each solvent aliquot of PASE. The average mass of analytes present in the three extracts was then added to give the total percent extraction efficiency of the PASE method for the GW sampler upon comparison to the known amount of PAHs spiked onto the GW sampler.

3.4.7 GC-MSD analysis

The PAH analysis for the 8 hr PASE with hexane (Section 3.4.8) was performed using a GC (Agilent 6890) connected to a MSD (Agilent 5975C) in electron impact (EI) ionisation mode. A 1 µL volume was injected splitless on a Restek Rxi® - PAH column (60 m long, 0.25 mm i.d., 0.10 µm df). Helium gas (high purity, Afrox, Gauteng) was used as the carrier gas at a constant flow of $1\ mL.min^{-1}$. The inlet temperature was 275 ºC and the GC oven temperature was held at 80 ºC for 1 min, then ramped at $30\ ºC.min^{-1}$ to 180 ºC, then subsequently to 320 ºC at $2\ ºC.min^{-1}$. The ionization potential was set to -70 eV, source temperature was set to 230 ºC whilst the quadrupole temperature was held at 150 ºC. A mass range of m/z 40 - 350 was recorded in full scan mode.

3.4.8 8 hr PASE with hexane

The 8 hr PASE with hexane study was carried out to investigate a possible way in which to further optimize PASE for the GW sampler. This study was undertaken due to the PASE procedure, as detailed in Section 3.4.4, resulting in ineffective extraction of analytes with the first extraction aliquot of PASE.

The GW samplers were spiked with 1 µL of a 400 ppm PAH standard (400 ng of each PAH). Once spiked with 400 ng of PAHs, the GW samplers were left to equilibrate for 10 min and were immediately plunged 10 times, so as to ensure all of the sorbent was in contact with the solvent. After which, the plunger was pulled up to the maximum capacity of the sampler and was left at the maximum length away from the sorbent so as to create a vacuum-like effect and hold the solvent up in the sorbent bed over a period of 8 hrs. The openings between both the rod of the plunger and the GW sampler, as well between the GW sampler and the polytop, were sealed with Parafilm as shown in Figure 3.4, so as to minimise solvent losses.

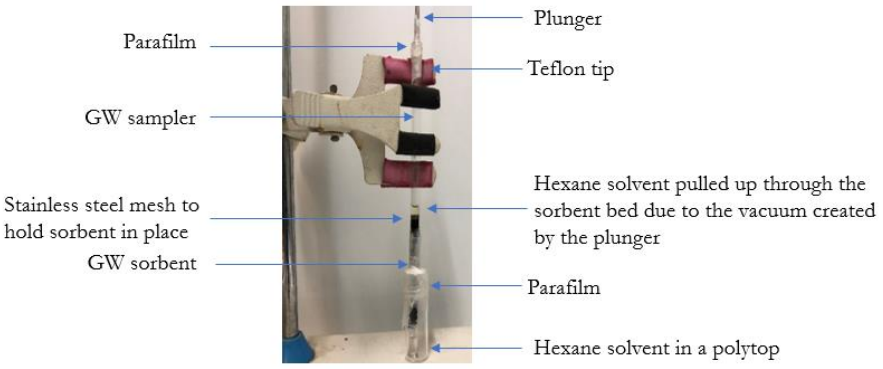

Figure 3.4: Image of how the plunger, GW sampler and polytop were sealed with Parafilm to minimise solvent losses during the PASE extraction; whereby the sorbent was soaked for 8 hrs with hexane.

After 8 hrs, the sampler was plunged 10 times so as to release the analyte containing solvent. PASE was then repeated four more consecutive times by plunging 10 times with another four aliquots of 0.75 mL of the hexane solvent (this equates to 3.75 mL of solvent used in total) to ensure only a negligible quantity of PAHs remained adsorbed by the GW after the plunging process. Extracts were pipetted into 5 mL amber vials, refrigerated at 5 °C until later analysis, similarly to Section 3.4.4. The results from this study were compared using peak areas.

B: TD

3.4.9 TD extraction

A Gerstel 3 TDS (Chemetrix, Midrand, SA) was employed at the back inlet of the LECO Pegasus 4D GCxGC-TOF-MS, described in Section 3.4.2, for sample introduction whereby the GW sampler was directly thermally desorbed. The GW samplers were thermally desorbed with a ramp from 30 °C (3 min hold) to 280 °C (5 min hold) at 60 °C.min^{-1}. The desorption flow rate was set to 100 mL.min^{-1}. The cooled injection system (CIS) method started at -50 °C and ended at 280 °C with a hold time of 5 min and a ramp rate of 12 °C.s^{-1}.

To start, a conditioned blank tube was analysed to ensure no contaminants were present in the system. As it was noted that from the TD of previous GW samplers, particles from the GW sampler were found inside the GC-MS inlet liner which was packed with glass wool. It was then decided to place ± 25 mg of QW ahead of the GW sampler in the sampler as shown by Figure 3.5 so as to minimize the amount of GW particles that enter the GC-MS inlet liner.

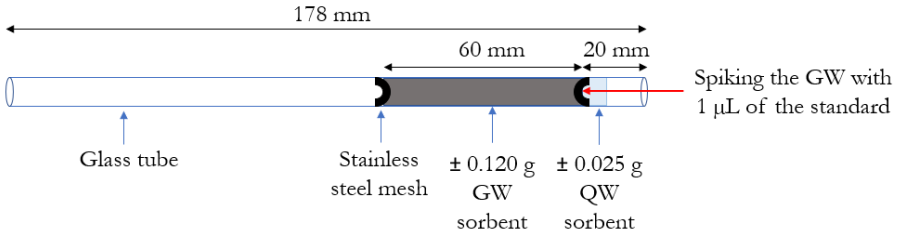

Figure 3.5: Schematic diagram of how the GW was spiked through the QW plug, preceding TD.

An empty sampler containing ± 25 mg of QW was spiked with 1 µL of a 6 ppm PAH mix standard (i.e. 6 ng) for a two-fold purpose. Firstly, it was done to gauge the peak area response for individual PAH analytes without the GW sorbent present and secondly, to determine the effect and possible analyte retention on the QW. ± 25 mg QW was then packed ahead of the sorbent inside the GW sampler. The GW sorbent was subsequently spiked with 1 µL of a 6 ppm PAH mix standard (*N*=3). The percent recovery was calculated using Equation 13.

$$\%\ Recovery = \frac{Peak\ area\ obtained\ by\ spiking\ GW + QW}{Peak\ area\ obtained\ by\ spiking\ empty\ tube + QW}\ x\ 100 \quad \ldots Eq\ 13$$

3.4.10 Quality control for TD-GCxGC-TOF-MS analyses

After spiking and desorbing the GW sampler, the same GW sampler was immediately re-desorbed and no carryover of the target analytes was observed, therefore no procedural blanks were used between analysis whilst a daily system and solvent blank was used to ensure no contamination took place during sample analysis by TD. The performance of the instrument was monitored daily through leak checks and tuning of the mass detector. The same quality control procedure was applied to all the TD analyses conducted throughout the studies.

3.5 Intra- and inter-sampler variability of selected analytes on the GW sampler

Before any real-life sampling is to be conducted, the intra- and inter-sampler variability of analysing the GW samplers spiked with a known quantity of VOCs and SVOCs was evaluated. Although directly spiking the GW sampler and instantly thermally desorbing it differs from sampling the gaseous form of the organic compounds, this was the first step used to evaluate the consistency of the analysis of GW samplers using TD. The internal standard (IS), d8-naphthalene (detailed in Table B1b in Appendix B), was used to improve the precision of the quantitative analysis of the VOCs.

3.5.1 Chemicals and standards used

For the transfer of VOCs, an SGE 008102: Syringe 1 mL FN Gastight 22ga/50/bevel (Stargate Scientific, SA) was used whilst for the transfer of SVOCs, a 10 µL Hamilton syringe (Supelco, Nevada US) was utilised.

All purchased standards were of ≥ 99% purity. A certified standard of a 60 component VOC mixture at 2 000 $ng.\mu L^{-1}$ in methanol was manufactured by AccuStandard, US and subsequently obtained from Stargate Scientific, SA. For the VOCs, Table A1 found in Appendix A lists all the analytes present in the VOC mixture with TLV® Basis whilst Table B1 in Appendix B notes the primary quantification ions with which each VOC target analyte was quantified, as well as the chemical structure of the analyte. The "TLV® Basis" found in Tables A1 - A3 in Appendix A lists the adverse effect(s) upon which the TLV® is based. Working solutions for all of the standards were prepared by means of appropriate dilutions of the stock solution prior to use. The deuterated IS used for the quantification of analytes in the VOC mixture was d8-naphthalene, purchased from Sigma-Aldrich.

A certified 2 000 ng.μL^{-1} PAH mix standard in dichloromethane (QTM, Sigma-Aldrich, SA) was used. Table B2 in Appendix B lists all the analytes present in this mixture. A certified hydrocarbon mixture (C_8 - C_{20}) was obtained from Sigma-Aldrich (Supelco, St Louis, MO) and is detailed in Table B3a in Appendix B. The deuterated IS, d34-hexadecane, used for quantification of the hydrocarbons, is shown in Table B3b in Appendix B and was also obtained from Sigma-Aldrich.

3.5.2 Analytical method for the TD of VOCs

A Gerstel 3 TDS (Chemetrix, Midrand, SA) was employed at the back inlet of the LECO Pegasus 4D GCxGC-TOF-MS (described in Section 3.4.2) for sample introduction whereby the GW sampler was directly thermally desorbed. The GW samplers were thermally desorbed at 60 mL.min^{-1} from 30 °C to 280 °C with a hold time of 30 min. The cooled injection system (CIS) method started at -100 °C and ended at 280 °C with a hold time of 30 min. Helium was used as the carrier gas at a flow rate of 1.40 mL.min^{-1}. The GC oven method started at 35 °C (held for 5 min), was ramped to 150 °C at 5 °C.min^{-1}, held for 3 min and then ramped to 280 °C at 20 °C.min^{-1} and was maintained at this temperature for 1 min. The transfer line temperature was set to 280 °C. The mass spectrometry method was set to scan from m/z 35 - 334 with an electron energy of -70 eV and an ion source temperature of 230 °C.

3.5.3 Analytical method for the TD of SVOCs

The same instrumentation was used for the TD and analysis of SVOCs as was described for the VOCs in Section 3.5.2. The GW samplers were thermally desorbed with a ramp from 30 °C (3 min hold) to 280 °C (5 min hold) at 60 °C.min^{-1}. The desorption flow rate was set to 100 mL.min^{-1}. The cooled injection system (CIS) method started at -50 °C and ended at 280 °C with a hold time of 5 min and a ramp rate of 12 °C.s^{-1}.

3.5.4 Procedure for determination of the GW intra- and inter-sampler variability

Once the VOC and SVOC methods had been established, the analytical variability of the GW sampler was tested for the target classes of compounds. These included the 60 analyte VOC mixture, which required a different GCxGC-TOF-MS analytical method to the SVOC compounds (PAHs and HCs), therefore the spiking of the VOCs and SVOCs was performed separately. To test the intra-sampler analytical variability of VOCs on the GW samplers, a selected GW sampler was spiked with 1 μL of a 20 ppm VOC mixture (20 ng) and analysed

according to Sections 3.5.2. Four replicate analyses (N=4) were used in the case of the VOCs, due to the increased uncertainty in the analysis of these analytes owing to their higher vapour pressures. Once intra-sampler variability had been established, four different GW samplers were selected at random and subsequently spiked similarly with the VOCs to determine inter-sampler variability of GW sampler analysis (N=4). The method detailed in Section 3.5.3 was utilised to determine the SVOC intra- and inter-sampler variability with N=3, by spiking and analysing a 1 µL volume of a 6 ppm PAH standard (6 ng) and a 1 µL volume of a 5 ppm HCs standard (5 ng), three subsequent times from the same sampler and then from three randomly selected GW samplers.

3.5.5 TEM images of the GW fibres

Strands of the GW material were dispersed in acetone, suspended onto copper grids (Agar Scientific Ltd, UK) and were left to dry overnight in a vacuum chamber. Images of the GW fibres were subsequently taken the next day using a JEOL 2100F field emission transmission electron microscope (TEM) (JEOL Ltd., Japan), operated at 200 kV.

3.6 Sampler tube retention volumes for individual analytes

It is crucial to be cognisant of the RVs of the target analytes on different sorbents as breakthrough can lead to misleading and otherwise inaccurate results. To conduct a comparative breakthrough study, four samplers, namely GW, QW, PDMS and an empty sampler, were secured in a GC oven; such that the selected sampler would act as the stationary phase of the chromatographic column (Peters and Bakkeren, 1994). This is to say that the purpose of arranging the sampler in such a fashion is to allow the gaseous analytes to interact with the sorbent of a selected type of sampler as if the sorbent itself is the stationary phase, as explained in Section 2.4.5. Therefore, the stronger the interaction between the sorbent of the selected sampler and the analyte of interest, the longer the analyte will take to pass through the sampler and reach the detector.

Analytes were selected based on differing associated BPs and polarities. To execute the elution technique as described in Section 2.4.5, 1 µL of the pure (undiluted) analytes were injected in duplicate (N=2) into the GC injection port. The RT from the chromatogram was used in Equation 14 (an adaptation of Equation 4 in Section 2.4.5) to determine the RV of an analyte for a given sorbent as detailed by Manura (2019).

3.6.1 Chemicals and instrumentation used

Methanol (≥ 99% purity) and n-hexane (≥ 97% purity) were purchased from Sigma-Aldrich. Propanol-2 (≥ 99% purity), butan-1-ol, (≥ 99% purity) and dodecane (≥ 99% purity) were purchased from Merck. Cyclohexanone (≥ 98.5% purity) was purchased from UNILAB whilst octane (≥ 99.5% purity) and hexadecane (≥ 99.5% purity) were purchased from BDH Laboratory Reagents. Acetone (≥ 97% purity) and toluene (≥ 99.5% purity) were obtained from ACE, SA. A 10 μL Hamilton syringe (Supelco, Nevada US) was used to inject the chosen analytes into the injection port of the GC.

Two fused silica capillaries (15 cm, 0.25 mm i.d., 0.363 mm d.f., SGE Analytical Science) were connected to each end of the GW sampler with one connected directly to the injection port of a Varian 6890A GC and the other end to the FID. The inlet pressure of the GC injection port was held 8 kPa and hydrogen was used as the carrier gas at a flow rate of 10 $mL.min^{-1}$. The FID hydrogen gas flow was set to 40 $mL.min^{-1}$ with the air and N_2 make-up flow rates at 400 $mL.min^{-1}$ and 10 $mL.min^{-1}$ respectively. The N_2 for the FID was generated by a Peak Scientific Nitrogen Generator whilst the hydrogen, dry air and helium (≥ 99.999% purity) were supplied by AFROX.

3.6.2 Procedure for the chromatographic test of the retention volume for selected analytes

The samplers tested included the GW, QW and PDMS samplers as well as an empty tube. The samplers were sequentially secured in the GC oven by a wire which cradled the sampler in front of the GC fan as shown in Figure 3.6 a). Once the sampler was connected to the uncoated capillaries and was securely positioned in the GC oven, the set-up was leak tested using a GL Sciences Inc. gas leak detector LD-223.

The solvent of choice would typically have been liquid CS_2 for FID analysis as the FID instrument is insensitive to this solvent (Nelson & De Ligny, 1968). However, due to the fact that the target analytes were pure and in liquid form, no solvent was needed, thus these analytes were injected neat. The FID chromatograms were produced by injecting 1 μL of each of the following nine analytes neat (according to the method of Manura, 2019) into the GC injection port; methanol (BP 64.7 °C), hexane (BP 68.7 °C), propanol-2-ol (BP 82.3 °C), toluene (BP 110.6 °C), butan-1-ol (BP 117.7 °C), octane (BP 125.6 °C), cyclohexanone (BP 155.4 °C), dodecane (BP 216.3 °C) and hexadecane (BP 286.8 °C). Over 430 injections were manually injected into the GC injection port for this study. The temperature intervals varied

between compounds and samplers; larger temperature intervals were used for situations in which wide Gaussian peaks were observed for corresponding analytes (which mainly occurred for the PDMS sampler.

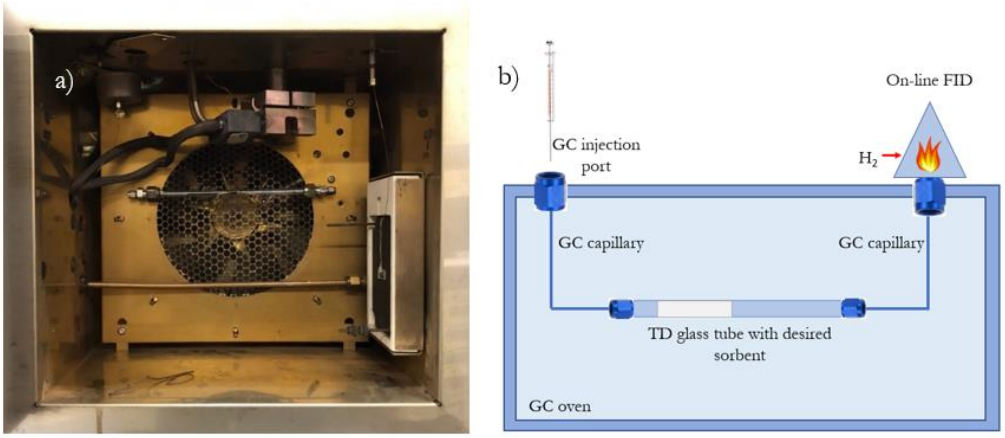

Figure 3.6: a) Photograph of the set-up inside the GC oven for the chromatographic test of tube retention volumes for selected analytes with **b)** schematic of the experimental set-up.

The GC column oven temperature was operated isothermally at set temperatures for each duplicate experimental run, thereafter the temperature was increased in subsequent runs by suitable increments (between 5 - 20 °C) until a satisfactory Gaussian peak was observed on the chromatogram. The set temperatures were between the ranges of 25 - 190 °C, 25 - 200 °C and 25 - 340 °C for the GW, QW and PDMS samplers, respectively. The duplicate chromatographic FID data was then averaged and the retention time of the selected analyte corresponding to the time at which the maximum signal occurred was taken from the averaged results. The RVs for the samplers were calculated using Equation 14, which does not include dead volume correction, as is included in Equation 4 in Section 2.4.5, as this value required the injection of a non-retained analyte into the GC port and typical non-retained analytes, such as methane (US Environmental Protection Agency, 1999), have been found to be adsorbed by graphene (Zhu and Zheng, 2016)

$$BV = \frac{(RT\ x\ Flow)}{Wa\ x\ 1000\ mL.L^{-1}} \quad \ldots \text{Eq 14}$$

BV - Breakthrough volume in $L.g^{-1}$
RT - Retention time of analyte in min
Flow - Carrier gas flow in $mL.min^{-1}$
Wa - Weight of sorbent resin in g
1000 mL/L - Conversion factor to convert data from $mL.g^{-1}$ to $L.g^{-1}$

The Wa accounted for specific sorbent mass of the tested sampler. In the case of the GW, QW and PDMS samplers employed, these weights were found to be 0.1410 g, 0.1200 g and 0.3657 g, respectively. The empty tube study allowed for a comparison of peak areas so as to determine if analytes were retained by the sorbents.

3.7 CAST campaign

3.7.1 Reagents and materials

The three fuels that were tested, namely petroleum derived diesel with no added biodiesel (B0), gas-to-liquid (GTL) and rapeseed oil methyl ester (RME) fuel, were all purchased from ASG Analytik-Service GmbH, Neusäss, Germany. An ultrasonic bath was utilised to degas each fuel for 30 min prior to use.

Individual stock standards of 36 VOCs and SVOCs along with 13 internal standards were purchased from the suppliers listed in Table G1 in Appendix G. The CAS numbers, quantification ions and chemical structures of these compounds can be found in Tables G2 and G3 in Appendix G. Working solutions were prepared by appropriate dilutions of the stock solutions prior use. For the extraction of analytes from the activated charcoal sampler, anhydrous carbon disulphide (CS_2) (> 99% purity) was purchased from Merck, Germany.

3.7.2 Sampler details

The PDMS traps consisted of twenty-two 55 mm long parallel PDMS tubes (Technical Products, Inc., Georgia, US) of 0.3 mm i.d. which were housed in a 89 mm long Supelco glass TD tube with an i.d. of 4 mm. GW was synthesised in-house as per the optimised conditions described by Schoonraad et al. (2020). The GW was synthesised from a quartz wool substrate purchased from Acros, Industrial Analytical, SA. For the assembly of the GW samplers, approximately 120 mg of GW was weighed out using a calibrated Sartorius Entris analytical balance and then packed into the same glass tubing as the PDMS traps, whilst maintaining a bed length of 60 mm for the GW sampler. The sorbent was held in place by stainless steel screens (Sigma Aldrich, SA) which are designed for Gerstel TD tubes. The traps were then conditioned using a multi-tube conditioner (TC-20 MARKES International, Germany) at 250 °C for 8 hrs under hydrogen gas flow and were then sealed using Shimadzu stainless steel tube caps. The activated charcoal type BIA tubes were purchased from Dräger, Germany.

3.7.3 CAST set-up

A Combustion Aerosol Standard generator (diesel CAST, Jing mini-CAST 5201D, Switzerland) based at the Helmholtz Zentrum (Munich, Germany), was operated with propane (99.95%, Linde AG, Germany). The settings were as follows: dilution air (10 L.min^{-1}), oxidation air (2.2 L.min^{-1}), quenching gas (10 L.min^{-1}, fixed), propane fuel (30 mL.min^{-1}, fixed) (refer to Mueller et al. (2016) for further details regarding the CAST). The fuel of choice was supplied to the CAST generator using an inlet from a HPLC pump at 50 mL.min^{-1}. In the viewing window, illustrated by number 4 of Figure 3.7, it could be seen that the flame changed from blue to orange once the fuel of interest was added to the propane already combusting in the CAST generator.

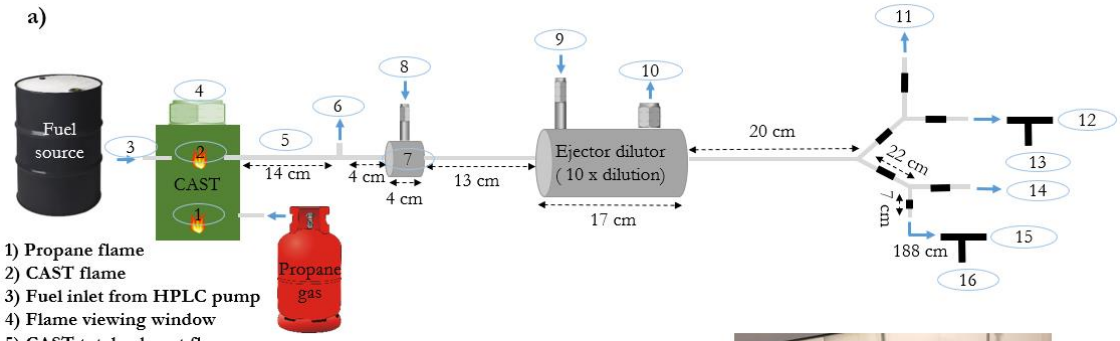

Figure 3.7: a) Schematic and **b)** photograph of the CAST generator sampling set-up.

The fuel was introduced to the CAST generator using polytetrafluoroethylene (PTFE) tubing (50 cm) and polyurethane (PU) tubing (5 cm) using a high-performance liquid chromatography (HPLC) pump (Kontron, type 420, Germany) and then subsequently, copper tubing was used to connect the HPLC pump to the CAST generator. Antistatic polyurethane hose of 12.0 mm o.d. x 8.0 mm i.d. (Riegler, Germany) was used for all the connections between the CAST and various dilutors, splitters and sampling instrumentation involved in this study. The CAST generated 22 L.min^{-1} of undiluted combustion exhaust. From the CAST generator, an exhaust outlet, shown by number 6 in Figure 3.7, allowed for the undiluted excess exhaust emissions to be released whilst continuously sampling 0.3

L.min^{-1} of this exhaust over the course of the 10 min sampling period for analysis by a flame ionization detector (FID) (SK-Electronik, GMBH), calibrated with propane (30 ppm) in nitrogen (Linde, Germany), and a Fourier-transform infrared spectroscopy (FT-IR) Gas Analyser (Gasmet, Model: DX4000, Finland). The FID sampled the undiluted CAST exhaust using a 380 °C heated transfer line. Thereafter, 0.3 L.min^{-1} (1.5 L.min^{-1} for GTL and RME) of the undiluted CAST exhaust was introduced to a porous tube dilutor (Mikro-Glasfaser Filterelement, Type GF-12-57-80E) to which 2.7 L.min^{-1} (1.5 L.min^{-1} for GTL and RME) of dry air was added to make up a total diluted flow of 3 L.min^{-1}. The ejector dilutor then drew the 3 L.min^{-1} from the porous dilutor and further diluted the CAST exhaust with laboratory air that was first cleaned by passing through Intersorb Plus (Intersurgical, Sankt Augustin, Germany) to remove CO_2, and then activated charcoal (Carl Roth, Karlsruhe, Germany) and finally through Silicagel (Azelis, Sankt Augustin, Germany) at 27 mL.min^{-1}. Any overpressure which may have occurred in the ejector dilutor was released through the outlet shown as number 10 in Figure 3.7.

From the ejector dilutor, a custom-built three-way Y-piece stainless steel splitter allowed for the diluted flow of the CAST exhaust to be directed to various sampling instrumentation as well as to the selected samplers. Two of the Y-piece exits lead directly to two sampling stations to which selected samplers were attached and diluted CAST exhaust was drawn through these at 500 mL.min^{-1} for 10 min by Gilian® GilAir® Plus Air Sampling Pumps (Sensidyne®, US).

The second Y-piece was utilised for the measurement of the light absorption properties of the CAST aerosols measured online by means of an Aethalometer® (Magee Scientific, Model AE33-7, Slovenia), which had an optimised diluted flow using a PALAS® VKL 10E dilutor as the Aethalometer® typically required a dilution of 1:10 000 to not over saturate the instrument. From the same PALAS® VKL 10E dilutor, the diluted CAST exhaust was additionally measured by a Condensation Particle Counter (CPC, TSI, Model 3022A, US) and an Electrostatic Classifier (TSI, Model 3082, US) connected to a CPC (TSI, Model 3750) in order to determine the stability of the particle number concentration produced from the CAST after changing fuel sources. The PM measurements were conducted to check the stability of the emissions and suitability of the dilution ratios of the different fuels. The combustion of B0 diesel resulted in a higher PM count therefore the emissions for gas phase sampling were diluted by a factor of a 100 whilst the GTL and RME emissions were diluted by a factor of 20.

3.7.4 Sample collection and extraction

Prior to introducing a new fuel into the CAST generator, the system was cleaned with cotton swabs, Kimtech wipes and a vacuum cleaner. Once cleaned, the selected degassed fuel was introduced into the CAST generator using the HPLC pump and the combustion emissions were monitored by the particle counter and the aethalometer to ensure that the CAST generator was stable and producing a consistent concentration of aerosols. A stainless-steel filter holder assembly was positioned between an empty glass tube upstream and the selected sorbent sampler downstream. The filter holder contained a 13 mm quartz-microfibre disc (Ahlstrom Munksjö, T 293) with a precipitation area diameter of 10 mm. The purchased activated charcoal samplers were opened using a TO 7000 Dräger Tube Opener. Each sampler was connected to a Gilian® GilAir® Plus Air Sampling Pump (Sensidyne®, US) using Teflon tubing (Figure 3.8), which was operated at 500 mL.min^{-1} for 10 min.

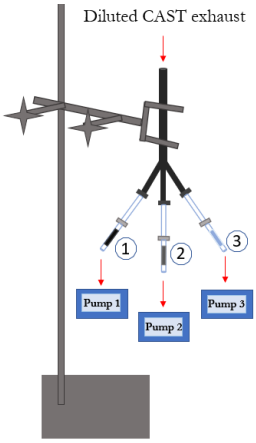

Figure 3.8: Schematic of the sampler set-up where numbers ①, ② and ③ illustrate the positions of the activated charcoal, GW and PDMS samplers, respectively, during CAST sampling events.

These sampling pumps were all calibrated for each specific sampler used prior to sampling by means of a Gilibrator 2® (Sensidyne®, US). This accounted for the individual differing back-pressures of the different sampler types. A Kestrel 4500 weather station (Envirocon, SA) was used to measure the ambient conditions at the time of the sampling event which are shown in Table G4 in Appendix G. After sampling, PDMS and GW samplers were end-capped and were subsequently wrapped in aluminium foil, sealed in zip lock polyethylene bags and were stored in a freezer at -18°C until analysis took place within 72 hrs.

The activated charcoal sampler was selected in this study due to its use in VOC methods published by the International Organisation for Standardization (ISO) and Methods for the

Determination of Hazardous Substances (MDHS) (International Organisation for Standardization ISO 9487 : 1991 (E); International Organisation for Standardization ISO 16200-1 : 2001 (E); Method for the Determination of Hazardous Substances MDHS 96 (2000)). Activated charcoal is also a cheaper alternative to graphitised materials such as Carbotrap®. The charcoal tubes were opened with an adjustable ORBO™ Tube Cutter after the sampling event, and the charcoal was emptied into 20 mL amber vials. 3 mL of CS_2 was added, the vials were then sealed and allowed to extract for 12 hr in a fume hood at room temperature. Although accredited methods such as the ISO 9487: 1991 (E) state that 500 µL of solvent be used in the extraction of analytes from activated charcoal sorbents, it was found that 3 mL of solvent was required to completely submerse the activated charcoal sorbent. After overnight extraction, the extract, with the activated charcoal still in contact with the solvent, was sonicated (Allpax Palsonic, Germany) for 15 min. The supernatant extract was subsequently transferred into a 5 mL amber GC vial and stored in a freezer at -18 °C until batch-wise analysis was conducted within 72 hrs.

3.7.5 GC-MS analysis

The PDMS and GW samplers were thermally desorbed using a Thermal Desorption System (TD-20, Shimadzu, Japan) using 60 mL.min^{-1} helium from 80 °C to 250 °C for the PDMS and to 280 °C for the GW sampler, both with a hold time of 30 min. The cooled injection system (CIS) method started at 5 °C and ended at 330 °C with a hold time of 30 min. A GC-2010 Plus was coupled to a MS-QP2010 Ultra (both Shimadzu, Japan) and helium was used as carrier gas at a flow rate of 1.6 mL.min^{-1}. A split ratio of 10:1 was applied whilst the column used was a VF-XMS (30 m, 0.25 mm i.d., 0.25 µm d.f.) column (Agilent, Netherlands). The GC oven method started with a hold time of 6 min at 60 °C and was ramped to 250 °C at 5 °C.min^{-1}. The transfer line temperature was set to 250 °C. The mass spectrometry method was set to scan from m/z 35 - 500 with an electron ionisation energy of -70 eV and an ion source temperature of 230 °C.

The charcoal extracts were injected by a 1 µL hot injection at 280 °C. Helium was used as the carrier gas with a flow rate of 1.5 mL.min^{-1}. A split ratio of 1:1 was applied to a SGE BX5 (25 m, 0.22 mm i.d., 0.25 µm d.f.) column. The oven started with a hold time of 1 min at 40 °C and was ramped to 250 °C at 5 °C.min^{-1} and then held for 2 min. The transfer line temperature was set to 270 °C. The mass spectrometry method was the same as for the PDMS and GW sampler analysis.

Chapter 4: Results and Discussion

4.1 Hygroscopicity

4.1.1 Part 1: Exploratory study

The graphene-water interactions were noted, in Chapter 2, to be highly dependent on the hydrophobicity of the GW material, with the hygroscopicity increasing with the number of layers present (Kozbial et al., 2014). The hygroscopicity of the QW substrate on which the GW layers were grown was compared to GW, for which the results in Table 4.1 were calculated using Equations 6 - 12 shown in Section 3.2.2.

Table 4.1: Average sorbent masses and the mass of adsorbed water for GW and QW in a SPE set-up (*N*= 3, ± SD).

Sorbent	Sorbent mass (mg)	Mass of $_dH_2O$ adsorbed (mg)	Mass of $_dH_2O$ retained by 1 mg of sorbent (mg)
QW	49.80 ± 2.26	14.30 ± 6.64	0.29 ± 0.47
GW	53.75 ± 3.32	23.80 ± 2.40	0.44 ± 0.12

From Table 4.1, it can be seen that the GW material retained ± 15% more $_dH_2O$ per 1 mg of sorbent as compared QW, which retained ± 30% of its mass in $_dH_2O$. This result may indicate that growing the graphene layers on the QW substrate increased the retention/entrainment of water by the material in a fully saturated environment. However, this study investigated the hygroscopicity of the GW in a compressed state which is not representative of the sorbent packing in a GW sampler. Therefore, the following chamber hygroscopicity study was undertaken to better understand the water retention of the GW sampler under various humidity conditions.

4.1.2 Part 2: Chamber hygroscopicity study

Once the hygroscopicity of the GW material was explored in terms of a fully saturated environment using the SPE set-up, it was of interest to investigate the hygroscopicity of the GW material in a manner more representative of real-life sampling.

For the first part of the chamber hygroscopicity study, three GW samplers were placed inside the chamber (*N*=3) with the fourth GW sampler attached to the outside of the chamber to confirm that the humidity conditions were the same inside and outside the chamber. The relative humidity in the laboratory was used which ranged from 48 - 72%. In these experiments, the sampler outside the chamber was included in the results (thus *N*=4). The

small standard deviation values shown in Table 4.2 indicate that the humidity conditions inside the chamber were the same as outside the chamber. Table 4.2 further shows that the mass of the GW increased due to adsorption/entrainment of water as humidity increased, however the amount of water retained below 72% humidity was negligible. A statistical t-test indicated that the mass difference of the GW sampler between 50-70% humidity is insignificant as the t-values for these were less than the t-critical value at 0.05 significance level. It can therefore be considered suitable to sample using a GW sampler in environments < 75% relative humidity.

Table 4.2: Mass of water adsorbed (± SD) by the GW samplers under different humidity conditions.

Average Humidity (%)	*N*= x	Mass of GW sampler (g)	GW sampler mass after exp (g)	Mass diff (g)	mg $_dH_2O$/g sampler	% $_dH_2O$ on sampler
50	4	6.3488 ± 0.0140	6.3475 ± 0.0152	0.0007 ± 0.0011	0* ± 0.0113	0* ± 1.1
60	4	6.3604 ± 0.0096	6.3605 ± 0.0093	0.0000 ± 0.0007	0.0003 ± 0.0056	0.02 ± 0.56
70	4	6.3612 ± 0.0100	6.3616 ± 0.0099	0.0004 ± 0.0001	0.0033 ± 0.0008	0.33 ± 0.084
80	3	6.3646 ± 0.0183	6.4272 ± 0.0047	0.1482 ± 0.0279	0.5114 ± 0.1198	51 ± 12

** An assumption of 0 was made as the mass difference was found to be negative within the measurement uncertainty.*

It is important to note that humidity ranges 48 - 72% did not have the mist maker switched on whereas the mist maker was used to simulate a humidity range of > 75%. Therefore, the amount of water retained by the sorbent at this ambient humidity may have been overestimated due to the synthetic generation of aerosols. As can be further seen from Table 4.2, since the GW sampler adsorbed nearly half its mass under moisture-saturated conditions, the GW sampler should not be used in highly humid environments with humidity > 80%, when liquid aerosols become visible to the naked eye. This observation is comparable with the SPE hygroscopicity study, as the GW sampler adsorbed a similar quantity of water in the form of mist in this study to what the GW material adsorbed in the SPE-based study (Table 4.1).

More water was retained by the GW sampler (Table 4.2) in the mist experiments as compared to GW in the SPE set-up. This could have primarily been due to the control in the SPE-

based study which accounted for water retained by the SPE cartridge and frits whilst in the chamber study, a control was not used to account for the amount of water retained by the glass tube. Additionally, this trend could be due to how the sorbent was packed in each set-up. The compact nature of how the GW and QW were packed in the SPE-based set-up, aided by the compression of the frits on either side of the materials, limited the amount of open space or volume available for water to be entrained. This is then compared to the GW and QW sampler set-up where the sorbents were loosely packed in comparison. The SPE study also made use of a vacuum manifold to extract entrained water from the GW sorbent. The removal of the entrained water for the chamber study was done by shaking out the GW sampler, after which water was removed from inside the glass sampler walls on either side of the GW by means of a cotton swab.

In the second part of the chamber hygroscopicity study, the water uptake of the GW sampler was compared to that of QW and PDMS samplers in saturated misty conditions of > 90% relative humidity, provided by the mist-maker. This part of the chamber study was similar to the previous one, with the exception that no additional sampler was attached to the outside of the chamber and additional samplers were investigated. Once the sampling period was concluded, the samplers were removed from the chamber and the outside of the sampler walls were dried with a paper towel, however there were still droplets visible on the inside of the tubes as shown in Figure 4.1 a). After weighing, the samplers were subsequently shaken and the interior glass walls of the GW samplers were dried, which resulted in the samplers as shown in Figure 4.1 b). Table 4.3 summarises the results from the second part of the chamber humidity study.

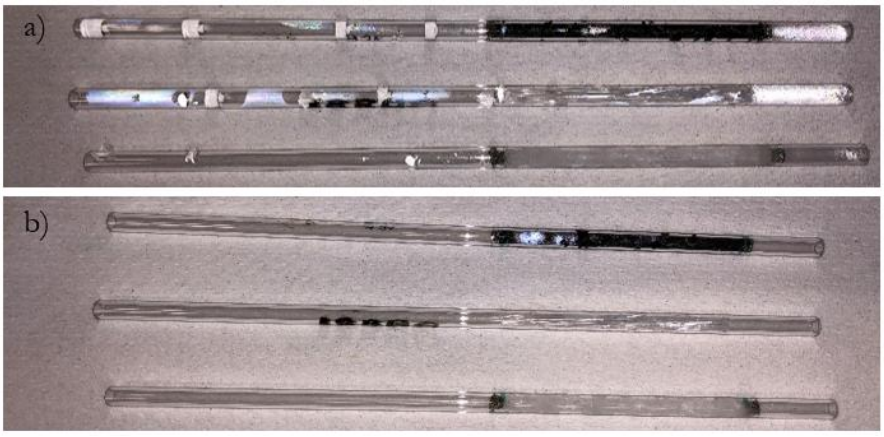

Figure 4.1: a) Photograph of the samplers after the chamber study in extreme humidity conditions (> 90%) **b)** samplers after drying by shaking and using a cotton swab to water

from the interior glass surfaces. *Top sampler is a GW sampler, middle sampler is a PDMS sampler and the bottom sampler is a QW sampler.*

Table 4.3: Mass of water retained by the GW, PDMS and QW samplers during sampling under extreme average humidity (> 90%) (*N*=4, ± SD).

Sampler type	Total average water retained (g)	g H_2O/g sampler	% H_2O on sampler
QW	0.15 ± 0.04	1.24	124
GW	0.10 ± 0.03	0.82	82
PDMS	0.02 ± 0.03	0.04	4

Table 4.3 shows expected results as the QW, which retained the most water, is the most polar sorbent which would therefore typically bind and retain more water than the non-polar PDMS sorbent. The PDMS sorbent retained the least amount of water, which indicates that the PDMS sampler can be used in more humid conditions. The QW sampler adsorbed more water than the GW, as expected, which is an opposing result to what the SPE-based hygroscopicity study showed in Section 4.1.1. This may be due to compression of the GW in the SPE set-up as compared to in the GW sampler, as previously discussed. Additionally, in the SPE-based study, the entrained water held in the compact sorbent may have been better removed by vacuum in the case of the QW material, whereas the GW material may have retained more water due to the way in which the sorbent was packed.

Overall, it was found that the GW sampler retained negligible water between humidity ranges of 48 - 72%, which illustrates a potential use of the GW sampler in a wide range of humidity conditions. In comparison, literature has indicated that the adsorption efficiency of activated charcoal sorbents may be affected by humidity whilst water molecules have been reported to displace analytes of interest in carbon molecular sieves (CMSs) (McMammon and Woebkenbery, 1998).

4.2 Back-pressure study

Since the change in back-pressure during a sampling event may be used as an indication of the restriction to air flow during sampling (at a constant flow rate), the back-pressure incurred by the GW sampler was comparatively evaluated to the QW and PDMS samplers at set flow rates. Throughout the sampling time of 10 min, the back-pressure recorded on the sampling pump when employing the GW sampler was found to be lower and more stable at the lower flow rates and increasingly higher and more unstable at higher flow rates. From

Figure 4.2 a) and b), it can be seen that sampling flow rates up to 400 mL.min^{-1} result in consistent back-pressures for both the GW sampler and the QW sampler. This is compared to the PDMS sampler where the back-pressure incurred was found to be much lower and very stable, at 1.3" H_2O for flow rates of both 400 mL.min^{-1} and 500 mL.min^{-1}, as shown by Figure 4.2 c). The higher back-pressures recorded which employing the GW and QW as compared to the PDMS sampler at equivalent flow rates may be attributed to the GW and QW samplers having a packed fibrous sorbent structure, as compared to the PDMS samplers which have an open-tubular structure.

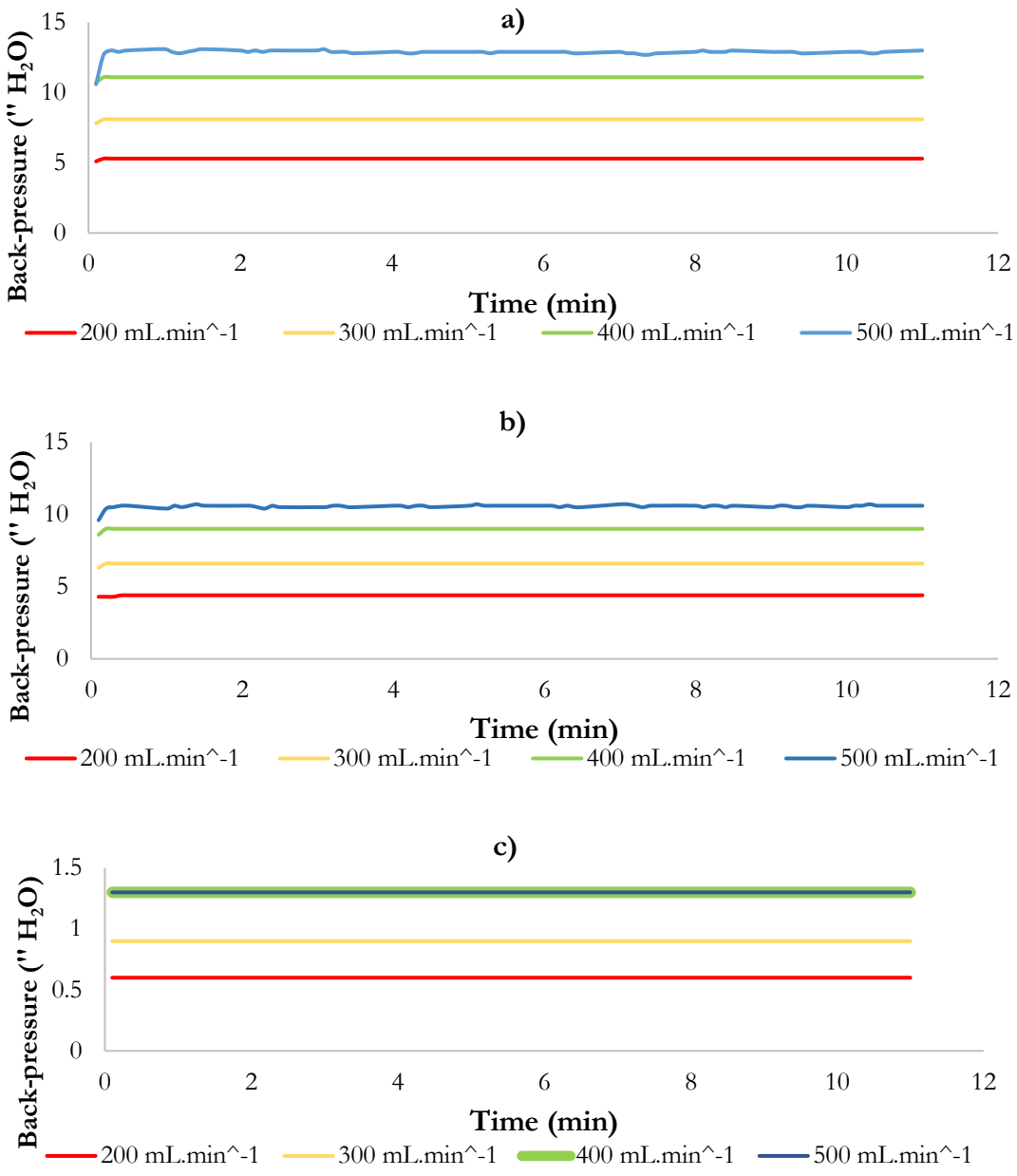

Figure 4.2: The variability of the back-pressure at various sampling flow rates for the **a)** GW sampler, **b)** QW sampler and **c)** PDMS sampler.

Whilst it is seen that stable back-pressures may be observed at 400 mL.min^{-1} for the QW and GW sampler, and at 500 mL.min^{-1} for the PDMS sampler, it is prudent to take literature into consideration. As previously mentioned in Chapter 2, for a glass tube sampler with an i.d. of 4.0 mm, the sampling flow rate should not exceed 250 mL.min^{-1} (Manura, 2019) whilst in two of the air sampling methods published by the International Organization for Standardization (ISO), namely ISO 9487 and ISO 16200-1, it has been stated that the maximum sampling flow rate should be 200 mL.min^{-1}. Further consideration of this may therefore need to be taken into account before sampling analytes of interest in real-world scenarios.

Once a stable back-pressure was found when employing the GW, QW and PDMS samplers, the consistency of how these samplers were packed in-house was explored. To do so, the flow rates of two additional GW and QW samplers were observed and recorded every 10 s at a set flow rate of 400 mL.min^{-1} whereas two additional PDMS samplers were tested at a flow rate of 500 mL.min^{-1}; as the back-pressure incurred was found to be consistent at these flow rates for the respective samplers.

As shown in Table 4.4, the average flow rate % RSD of the samplers was similar; 0.37 % RSD was found for the QW sampler whilst the % RSD of both the GW and PDMS samplers was 0.49%. Comparatively, the flow rate variation between the randomly selected PDMS samplers showed that there was the same variability in the measurements recorded (% RSD of 0.49%) as compared to that of the GW sampler, even though the % RSD relating to the mass difference between the PDMS samplers was larger (13.45%) compared to the % RSD of the mass difference of the GW samplers (1.22%). This shows that the structure of the sampler (packed fibres versus open-tubular) had more of an impact on any variations in flow rates than the amount of sorbent within the mass range tested.

Table 4.4: Average flow rates (± SD) per sampler, where the flow rates for the GW and QW samplers were set at 400 mL.min^{-1} and the PDMS samplers were set at 500 mL.min^{-1} (*N*=3).

Sampler type	Average flow rate (mL.min^{-1})	% RSD
GW	400 ± 1.97	0.49
QW	400 ± 1.46	0.37
PDMS	500 ± 2.43	0.49

The back-pressure incurred by the samplers can be reduced by decreasing the sampling flow rate, although this requires an increase in the sampling time to ensure analytes are sufficiently pre-concentrated on the sorbent. This would increase the probability that atmospheric concentration fluctuations, as well as possible degradative reactions on the sorbent, may take place during sampling (Hart et al., 1992). High back-pressures can also be reduced by increasing the inner diameter of the sampler, however this may then result in the sampler not being compatible with commercially available TDSs, therefore samplers would require solvent extraction using PASE, for example. Alternatively, the sorbent packing process may be varied to increase sorbent porosity by reducing the sorbent packing density via extending the sorbent bed length for the same sorbent mass.

Although the back-pressures observed when employing the GW sampler were higher than the PDMS sampler, these back-pressures may be lower than those incurred by some other samplers containing packed beds. Literature has reported that a 150 mg activated charcoal tube would typically be utilised at low flow rates of 10 - 200 $cc.min^{-1}$ (Roberson, 2012). It was observed that the activated charcoal sampler which was employed in the CAST campaign (refer to Section 4.6) incurred approximately 2" H_2O lower back-pressures at equivalent flow rates to the GW sampler. If the back-pressure incurred by the sampler is too high, portable low volume sampling pumps can no longer be used, which reduces possible applications of the sampler concerned. In the case of the GW sampler, however, this was not the case and the portable sampling pump reflected a stable back-pressure of ± 13" H_2O at 400 $mL.min^{-1}$.

4.3 Extraction techniques: PASE versus TD

4.3.1 Standard PASE procedure

The concentrations of the PAHs investigated in this study were determined by multiplying the ng of PAHs detected, as determined from the relevant calibration curves, with the volume of hexane calculated using analytical mass differences and the density of hexane which was reported in literature to be 0.659 $g.mL^{-1}$ (Sigma Aldrich, 2019). It was noted during the PASE procedure that the resulting extracts had various volumes, although they were fairly reproducible as shown in Table 4.5. The first PASE extract contained ± 50% less volume as compared to extracts 2 and 3, as half of the solvent in the first extract is largely lost to wetting the sorbent bed of the GW sampler and thereby half of the solvent is retained in the GW sorbent bed.

Table 4.5: Experimentally determined hexane volumes (µL) (± SD) of sequential extracts 1, 2 and 3 resulting from three PASE trials with different GW samplers.

Extract number	GW Sampler 1	GW Sampler 2	GW Sampler 3	Average (µL)	% RSD
1	344.31	375.27	372.38	363.99 ± 17.10	4.7
2	708.19	692.11	712.90	704.40 ± 10.90	1.6
3	652.66	697.12	734.29	694.69 ± 40.87	5.9

Once the volume for each extraction with PASE was optimised from 1 mL, as used for PDMS samplers (Munyeza et al., 2018), to 0.75 mL for GW samplers, the chromatographic parameters (Section 3.4.3) were optimised and applied to the GCxGC-TOF-MS, described in Section 3.4.2, to yield the chromatogram shown in Figure 4.3.

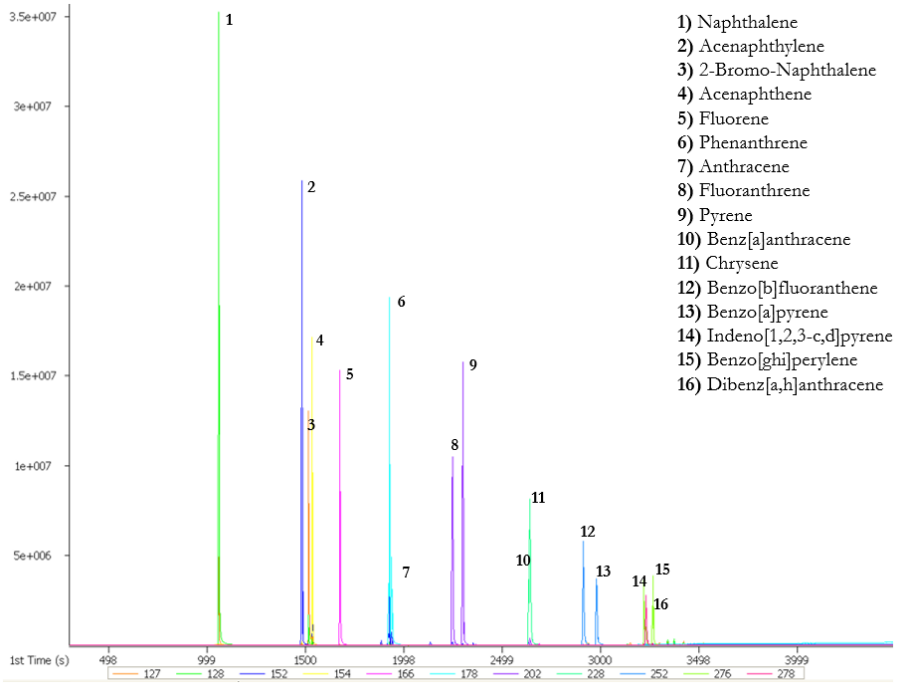

Figure 4.3: Extracted ion chromatogram (EIC) of the target analytes by means of specific molecular ion masses.

An example of an instrument calibration curve for naphthalene derived by direct injection of 1 µL of standard solutions into the injection port of the GC is shown in Figure 4.4, with the rest of the calibration curves included in Appendix D. In addition to the calibration curve shown in Figure 4.4, Figure 4.5 shows a method calibration curve for naphthalene which was generated by spiking different amounts of the PAH onto the GW. Figure 4.5 was derived by applying the optimised PASE method, analysing each extract separately, dividing the

calculated peak area by the total volume of the relevant extract and plotting the summation of the three extract concentrations on the y-axis. The calibration curves for the other analytes generated using this method may be found in Appendix E. Figure 4.5 shows that a method calibration curve obtained by standard addition is possible in future applications of PASE of GW samplers which would account for factors such as incomplete extraction and analyte losses due to volatilisation during PASE plunging or injection. Incomplete extraction would be expected to be more of a problem with the heavier PAHs, whilst naphthalene would be most affected by volatilisation losses. From the instrument calibration curves in Figure 4.4 and in Appendix D, the LODs and LOQs for the target analytes in Table 4.6 were calculated using Equations 2 and 3, respectively.

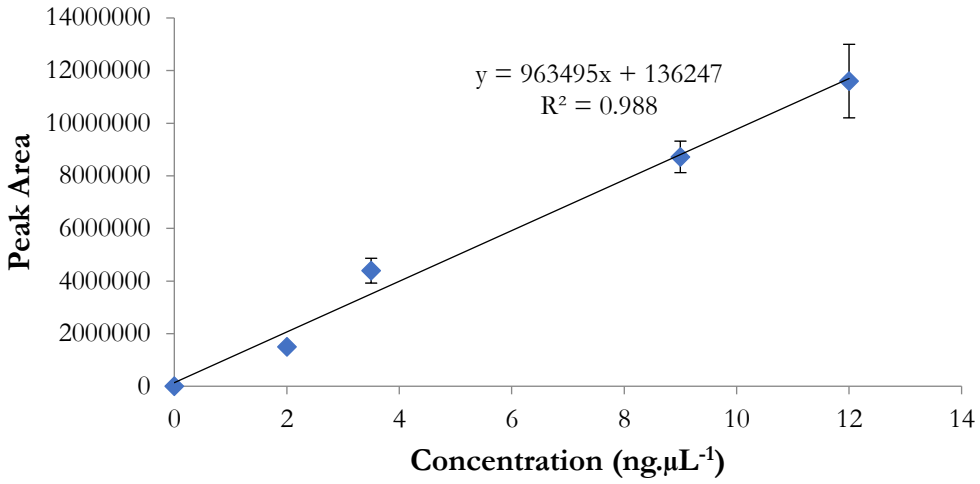

Figure 4.4: A 5-point instrument calibration curve for naphthalene in neat hexane.

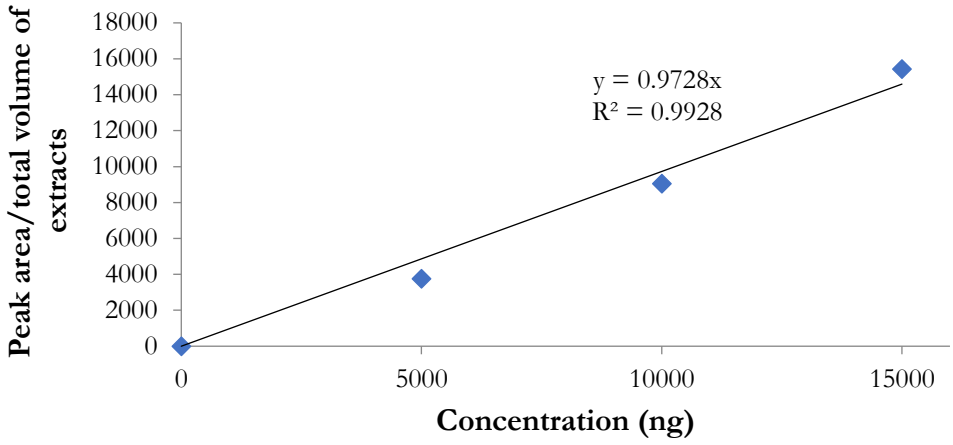

Figure 4.5: An illustrative 4-point method calibration curve for naphthalene to show the possibility of generating a calibration curve based on spiking GW with a known amount of standard.

Table 4.6: Instrument-derived LODs and LOQs of the target PAHs investigated in this study using the method detailed in Section 3.4.3 on the GCxGC-TOF-MS described in Section 3.4.2.

Target PAH	Abbreviation	LOD (ng.µL^{-1})	LOQ (ng.µL^{-1})
Naphthalene	Naph	0.001	0.005
Acenaphthylene	AceY	0.001	0.005
Acenaphthene	AceE	0.004	0.013
Fluorene	FluE	0.004	0.013
Phenanthrene	Phe	0.023	0.075
Anthracene	Anth	0.006	0.019
Fluoranthene	FluA	0.003	0.011
Pyrene	Pyr	0.030	0.099
Naphthalene, 2-bromo-	Naph-2Br	0.011	0.036
Benz[a]anthracene	Benz[a]Ant	0.013	0.044
Chrysene	Chry	0.012	0.040
Benzo[b]fluoranthene	Benzo[b]FluA	0.025	0.083
Benzo[a]pyrene	Benzo[a]Pyr	0.020	0.068
Indeno[1,2,3-cd]pyrene	Indeno[1,2,3-cd]Pyr	0.029	0.097
Benzo[ghi]perylene	Benzo[g,h,i]Per	0.042	0.140
Dibenz[a,h]anthracene	Dibenz[a,h]Anth	0.093	0.311

To then further investigate the real-world applicability and relevance of performing PASE of GW samplers, the LOQs of each of the target analytes were multiplied by the average volumes of extracts 1, 2 and 3. This value was then divided by a set average air sampling volume of 5 L and the units were converted to µg.m^{-3}, as shown in Table 4.7. It is evident that the concentration of the PAHs in the sampled air must be relatively high to effectively apply this extraction method and accurately quantify the target PAH analytes, such as in monitoring emissions produced by household cooking devices (Munyeza et al., 2020). A possible solution to this problem would be blow down the extract in future studies before analysis so as to concentrate the target analytes.

Table 4.7: Minimum PAH concentrations which can be quantified by PASE extraction of the GW sampler, based on LOQs reported in Table 4.6.

	PAH concentration in ambient air (µg.m^{-3})			
PAH analyte	**Extract 1 = 360.39 µL**	**Extract 2 = 689.83 µL**	**Extract 3 = 694.42 µL**	**Total**
Naphthalene	0.33	0.63	0.63	1.59
Acenaphthylene	0.35	0.66	0.67	1.68
Acenaphthene	0.93	1.79	1.80	4.52
Fluorene	0.94	1.79	1.80	4.53
Phenanthrene	5.42	10.37	10.44	26.23
Anthracene	1.35	2.58	2.59	6.52
Fluoranthene	0.79	1.51	1.52	3.82
Pyrene	7.17	13.73	13.82	34.72
Naphthalene, 2-bromo-	2.56	4.91	4.94	12.41
Benz[a]anthracene	3.19	6.10	6.14	15.43
Chrysene	2.90	5.55	5.58	14.03
Benzo[b]fluoranthene	5.97	11.43	11.51	28.91
Benzo[a]pyrene	4.93	9.43	9.49	23.85
Indeno[1,2,3-cd]pyrene	6.98	13.35	13.44	33.77
Benzo[ghi]perylene	10.07	19.27	19.40	48.74
Dibenz[a,h]anthracene	22.41	42.89	43.17	108.47

Once initial optimisations of the PASE procedure for GW samplers were deemed sufficient, reproducibility thereof was investigated. Initial studies started with spiking 400 ng of PAHs onto the GW but after sensitivity issues were experienced with the GCxGC-TOF-MS, the GW samplers were rather spiked with 10 000 ng of the PAH standard (5 µL of 2 000 ppm PAH standard). At these higher spiking concentrations, carryover was observed and can be seen by high extracted masses of PAHs for sampler 3 in Figure 4.6 a), b) and c), and in Table 4.8.

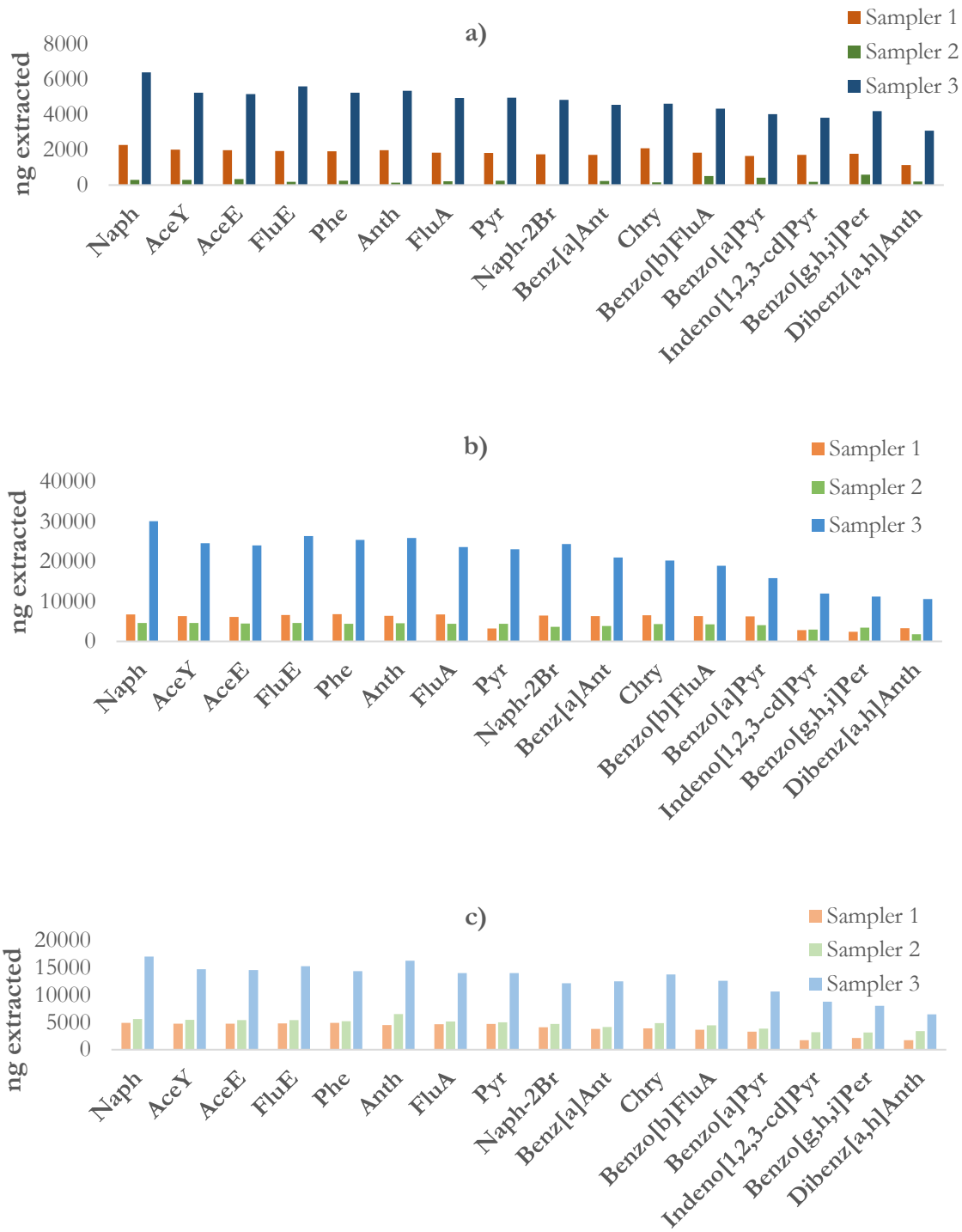

Figure 4.6: Amount of individual PAHs (in ng) extracted by three sequential extractions with PASE of three spiked GW samplers in **a)** extract 1, **b)** extract 2 and **c)** extract 3. *Abbreviations are defined in Table 4.6 and 4.8.*

As a comparison to explore the impact of reuse on results, sampler 3 was re-used whilst samplers 1 and 2 were freshly made and conditioned as described in Section 3.1.1, therefore this effect was avoided in this experiment. However, results showed percent extraction

efficiencies over 100% for most analytes on sampler 1 and some analytes on sampler 2 (Table 4.8). These results were obtained after all volumes were accounted for and the ng extracted in each extract were pooled and divided by the initial amount of 10 000 ng of PAHs spiked onto the sampler. Disproportionate solvent to analyte evaporation is noted as a possible cause of the percent efficiency being > 100% in these cases, as lighter, more volatile PAHs such as naphthalene, showed larger percent extraction efficiencies as compared to heavier PAHs such as dibenz[a,h]anthracene.

Table 4.8: Percent extraction efficiency (% EE) of the sum of 3 sequential extractions using PASE for GW samplers 1, 2 and 3.

PAH	Abbreviation	% EE Sampler 1	% EE Sampler 2	% EE Sampler 3
Naphthalene	Naph	140	106	536
Acenaphthylene	AceY	131	104	446
Acenaphthene	AceE	129	103	439
Fluorene	FluE	134	102	473
Phenanthrene	Phe	137	98	451
Anthracene	Anth	129	112	476
Fluoranthene	FluA	132	98	427
Pyrene	Pyr	98	97	421
Naphthalene, 2-bromo-	Naph-2Br	124	83	415
Benz[a]anthracene	Benz[a]Ant	118	83	381
Chrysene	Chry	126	94	387
Benzo[b]fluoranthene	Benzo[b]FluA	118	92	359
Benzo[a]pyrene	Benzo[a]Pyr	113	84	306
Indeno[1,2,3-cd]pyrene	Indeno[1,2,3-cd]Pyr	63	63	246
Benzo[ghi]perylene	Benzo[g,h,i]Per	64	72	235
Dibenz[a,h]anthracene	Dibenz[a,h]Anth	62	54	202

However, even though sampler 3 did show far higher percent extraction efficiencies due to carry over from previous PASE studies utilising that sampler, the trend remained more or less the same between samplers 1 and 3 with a difference in the results for sampler 2 as observed by Figure 4.7. The variation between samplers 1 and 2, as shown by Figure 4.7 a) and b), respectively, may be due to non-uniformity in the graphene layers are grown on the QW, which is further discussed in Section 4.4. In sampler 1, the graphene layers of the GW may have been thinner than in sampler 2. This would then lead to the GW in sampler 2

adsorbing the analytes more strongly, causing a lower extraction efficiency in the first extraction as shown in Figure 4.7 b). This possible variation in the GW needs to be addressed before widespread application of the GW sampler can be embarked on.

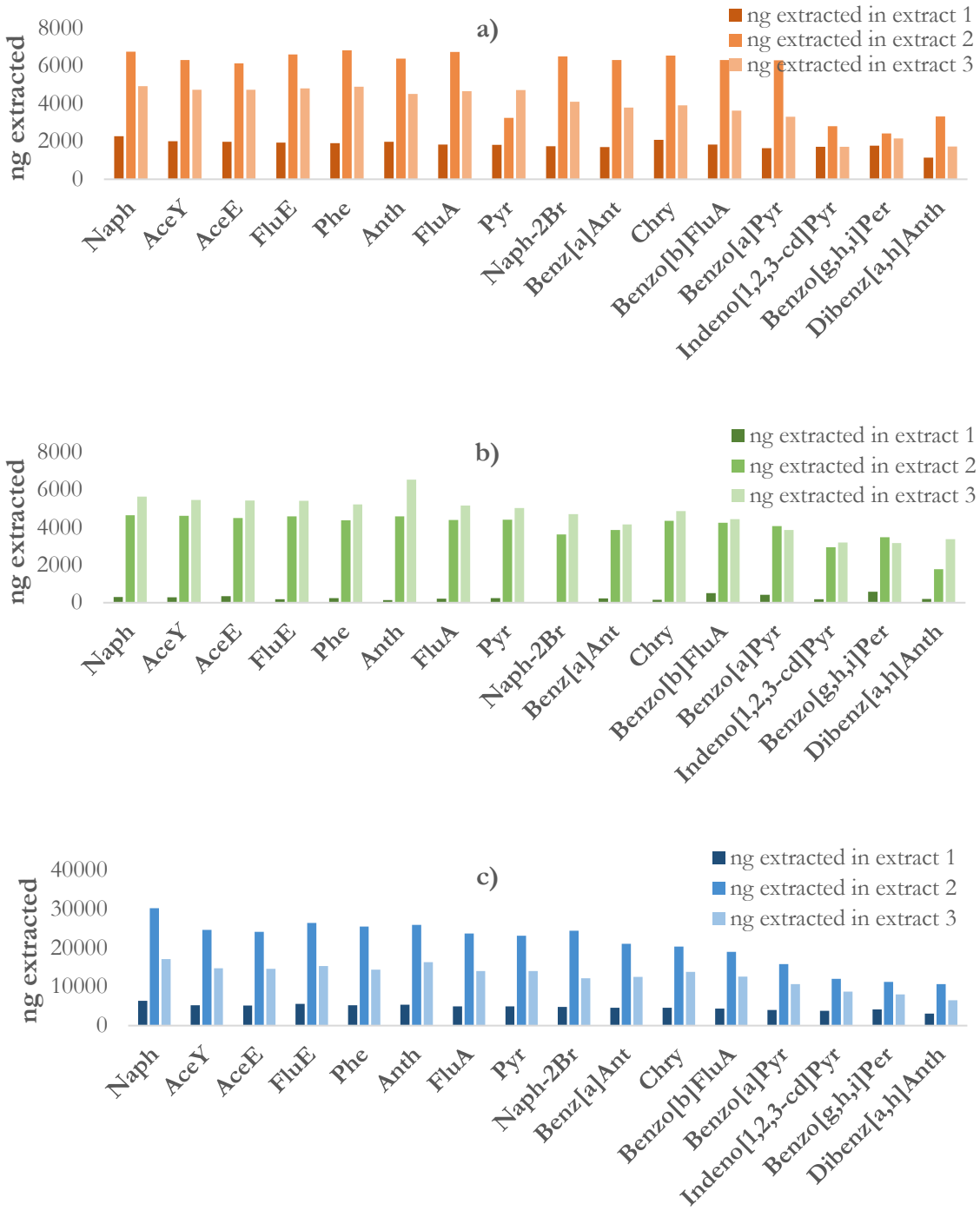

Figure 4.7: Amount of PAHs (in ng) in three sequential PASE extractions of GW samplers **a)** 1, **b)** 2 and **c)** 3.

From Figure 4.7, it can be noted that there is a large concentration of all of the analytes still present in the third PASE extract. This is undesirable as a liquid extraction technique would be preferentially able to extract the bulk of the analytes in the first extraction so as to not use more solvent than necessary and further dilute the sample before analysis. To investigate a possible optimisation in this regard, an 8 hr PASE extraction was applied to the GW sampler.

4.3.2 8 hr PASE using hexane

After a fresh GW sampler was spiked with 400 ng of the PAH mix (400 ng of each PAH), the sorbent was soaked with the solvent (hexane) for 8 hrs as described in Section 3.4.7. Thereafter, the same PASE procedure was used as what was applied Section 4.3.1 except additional PASE extractions were conducted to investigate how many extractions were required before analytes were below the LOD in the extracts. Figure 4.8 shows five extractions were required to extract the PAHs after the sorbent was soaked in hexane for 8 hrs prior to extraction.

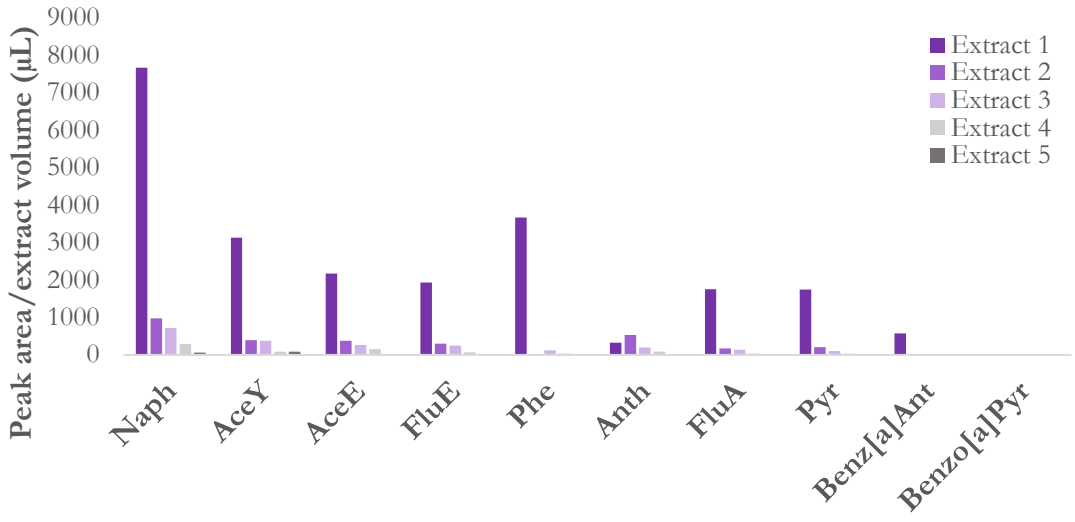

Figure 4.8: Amount of PAHs extracted (Peak area/extract volume (µL)) per sequential PASE extract conducted after the 8 hr soak with hexane.

It is noted however that, with the exception of acenaphthene (AceE) and anthracene (Anth), extracts 4 and 5 yielded < 4% of the analytes which were detected in extract 1. Analytes heavier than benzo[a]pyrene (Benzo[a]pyr) were, however, undetected. This optimisation of PASE is very promising as most of the analytes were extracted in the first extract, therefore solvent soaking prior to PASE extraction of PAHs from GW samplers is recommended. The actual soaking time required to achieve good extraction requires optimisation to possibly

reduce the time required. An additional consideration for the optimisation of PASE for the GW sampler is using different solvents which is addressed at the end of Section 4.3.3.

4.3.3 Thermal desorption efficiency

Since TD of samplers is seen to be ideal in terms of the simplicity and ease of the method in most cases, which requires no form of solvent extraction, it was of interest to investigate the efficiency of TD for the extraction of PAHs from the GW sampler as compared to TD from an empty glass sampler tube, using the TD-GCxGC-TOF-MS method detailed in Section 3.4.8. As can be seen in Figure 4.9 and Table 4.9, lighter PAHs such as naphthalene had an excellent percent recovery of ± 97%, although naphthalene had the highest % RSD likely due to volatilisation losses. However, the percent recovery of the PAHs decreased as the molecular mass of the PAHs increased. The thermal desorption program was set to 280 °C whereas the maximum temperature of the specific thermal desorber used is 300 °C, therefore it is predicted that increasing the TD temperature by 20 °C will not greatly improve the percent recovery of the heavier compounds, which is likely due to these analytes adsorbing strongly to the GW adsorbent and their low vapour pressures. Good TD efficiencies have been previously reported for the TD of PAHs from PDMS samplers, ranging from 66 - 93% recovery (Munyeza et al., 2018). Retention of analytes is achieved by strong adsorptive processes in the case of GW, whilst more easily reversible absorption occurs with PDMS.

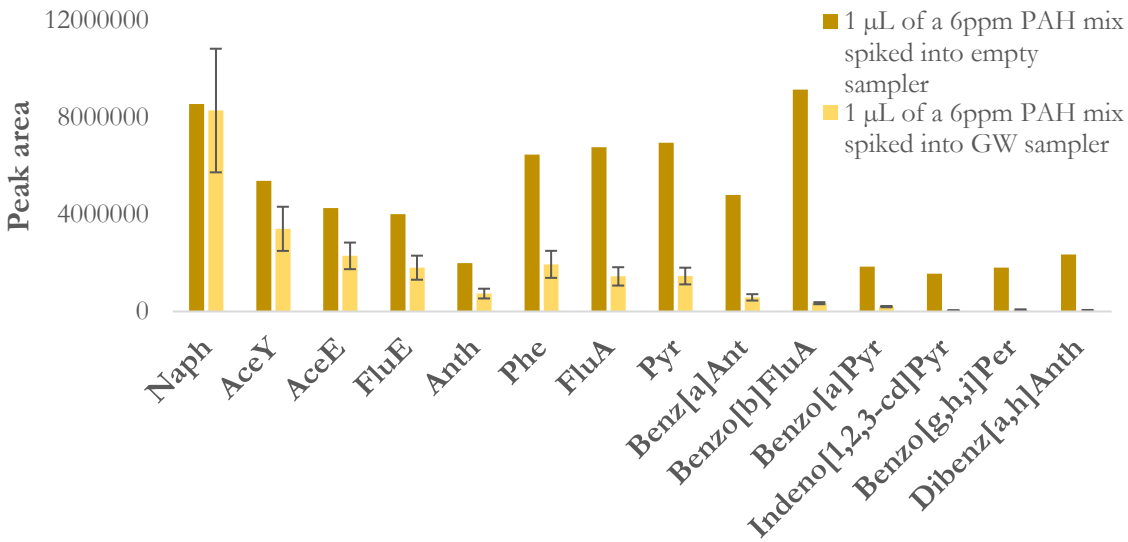

Figure 4.9: Comparative peak areas of PAHs extracted by TD of GW samplers (*N*=3) as compared to peak areas of PAHs extracted from TD of an empty sampler spiked with PAHs.

Table 4.9: The extraction efficiency calculated for the TD of selected PAHs from GW samplers (*N*=3).

PAH	Abbr.	Molecular mass	% RSD	% Recovery
Naphthalene	Naph	128	30.76	97
Acenaphthylene	AceY	152	26.71	63
Acenaphthene	AceE	154	23.92	54
Fluorene	FluE	166	27.46	45
Anthracene	Anth	178	27.15	37
Phenanthrene	Phe	178	28.68	30
Fluoranthene	FluA	202	26.14	21
Pyrene	Pyr	202	23.56	21
Benz[a]anthracene	Benz[a]Ant	228	22.58	12
Benzo[b]fluoranthene	Benzo[b]FluA	252	21.86	3.8
Benzo[a]pyrene	Benzo[a]Pyr	252	12.24	11
Indeno[1,2,3-cd]pyrene	Indeno[1,2,3-cd]Pyr	276	12.86	2.2
Benzo[g,h,i]perylene	Benzo[g,h,i]Per	276	62.64	3.2
Dibenz[a,h]anthracene	Dibenz[a,h]Anth	278	52.82	1.8

As a result of the TD proving inadequate, with low percent recoveries recorded for the TD of heavier PAHs from GW samplers, it may be of use to test various other solvents for the analysis of SVOCs sampled onto GW samplers using the PASE method to optimise recoveries of the heavier PAH analytes. Possible solvents to investigate include CS_2 and acetonitrile as recommended by Supelco (1986) for Carbotrap adsorbents.

4.4 Intra- and inter- variability of selected analytes on the GW sampler

In the previous section, GW sampler TD efficiencies focused on PAHs. In this section TD of a wider volatility range of analytes from GW was investigated. Therefore, further investigations were conducted into the consistency of the TD of analytes from the GW sampler, as a means of better understanding variabilities in re-use of a GW sampler as well as variability between GW samplers, VOCs and SVOCs (specifically PAHs and HCs) were thermally desorbed as per the methods described in Sections 3.5.2 and 3.5.3, respectively. Due to the high vapour pressure of the VOCs which could lead to losses, the peak areas of these analytes were divided by the area of the internal standard, d8-naphthalene, (the peak area ratios were recorded and presented in Figures 4.10 and 4.11), whilst the reproducibility

of the PAHs and HCs were quantified without the use of an internal standard. It should be noted that some of the peak areas of the analytes with similar molecular masses and fragmentation patterns were added (such as the xylene isomers and trimethylbenzene isomers in Figure 4.10 and 4.11) as no individual standards were available to distinguish these analytes based on their retention times.

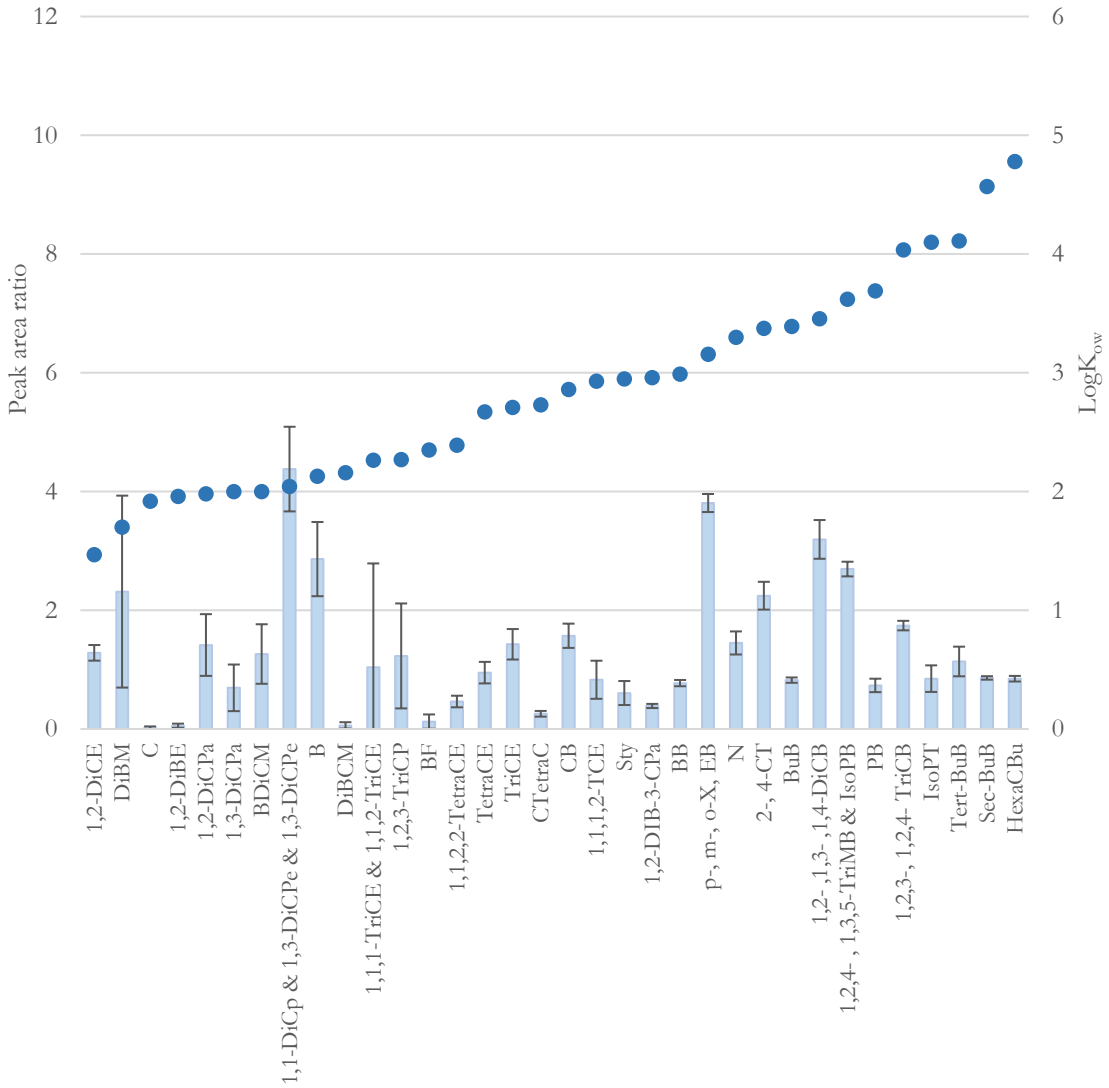

Figure 4.10: Intra-sampler variability of VOCs when spiked onto a GW sampler and analysed by TD-GCxGC-MS. The bar graphs correspond to the left y-axis which denotes the ratio of analyte peak area/ peak area of d8-naphthalene, whilst the circular data points correspond to the right y-axis which denotes $LogK_{ow}$ values. *The error bars are based on the SD between sampler runs with N=4. Abbreviations are defined in Table 4.10.*

In Figures 4.10 and 4.11, the VOCs are arranged in order of their $LogK_{ow}$, increasing from left to right. The HCs are arranged in order of their molecular masses, increasing from left

to right in Figures 4.12 and 4.13. PAHs, as shown in Figures 4.14 and 4.15, are arranged in order of their molecular masses, increasing from left to right, similarly to the HCs. The % RSDs are stated in Table 4.10 for both the intra- and inter-sampler variability analysis.

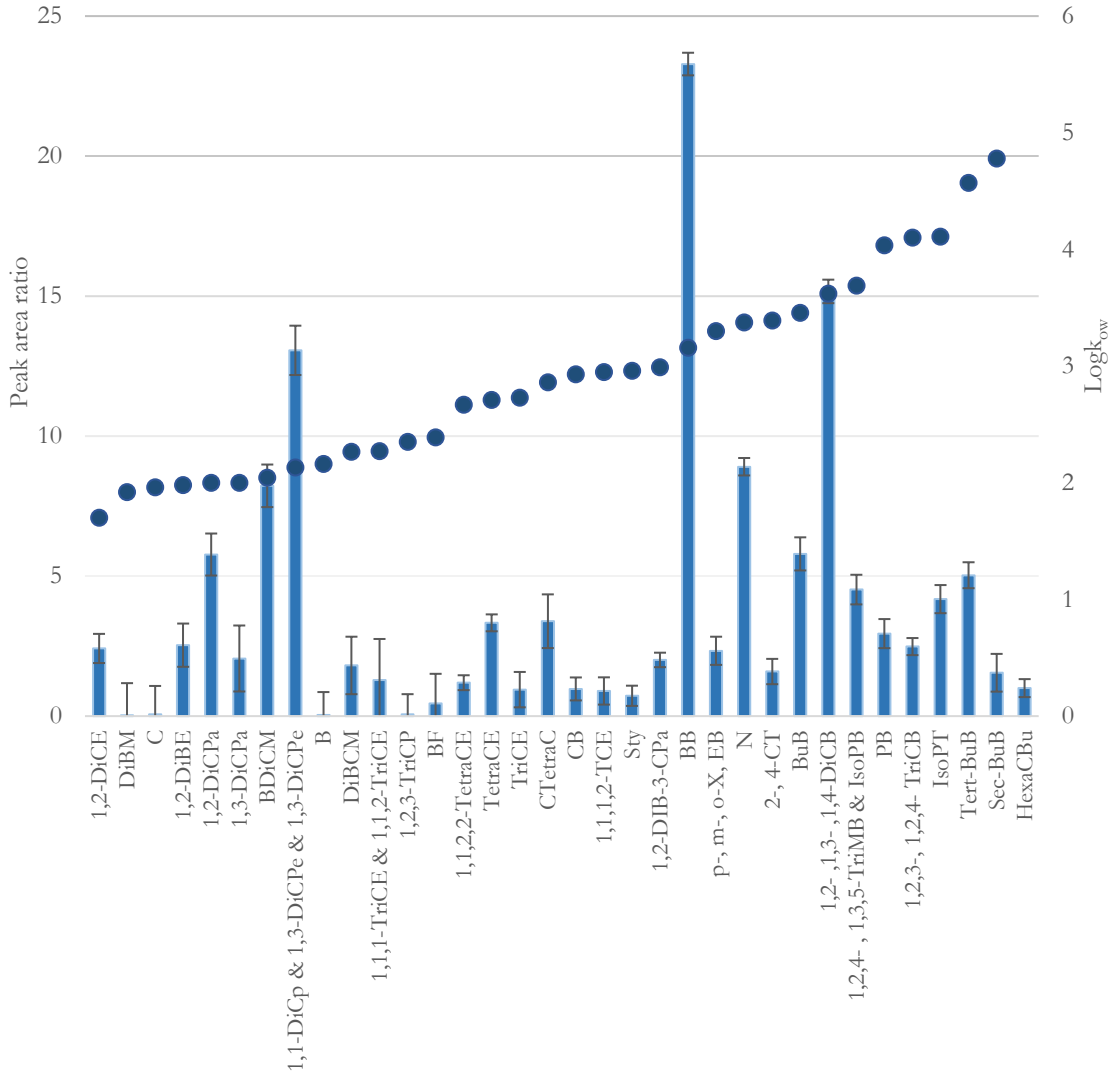

Figure 4.11: Inter-sampler variability of VOCs when spiked onto different graphene wool samplers. The bar graphs correspond to the left y-axis which denotes the ratio of analyte peak area/ peak area of d8-naphthalene, whilst the circular data points correspond to the right y-axis which denotes LogK$_{ow}$ values. *The error bars are based on the SD between samplers with N=4. Abbreviations are defined in Table 4.10.*

From Figure 4.10 and Table 4.10, it can be seen that there was generally a greater variability in the peak areas of analytes with lower LogK$_{ow}$ values. This is most likely due to volatilisation losses whilst spiking the sampler and may also be due to how these polar analytes interact with the non-polar GW sorbent. Overall, 15 and 14 of the 34 analyte groups had % RSDs <

20% in terms of intra- and inter-sampler variability, respectively. However, benzene was quantified with < 30% RSD which has been previously accepted by the European Union (European Union, 2000). The inter-trap variability was very good as seen in Figure 4.13, however a lack of uniformity in the graphene layers in the GW batches could have contributed to higher variations with respect to the remaining analytes.

Table 4.10: % RSDs for the intra- and inter-sampler variability of TD of VOCs from the GW samplers (*N*=4).

VOC	Abbreviation	% RSD of intra-sampler	% RSD of inter-sampler
1,2-Dichloroethane	1,2-DiCE	10	8.5
Dibromomethane	DiBM	70	47
Chloroform	C	116	2935
1,2-Dibromoethane	1,2-DiBE	64	1181
1,2-Dichloropropane	1,2-DiCPa	37	30
1,3-Dichloropropane	1,3-DiCPa	57	20
Bromodichloromethane	BDiCM	40	37
1,1-Dichloropropene & cis-1,3-Dichloropropene & trans-1,3-Dichloropropene	1,1-DiCp & 1,3-DiCPe & 1,3-DiCPe	16	11
Benzene	B	22	6.2
Dibromochloromethane	DiBCM	88	2250
1,1,1-Trichloroethane & 1,1,2-Trichloroethane	1,1,1-TriCE & 1,1,2-TriCE	168	81
1,2,3-Trichloropropane	1,2,3-TriCP	72	56
Bromoform	BF	96	1615
1,1,2,2-Tetrachloroethane	1,1,2,2-TetraCE	21	59
Tetrachloroethene	TetraCE	19	25
Trichloroethene	TriCE	18	19
Carbon tetrachloride	CTetraC	19	101
Chlorobenzene	CB	13	12
1,1,1,2-Tetrachloroethane	1,1,1,2-TCE	39	50
Styrene	Sty	33	40
1,2-Dibromo-3-chloropropane	1,2-DIB-3-CPa	9.1	36
Bromobenzene	BB	6.8	20
p-Xylene, m-Xylene and o-Xylene & ethylbenzene	p-, m-, o-X, EB	4.0	2.2
Naphthalene	N	13	13
2-Chlorotoluene and 4-Chlorotoluene	2-, 4-CT	10	5.1
n-Butylbenzene	BuB	5.5	37
1,2-Dichlorobenzene & 1,3-Dichlorobenzene & 1,4-Dichlorobenzene	1,2- ,1,3- ,1,4-DiCB	10	7.3

1,2,4-Trimethylbenzene & 1,3,5-Trimethylbenzene & Isopropylbenzene (Cumene)	1,2,4- , 1,3,5-TriMB & IsoPB	4.6	3.5
n-Propylbenzene	PB	15	11
1,2,3-Trichlorobenzene & 1,2,4-Trichlorobenzene	1,2,3-, 1,2,4-TriCB	4.6	10
p-Isopropyltoluene (p-Cymene)	IsoPT	26	20
tert-Butylbenzene	Tert-BuB	22	11
sec-Butylbenzene	Sec-BuB	3.4	13
Hexachlorobutadiene	HexaCBu	5.6	21

The HCs were detected by selectively extracting m/z 57 as shown in Figure 4.12, which shows excellent separation of the target analytes. The intra-sampler variability for TD of HCs spiked onto GW samplers, as seen in Figure 4.13, showed an increasing variability as the HCs increased in size from C_{12} - C_{20}. In terms of the inter-sampler variability, there was large variation observed for C_{14} - C_{16} HCs (Figure 4.14).

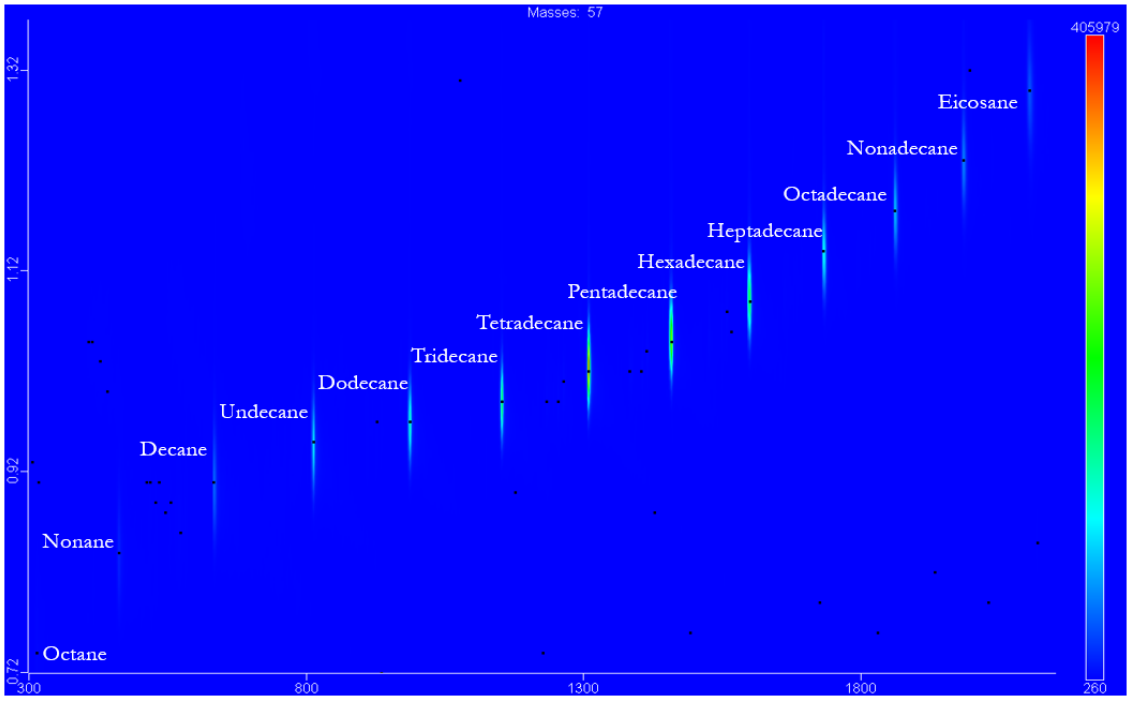

Figure 4.12: Extracted 2D ion TD-GCxGC-TOF-MS chromatogram of hydrocarbons (C_8 - C_{20}) for m/z 57.

The % RSDs for the HCs may be found in Table 4.11. The variability in this group of compounds may be due to variations in the GW. Additionally, heavier HCs may exhibit a similar trend to that of the PAHs in Section 4.3.3; the heavier HCs may be incompletely desorbed. Overall, 6 and 0 of the 12 HC analytes had % RSDs < 20% in terms of intra- and inter-sampler variability, respectively.

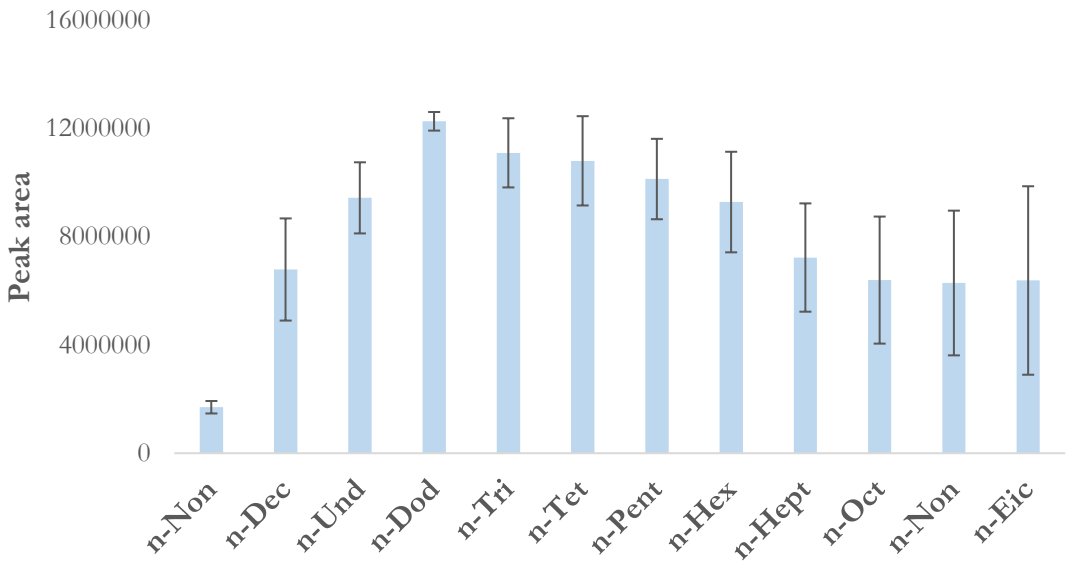

Figure 4.13: Intra-sampler variability of hydrocarbons (C_8 - C_{20}) when thermally desorbed from a GW sampler. *The error bars are based on the SD between sampler runs with N=3.*

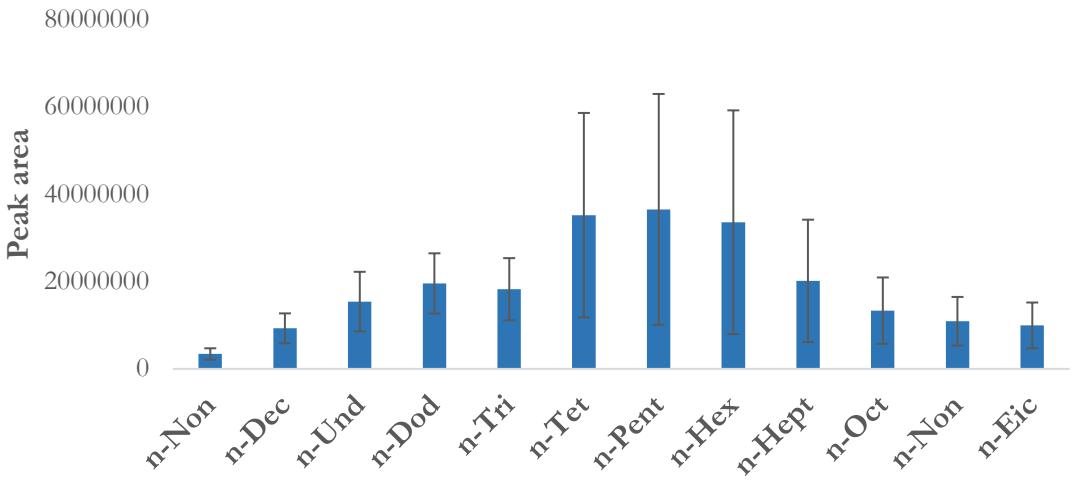

Figure 4.14: Inter-sampler variability of hydrocarbons (C_8 - C_{20}) when thermally desorbed from a GW sampler. *The error bars are based on the SD between samplers with N=3.*

Table 4.11: % RSDs for the intra- and inter-sampler variability of TD of HCs from the GW samplers (*N*=3).

HC	Abbreviation	% RSD of intra-sampler	% RSD of inter-sampler
n-Nonane	n-Non	14	38
n-Decane	n-Dec	28	37
n-Undecane	n-Und	14	44

n-Dodecane	n-Dod	2.8	35
n-Tridecane	n-Tri	12	39
n-Tetradecane	n-Tet	15	66
n-Pentadecane	n-Pent	15	72
n-Hexadecane	n-Hex	20	76
n-Heptadecane	n-Hept	28	69
n-Octadecane	n-Oct	37	57
n-Nonadecane	n-Non	43	51
n-Eicosane	n-Eic	55	53

In the case of the PAHs, the intra- (Figure 4.15) and inter-sampler (Figure 4.16) variability profiles of these analytes were the most similar in terms of the groups of compounds studied. The % RSD values for these compounds (Table 4.12) are generally of a similar magnitude for intra- and inter-sampler studies respectively, compared to the other compound classes. This could be due to these compounds containing aromatic structures with delocalised pi electrons which would interact and bind with the graphene layer in the GW sorbent through pi-pi interactions in a reproducible manner.

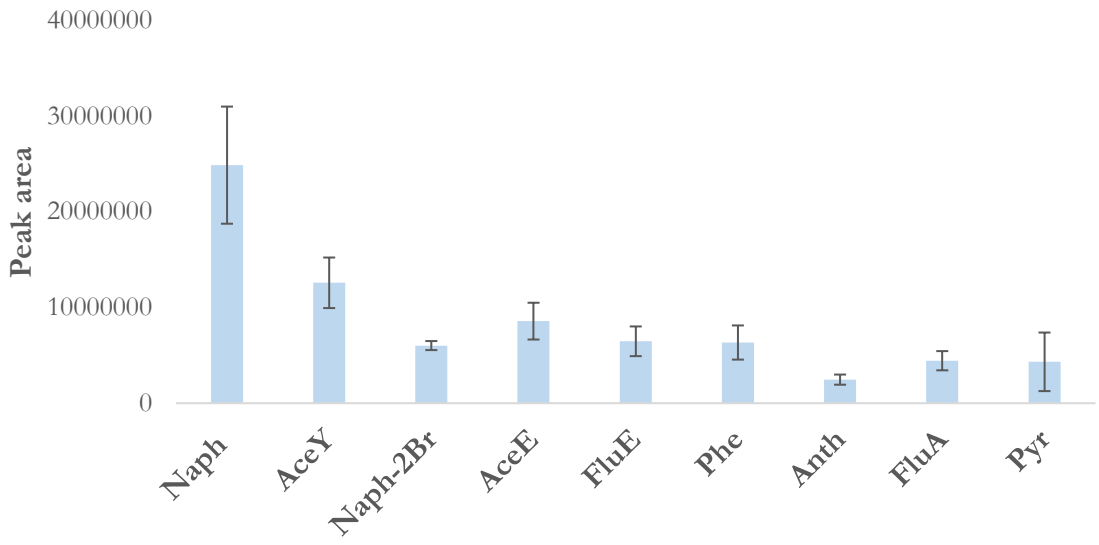

Figure 4.15: Intra-sampler variability of PAHs when thermally desorbed from a GW sampler. *The error bars are based on the SD between sampler runs with N=3.*

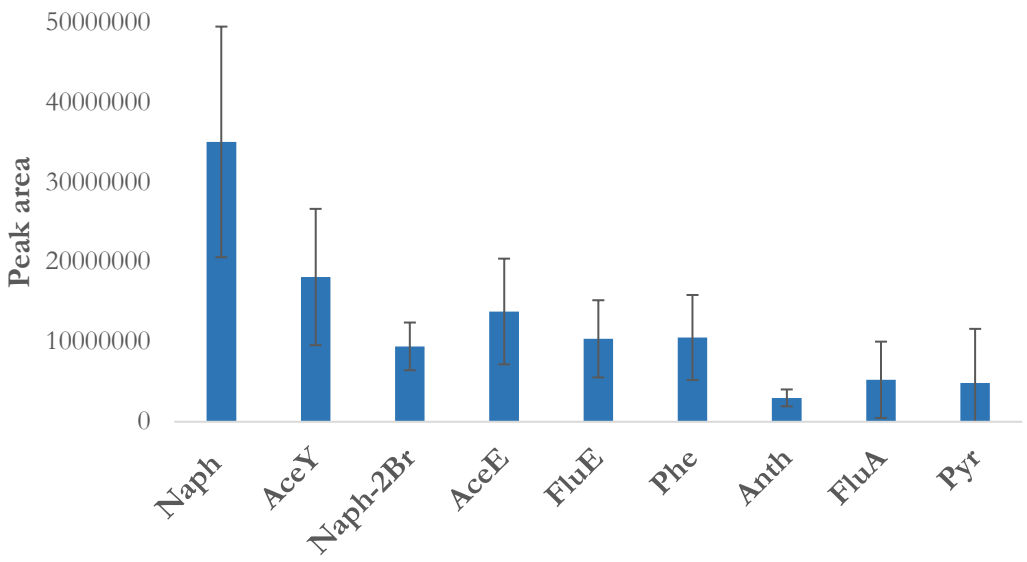

Figure 4.16: Inter-sampler variability of PAHs when thermally desorbed from a GW sampler. *The error bars are based on the SD between samplers with N=3.*

Table 4.12: % RSDs for the intra- and inter-sampler variability of TD of PAHs from the GW samplers (*N*=3).

PAH	Abbreviation	% RSD of intra-sampler	% RSD of inter-sampler
Naphthalene	Naph	25	41
Acenaphthylene	AceY	21	47
2-Bromo-napthalene	Naph-2Br	7.9	32
Acenaphthene	AceE	22	48
Fluorene	FluE	24	47
Phenanthrene	Phe	28	50
Anthracene	Anth	21	35
Fluoranthene	FluA	23	91
Pyrene	Pyr	71	139

It is noted that the inter-sampler variability upon TD analysis of the PAH spiked samplers is larger than the intra-sampler variability, as expected. The increase in the variability upon inter-sampler spiking and subsequent analysis could further support the need to optimise the uniformity of the graphene layers in the GW sampler, as the adsorption of compounds may be sensitive to how evenly the graphene is grown on the QW substrate and subsequently how the GW is assembled as a GW sampler. This was further investigated by TEM analysis.

To investigate the graphene layering grown on the QW in the GW material, TEM was used to take images of the GW fibres. Figure 4.17 a) shows the multi-layered nature of the

graphene grown on the QW with 3 - 5 layers present as stated by Schoonraad et al. (2020). However, Figure 4.17 b) shows a QW fibre with barely any graphene grown on the surface. Both of the images shown in Figure 4.17 were taken of the same batch of GW, which shows an inconsistency in the uniformity of the graphene layers which would not only increase the hydrophilicity of the GW material but also decrease the potential surface area of the GW material for adsorption of target analytes, reducing the breakthrough volume. The synthesis of the GW layers should therefore be further optimised to ensure that the graphene layers are grown more uniformly on the QW substrate fibres to improve reproducibility of GW samplers in use.

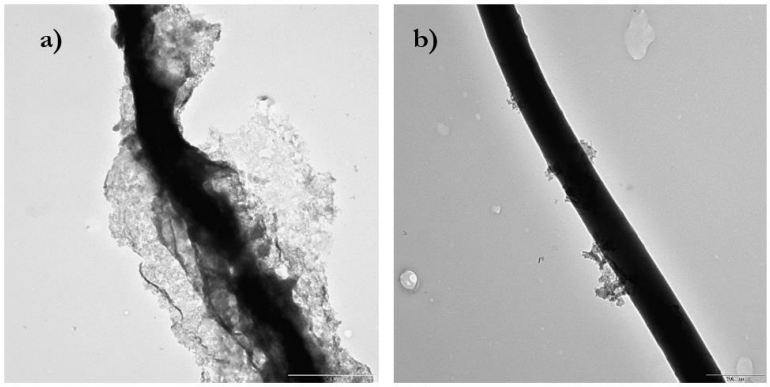

Figure 4.17: TEM images showing **a)** multi-layering of the graphene on a QW fibre alongside the **b)** lack of graphene layering on a different QW fibre from the same GW batch.

4.5 Sampler tube retention volumes for individual analytes

The RVs of GW, PDMS and QW samplers for nine analytes with varying BPs and polarities were investigated so as to better understand the adsorption capacity of the GW sampler, as compared to the QW substrate from which the GW was made and the PDMS sampler which has been used in multiple air quality studies (for example Munyeza et al., 2019 and 2018; Forbes et al., 2012). To achieve this aim, the samplers were sequentially fitted in place between two uncoated capillaries in a GC oven in order for each of the samplers to act as the stationary phase with which the vaporized injected analytes would interact. After leak checks, the FID chromatograms were produced by injecting 1 µL of the following nine analytes into the GC injection port at 250 °C; methanol (BP 64.7 °C), hexane (BP 68.7 °C), propanol-2-ol (BP 82.3 °C), toluene (BP 110.6 °C), butan-1-ol (BP 117.7 °C), octane (BP 125.6 °C), cyclohexanone (BP 155.4 °C), dodecane (BP 216.3 °C) and hexadecane (BP 286.8 °C). Over 430 manual injections were performed for this study. The GC column oven

temperature operated isothermally at set temperatures for each duplicate experimental run, thereafter the temperature was increased in subsequent runs by suitable increments (between 5 - 20 °C) until a satisfactory Gaussian peak was observed on the chromatogram. The set temperatures ranged between 25 - 190 °C for GW, 25 - 200 °C for QW and 25 - 340 °C for PDMS. The PDMS sampler required many of the analytes to be run at higher isothermal temperatures with larger increments between runs than for the GW and QW samplers due to the analyte retention observed for the PDMS sampler at lower temperatures.

Figure 4.18 shows overlaid chromatograms acquired for the different samplers for methanol at 25 °C. The retention time (RT) used for the calculation of the breakthrough volume for selected samplers was taken as the average time at which the maximum signal for the particular analyte occurred for the duplicate injection of that analyte at a particular isothermal temperature for the GC-FID run. For example, in Figure 4.18 the retention times for the empty tube, the QW sampler, the GW sampler and the PDMS sampler were 0.36, 0.37, 0.43 and 0.82 min, respectively.

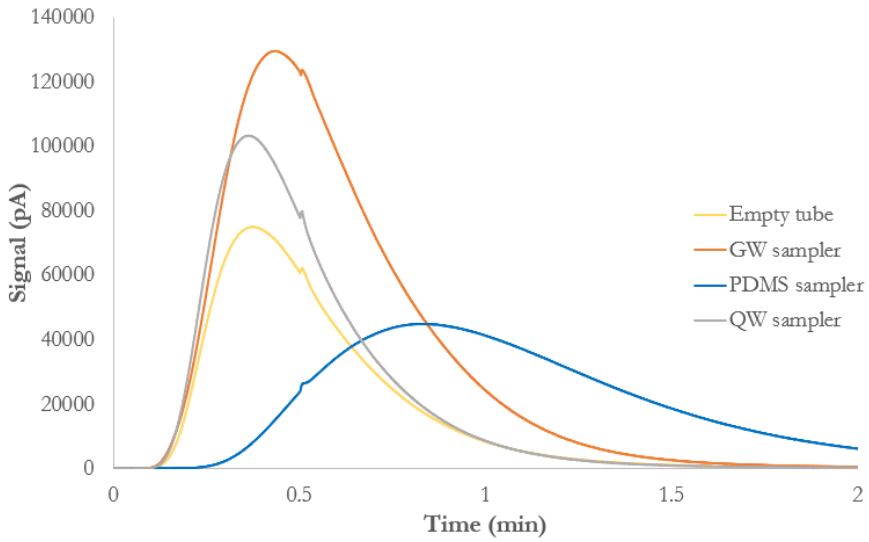

Figure 4.18: Overlaid chromatograms illustrating the differing retention times and peak areas of 1 µL of methanol which was run isothermally at 25 °C for the sorbents used in the breakthrough study.

The purpose of injecting the empty tube with the analytes of interest at various isothermal temperatures was to compare the peak areas obtained to that of the GW, QW and PDMS samplers to determine whether complete desorption occurred from the sorbents. Once the chromatograms were overlaid (Figure 4.18) and the recorded peak areas of the methanol injected isothermally at 25 °C onto different samplers were compared (Table 4.13), it was

noted that the peak area recorded for the GW sampler repeatedly differed to the peak areas obtained for the other samplers. This may indicate that methanol might be causing some of the graphene to detach from the QW and thus cause the FID to give larger peak area responses in the case of the methanol injection. Other deviations in peak area may be as a result of discrepancies in the manual injection of the analytes.

Table 4.13: Recorded peak areas resulting from the direct injection of 1 µL of methanol (with the GC oven set to an isothermal temperature of 25 °C) through an empty, QW, GW and PDMS sampler. *N=1 for the samplers with N=2 for injections.*

Sampler	Peak area			
	1st injection (x 100 000)	2nd injection (x 100 000)	Average ± SD	% RSD
Empty Tube	20.59	21.01	20.80 ± 0.30	1.5
GW	41.92	41.12	41.52 ± 0.56	1.4
QW	28.46	25.09	26.78 ± 2.38	8.9
PDMS	27.26	27.52	27.39 ± 0.18	0.66

Subsequently, the chromatograms of another analyte, specifically hexane, at 25 °C were overlaid (Figure 4.19), and the peak areas were compared (Table 4.14) and it was found that the peak areas were reasonably similar for this analyte. A lower peak area was found for the PDMS sampler than for the empty tube which indicates that the PDMS sampler showed partial retention of hexane under these conditions. Due to technological issues relating to the software, the peak areas of the other analytes at the various isothermal temperatures could not be further investigated, however this result may require further investigation to determine how the GW material interacts with polar versus non-polar solvents and whether breakdown of the material indeed takes place when in contact with certain solvents.

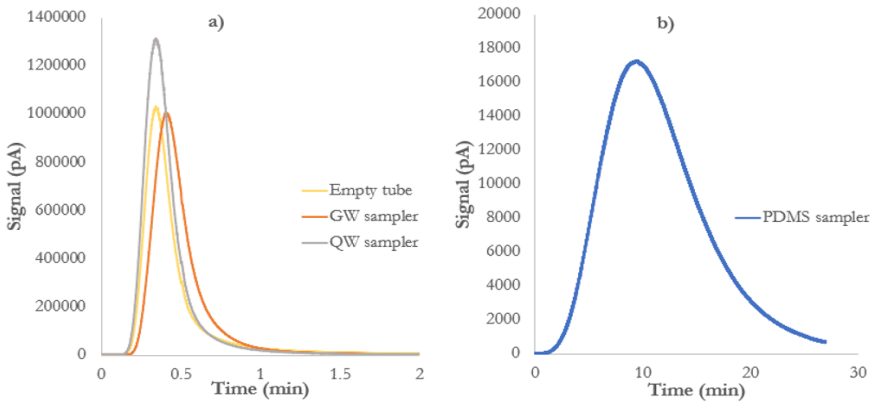

Figure 4.19: Overlaid chromatograms illustrating the differing retention times and peak areas of hexane at 25 °C for samplers used in the breakthrough study.

Table 4.14: Recorded peak areas resulting from the direct injection of 1 µL of hexane (with the GC oven set to an isothermal temperature of 25 °C) through an empty, QW, GW and PDMS sampler. *N=1 for the samplers with N=2 for injections.*

Sampler	Peak area			
	1st injection (x 100000)	2nd injection (x 100000)	Average ± SD	% RSD
Empty Tube	159.07	133.09	146.08 ± 18.37	13
GW	168.92	163.96	166.44 ± 3.51	2.1
QW	179.24	180.97	180.10 ± 1.22	0.68
PDMS	108.01	107.02	107.51 ± 0.70	0.65

Once the retention times (RTs) were acquired and the carrier gas flow rate was set to 10 $mL.min^{-1}$, Equation 14 was then used to calculate the RVs for the GW, QW and PDMS samplers at 25 °C for each analyte and the results are presented in Table 4.15. Correction for dead volume was not done as this requires the injection of a non-retained analyte into the GC port and typical non-retained analytes, such as methane, have been found to be adsorbed by graphene (Zhu and Zheng, 2016), as previously stated in Section 3.6.

$$BV = \frac{(RT\ x\ Flow)}{Wa\ x\ 1000\ mL.L^{-1}} \quad \ldots \text{Eq 14}$$

BV - Breakthrough volume ($L.g^{-1}$)
RT - Retention time of analyte (min)
Flow - Carrier gas flow ($mL.min^{-1}$)
Wa - Weight of sorbent resin (g)
1000 mL/L - Conversion factor to convert data from $mL.g^{-1}$ to $L.g^{-1}$

Subsequently, an alternative breakthrough study could be conducted with a second downstream GW sampler, which would aid in the validation of the retention volumes determined in here at set pressures and temperatures. The sorbent weight of the GW, QW and PDMS samplers were 0.1410 g, 0.1200 g and 0.3657 g, respectively. Shown in Tables F1 - 3 in Appendix F are the RT values from which the RV curves in Figure 4.20 and 4.21 were plotted.

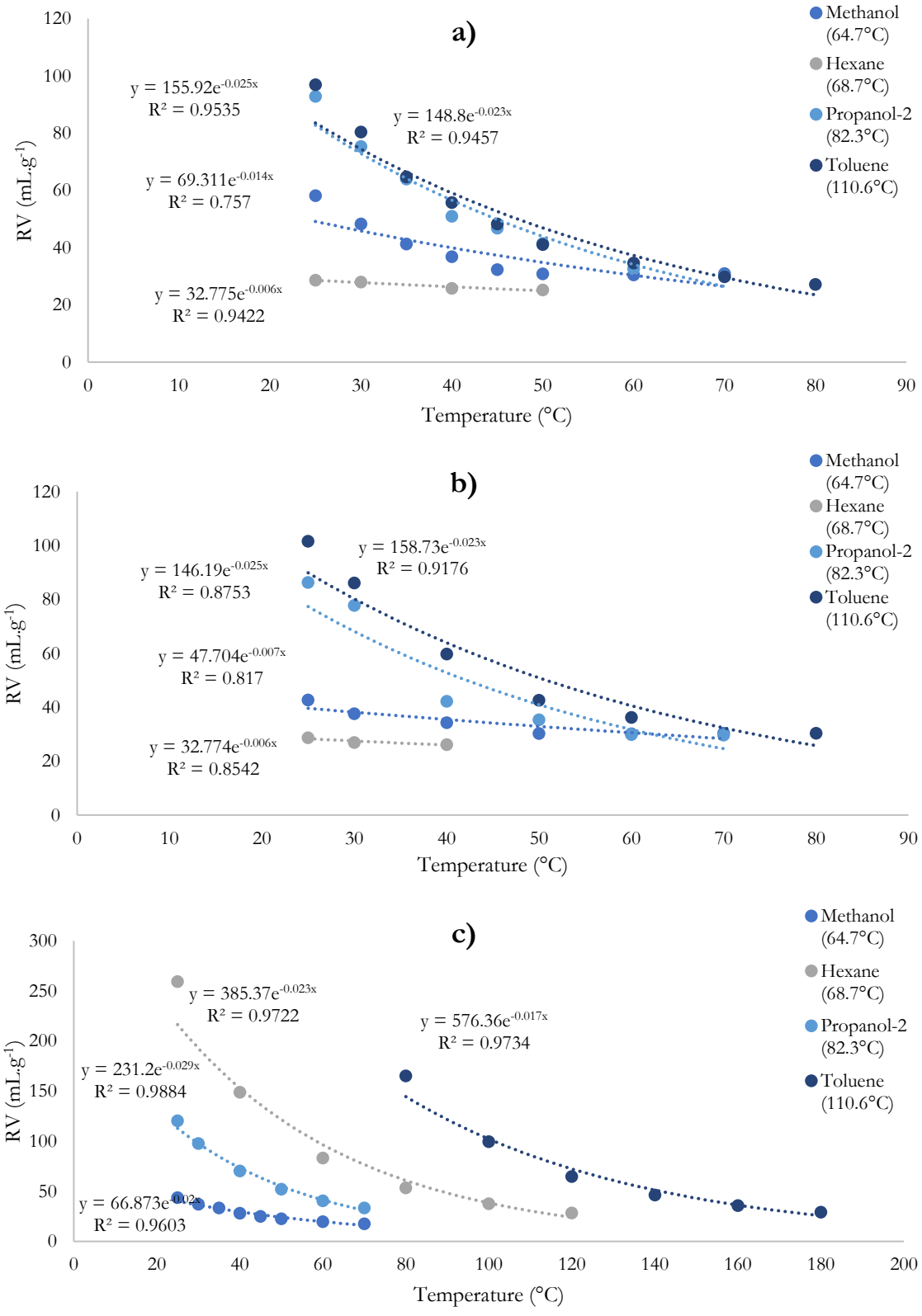

Figure 4.20: Retention volume curves for the lower BP analytes (BP in brackets under corresponding analyte) when injected onto **a)** GW, **b)** QW and **c)** PDMS samplers in the breakthrough volume set-up at various isothermal temperatures.

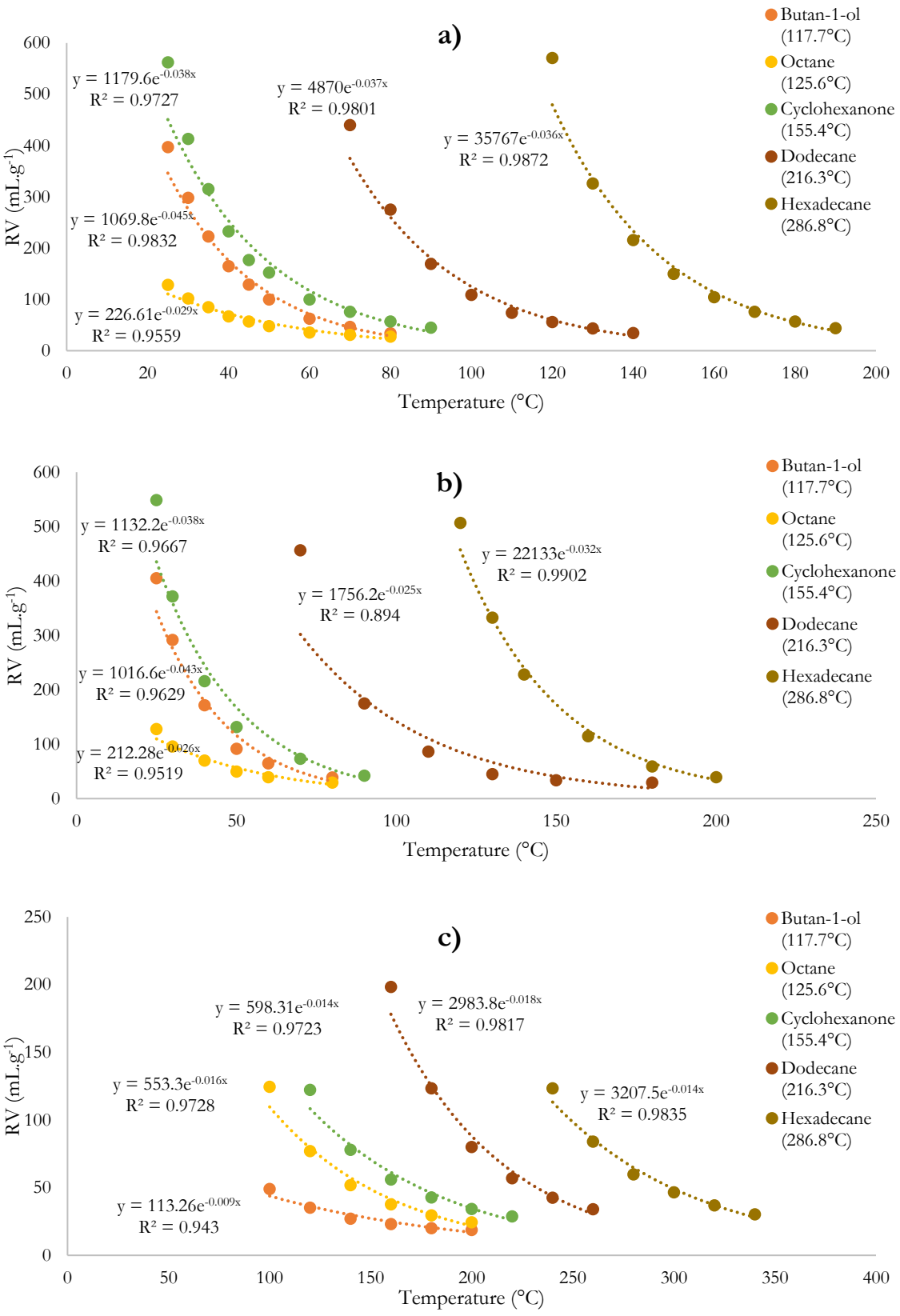

Figure 4.21: Retention volume curves for the higher BP analytes (BP in brackets under corresponding analyte) when injected onto **a)** GW, **b)** QW and **c)** PDMS samplers in the breakthrough volume set-up at various isothermal temperatures.

The exponential equations derived from the RV curves can be found in Table F4 in Appendix F. As can be seen from Table F5 in Appendix F, all of the R^2 values were above 0.75 with all but four R^2 values being above 0.90, which allows for their extrapolation to 25 °C. This allows for the breakthrough volumes at ambient sampling temperatures (25 °C) to be determined for analytes for which this could not be measured experimentally due to retention by sorbents at this temperature. Therefore, the exponential equations derived from the curves in Figures 4.20 and 4.21 were used to calculate some of the RV values presented in Table 4.15. These calculated values are distinguished from the experimentally determined values by a superscript "#". This difference in the source of the data included in Table 4.15 has to be kept in mind when comparing the data, especially for a particular analyte across the different samplers.

Table 4.15: RVs of QW, GW and PDMS samplers for a range of analytes along with their boiling points, molecular masses and densities at 25 °C. ***Source:** adapted from (PubChem, 2020). Calculated values are distinguished from the experimentally determined values by "#".*

Analyte with corresponding BP*	RV at 25 °C (mL. g^{-1})			Polarity* expressed as $LogK_{ow}$	MM of analyte (g.mol^{-1})	Density* at 25 °C (g.L^{-1})
	GW	QW	PDMS			
Polar analytes						
Methanol (64.7°C)	58	43	44	-0.77	32	0.75
Propanol-2 (82.3°C)	93	86	120	0.05	60	0.79
Butan-1-ol (117.7°C)	397	405	168#	0.88	74	0.81
Cyclohexanone (155.4°C)	563	549	227#	0.81	98	0.94
Non-polar analytes						
Hexane (68.7°C)	29	29	259	3.90	86	0.66
Toluene (110.6°C)	97	102	185#	2.73	92	0.86
Octane (125.6°C)	129	128	194#	5.18	114	0.70
Dodecane (216.3°C)	142#	170#	266#	6.10	170	0.75
Hexadecane (286.8°C)	202#	212#	347#	8.20	226	0.77

In a real-world application, the RVs shown in Table 4.15 are low considering that the GW sampler has been optimised for ± 0.120 g of sorbent per sampler whilst the PDMS has been optimised for ± 0.365 g of sorbent per sampler. Thus, if cyclohexanone was, for example, sampled by the GW sampler at 500 mL.min^{-1}, breakthrough would theoretically occur within

8 s of sampling. Therefore, before real-world application may be explored, it would be of use to further optimise the packing of the GW sorbent. These results also indicate that the GW sampler would be best applied to sampling compounds with mid-range BPs.

From Table 4.15, it can be observed that of the analytes injected and passed through the various samplers, it was found that the PDMS sampler had the largest calculated RVs for six of the nine analytes. The GW sampler showed increased retention for four of the nine analytes as compared to the QW sampler. Two of the nine analytes were extrapolated for the GW and QW samplers using the equations generated in Figure 4.21 for which the R^2 values ranged from 0.89 - 0.99; indicating a good fit for the trendlines. The primary hypothesis for why a clearer difference between GW and QW RVs was not observed was that only one sampler of each sorbent type was used in these experiments. Since it has been shown that the graphene layers are not grown uniformly on the QW substrate, it is possible that the chosen GW sampler had a significant number of QW fibres that were not adequately layered with graphene. In addition, channelling may have occurred in the GW sorbent bed, whereby the analytes followed the path of least resistance, due to the differences in packing density across the bed, leading to saturation of available active sites along the channel but not in the sampler bed as a whole.

For the GW sampler, Figure 4.22 illustrates a distinct trend of how the RVs for polar analytes greatly increased within a smaller BP range as compared to the RVs for non-polar analytes, although the same trend was noted for QW. This may further imply that, in its current state, the GW sampler targets polar analytes due to exposed QW fibres, leading to a higher affinity of the material to retain polar analytes with somewhat higher BPs as compared to non-polar analytes at equivalent BPs. Therefore, it is hypothesized that the GW sampler will have a larger retention volume for non-polar analytes once the uniformity and layering of the graphene layers on the QW substrate has been optimised.

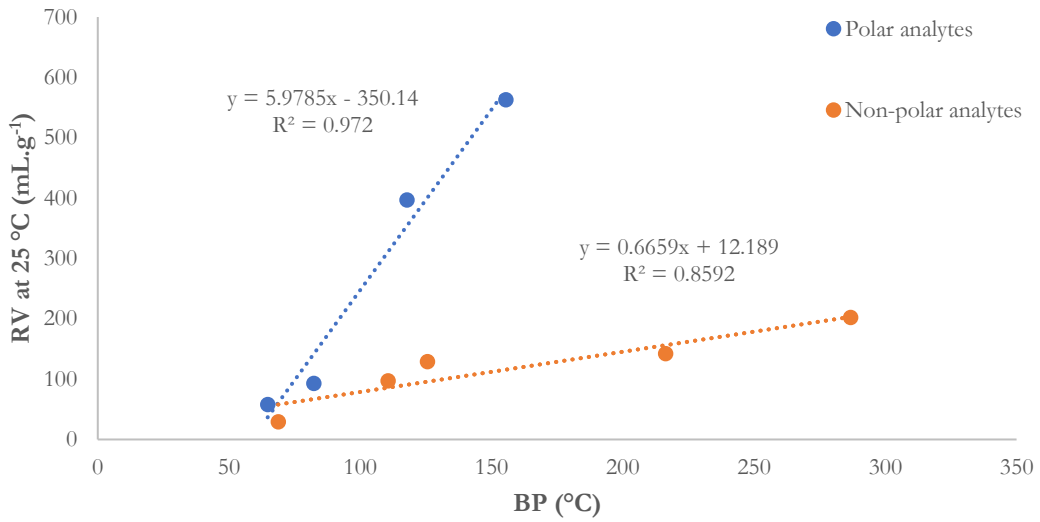

Figure 4.22: Relationship between the RVs for the GW sampler at 25 °C (mL.g^{-1}) and the BPs (°C) of polar and non-polar analytes.

In addition, from these results the sorbent bed possibly requires further optimisation to prevent channelling. The GW sampler may be optimised to contain more of the sorbent per sampler to increase the RVs and a second GW sampler downstream of the first (primary) GW sampler could act as a gauge for breakthrough from which Equation 5 may be used to calculate percent breakthrough. This will further allow for more accurate quantification of the specific breakthrough volume (SBV) for target analytes at relevant sampling conditions to include factors such as ambient temperature, humidity etc., during sampling.

$$BV\ (\%) = \frac{S}{S + P} \times 100 \quad \ldots \text{Eq 5}$$

S - Concentration found on secondary (2°) bed

P - Concentration found on primary (1°) bed

4.6 CAST campaign

Throughout the sampling period, the ambient temperature differed slightly from 26.8 - 27.7 °C with a % RSD of 1.56 whilst the barometric pressure ranged from 955.5 - 956.2 hPa with a % RSD of 0.03, as shown in Table G4. This showed that the ambient conditions during sampling were fairly consistent and thereby allowed for the comparison of the fuel measurements and the CAST system over the sampling period.

4.6.1 FID/FTIR analysis

Since this study occurred over a period of three days, it was of interest to investigate the inter-day CAST generator combustion and emission stability using the FID and FTIR over the sampling period to determine the reliability of the CAST system for organic gas-phase emission sampling. In order to do this, the sampling of the emissions from the CAST generator started with the B0 fuel type, which was used as a basis for comparison of the other two fuels tested, as petroleum-derived diesel is widely used throughout the world. The experiments then continued onto the gas-to-liquid (GTL) and rapeseed oil methyl ester (RME) fuel types, respectively, and ended with sampling the B0 fuel type as a bracket test to gauge the reproducibility of the CAST emissions between the duplicate measurements sampled over the course of the days over which the sampling took place.

In Table 4.16, each fuel type is allocated numbers 1 - 4, where 1 and 2 designate the duplicate measurements of the first round of sampling the emissions from each fuel, which were carried out directly after each other, whereas numbers 3 and 4 relate to the duplicate measurements of the second sampling event of the same fuel which were carried out sequentially on a different day. As can be seen from Table 4.16, the response of the FID showed higher gas phase organic emissions from each fuel type during the first sampling event as compared to the second sampling event. Although the duplicate sampling events for each fuel type were carried out on different days, no rinsing occurred for intra-fuel sampling events of the GTL and RME fuel types. This could have in turn contributed to the smaller FID measurement difference (i.e. lower % RSD) in the combustion fuel emissions of these fuel types, measured between the duplicate fuel measurements, as compared to B0 which was sampled as a bracket test. Nevertheless, the fuel combustion emissions recorded by the FID, for all of the fuel types, showed that the combustion emissions were significantly different between days, using a statistical t-test at a 95% confidence level. This implies that it is preferable to conduct all tests of a particular fuel type sequentially on one day when using the CAST system, to reduce these uncertainties. During the sampling events of each fuel type, additional measurements were taken of the H_2O, CO_2, O_2 percentage and amount of CO (ppm) contained within the combustion emissions from the CAST exhaust. These values were found to not differ significantly during the sampling period (Table G5 in Appendix G).

Table 4.16: Mean FID results for the sampling events of the undiluted fuel emissions over each 10 min sampling period.

	FID (ppm)		
Sampling event	**B0**	**GTL**	**RME**
1	8.87	7.33	5.60
2	8.75	7.27	5.57
3	7.63	7.09	5.30
4	7.60	7.05	5.49
Mean	8.21	7.19	5.49
SD	0.69	0.14	0.13
% RSD	8.42	1.89	2.46

In order to compare the performance of the samplers, the results from the second sampling events of the B0 and GTL combustion were used, i.e. numbers 3 and 4 for B0 and GTL respectively in Table 4.16, as these results proved to be more reliable from the FID measurements; in that lower % RSDs were recorded over each sampling event. Additionally, it was found that the first round of sampling of the B0 and GTL yielded target analyte concentrations that were significantly larger with greater variation than in the second round of sampling as shown in Figure G1 in Appendix G. Since the RME fuel did not contain additives i.e. stabilizers, polymerisation of the combustion products occurred around the flame tip during the second sampling event. These combustion products caused a partial blockage with related potential inconsistencies in results, therefore the duplicates from the first sampling event for that fuel type, i.e. RME 1 and 2 in Table 4.16, were used for the comparison of the samplers and fuel types.

4.6.2 Comparison of the analytes detected on each sampler type

The highest number of target analytes were detected from the emissions of B0, where thermal desorption of the PDMS sampler resulted in the detection of 33 target analytes, whilst 34 were detected upon TD analysis of the GW sampler. Analysis of the charcoal sampler extracts after solvent extraction resulted in the detection of only two of the 36 target analytes in all fuel types sampled; namely benzene and toluene, of which only benzene was above the LOQ. The low number of analytes detected was likely due to the dilution volume. After analysis of a blank extraction of the activated charcoal sorbent, it was evident that the detected analytes were from the sorbent itself, which contained particularly high levels of

benzene. The blank analysis data of the three samplers is shown in Table G6 in Appendix G. Therefore, the comparison of the concentrations of benzene and toluene emitted upon combustion of different fuels is based only on the analysis of the PDMS and GW samplers (as shown in Figure 4.23 and detailed further in Section 4.6.3 and 4.6.4).

There are a number of factors contributing to the lack of analytes detected upon analysis of the activated charcoal sampler extracts as compared to the number of analytes detected upon analysis of the PDMS and GW samplers, as shown in Figure 4.23 (also refer to Tables G7 and G8). Firstly, the volume of solvent experimentally determined to be required (3 mL) for the extraction of the activated charcoal may have diluted the sampled analytes to below the limit of detection (LOD) of the analytical method.

The charcoal sampler was preliminarily calibrated for only 8 of the 36 target analytes. Further calibration of the remaining 28 target analytes did not occur as no other target analytes other than benzene and toluene were detected upon analysis of the activated charcoal extracts. The LODs for the activated charcoal sampler were calculated to range from 0.48 $\mu g.m^{-3}$ for naphthalene to 2.26 $\mu g.m^{-3}$ for m-xylene (Tables G9a and G9b). Comparatively, the LODs for PDMS ranged from 0.0001 $\mu g.m^{-3}$ for 1,2-dimethylnaphthalene to 0.80 $\mu g.m^{-3}$ for n-octane, whilst the LODs for GW ranged from 0.002 $\mu g.m^{-3}$ for toluene to 0.79 $\mu g.m^{-3}$ for n-octane and n-nonane.

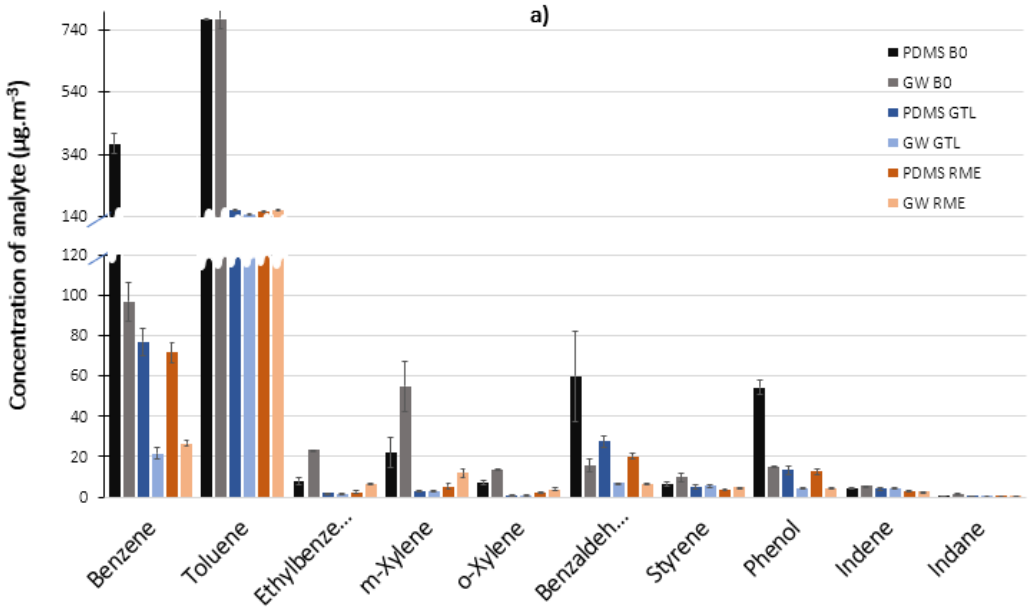

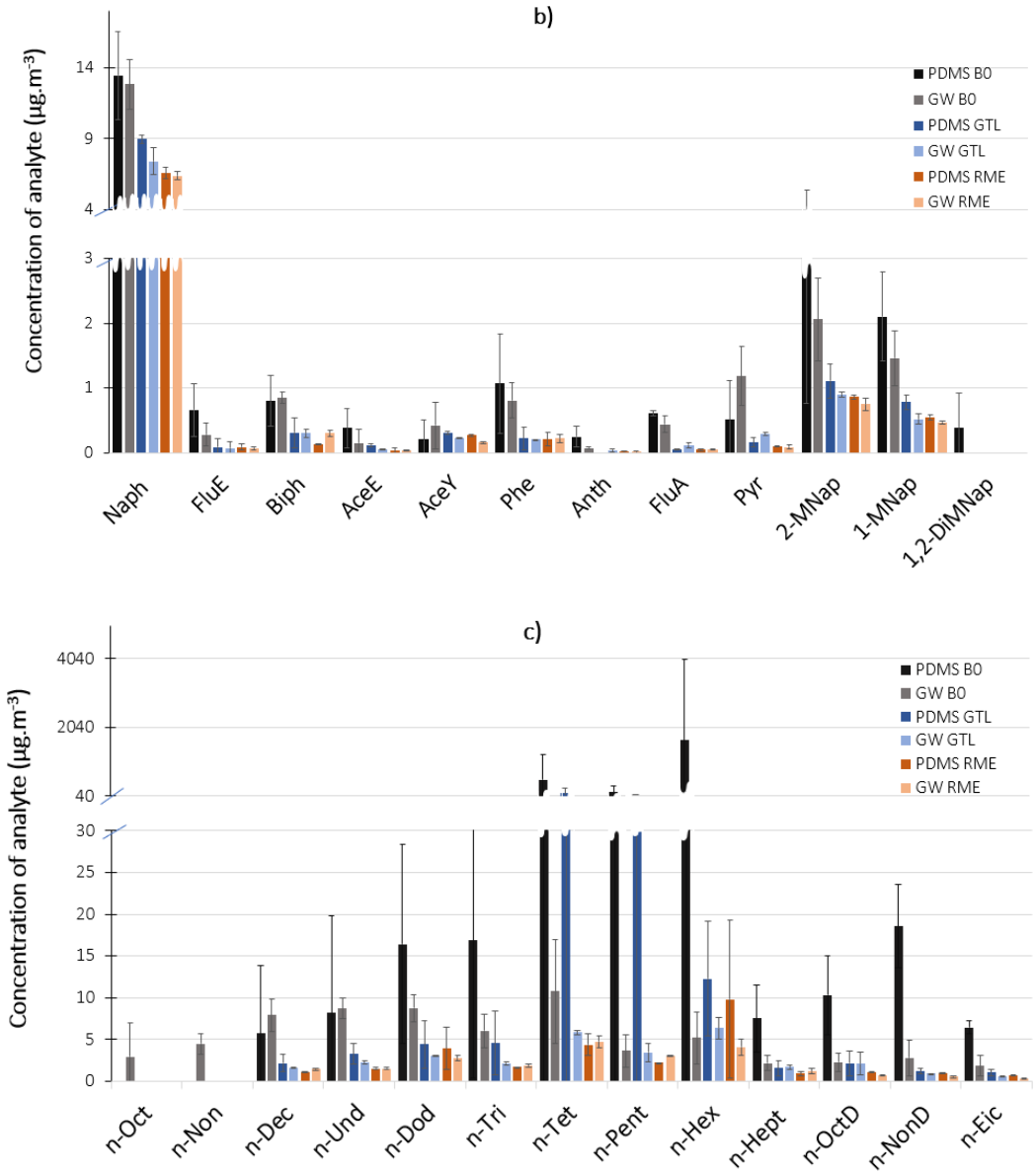

Figure 4.23: Detected concentrations of **a)** VOCs, **b)** PAHs and **c)** HCs from the combustion of fuel types B0, GTL and RME sampled from the CAST generator exhaust using PDMS and GW samplers. *The error bars are based on the SD of duplicate measurements and abbreviations can be found listed in Tables 9a and 9b in Appendix G.*

As can be seen from Figure 4.23 c), the GW sampler was found to be more effective than PDMS in retaining the lighter HCs such as n-octane and n-nonane. However, analysis of the GW sampler generally gave lower concentrations of each target analyte than the PDMS sampler (Figures 4.23 a) - c)). This may be indicative of the GW sampler having a lower breakthrough volume compared to the PDMS sampler as determined in Section 4.5 however, the main cause is probably due to the TD parameters being optimised for the PDMS sampler and not for GW desorption. Therefore, the lower concentrations of analytes

determined upon analysis of the GW samplers are most likely due to the incomplete TD of analytes from the GW sampler, as was found in Section 4.3.3, as the GW sampler retains analytes more strongly by adsorption rather than by sorption as in the case of PDMS.

4.6.3 Comparison of the variability between the samplers

As previously stated, the analysis of the PDMS samplers reflected higher concentrations of the target analytes as compared to the GW samplers (Figures 4.23). However, the reported concentrations from the analysis of the PDMS samplers showed larger SDs as compared to the GW samplers. This could be due to PDMS functioning as a sampler through the action of absorption as opposed to the GW sampler, which functions by adsorbing analytes. Additionally, the structure of the GW sorbent itself, which involves a 2D monolayered structure of one atom thickness, leads to a large number of active sites being open and available for adsorption, although it may be more difficult to desorb analytes from the GW sampler than from the PDMS sampler.

The range of target analytes were dominated by non-polar compounds which would theoretically tend to interact better with the non-polar GW sorbent as compared to the less non-polar PDMS sorbent. The results thus indicate that the GW samplers used in the CAST study had good graphene coverage on the QW substrate (as compared to the GW sampler used in Section 4.5), although it is important to note that in the CAST experiments analyte concentrations were at trace levels, whilst in the RV experiments analytes were at significantly higher concentrations in their pure forms. The lower standard deviation (SD) in the concentrations reported through the analysis of the GW samplers as compared to the analysis of the PDMS samplers is particularly noticeable for the concentrations of the PAHs detected (Figure 4.23 b) but even more so for the concentrations of HCs detected (Figure 4.23 c). Therefore, due to the lower degree of uncertainty in concentrations reported upon analysis of the GW sampler and the greater number of compounds detected by the GW sampler as compared to the other two samplers, the GW sampler proved to be the superior sampler as compared to the activated charcoal sampler and the PDMS sampler for the sampling of the selected VOCs, PAHs and HCs in this case study. The strengths and weaknesses of the various samplers employed are summarised in Table 4.17. The user would need to take these advantages and disadvantages into account when deciding which sampler would work best for an intended application.

Table 4.17: The relative advantages and disadvantages of GW, PDMS and charcoal samplers for the sampling of the selected VOCs, PAHs and HCs.

	GW Sampler	PDMS Sampler	Activated Charcoal Sampler
Advantages	Low background noise	-	-
	Can be reused	Can be reused	R67 per sampler
	On average, the lowest SD in recorded duplicate measurements	-	-
	Largest number of analytes detected	A large number of analytes detected	-
	Similar analysis time to PDMS	Similar analysis time to GW	-
	Can be thermally desorbed therefore requires no solvents in preparation for analysis	Can be thermally desorbed therefore requires no solvents in preparation for analysis	Does not require a lab equipped with a TD system
Disadvantages	-	Sorbent background (due to siloxanes)	Sorbent background (for toluene and benzene)
	R141 per sampler	R155 per sampler	Single use
	Lower concentrations of several target analytes reported as compared to PDMS	Larger SD in recorded duplicate measurements as compared to the GW sampler, especially for the HCs	Largest SD in recorded duplicate measurements of benzene
	Requires a lab equipped with TD system	Requires a lab equipped with a TD system	Lowest number of analytes detected
	-	-	Long extraction time
	-	-	Incomplete sample recovery
	-	-	Toxicity of solvent used for extraction i.e. CS_2

4.6.4 Effect of the different fuels on the combustion emission profiles

Most of the CAST combustion emission compound profiles for the different fuels tested reflected a similar trend as seen in Figure 4.23, when sampled by the PDMS and the GW sampler. Since it has been identified that the PDMS sampler had more variability in the resultant concentrations reported as compared to the GW sampler, the relative concentrations of target analytes within each fuel type emission profile will be discussed in terms of the results reported through the analysis of the GW samplers. Comparing the three fuel types sampled in this study, the combustion of B0 diesel resulted in higher concentrations of target analytes in most cases, with the exception of hexadecane in the combustion emissions of GTL (Figure 4.24). As expected, the combustion emissions of RME reflected lower concentrations of targeted VOCs and SVOCs as compared to diesel

and GTL, with the exception of ethylbenzene and the xylene isomers in the case of GTL (Figure 4.24 c). These reported results align with the visual analysis of the filter papers which were placed upstream of the samplers. It can be seen in Figure 4.25 that the PM filter from B0 combustion is considerably darker than the filters relating to GTL and RME combustion. The same trend was also observed in the duplicate sampling events conducted with B0 and GTL and RME.

In the broader context of fuel emission monitoring, the percent carbon content and total unburned hydrocarbons (THCs) are typically reported in the literature to be the largest in diesel whilst GTL tends to have less, and biodiesels, such as RME, have been reported to have the lowest concentrations (Dagaut et al., 2019; Damanik et al. 2018; Soriano et al. 2018). The measurements are done on % w/w of the fuel before combustion or the measurements of the target molecules are accomplished though the analysis of the PM phase formed after the combustion of the fuel. The compounds present in the different fuels and the relative abundancies in terms of engine emissions are also reported. It is important to note that the CAST generator pyrolyzes the fuel by means of a diffusion flame therefore the combustion conditions and consequently the emissions, would differ to real-world engine emission scenarios making direct comparisons to other studies difficult. Furthermore, compounds present in various fuel sources are often reported in terms of total carbon (TC); which is the summation of elemental carbon (EC) and organic carbon (OC) fractions with little detail regarding which specific analytes are present in the OC fraction (Atiku et al., 2016; Nyström et al., 2016; Shen et al., 2013; Zhou, Zhou, & Zhu, 2019). This indicates that it is important to conduct the type of sampling undertaken in this study to better monitor the emission of VOCs and SVOCs generated by combustion processes.

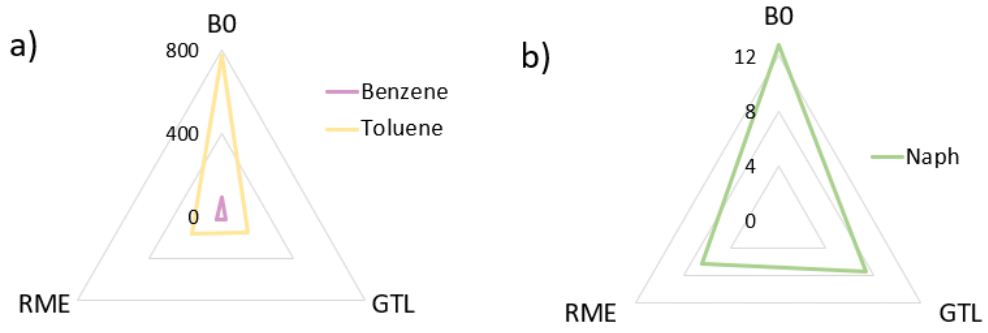

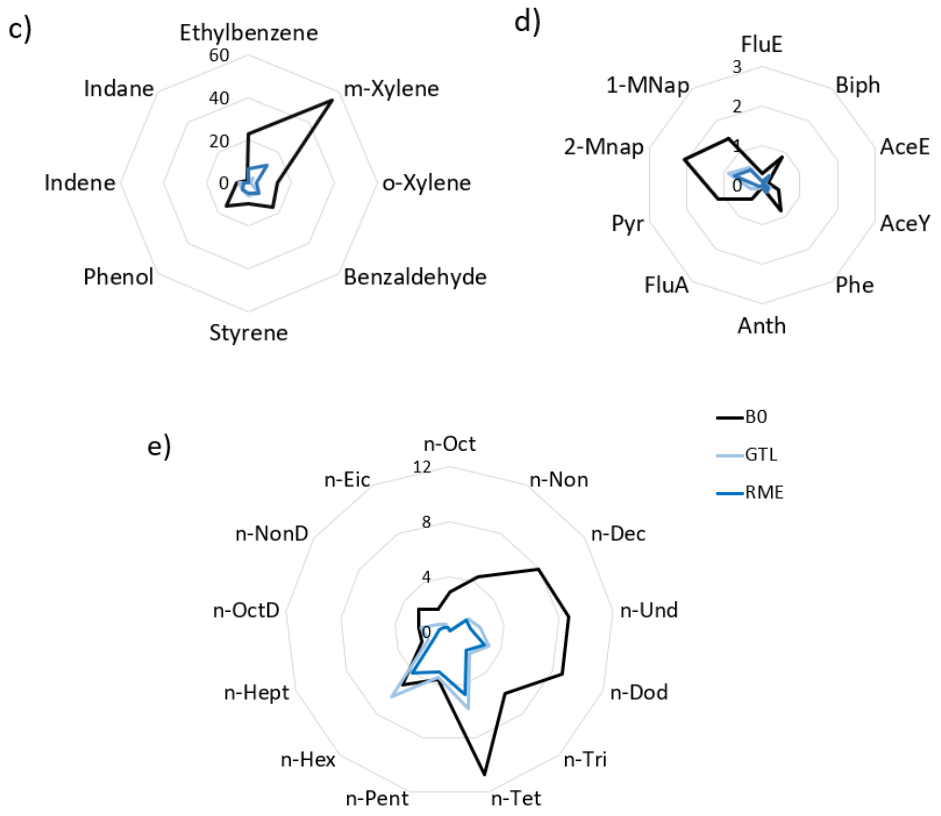

Figure 4.24: Relative abundance (μg.m^{-3}) of various analytes detected upon analysis of the GW sampler after sampling the gas phase emissions from B0, GTL and RME. Shown are the detected combustion emission levels of **a)** benzene and toluene, **b)** naphthalene **c)** VOCs, **d)** PAHs and **e)** HCs.

In terms of bettering the fuel source for many forms of machinery in order to reduce emissions which are potentially hazardous for human health, it will be important to determine emission profiles of fuels not only in terms of the PM generated, but also specifically which volatile and semi-volatile organic compounds are being released into the atmosphere as these can also be detrimental to the environment and to human health, even though they may not be visible.

Figure 4.25: PM filtered from **a)** B0, **b)** GTL and **c)** RME CAST emissions prior to gas phase sampling.

Chapter 5: Conclusions and Future Work

5.1 Conclusions regarding the laboratory-based studies

The hygroscopicity studies showed that the GW material retained more water than QW when both materials were in a compressed state, under vacuum conditions, as in the SPE set-up. However, in a sampler set-up, whereby the materials were packed in a less dense manner, the QW sampler showed the greatest retention of water, as compared to the GW and PDMS sampler. This is expected due to their respective polarities. The GW sampler retained a negligible amount of water between the humidity ranges of 48 - 72%, however when the mist maker was switched on to generate an ambient humidity > 75%, it was observed that the GW sampler retained more than half its weight in water. The negligible adsorption of water at humidity ranges < 80% is desirable as this, in turn, indicates a negligible competition for active sites on the GW sorbent between target analytes and water, and further infers that the GW sampler is compatible with GC-MS analysis as GC-MS is incompatible with water. It was shown that water retention will not be a problem when using the GW sampler under ambient conditions not exceeding 80% humidity.

The back-pressure incurred by the GW sampler in comparison to that incurred by the QW and PDMS samplers was investigated under constant flow rates. The samplers made out of QW and GW were similar with respect to back-pressure consistency measured at the sampling pump with steady back-pressures up to, and including, flow rates of 400 $mL.min^{-1}$. As a result of the open tubular structure of the PDMS samplers, these samplers incurred a low and steady back-pressure during sampling at 400 and 500 $mL.min^{-1}$. This is in contrast to the GW and QW samplers which are composed of fibrous packed sorbent beds that pose a greater resistance to flow and therefore incur higher back-pressures than the PDMS samplers at equivalent flow rates. Based on these results the back-pressure incurred by the GW samplers was found to be stable at a flow rate of 400 $mL.min^{-1}$. Although it is recommended to sample at a flow rate of 200 - 250 $mL.min^{-1}$ by Manura (2019) and the International Organisation for Standardization (2001 and 1991), this result is positive as GW has shown to incur low flow resistance.

In order to compare extraction techniques, namely PASE and TD, in terms of their efficiencies to extract spiked PAHs from the GW samplers, the percent extraction efficiencies of these two methods were compared. Performing PASE with hexane was shown to be a promising means by which to extract target analytes from the GW. The

limitation is, however, that this would only be applicable to sampling concentrations of target analytes (PAHs) in polluted environments, as the instrumental LOQ is heavily impacted by solvent dilution. A possible solution to this problem would be blow down the extract before analysis so as to concentrate the target analytes. The 8 hr hexane soak of the GW sorbent using PASE showed promising results for the extraction of PAHs from the GW sampler, as most of the PAHs were extracted in the first PASE extract whereas most of the PAHs were extracted in the second and third extracts without the 8 hr hexane soak. Method calibration curves using the summation of the concentration of three sequential extracts to effectively account for irreversible adsorption of certain larger non-polar molecules should be used for quantitation.

TD of the GW sampler resulted in good extraction efficiencies for the lighter PAHs such as naphthalene (96.89% recovery), however, the extraction efficiency was observed to decrease as the molecular mass of the PAHs increased. An example of which is the 1.80% recovery of dibenz[a,h]anthracene from the GW sampler. This result indicates that the larger molecules are more susceptible to being irreversibly adsorbed onto the GW and therefore should not be targeted when using the GW sampler. It may thus be advantageous to optimise PASE, whilst exploring solvents used such as CS_2 and acetonitrile, for PAH extraction from GW samplers.

The intra- and inter- sampler variability studies involved the spiking of VOCs and SVOCs (PAHs and HCs) onto randomly selected fresh GW samplers with subsequent analysis of these spiked samplers using TD-GCxGC-TOF-MS. Greater variability, in both the intra- and inter- sampler variability results, were generally found for more polar VOCs and heavier SVOCs. The intra- and inter- sampler profiles of the VOCs were similar, with the exception of 6 out of 34 VOC analyte groupings (some of the VOC analytes were grouped due to the similarity of their fragmentation patterns, as no individual standards were available to distinguish these analytes based on their retention times). The variability of the intra-sampler analysis of the HCs increased as the molecular masses increased which may have occurred as a result the irreversible adsorption of heavier non-polar compounds. The analysis of inter-sampler variability of thermally desorbing the PAHs from the GW sampler reflected % RSDs of approximately twice that of the intra-sampler analysis. Discrepancies in the inter-sampler variability results from the analysis of the VOCs and SVOCs may have occurred due to the inconsistency in the uniformity of the graphene layering in the GW material as confirmed by TEM images.

In the final laboratory-based study, chromatographic tests of the tube retention volume were determined using representative analytes for the GW, QW and PDMS samplers. It was found that GW had larger BVs for three of the nine analytes, as compared to the other two samplers. The generally low RVs of the GW sampler are primarily attributable to three factors. Firstly, this experiment involved very concentrated samples in large volumes. Therefore, conducting further experiments in a more representative method to real-case scenarios such as using headspace sampling may be further investigated in future studies, as expanded on in Section 5.3. Furthermore, the lack of uniformity of the graphene layers on the QW substrate and suspected channelling within the sampler may have further reduced the RVs of the GW sampler. Channelling would have caused the GW to show decreased retention of the analytes, without exceeding the adsorption capacity of the sampler. This may be overcome in future studies by optimising the uniformity of the graphene layers and optimising the packing of the sorbent to minimise channelling effects. In terms of comparing the GW sampler to the PDMS sampler, it can be seen that the GW sampler had the highest RV for methanol, whilst both the GW and QW samplers had higher RVs butan-1-ol and cyclohexanone as compared to PDMS. This may be primarily attributed to exposed QW fibres retaining polar analytes better, as compared to non-polar analytes, contrary to expectations. This can be overcome by increasing the graphene layering on the QW substrate to enhance the retention of non-polar analytes.

5.2 Conclusions regarding the CAST campaign

In this study it was found that the commercial activated charcoal sampler was not effective in sampling the target analytes produced upon combustion of the fuels tested by the CAST. This could be due to the sample being too dilute and below the LOD due to the volume of the extraction solvent required, as well as the low levels of gas phase VOCs and SVOCs produced by the CAST system and the small sample volume. In addition to the target analytes being below the LOD for the activated charcoal extracts, the activated charcoal sampler may have irreversibly adsorbed the target analytes. It is also noted that the extraction method for the activated charcoal sampler was time consuming, required a toxic solvent and high background concentrations were found for some analytes. The activated charcoal sampler proved to be the cheapest however, with a once-off use, whilst the PDMS and GW have the advantage of being able to be reconditioned and reused.

The results of the PDMS sampler analysis reflected relatively higher concentrations of the VOC and SVOC target analytes detected to that of the GW sampler. However, the results

from the PDMS sampler analysis also showed a higher variability in the duplicate concentrations reported, particularly for the HCs. The analysis of the GW sampler showed that target analytes were determined with lower uncertainties than with the PDMS sampler and lighter n-alkanes, such as octane and nonane were detected with the GW sampler but not with the other two samplers. The analysis of the GW samplers did reflect lower concentrations of all target analytes sampled as compared to the concentrations reflected by the PDMS samplers. This could be due to the TD parameters which were optimal for the PDMS but resulted in incomplete desorption from the GW sorbent which therefore requires further optimisation such as a higher desorption temperature. Overall, the GW sampler has proven to be superior, as compared to the activated carbon as well as the PDMS sampler in the sampling of the selected trace levels of VOCs, PAHs and the lighter n-alkanes (such as n-octane and n-nonane) in this case study. These results indicate that the GW sampler may be used to target trace concentrations of lighter non-polar analytes, which indicates that in this case the GW sampler employed had more complete layering of graphene on the QW. In terms of fuel comparisons, B0 produced the highest concentration of VOCs and SVOCs upon combustion in the CAST, as compared to RME and GTL fuels.

Regarding the CAST generator itself, it is suggested that one fuel type is used and sampled over a continuous period to definitively establish the reproducibility of the CAST, as significant variation was observed when sampling the fuel emissions on different days, although this variability was compounded by the low levels of target analytes produced by the CAST system. In future comparisons, the final extract volume for the charcoal sampler should be reduced to improve detection limits, especially in light of the low emission levels from the CAST system. It may also be of use to analyse the various fuel types before combustion to determine the aromatic content thereof and compare these to the combustion profiles reported in this study, as well as to compare the samplers using another combustion source which generates higher levels of target VOCs and SVOCs.

5.3 Recommendations for additional future research

As a primary recommendation for the GW sampler, it is advised to firstly deploy resources into optimising the uniformity of the graphene layers grown on the QW substrate fibres. It may also be possible to tune the synthesised material to target either more or less polar gaseous analytes; depending on how many layers are grown on the QW substrate. Further optimisations of the GW material are also possible through the use of surface chemistry. Possible surface chemistry adaptations of graphene include combining it with mesoporous

silica (G@SiO_2) (Abdelhamid et al., 2014). This has been found to decrease interactions of analytes with graphene nanosheets, for instance aromatic compounds that interact via π-π interactions, which may reduce irreversible adsorption of heavier target analytes by modified GW. In the case of lighter target analytes, it would be beneficial to investigate storage stability of these analytes when sampled onto GW.

From the laboratory-based studies conducted on the GW sampler, it may be of benefit to focus on certain aspects and expand thereon in future research, such as optimising the bed length of the GW sampler, with back-pressure and flow rate consistency in mind, and to have a second GW sampler downstream of the sampling set-up so as to definitely determine breakthrough at set flow rates and sampling volumes. An additional breakthrough volume study involving headspace sampling instead of injecting 1 µL of neat sample should be considered. Also, the comparison of the breakthrough of naphthalene from the GW sampler by means of a permeation tube and directly comparing it to the PDMS sampler which has already been validated for the sampling 5 L of naphthalene at 500 $mL.min^{-1}$. The advantages of permeation tubes are their versatility, portability and ease of use (Forbes, 2010). This can be done through the experimental set-up as illustrated by Figure 5.1. The upstream activated charcoal acts as air filtration for organic compounds naturally present in the laboratory air and the permeation tubes are weighed so as to account for the amount of naphthalene vaporising and being adsorbed onto the GW sampler.

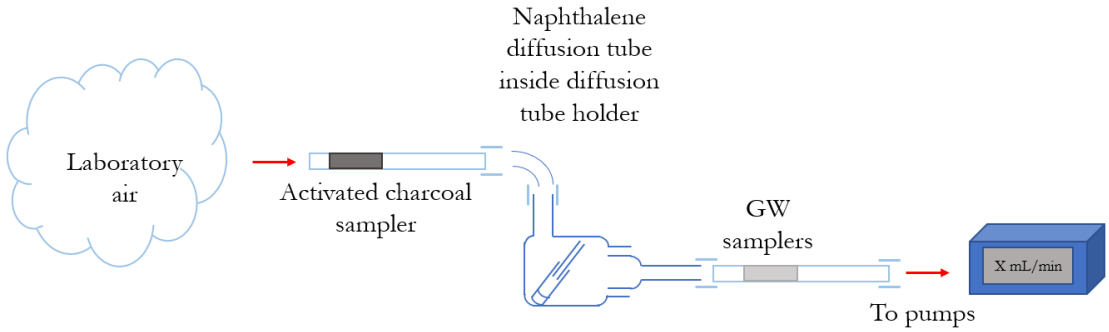

Figure 5.1: Schematic for the collection of naphthalene generated from a permeation tube onto a GW sampler.

5.4 Concluding comments

There are notably numerous potential applications of GW in environmental monitoring such as for airborne VOC and SVOC monitoring, which was studied in this dissertation. In terms of medical research, the GW may find use as a non-invasive sampling technique for VOCs in breath, which would be indicative of diseases. Additionally, GW may be explored for its

ability in detecting toxic VOCs release by fungi and moulds, that are found in households and industrial areas, which can cause adverse health effects to people unknowingly being exposed.

Finally, the GW material may even find potential application in the adsorption of viral particles so as to manufacture safety equipment and filtration devices with larger capacities than what is currently available. There are numerous possible applications of the GW material, however, it would be prudent to optimise the graphene layer uniformity on the substrate before future applications and properties of this material are investigated.

References

Abdelhamid, H.N., Wu, B.S., and Wu, H.F. **2014**. Graphene coated silica applied for high ionization matrix assisted laser desorption/ionization mass spectrometry: a novel approach for environmental and biomolecule analysis. *Talanta,* 126, 27-37.

ACGIH. **2012**. ACGIH® threshold limit values (TLVs®) and biological exposure indices (BEIs®). [Online] Available at: https://www.nsc.org/Portals/0/Documents/facultyportal/Documents/fih-6e-appendix-b.pdf

AcuRite. **2017**. How to measure humidity. [Online] Available at: https://www.acurite.com/blog/how-to-measure-humidity.html

Adeola, A.O., and Forbes, P.B.C. **2020**. Optimization of the sorption of selected polycyclic aromatic hydrocarbons by regenerable graphene wool. *Water Science & Technology*, 80(10), 1931-1943.

Afework, B., Hanania, J., Sheardown, A., Stenhouse, K., and Donev, J. **2019**. Secondary pollutant. [Online] Available at: https://energyeducation.ca/encyclopedia/Secondary_pollutant

Arias, M., Penichet, I., Ysambertt, F., Bauza, R., Zougagh, M., and Ríos, Á. **2009**. Fast supercritical fluid extraction of low- and high-density polyethylene additives: comparison with conventional reflux and automatic Soxhlet extraction. *The Journal of Supercritical Fluids,* 50(1), 22-28.

Arsat, R., Breedon, M., Shafiei, M., Spizziri, P., Gilje, S., Kaner, R., Kalantar-zadeh, K., and Wlodarski, W. **2009**. Graphene-like nano-sheets for surface acoustic wave gas sensor applications. *Chemical Physics Letters,* 467(4-6), 344-347.

Atiku, F.A., Mitchell, E.J.S., Lea-Langton, A.R., Jones, J.M., Williams, A., and Bartle, K.D., **2016**. The impact of fuel properties on the composition of soot produced by the combustion of residential solid fuels in a domestic stove. *Fuel Processing Technology,* 151, 117-125.

Azwanida, N.N. **2015**. A review on the extraction methods use in medicinal plants, principle, strength and limitation. *Medicinal and Aromatic Plants,* 4(196), 2167-2173.

Barro, R., Regueiro, J., Llompart, M., and Garcia-Jares, C. **2009**. Analysis of industrial contaminants in indoor air: part 1. Volatile organic compounds, carbonyl compounds, polycyclic aromatic hydrocarbons and polychlorinated biphenyls. *Journal of Chromatography A,* 1216(3), 540-566.

Basu, S., and Bhattacharyya, P. **2012**. Recent developments on graphene and graphene oxide based solid state gas sensors. *Sensors and Actuators B: Chemical,* 173, 1-21.

Berglund, B., Clausen, G., De Ceaurriz, J., Kettrup, A., Lindvall, T., Maroni, M., Mølhave L., Pickering, A.C., Risse, U., and Rothweiler, H. **1997**. Total volatile organic compounds (TVOC) in indoor air quality investigations: European Collaborative Action. Report number 9.

Bernstein, J.A., Alexis, N., Barnes, C., Bernstein, I.L., Nel, A., Peden, D., Diaz-Sanchez, D., Tarlo, S.M., and Williams, P.B. **2004**. Health effects of air pollution. *Journal of Allergy and Clinical Immunology,* 114(5), 1116-1123.

Bertoni, G., Bruner, F., Liberti, A., and Perrino, C. **1981**. Some critical parameters in collection, recovery and gas chromatographic analysis of organic pollutants in ambient air using light adsorbents. *Journal of Chromatography A,* 203, 263-270.

Bhatt, R.V., **2000**. Environmental influence on reproductive health. *International Journal of Gynecology and Obstetrics,* 70(1), 69-75.

Bielicka-Daszkiewicz, K., and Voelkel, A. **2009**. Theoretical and experimental methods of determination of the breakthrough volume of SPE sorbents. *Talanta,* 80(2), 614-621.

Brownson, D.A.C., Kampouris, D.K., and Banks, C.E. **2012**. Graphene electrochemistry: fundamental concepts through to prominent applications. *Chemical Society Reviews,* 41(21), 6944-6976.

Chen, G., Paronyan, T.M., and Harutyunyan, A.R. **2012**. Sub-ppt gas detection with pristine graphene. *Applied Physics Letters,* 101(5), 1-4.

Cheremukhin, A., Golosov, M., Guriev, S., and Tsyvinski, A. **2015**. The economy of people's republic of China from 1953. *National Bureau of Economic Research Working Paper Series,* 21397, 1-111.

Chin, J.Y., Godwin, C., Jia, C., Robins, T., Lewis, T., Parker, E., Max, P., and Batterman, S. **2013**. Concentrations and risks of p-dichlorobenzene in indoor and outdoor air. *Indoor Air,* 23(1), 40-49.

Chu, J. **2015**. Can rain clean the atmosphere? [Online] Available at: http://news.mit.edu/2015/rain-drops-attract-aerosols-clean-air-0828#targetText=As%20a%20raindrop%20falls%20through,%2C%20sulfates%2C%20and%20organic%20particles.

Collins. **2019**. Aerosol. [Online] Available at: https://www.collinsdictionary.com/dictionary/english/aerosol

Dagaut, P., Bedjanian, Y., Dayma, G., Foucher, F., Grosselin, B., Romanias, M., and Shahla, R. **2019**. Emission of carbonyl and polyaromatic hydrocarbon pollutants from the combustion of liquid fuels: impact of biofuel blending. *Journal of Engineering for Gas Turbines and Power,* 141(3), 031028. 1-8.

Damanik, N., Ong, H.C., Tong, C.W., Mahlia, T.M.I., and Silitonga, A.S. **2018**. A review on the engine performance and exhaust emission characteristics of diesel engines fueled with biodiesel blends. *Environmental Science and Pollution Research*, 25(16), 15307-15325.

Deng, S., Tjoa, V., Fan, H.M., Tan, H.R., Sayle, D.C., Olivo, M., Mhaisalkar, S., Wei, J., and Sow, C.H. **2012**. Reduced graphene oxide conjugated Cu_2O nanowire mesocrystals for high-performance NO_2 gas sensor. *Journal of the American Chemical Society,* 134(10), 4905-4917.

Department of Environmental Affairs **2018**. The 2017 National Framework for air quality management in the Republic of South Africa. [Online] Available at: https://saaqis.environment.gov.za/Pagesfiles/2017_National_Framework.pdf

Department of Environmental Affairs **2015**. Ammendments to the list of activities which result in atmospheric emission which have or may have a significant detrimental effect on the environment, including health, social conditions, economic conditions, ecological conditions or cultural heritage. [Online] Available at: https://www.gov.za/sites/default/files/gcis_document/201506/38863gen551.pdf

Department of Environmental Affairs **2009**. National ambient air quality standards. [Online] Available at: https://www.environment.gov.za/sites/default/files/legislations/nemaqa_airquality_g32816gon1210_0.pdf

Department of Labour. **2018**. Draft regulations for hazardous chemical agents. [Online] Available at: https://www.gov.za/sites/default/files/gcis_document/201810/draftregforhazardousregulatios.pdf

Dettmer, K., and Engewald, W. **2002**. Adsorbent materials commonly used in air analysis for adsorptive enrichment and thermal desorption of volatile organic compounds. *Analytical and Bioanalytical Chemistry,* 373(6), 490-500.

Dhanani, T., Shah, S., Gajbhiye, N.A., and Kumar, S. **2017**. Effect of extraction methods on yield, phytochemical constituents and antioxidant activity of Withania somnifera. *Arabian Journal of Chemistry,* 10, S1193-S1199.

Eiserbeck, C., Nelson, R.K., Reddy, C.M., Grice, K. **2014**. Advances in Comprehensive Two-dimensional Gas Chromatography (GCxGC). Volume 4. Chapter 12.

European Union. **2000**. Directive 2000/69/EC of The European Parliament and of The Council. L313/12.

Figge, K.., Rabel, W., and Wieck, A. **1987**. Adsorptionsmittel zur anreicherung von organischen luftinhaltsstoffen; adsorbents for the enrichment of organic atmospheric trace compounds. Experimental determination of specific retention and break-through volumes. *Fresenius' Zeitschrift für analytische Chemie,* 327(3-4), 261-278.

Finlayson-Pitts, B.J., and Pitts, J.N. **1997**. Tropospheric air pollution: ozone, airborne toxics, polycyclic aromatic hydrocarbons, and particles. *Science,* 276(5315), 1045-1051.

Finlayson-Pitts, B.J., and Pitts Jr, J.N. **1999**. Chemistry of the Upper and Lower Atmosphere: Theory, Experiments, and Applications: *Elsevier.*

Fogelström, M. **2014**. Graphene science | Mikael Fogelström | TEDxGöteborg. In. [Online] Available at: https://www.youtube.com/watch?v=eh3dA8xnZ4Y

Forbes, P.B.C. **2010**. Development of a laser induced fluorescence technique for the analysis of organic air pollutants. 18-24.

Forbes, P.B.C., Karg, E.W., Zimmermann, R., and Rohwer, E.R. **2012**. The use of multi-channel silicone rubber traps as denuders for polycyclic aromatic hydrocarbons. *Analytica Chimica Acta,* 730, 71-79.

Forbes, P.B.C., and Rohwer, E.R. **2009**. Investigations into a novel method for atmospheric polycyclic aromatic hydrocarbon monitoring. *Environmental Pollution,* 157(8-9), 2529-2535.

Fowler, J.D., Allen, M.J., Tung, V.C., Yang, Y., Kaner, R.B., and Weiller, B.H. **2009**. Practical chemical sensors from chemically derived graphene. *ACS Nano,* 3(2), 301-306.

Ge, S., Lan, F., Yu, F., and Yu, J. **2015**. Applications of graphene and related nanomaterials in analytical chemistry. *New Journal of Chemistry,* 39(4), 2380-2395.

Geldenhuys, G., Rohwer, E.R., Naudé, Y., and Forbes, P.B.C. **2015**. Monitoring of atmospheric gaseous and particulate polycyclic aromatic hydrocarbons in South African platinum mines utilising portable denuder sampling with analysis by thermal desorption–comprehensive gas chromatography–mass spectrometry. *Journal of Chromatography A,* 1380, 17-28.

Goldemberg, J., Martinez-Gomez, J., Sagar, A., and Smith, K.R. **2018**. Household air pollution, health, and climate change: cleaning the air. *Environmental Research Letters,* 13(3), 030201. 1-12.

Graphene Flagship. **2020**. Graphene goes to space. [Online] Available at: https://graphene-flagship.eu/news/Pages/Graphene-goes-to-space.aspx

Hales, A. **2018.** Why do we need exhaust back pressure? [Online] Available at: https://www.quora.com/Why-do-we-need-exhaust-back-pressure.

Han, T.H., Huang, Y.K., Tan, A.T., Dravid, V.P., and Huang, J. **2011**. Steam etched porous graphene oxide network for chemical sensing. *Journal of the American Chemical Society,* 133(39), 15264-15267.

Harper, M. **1993**. Critical tests of volatile organic sampling methods–high temperatures, high humidities and low concentrations. Paper presented at the volatile organic compounds in the environment. Proceedings of the International Conference held in London, Lonsdale Press Ltd, London.

Harper, M. **1992.** Evaluation of solid sorbent sampling methods by breakthrough volume studies. *Journal of Occupational and Environmental Hygiene,* 37(1), 65-88.

Hart, K.M., Isabelle, L.M., and Pankow, J.F. **1992**. High-volume air sampler for particle and gas sampling. 1. Design and gas sampling performance. *Environmental Science and Technology,* 26, 1048-1052.

Helen, G.S., Liakoni, E., Nardone, N., Addo, N., Jacob, P., and Benowitz, N.L. **2020**. Comparison of systemic exposure to toxic and/or carcinogenic volatile organic compounds (VOCs) during vaping, smoking, and abstention. *Cancer Prevention Research*, 13(2), 153-162.

Hemminki, K., and Pershagen, G. **1994**. Cancer risk of air pollution: epidemiological evidence. *Environmental Health Perspectives,* 102(4), 187-192.

Ho, S.S.H., Chow, J.C., Watson, J.G., Wang, L., Qu, L., Dai, W., Huang, Y., and Cao, J. **2017.** Influences of relative humidities and temperatures on the collection of C_2-C_5 aliphatic hydrocarbons with multi-bed (Tenax TA, Carbograph 1TD, Carboxen 1003) sorbent tube method. *Atmospheric Environment,* 151, 45-51.

Hobbs, P., Webb, J., Mottram, T.T., Grant, B., and Misselbrook, T.M. **2004**. Emissions of volatile organic compounds originating from UK livestock agriculture. *Journal of the Science of Food and Agriculture,* 84(11), 1414-1420.

Hu, N., Wang, Y., Chai, J., Gao, R., Yang, Z., Kong, E.S.W., and Zhang, Y. **2012**. Gas sensor based on p-phenylenediamine reduced graphene oxide. *Sensors and Actuators B: Chemical,* 163(1), 107-114.

Hwang, S., Lim, J., Park, H.G., Kim, W.K., Kim, D.H., Song, I S., Kim, J.H., Lee, S., Woo, D.H., and Chan, J.S. **2012.** Chemical vapor sensing properties of graphene based on geometrical evaluation. *Current Applied Physics,* 12(4), 1017-1022.

International Organization for Standardization 9487. **1991**. Workplace air - determination of vaporous aromatihydrocarbons - charcoal tube/solvent desorption/gas chromatographic method. ISO 9487 : 1991 (E)

International Organization for Standardization 16200-1. **2001**. Workplace air quality - sampling and analysis of volatile organic compounds by solvent desorption/gas chromatography – part 1: pumped sampling method. ISO 16200-1 : 2001(E).

Jia, C., Batterman, S., and Godwin, C. **2008**. VOCs in industrial, urban and suburban neighborhoods, part 1. Indoor and outdoor concentrations, variation, and risk drivers. *Atmospheric Environment,* 42(9), 2083-2100.

Jing, L. **2009**. CAST principle. [Online] Available at: http://www.sootgenerator.com/CAST_principle.htm

Jing, L. **2002.** Influence of air on the soot particles in co-flow diffusion flame. [Online] Available at: http://www.sootgenerator.com/documents/jing_b.pdf

Jorio, A., Dresselhaus, G., Saito, R., and Dresselhaus, G. **2011**. Raman spectroscopy in graphene related systems. *Wiley-VCH, Europe.*

Kasper, M. **2009**. CAST - Combustion aerosol standard: principle and new applications. [Online] Available at: http://www.sootgenerator.com/documents/Kasper.pdf

Keith, L.H. **2015**. The source of US EPA's sixteen pah priority pollutants. *Polycyclic Aromatic Compounds,* 35(2-4), 147-160.

Kesselmeier, J., and Staudt, M. **1999**. Biogenic volatile organic compounds (VOC): an overview on emission, physiology and ecology. *Journal of Atmospheric Chemistry,* 33(1), 23-88.

Kim, S.J., Murthy, H.N., Hahn, E.J., Lee, H L., and Paek, K.Y. **2007**. Parameters affecting the extraction of ginsenosides from the adventitious roots of ginseng (Panax ginseng C.A. Meyer). *Separation and Purification Technology,* 56(3), 401-406.

Kok, L. **2014**. IB chemistry on allotrope of carbon, graphene, alloy and metallic bonding. In. [Online] Available at: https://www.slideshare.net/wkkok1957/ib-chemistry-on-a

Kong, J., Franklin, N.R., Zhou, C., Chapline, M.G., Peng, S., Cho, K., and Dai, H. **2000**. Nanotube molecular wires as chemical sensors. *Science,* 287(5453), 622-625.

Kozbial, A., Li, Z., Sun, J., Gong, X., Zhou, F., Wang, Y., Xu, H., Liu, H., and Li, L. **2014**. Understanding the intrinsic water wettability of graphite. *Carbon,* 74, 218-225.

Kroll, J.H., and Seinfeld, J.H. **2008**. Chemistry of secondary organic aerosol: formation and evolution of low-volatility organics in the atmosphere. *Atmospheric Environment,* 42(16), 3593-3624.

Kuila, T., Bose, S., Khanra, P., Mishra, A.K., Kim, N.H., and Lee, J.H. **2011**. Recent advances in graphene-based biosensors. *Biosensors and Bioelectronics,* 26(12), 4637-4648.

Kumar, R. **2015.** What is the difference between pressure drop and back pressure? [Online] Available at: https://www.researchgate.net/post/What_is_the_difference_between_Pressure_Drop_and_Back_Pressure

Landrigan, P.J., Fuller, R., Acosta, N.J., Adeyi, O., Arnold, R., Baldé, A.B., Bertollini, R., Bose-O'Reilly, S., Boufford, J.L., and Breysse, P.N. **2018**. The Lancet Commission on pollution and health. *The Lancet,* 391(10119), 462-512.

Landrigan, P.J., Fuller, R., Fisher, S., Suk, W. A., Sly, P., Chiles, T.C., and Bose-O'Reilly, S. **2019**. Pollution and children's health. *Science of the Total Environment,* 650, 2389-2394.

Lerner, J.E.C., de los Angeles Gutierrez, M., Mellado, D., Giuliani, D., Massolo, L., Sanchez, E.Y., and Porta, A. **2018**. Characterization and cancer risk assessment of VOCs in home and school environments in gran La Plata, Argentina. *Environmental Science and Pollution Research,* 25(10), 10039-10048.

Li, J., Lu, Y., Ye, Q., Cinke, M., Han, J., and Meyyappan, M. **2003**. Carbon nanotube sensors for gas and organic vapor detection. *Nano Letters,* 3(7), 929-933.

Li, W., Geng, X., Guo, Y., Rong, J., Gong, Y., Wu, L., Zhang, X., Li, P., Xu, J., and Cheng, G. **2011**. Reduced graphene oxide electrically contacted graphene sensor for highly sensitive nitric oxide detection. *ACS Nano,* 5(9), 6955-6961.

Lin, Y., Gong, D., Lv, S., Ding, Y., Wu, G., Wang, H., Li, Y., Wang, Y., Zhou, L., and Wang, B. **2019**. Observations of high levels of ozone-depleting CFC-11 at a remote mountain-top site in southern China. *Environmental Science and Technology Letters*, 6(3), 114-118.

Longworth, J., Krueger, B.P., and Fleming, G.R. **2018**. Photochemical reaction. *Encyclopaedia Britannica*. [Online] Available at: https://www.britannica.com/science/photochemical-reaction

Lu, G., Ocola, L.E., and Chen, J. **2009**. Reduced graphene oxide for room-temperature gas sensors. *Nanotechnology,* 20(44), 445502, 1-9.

Lucattini, L., Poma, G., Covaci, A., de Boer, J., Lamoree, M.H., and Leonards, P.E.G. **2018**. A review of semi-volatile organic compounds (SVOCs) in the indoor environment: occurrence in consumer products, indoor air and dust. *Chemosphere,* 201, 466-482.

Lübeck. **2015**. Dräger-tubes and CMS-handbook: soil, water, and air investigations as well as technical gas analysis. [Online] Available at: https://www.draeger.com/Library/Content/tubes-ca-9092086-en.pdf

Manahan, S. **2017**. Environmental Chemistry. *CRC Press,* 10, 1-784.

Manura, J.J. **2019**. Calculation and use of breakthrough volume data. [Online] Available at: https://www.sisweb.com/index/referenc/resin10.htm

Mastrogiacomo, A.R., Pierini, E., and Sampaolo, L. **1995**. A comparison of the critical parameters of some adsorbents employed in trapping and thermal desorption of organic pollutants. *Chromatographia,* 41(9-10), 599-604.

McMammon C.S., and Woebkenbery, M.L. **1998**. General considerations for sampling airborne contaminants. *NIOSH Manual of Analytical Methods,* 18-20.

Melios, C., Giusca, C.E., Panchal, V., and Kazakova, O. **2018**. Water on graphene: review of recent progress. *2D Materials,* 5(2), 02200, 1-37.

Mueller, L., Schnelle-Kreis, J., Jakobi, G., Orasche, J., Jing, L., Canonaco, F., Prevot, A.S.H., 595 Zimmermann, R. **2016**. Combustion process apportionment of carbonaceous

particulate 596 emission from a diesel fuel burner. *Journal of Aerosol Science*, 100, 61-72.

Mercier, F., Glorennec, P., Thomas, O., and Bot, B.L. **2011**. Organic contamination of settled house dust, a review for exposure assessment purposes. *Environmental Science and Technology,* 45(16), 6716-6727.

Methods for the Determination of Hazardous Substances. **2000**. Volatile Organic Compounds in Air (4). Laboratory method using pumped solid sorbent tubes, solvent desorption and gas chromatography. MDHS 96.

Munyeza, C.F., Osano, A.M, Maghanga, J.K. and Forbes, P.B.C. **2020**. Polycyclic aromatic hydrocarbon gaseous emissions from household cooking devices: a Kenyan case study. *Environmental Toxicology and Chemistry,* 39(3), 538-547.

Munyeza, C.F., Rohwer, E.R., and Forbes, P.B.C. **2019**. A review of monitoring of airborne polycyclic aromatic hydrocarbons: an African perspective. *Trends in Environmental Analytical Chemistry*, e00070.

Munyeza, C.F., Dikale, O., Rohwer, E.R., and Forbes, P.B.C. **2018**. Development and optimization of a plunger assisted solvent extraction method for polycyclic aromatic hyäocarbons sampled onto multi-channel silicone rubber traps. *Journal of Chromatography A,* 1555, 20-29.

National Aeronautics and Space Administration. **2018**. Introduction to ozone air pollution. [Online] Available at: https://science-edu.larc.nasa.gov/ozonegarden/ozone.html

National Environment Management. **2017**. No. 39 of 2004: National Environment Management: Air Quality Act, 2004. *Government Gazette,* 26 October 2018.

National Research Council. **2001**. Climate change science: an analysis of some key questions. *National Academies Press*, 6-7.

Nelson, H.D., and De Ligny, C.L. **1968**. The determination of the solubilities of some n-alkanes in water at different temperatures, by means of gas chromatography. *Recueil des Travaux Chimiques des Pays-Bas,* 87(5), 528-544.

Nollet, L.M.L., and Lambropoulou, D.A. **2017**. Chromatographic Analysis of the Environment : Mass Spectrometry Based Approaches. *Chromatographic Science Series.* 4th Edition.

Nomani, M.W.K., Shishir, R., Qazi, M., Diwan, D., Shields, V.B., Spencer, M.G., Tompa, G.S., Sbrockey, N.M., and Koley, G. **2010**. Highly sensitive and selective detection of NO_2 using epitaxial graphene on 6H-SiC. *Sensors and Actuators B: Chemical,* 150(1), 301-307.

Nørgaard, A.W., Kudal, J., Kofoed-Sørensen, V., Koponen, I., and Wolkoff, P. **2014**. Ozone-initiated VOC and particle emissions from a cleaning agent and an air freshener: risk assessment of acute airway effects. *Environment International,* 68, 209-218.

Novoselov, K.S., Geim, A.K., Morozov, S.V., Jiang, D., Zhang, Y., Dubonos, S.V., Grigorieva and Firsov, A.A. **2004**. Electric field effect in atomically thin carbon films. *Science*, 306(5696), 666-669.

Nyström, R., Sadiktsis, I., Ahmed, T.M., Westerholm, R., Koegler, J.H., Blomberg, A., Sandström T., and Boman, C. **2016**. Physical and chemical properties of RME biodiesel exhaust particles without engine modifications. *Fuel,* 186, 261-269.

O'Keefe B. **2013**. Recent trends in air quality standards in Europe and Asia: what's next? HEI Annual Conference 2012. [Online] Available at: http://www.healtheffects.org/Slides/AnnConf2013/OKeefe-Sun.pdf

Olumayede, E.G. **2014**. Atmospheric volatile organic compounds and ozone creation potential in an urban center of southern Nigeria. *International Journal of Atmospheric Sciences,* 2014. 1-7.

Ortner, E.K., and Rohwer, E.R. **1996**. Trace analysis of semi-volatile organic air pollutants using thick film silicone rubber traps with capillary gas chromatography. *Journal of High Resolution Chromatography*, 19(6), 339-344.

Pan, X., Niu, G., and Liu, H. **2003**. Microwave-assisted extraction of tea polyphenols and tea caffeine from green tea leaves. *Chemical Engineering and Processing: Process Intensification,* 42(2), 129-133.

Pennerman, K.K., AL-Maliki, H.S., Lee, S., and Bennett J.W. **2016**. Chapter 7 – Fungal volatile organic compounds (VOCs) and the Genus *Aspergillus*. *New and Future Developments in Microbial Biotechnology and Bioengineering,* 95-115.

Peters, R.J., and Bakkeren, H.A. **1994**. Sorbents in sampling. Stability and breakthrough measurements. *Analyst,* 119(1), 71-74.

Points, J. **2019**. Global VOC standards to address a volatile global problem: Dr. Ehrenstrofer.

Pöschl, U. **2005**. Atmospheric aerosols: composition, transformation, climate and health effects. *Angewandte Chemie International Edition,* 44(46), 7520-7540.

PubChem. **2020**. [Online] Available at: https://pubchem.ncbi.nlm.nih.gov/

Qu, C., Bai, Y., Jin, X., Wang, Y., Zhang, K., You, J., and Zhang, H. **2009**. Study on ginsenosides in different parts and ages of Panax quinquefolius L. *Food Chemistry,* 115(1), 340-346.

Raza, N., Hashemi, B., Kim, K.H., Lee, S.H., and Deep, A. **2018**. Aromatic hydrocarbons in air, water, and soil: sampling and pretreatment techniques. *TrAC Trends in Analytical Chemistry,* 103, 56-73.

Robinson, J.T., Perkins, F.K., Snow, E.S., Wei,Z., and Sheehan, P.E. **2008**. Reduced graphene oxide molecular sensors. *Nano Letters,* 8(10), 3137-3140.

Roberson, R,. **2012**. GolAir Plus QuadModeSM – split sampling in the highh flow mode. [Online] Available at: https://www.sysmex.nl/fileadmin/media/f102/Environment_Safety/Brochure/GilAir_Plus_QuadMode-High-Flow-Article.pdf

Rohde, A.R., and Muller, R.A**. 2015**. Air pollution in China: mapping of concentrations and sources. *PLoS ONE,* 10(8), e0135749.

Sadasivuni, K.K., Ponnamma, D., Kim, J., and Thomas, S. **2015**. Graphene-based polymer nanocomposites in electronics. *Springer*, 1-382.

Schedin, F., Geim, A., Morozov, S., Hill, E., Blake, P., Katsnelson, M., and Novoselov, K. **2007**. Detection of individual gas molecules adsorbed on graphene. *Nature Materials,* 6(9), 652.

Schoonraad, G.L., Madito, M.J., Manyala, N., and Forbes, P.B.C. **2020**. Synthesis and optimisation of a novel graphene wool material by atmospheric pressure chemical vapour deposition. *Journal of Materials Science*, 55(2), 545-564.

Schoonraad and Forbes; filed on 1 February **2019**. Air pollutant trap, SA provisional patent application 2019/00674 (a).

Schoonraad and Forbes; filed on 1 February **2019**. System and method for manufacturing graphene wool, SA provisional patent application 2019/00675 (b).

Shen, G., Xue, M., Wei, S., Chen, Y., Zhao, Q., Li, B., Wu, H., and Tao, S. **2013**. Influence of fuel moisture, charge size, feeding rate and air ventilation conditions on the emissions of PM, OC, EC, parent PAHs, and their derivatives from residential wood combustion. *Journal of Environmental Sciences,* 25(9), 1808-1816.

Sigma Aldrich. **2019**. Hexane. [Online] Available at: https://www.sigmaaldrich.com/technical-documents/articles/biology/hexane-center.html

Sitko, R., Zawisza, B., and Malicka, E. **2013**. Graphene as a new sorbent in analytical chemistry. *TrAC Trends in Analytical Chemistry,* 51, 33-43.

Sorbent Systems. **2006**. Desiccant chart comparisons. [Online] Available at: https://www.sorbentsystems.com/desiccants_charts.html

Soriano, J.A., García-Contreras, R., Leiva-Candia, D., and Soto, F. **2018**. Influence on performance and emissions of an automotive diesel engine fueled with biodiesel and paraffinic fuels: GTL and biojet fuel farnesane. *Energy and Fuels,* 32(4), 5125-5133.

Suehiro, J., Zhou, G., and Hara, M. **2003**. Fabrication of a carbon nanotube-based gas sensor using dielectrophoresis and its application for ammonia detection by impedance spectroscopy. *Journal of Physics D: Applied Physics,* 36(21), L109.

Supelco. **1986**. Carbotrap carbon black: an excellent adsorbent for solvent or thermal desorption/GC analyses of airborne organic compounds. [Online] Available at: https://www.sigmaaldrich.com/content/dam/sigma-aldrich/docs/Supelco/Bulletin/4501.pdf

Tang, J., Xu, Y., Ma, M., and Wang, Z. **2012**. Comparison of different triolein-based composite semipermeable membranes for passive sampling of organochlorine pesticides. *Chinese Science Bulletin,* 57(15), 1788-1795.

Tang, X., Misztal, P.K., Nazaroff, W.W., and Goldstein, A.H. **2016**. Volatile organic compound emissions from humans indoors. *Environmental Science and Technology,* 50(23), 12686-12694.

Taylor, O. **1969**. Importance of peroxyacetyl nitrate (PAN) as a phytotoxic air pollutant. *Journal of the Air Pollution Control Association,* 19(5), 347-351.

US Environmental Protection Agency. **2018**. What are the trends in indoor air quality and their effects on human health? [Online] Available at: https://www.epa.gov/report-environment/indoor-air-quality

US Environmental Protection Agency. **2017**. Technical overview of volatile organic compounds. [Online] Available at: https://www.epa.gov/indoor-air-quality-iaq/technical-overview-volatile-organic-compounds#8

US Environmental Protection Agency. **1999**. Compendium method TO-17 determination of volatile organic compounds in ambient air using active sampling onto sorbent tubes. [Online] Available at: https://www3.epa.gov/ttnamti1/files/ambient/airtox/to-17r.pdf

US Environmental Protection Agency. **1986**. Compendium of methods for the determination of air pollutants in indoor air: IP-1B. [Online] Available at: https://archive.epa.gov/region1/info/testmethods/web/pdf/600490010_epa_compendmethod-indoorairpollutants_p1.pdf

Valentini, L., Mercuri, F., Armentano, I., Cantalini, C., Picozzi, S., Lozzi, L., Santucci, S., Sgamellotti, A., and Kenny, J. **2004**. Role of defects on the gas sensing properties of carbon nanotubes thin films: experiment and theory. *Chemical Physics Letters,* 387, 356-361.

Vandenbroucke, A. **2015**. Abatement of volatile organic compounds by combined use of non-thermal plasma and heterogeneous catalysis. Doctoral dissertation, Ghent University.

Vyskocil, A., Viau, C., and Lamy, S. **1998**. Peroxyacetyl nitrate: review of toxicity. *Human and Experimental Toxicology,* 17(4), 212-220.

Wang, S., Wu, D., Wang, X.M., Fung, J.C.H., and Yu, J.Z. **2013**. Relative contributions of secondary organic aerosol formation from toluene, xylenes, isoprene, and monoterpenes in Hong Kong and Guangzhou in the Pearl River Delta, China: an emission-based box modeling study. *Journal of Geophysical Research: Atmospheres,* 118(2), 507-519.

Wang, X., Liu, B., Lu, Q., and Qu, Q. **2014**. Graphene-based materials: fabrication and application for adsorption in analytical chemistry. *Journal of Chromatography A,* 1362, 1-15.

Warwick. **2010**. Transission electron microscpy (TEM). [Online] Available at: https://warwick.ac.uk/fac/sci/physics/current/postgraduate/regs/mpagswarwick/ex5/techniques/structural/tem/

Weingartner, E., Burtscher, H., and Baltensperger, U. **1997**. Hygroscopic properties of carbon and diesel soot particles. *Atmospheric Environment,* 31(15), 2311-2327.

World Health Organization. **2019**. Air pollution. [Online] Available at: https://www.who.int/airpollution/en/

World Health Organization. **2014.** WHO methods and data sources for global causes of death 2000–2012. [Online] Available at: http://www.who.int/entity/healthinfo/global_burden_disease/GlobalCOD_method_2000_2012.pdf

World Health Organization. **2012**. Burden of disease from the joint effects of household and ambient air pollution for 2012. WHO Technical Report. [Online] Available at: http://www.who.int/phe/health_topics/outdoorair/databases/AP_jointeffect_BoD_results_March2014.pdf

World Health Organization. **1989**. Indoor air quality: organic pollutants. *Environmental Technology Letters,* 10(9), 855-858.

World Meteorological Organization. **2017**. GAW research on reactive gases. [Online] Available at: http://www.wmo.int/pages/prog/arep/gaw/reactive_gases.html

Woolfenden, E. **2010**. Sorbent-based sampling methods for volatile and semi-volatile organic compounds in air. Part 2: sorbent selection and other aspects of optimizing air monitoring methods. *Journal of Chromatography A,* 1217(16), 2685-2694.

World Population Review. **2019**. China population. [Online] Available at: http://worldpopulationreview.com/countries/china-population/

Wu, W., Zhao, B., Wang, S., and Hao, J. **2017**. Ozone and secondary organic aerosol formation potential from anthropogenic volatile organic compounds emissions in China. *Journal of Environmental Sciences,* 53, 224-237.

Xu, Y., and Zhang, J. **2011**. Understanding SVOCs. *ASHRAE Journal,* 53(12), 121-125.

Yan, B., Liu, S., Zhao, B., Li, X., Fu, Q., and Jiang, G. **2018**. China's fight for clean air and human health. *ACS Publications*, 8063-8064.

Yang, K., Feng, L., and Liu, Z. **2015**. The advancing uses of nano-graphene in drug delivery. *Expert Opinion on Drug Delivery,* 12(4), 601-612.

Yang G., Wang Y., Zeng Y., Gao G.F., Liang X., Zhou M., Wan, X., Yu, S., Jiang, Y., Naghavi, M., Vos, T., Wang, H., Lopez, A.D., Murray, C.J.L. **2013.** Rapid health transition in China, 1990– 2010: findings from the Global Burden of Disease Study 2010. *Lancet*, 381, 1987-2015.

Yi, J., Lee, J.M., and Park, W.I. **2011**. Vertically aligned ZnO nanorods and graphene hybrid architectures for high-sensitive flexible gas sensors. *Sensors and Actuators B: Chemical,* 155(1), 264-269.

Yu, C.W.F., and Kim, J.T. **2010**. Building pathology, investigation of sick buildings—VOC emissions. *Indoor and Built Environment,* 19(1), 30-39.

Yuan, W., Liu, A., Huang, L., Li, C., and Shi, G. **2013**. High-performance NO_2 sensors based on chemically modified graphene. *Advanced Materials,* 25(5), 766-771.

Yuan, W., and Shi, G. **2013**. Graphene-based gas sensors. *Journal of Materials Chemistry A,* 1(35), 10078-10091.

Zaranksi, M.T., and Bidlemen, T.F. **1987**. High-volume elution chromatography of dichlorobenzenes on a polyurethan foam-Tenx sandwich cartridge. *Journal of Chromatography,* 409, 235-242.

Zhang, L., Li, C., Liu, A., and Shi, G. **2012**. Electrosynthesis of graphene oxide/polypyrene composite films and their applications for sensing organic vapors. *Journal of Materials Chemistry,* 22(17), 8438-8443.

Zhang, S., Chen, R., Wu, H., and Wang, C. **2006**. Ginsenoside extraction from Panax quinquefolium L. (American ginseng) root by using ultrahigh pressure. *Journal of Pharmaceutical and Biomedical Analysis,* 41(1), 57-63.

Zhang, Z., Zou, R., Song, G., Yu, L., Chen, Z., and Hu, J. **2011**. Highly aligned SnO_2 nanorods on graphene sheets for gas sensors. *Journal of Materials Chemistry,* 21(43), 17360-17365.

Zhao, J., Ren, W., and Cheng, H.M. **2012**. Graphene sponge for efficient and repeatable adsorption and desorption of water contaminations. *Journal of Materials Chemistry,* 22(38), 20197-20202.

Zhou, S., Zhou, J., and Zhu, Y. **2019**. Chemical composition and size distribution of particulate matters from marine diesel engines with different fuel oils. *Fuel,* 235, 972-983.

Zhu, Z.W., and Zheng Q.R. **2016**. Methane adsorption on the graphene sheets, activated carbon and carbon black. *Applied thermal Engineering,* 108, 605-613.

Züttel, A., Sudan, P., Mauron, P., and Wenger, P. **2004**. Model for the hydrogen adsorption on carbon nanostructures. *Applied Physics A,* 78(7), 941-946.

Appendices

Appendix A: TWA, STEL and TLV® Basis of VOCs and SVOCs investigated in the laboratory-based studies

Table A1: A list of the 60 VOCs used in selected studies with associated CAS no.s, TWAs, STELs, TLV® basis.

Compound name	CAS no.	TWA (ppm)	STEL (ppm)	TLV® Basis	Source
Chloromethane (gas)	74-87-3	50	100	CNS impairment; liver & kidney damage; testicular damage; teratogenic effects	(ACGIH 2012)
Vinyl chloride (gas)	75-01-4	1	-	Lung cancer; liver damage	(ACGIH 2012)
Chloroethane (gas)	75-00-3	100	-	Liver damage	(ACGIH 2012)
Benzene	71-43-2	0.5	2.5	Leukaemia	(ACGIH 2012)
Dichloromethane	75-09-2	50	-	COHb-emia; CNS impairment	(ACGIH 2012)
Toluene	108-88-3	20	-	Visual impairment; female reproductive damage; pregnancy loss	(ACGIH 2012)
Bromomethane (gas)	74-83-9	1	-	URT & skin irritation	(ACGIH 2012)
1,1-Dichloroethene (Vinylidene chloride)	75-35-4	5	-	Liver & kidney damage	(ACGIH 2012)
trans-1,2-dichloroethene (trans-1,2-dichloroethylene)	156-60-5	200	-	CNS impairment; eye irritation	(ACGIH 2012)
cis-1,2-Dichloroethene	156-59-2	200	-	CNS impairment; eye irritation	(ACGIH 2012)
1,2-Dichloroethane (Ethylene dichloride)	107-06-2	10	-	Liver damage; nausea	(ACGIH 2012)
1,1-Dichloroethane	75-34-3	100	-	URT & eye irritation; liver & kidney damage	(ACGIH 2012)
Styrene	100-42-5	20	40	CNS impairment; URT irritation; peripheral neuropathy	(ACGIH 2012)

Ethylbenzene	100-41-4	20	-	URT irritation; kidney damage (nephropathy); cochlear impairment	(ACGIH 2012)
m-Xylene	108-38-3	100	150	URT & eye irritation; CNS impairment	(ACGIH 2012)
o-Xylene	95-47-6	100	150	URT & eye irritation; CNS impairment	(ACGIH 2012)
p-Xylene	106-42-3	100	150	URT & eye irritation; CNS impairment	(ACGIH 2012)
1,1-Dichloropropene	563-58-6	-	-	-	-
cis-1,3-Dichloropropene	10061-01-5	1	-	Eyes & Skin & URT irritation; CNS impairment; liver & kidney damage	(NIOSH 2018d)
trans-1,3-Dichloropropene	10061-02-6	1	-	Eyes & skin & URT irritation; CNS impairment; kidney and liver damage	(NIOSH 2018d)
Chlorobenzene	108-90-7	10	-	Liver damage	(ACGIH 2012)
1,2-Dichloropropane (Propylene dichloride)	78-87-5	10	-	URT irr; body weight effects	(ACGIH 2012)
1,3-Dichloropropane	142-28-9	-	-	-	-
2,2-Dichloropropane	594-20-7	-	-	-	-
Chloroform	67-66-3	10	-	Liver damage; embryo/fetal damage; CNS impairment	(ACGIH 2012)
Isopropylbenzene (Cumene)	98-82-8	50	-	Eye, Skin and URT irritation; CNS impairment	(ACGIH 2012)
1,3,5-Trimethylbenzene	108-67-8	25	-	Eye & skin & URT irritation; CNS impairment; hypochromic anaemia	(NIOSH 2018e)
Propylbenzene	103-65-1	-	-	-	-
1,2,4-Trimethylbenzene	95-63-6	25	-	Eye & skin & URT irritation; CNS impairment; hypochromic anaemia	(NIOSH 2018c)
Dichlorodifluoromethane (gas)	75-71-8	1000	-	Cardiac sensitization	(ACGIH 2012)
2-Chlorotoluene	95-49-8	50	-	URT, eye & skin irritation	(ACGIH 2012)

4-Chlorotoluene	106-43-4	-	-	-	-
Naphthalene	91-20-3	5	-	URT irritation	(ACGIH 2012)
Bromochloromethane	74-97-5	200	-	CNS impairment; liver damage	(ACGIH 2012)
Trichloroethene	79-01-6	10	25	CNS impairment; cognitive decrements; renal toxicity	(ACGIH 2012)
1,1,2-Trichloroethane	79-00-5	10	-	CNS impairment; liver damage	(ACGIH 2012)
1,1,1-Trichloroethane (methyl chloroform)	71-55-6	350	450	CNS impairment; liver damage	(ACGIH 2012)
n-Butylbenzene	104-51-8	-	-	-	-
p-Isopropyltoluene	99-87-6	-	-	-	-
sec-Butylbenzene	135-98-8	-	-	-	-
tert-Butylbenzene	98-06-6	-	-	-	-
Trichlorofluoromethane (gas)	75-69-4	-	C 1000	Cardiac sensitization	(ACGIH 2012)
1,3-Dichlorobenzene	541-73-1	10		Liver & kidney damage	(Toxnet 2008)
1,2-Dichlorobenzene	95-50-1	25	50	URT & eye irritation; liver damage	(ACGIH 2012)
1,4-Dichlorobenzene	106-46-7	10	-	Eye irritation; kidney damage	(ACGIH 2012)
1,2,3-Trichloropropane	96-18-4	0.05	-	Cancer; eye & URT irritation; liver damage	(ACGIH 2012)
Carbon tetrachloride	56-23-5	5	10	Liver damage	(ACGIH 2012)
Bromobenzene	108-86-1	0.5	-	Eye & skin & URT irritation	(Molbase 2015)
Bromodichloromethane	75-27-4	-	-	-	-
Tetrachloroethene	127-18-4	25	100	CNS impairment	(ACGIH 2012)

1,1,1,2-Tetrachloroethane	79-34-5	1	-	Liver damage	(ACGIH 2012)
1,1,2,2-Tetrachloroethane	79-34-5	1	-	Liver damage	(ACGIH 2012)
Dibromomethane	74-95-3	0.045	C 0.13 (15min)	Eyes & skin & URT irritation; Liver & kidney & reproductive damage	(NIOSH 2018f)
1,2,3-Trichlorobenzene	87-61-6	-	2.25	Eye & skin & URT irritation	(ATSDR 2010)
1,2,4-Trichlorobenzene	120-82-1	-	C 5	Eye & URT irritation	(ACGIH 2012)
1,2-Dibromoethane (Ethylene dibromide)	106-93-4	0.045	C 0.13 (15 min)	Eyes & skin & URT irritation; liver & kidney and reproductive system damage	(NIOSH 2018b)
Dibromochloromethane	124-48-1	-	-	-	-
1,2-Dibromo-3-Chloropropane	96-12-8	0.001	-	Eyes & skin & URT irritation; CNS impairment; liver & kidney & spleen & reproductive system & digestive system damage	(NIOSH 2018a)
Bromoform	75-25-2	0.5	-	Liver dam; URT and eye irritation	(ACGIH 2012)
Hexachlorobutadiene	87-68-3	0.02	-	Kidney damage	(ACGIH 2012)

Abbreviations: C; *Ceiling limit - a value that may not be exceeded for any amount of time,* ***CAS no****; Chemical Abstracts Service number,* ***CNS;*** *Central nervous system,* ***COHb-emia;*** *Carboxyhemoglobinemia,* ***ppm;*** *Parts of vapor or gas per million parts of contaminated air by volume at NTP conditions (25°C; 760 Torr),* ***Q;*** *Quantification,* ***Skin;*** *Danger of cutaneous absorption,* ***STEL;*** *Short-term exposure limit,* ***TLV®;*** *Threshold limit value,* ***TLV® basis;*** *the adverse effect(s) upon which the TLV® is based,* ***TWA;*** *time-weighted average,* ***URT;*** *Upper respiratory tract.*

Table A2: A list of the 16 PAH SVOCs used in selected studies with associated CAS no.s, TWAs, STELs, TLV® basis.

Compound name	Abbr.	CAS no.	TWA	STEL	TLV® Basis	Source
Naphthalene	NAP	91-20-3	10 ppm	15 ppm	URT irritation; cataracts; haemolytic anaemia	(ACGIH 2012)
Acenaphthylene	ACY	208-96-8	-	-	Eyes & skin & URT irritation	(PubChem 2018a)
Acenaphthene	ACE	83-32-9	-	-	Eyes & skin & URT irritation; kidney and liver damage	(NOISH 2018)
Fluorene	FLU	86-73-7	-	-	Eyes & skin & URT irritation	(PubChem 2018h)
Anthracene	ANTH	120-12-7	0.2 $mg.m^{-3}$	-	Eyes & skin & URT irritation; carcinogenic; female reproductive damage; danger to unborn child	(PubChem 2018b; US Department of Labour, 2020)
Phenanthrene	PHEN	85-01-8	-	-	Eyes & skin & URT irr; kidney damage	(NOISH 2018)
Fluoranthene	FLTH	206-44-0	-	-	Eyes & skin & URT irr; cardiac sensitization; liver damage	(PubChem 2018g)
Pyrene	PYR	129-00-0	0.2 $mg.m^{-3}$	-	Eyes & skin & URT irritation	(NOISH 2018 US Department of Labour, 2020)
Benzo[a]anthracene	B[a]A	56-55-3	-	-	Carcinogenic	(PubChem 2018c)
Chrysene	CHRY	218-01-9	0.2 $mg.m^{-3}$	-	Carcinogenic	(NOISH 2018; ACGIH 2012 US Department of Labour, 2020)
Benzo[a]pyrene	B[a]P	50-32-8	0.2 $mg.m^{-3}$	-	Eyes & skin & URT irritation; carcinogenic; female reproductive damage; danger to unborn child	(NOISH 2018 US Department of Labour, 2020)
Benzo[a]fluoranthene	B[a]F	203-33-8	-	-	-	-
Benzo[k]fluoranthene	B[k]F	207-08-9	-	-	Carcinogenic	(PubChem 2018e)

Benzo[g,h,i]perylene	B[ghi]P	191-24-2	-	-	Eyes & skin & URT irritation	(PubChem 2018d)
Indeno[1,2,3-c,d]pyrene	IND	193-39-5	-	-	Carcinogenic	(PubChem 2018i)
Dibenz[a,h]anthracene	D[ah]A	53-70-3	-	-	Carcinogenic	(PubChem 2018f)

Abbreviations: CAS no*; Chemical Abstracts Service number,* ***ppm;*** *Parts of vapor or gas per million parts of contaminated air by volume at NTP conditions (25°C; 760 Torr),* ***Q;*** *Quantification,* ***Skin;*** *Danger of cutaneous absorption,* ***STEL;*** *Short-term exposure limit,* ***TLV®;*** *Threshold limit value,* ***TLV® basis;*** *the adverse effect(s) upon which the TLV® is based,* ***TWA;*** *Time-weighted average,* ***URT;*** *Upper respiratory tract.*

Table A3: A list of the 13 HC SVOCs used in selected studies with associated CAS no.s, TWAs, STELs, TLV® basis.

Compound name	CAS no.	TWA (ppm)	STEL (ppm)	TLV® Basis	Source
n-Octane	111-65-9	300	-	URT irr	(ACGIH 2012)
n-Nonane	111-84-2	200	-	CNS impair	(ACGIH 2012)
n-Decane	1224-18-5	-	-	-	-
n-Undecane	1120-21-4	-	-	-	-
n-Dodecane	112-40-3	-	-	-	-
n-Tridecane	629-50-5	-	-	-	-
n-Tetradecane	629-59-4	-	-	-	-
n-Pentadecane	629-62-9	-	-	-	-
n-Hexadecane	544-76-3	-	-	-	-
n-Heptadecane	629-78-7	-	-	-	-
n-Octadecane	593-45-3	-	-	-	-
n-Nonadecane	629-92-5	-	-	-	-
n-Eicosane	112-95-8	-	-	-	-

Abbreviations: CAS no*; Chemical Abstracts Service number,* ***CNS;*** *Central nervous system,* ***ppm;*** *Parts of vapor or gas per million parts of contaminated air by volume at NTP conditions (25°C; 760 Torr),* ***STEL;*** *Short-term exposure limit,* ***TLV®;*** *Threshold limit value,* ***TLV® basis;*** *the adverse effect(s) upon which the TLV® is based,* ***TWA;*** *Time-weighted average,* ***URT;*** *Upper respiratory tract.*

Appendix B: Molecular masses, quantification ions and chemical structures of VOCs and SVOCs investigated in the laboratory-based studies

Table B1a: 60 compound VOC analyte mixture with associated CAS numbers, molecular weights, primary and secondary quantification ions as well as their chemical structures.

VOCs				
Compound name	CAS no.	MM ($g.mol^{-1}$)	1°; 2° Q ion	Structure
Chloromethane (gas)	74-87-3	50	50; 15	
Vinyl chloride (gas)	75-01-4	62	27; 62	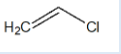
Chloroethane (gas)	75-00-3	64	64; 28	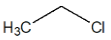
Benzene	71-43-2	78	78; 77	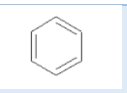
Dichloromethane	75-09-2	84	49; 84	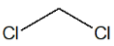
Toluene	108-88-3	92	91; 92	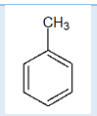
Bromomethane (gas)	74-83-9	94	94; 96	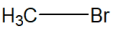
1,1-Dichloroethene (Vinylidene chloride)	75-35-4	96	61; 96	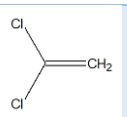
trans-1,2-dichloroethene (trans-1,2-dichloroethylene)	156-60-5	96	61; 96	
cis-1,2-Dichloroethene	156-59-2	96	61; 96	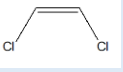
1,2-Dichloroethane (Ethylene dichloride)	107-06-2	98	62; 64	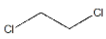
1,1-Dichloroethane	75-34-3	98	63; 65	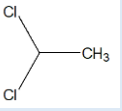
Styrene	100-42-5	104	104; 78	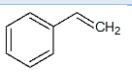
Ethylbenzene	100-41-4	106	91; 106	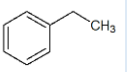

m-Xylene	108-38-3	106	91; 106	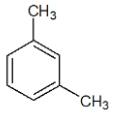
o-Xylene	95-47-6	106	91; 106	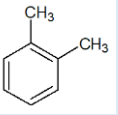
p-Xylene	106-42-3	106	91; 106	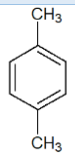
1,1-Dichloropropene	563-58-6	110	75; 39	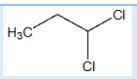
cis-1,3-Dichloropropene	10061-01-5	110	75; 39	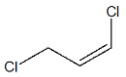
trans-1,3-Dichloropropene	10061-02-6	110	75; 39	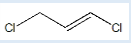
Chlorobenzene	108-90-7	112	112; 77	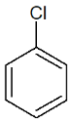
1,2-Dichloropropane (Propylene dichloride)	78-87-5	112	63; 62	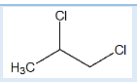
1,3-Dichloropropane	142-28-9	112	76; 41	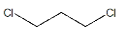
2,2-Dichloropropane	594-20-7	112	77; 41	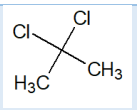
Chloroform	67-66-3	118	83; 85	
Isopropylbenzene (Cumene)	98-82-8	120	105; 120	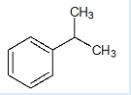
1,3,5-Trimethylbenzene	108-67-8	120	105; 120	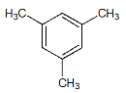
Propylbenzene	103-65-1	120	91; 120	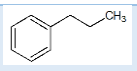
1,2,4-Trimethylbenzene	95-63-6	120	105; 120	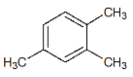
Dichlorodifluoromethane (gas)	75-71-8	120	85; 87	

2-Chlorotoluene	95-49-8	126	91; 126	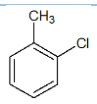
4-Chlorotoluene	106-43-4	126	91; 126	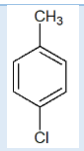
Naphthalene	91-20-3	128	128	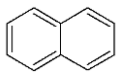
Bromochloromethane	74-97-5	128	49; 130	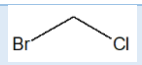
Trichloroethene	79-01-6	130	130; 95	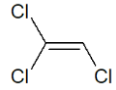
1,1,2-Trichloroethane	79-00-5	130	130; 95	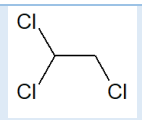
1,1,1-Trichloroethane (methyl chloroform)	71-55-6	132	97; 99	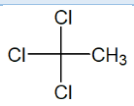
n-Butylbenzene	104-51-8	134	91; 92	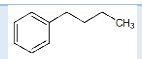
p-Isopropyltoluene	99-87-6	134	119; 134	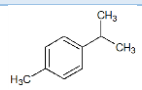
sec-Butylbenzene	135-98-8	134	105; 134	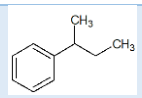
tert-Butylbenzene	98-06-6	134	119; 91	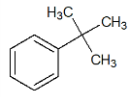
Trichlorofluoromethane (gas)	75-69-4	136	101; 103	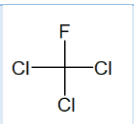
1,3-Dichlorobenzene	541-73-1	146	146; 148	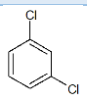
1,2-Dichlorobenzene	95-50-1	146	146; 148	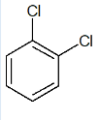
1,4-Dichlorobenzene	106-46-7	146	146; 148	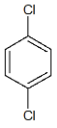
1,2,3-Trichloropropane	96-18-4	146	75; 101	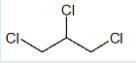

Carbon tetrachloride	56-23-5	152	117; 119	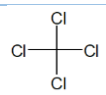
Bromobenzene	108-86-1	156	77; 156	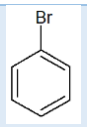
Bromodichloromethane	75-27-4	162	83; 85	
Tetrachloroethene	127-18-4	164	166; 164	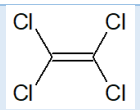
1,1,1,2-Tetrachloroethane	79-34-5	166	131; 133	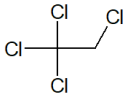
1,1,2,2-Tetrachloroethane	79-34-5	166	83; 85	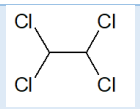
Dibromomethane	74-95-3	172	174; 93	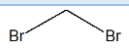
1,2,3-Trichlorobenzene	87-61-6	180	180; 182	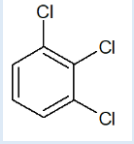
1,2,4-Trichlorobenzene	120-82-1	180	180; 182	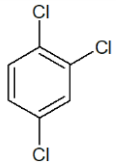
1,2-Dibromoethane (Ethylene dibromide)	106-93-4	186	107; 109	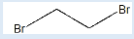
Dibromochloromethane	124-48-1	206	129; 127	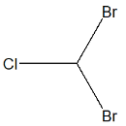
1,2-Dibromo-3-Chloropropane	96-12-8	234	157; 75	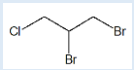
Bromoform	75-25-2	250	173; 171	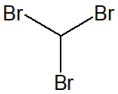
Hexachlorobutadiene	87-68-3	258	225; 223	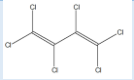

Abbreviations: CAS no*; Chemical Abstracts Service number,* ***MM****; molecular mass,* ***1º****; primary,* ***2º****; secondary,* ***Q****; quantification.*

Table B1b: The deuterated VOC internal standard

Deuterated IS			
Compound name	CAS no	MM (g.mol^{-1}); Q ion	Structure
d8-naphthalene	1146-65-2	136	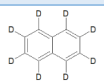

Abbreviations: ***CAS no****; Chemical Abstracts Service number,* ***MM****; molecular mass,* ***1°****;* ***Q****; quantification.*

Table B2: 16 compound PAH mixture along with the associated CAS numbers, molecular masses, primary quantification ions as well as their chemical structures.

PAHs				
Compound name	Abbr.	CAS no.	MM (g.mol^{-1}); Q ion	Structures
Naphthalene	NAP	91-20-3	128	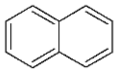
2-Bromonaphthalene	BNAP	580-13-2	206; 127	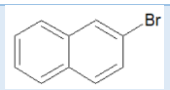
Acenaphthylene	ACY	208-96-8	152	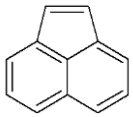
Acenaphthene	ACE	83-32-9	153	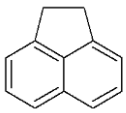
Fluorene	FLU	86-73-7	166	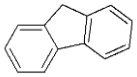
Phenanthrene	PHEN	85-01-8	178	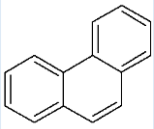
Anthracene	ANTH	120-12-7	178	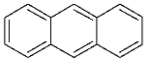
Fluoranthene	FLTH	206-44-0	202	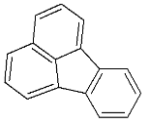
Pyrene	PYR	129-00-0	202	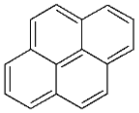
Benzo[a]anthracene	B[a]A	56-55-3	228	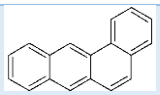

Chrysene	CHRY	218-01-9	228	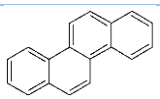
Benzo[a]fluoranthene	B[a]F	203-33-8	252	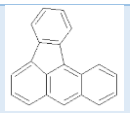
Benzo[a]pyrene	B[a]P	50-32-8	252	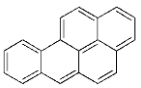
Benzo[g,h,i]perylene	B[ghi]P	191-24-2	276	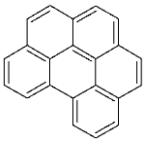
Indeno[1,2,3-c,d]pyrene	IND	193-39-5	276	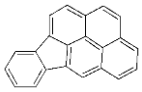
Dibenz[a,h]anthracene	D[ah]A	53-70-3	278	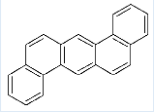

Abbreviations: CAS no*; Chemical Abstracts Service number,* ***MM****; molecular mass,* ***1°****; primary,* ***Q****; quantification.*

Table B3a: Hydrocarbon (C_8-C_{20}) mixture with associated CAS numbers, molecular masses along with associated primary quantification ions as well as their chemical structures.

Alkanes				
Compound name	CAS no.	MM ($g.mol^{-1}$)	1° Q ion	Structures
n-Octane	111-65-9	114	57	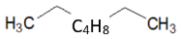
n-Nonane	111-84-2	128	57	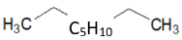
n-Decane	1224-18-5	142	57	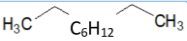
n-Undecane	1120-21-4	156	57	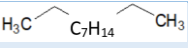
n-Dodecane	112-40-3	170	57	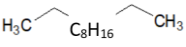
n-Tridecane	629-50-5	184	57	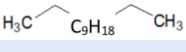
n-Tetradecane	629-59-4	198	57	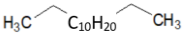
n-Pentadecane	629-62-9	212	57	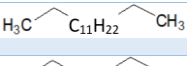
n-Hexadecane	544-76-3	226	57	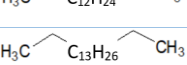
n-Heptadecane	629-78-7	240	57	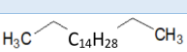
n-Octadecane	593-45-3	254	57	

n-Nonadecane	629-92-5	268	57	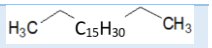
n-Eicosane	112-95-8	282	57	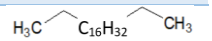

Abbreviations: CAS no*; Chemical Abstracts Service number,* ***MM****; molecular mass,* ***1°****; primary,* ***Q****; quantification.*

Table B3b: The deuterated standard with which hydrocarbon target analytes were quantified.

Deuterated IS				
Compound name	CAS no.	MM ($g.mol^{-1}$)	1° Q ion	Structure
d34-hexadecane	544-76-3	260	50	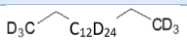

Abbreviations: CAS no*; Chemical Abstracts Service number,* ***MM****; molecular mass,* ***1°****; primary,* ***Q****; quantification.*

Appendix C: Summary of sampling and analytical techniques

Table C1: A summary of sampling techniques, the retaining media used and the subsequent analytical techniques used to target specific compounds from stated sampling sites. ***Source:*** *Adapted from Nollet and Lambropoulou (2017).*

Sampling Technique	Retaining Media	Analytical Technique	Target Compounds	Sampling Site	Source
Cryogenic trap	Glass bead trap (-170'C)	GC-MS	Aromatic hydrocarbons, chlorofluorocarbons, and chlorinated hydrocarbons	Buildings in nuclear power plants	(Hsieh et al. 2006)
Impinger	Water	HPLC-UV and IC	Thioglycolic acid, dithioglycolic acid, and ammonia	Beauty salon	(Oikawa et al. 2012)
OTT	PDMS	GC-FID and GC-MS	Aromatic hydrocarbons and acetate esters	Wood working shop	(Dudek et al. 2002)
SPME	PDMS	GC-MS	Alkanes, aromatics, and chlorinated hydrocarbons	Flat rooms and chemical laboratories	(Gorlo et al. 1999)
SPME	PDMS; PEG	GC-MS	Phenol	Biologics production areas	(Es-haghi, Baghernejad , and Bagheri 2012)
SPME	PDMS	GC-NPD	Organophosphate triesters	Lecture room	(Isetun, Nilsson, and Colmsjö 2004)
NTD	MA/EGDMA; Tenax TA; activated carbon; DVB	GC-MS	Aromatic hydrocarbons	Rooms	(Ueta et al. 2012)
NTD	Tenax TA; Carbopack X	GC-MS	Alkanes, aromatic hydrocarbons, acetate esters, aldehydes, ketones, furans, and chlorinated hydrocarbons	Chemical laboratories	(Alonso et al. 2011)
SPDE	PDMS	GC-FID	Toluene	Room	(Van Durme et al. 2007)
GPE	PDMS	GC-MS	Nicotine	Hospital rooms	(Baltussen et al. 1999)
Adsorption system	Chromosorb 102	GC-FPD	Organophosphorus pesticides	Home and childcare facilities in an agricultural community	(Kawahara et al. 2005)
Adsorption system	Tenax GR and Carbosieve SIII	GC-MS	Alkanes, aromatic hydrocarbons, PAHs, alcohols, ketones, halogenated hydrocarbons, and trepenoids	Residences in industrial, urban, and suburban areas	(Jia, Batterman, and Godwin 2008b)
Adsorption system	Carbograph 4	GC-MS	α-Pinene, 3-carene, and D-limonene	Residences in urban areas	(Król, Namieśnik,

					and Zabiegała 2014)
Adsorption trap/ SPME	Tenax TA/PS; PDMS; PDMS/DVB; CAR/PDMS; DVB/CAR/PDMS	GC-MS	Synthetic musks	Residential area	(Regueiro et al. 2009)
MESI	Tenax	GC-FID	α-Pinene, eucalyptol and γ-terpinene	Greenhouse	(Liu et al. 2004)
Cryogenic Trap	Glass wool trap (-186'C or -196'C)	GC-FPD	Reduced sulfur compounds	Tropical urban area	(Campos et al. 2010)
Cryogenic Trap	Glass bead trap (-170'C)	GC-FID and GC-MS	Alkanes, alkenes, alkynes, aromatic hydrocarbons, halogenated hydrocarbons, ethers, esters, ketones, furans and VSC's	Urban areas	(Wang, Chang, and Lee 2012)
Cryogenic Trap	Glass bead trap (-170'C)	GC-MS and GC-FID	MTBE, alkanes, alkenes, alkynes, aromatic hydrocarbons, and halogenated hydrocarbons	Urban areas	(Chang et al. 2003)
Annular denuder	DNPH and phosphoric acid in acetonitrile	HPLC-UV	Formaldehyde and acetaldehyde	Urban areas	(Komazaki et al. 1999)
Annular denuder	Citric acid in water	HPLC-FLD	Ammonia and four alkylamines	Urban and semi-rural areas	(Huang, Hou, and Zhou 2009)
NTD	Tenax TA; Carbopack X	GC-MS	Aromatic hydrocarbons, aldehydes, ketones, and furans	Pedestrian areas	(Alonso et al. 2011)
GPE	PDMS	GC-MS and GC-ECD	PAHs and nitro-PAHs	Rural area	(Baltussen et al. 2005)
Adsorption system	Activated carbon; Carbotrap B	GC-MS and GC-FID	Aromatic hydrocarbons	Urban area	(Czaplicka and Klejnowski 2002)
Adsorption system	Chromosorb 102	GC-FPD	Organophosphorus pesticides	Area nearby a pesticide-applied farm	(Kawahara et al. 2005)
Adsorption system	Tenax GR and Carbosieve SIII	GC-MS	Alkanes, aromatic hydrocarbons, PAHs, alcohol, ketones, halogenated hydrocarbons, and terpenoids	Industrial, urban and suburban areas	(Jia, Batterman, and Godwin 2008a)
Adsorption system	Activated carbon; Tenax TA and Carbograph ITD	GC-MS	Alkanes, alkenes, aromatic hydrocarbons, PAHs, alcohol, ethers, furans, nitriles, and halogenated hydrocarbons	Area nearby a petrochemical complex	(Ramirez et al. 2010)
Adsorption system	Carbograph 4	GC-MS	Benzene	Urban areas	(Krol, Zabiegala,

					and Namiesnik 2012)
SPMD	Triolein	GC-MS	PAHs and PCBs	Area nearby wind tunnel	(Söderström and Bergqvist 2004)

***Abbreviations**: **GC-ECD**; gas chromatography coupled to an electron capture detector, **GC-FID**; gas chromatography coupled to flame ionization detector, **GC-FPD**; gas chromatography coupled to a flame photometric detector, **GC-MS**; gas chromatography coupled to mass spectrometry, **GC-NPD**; gas chromatography coupled to nitrogen phosphorous detector, **GPE**; gum-phase extraction, **HPLC-FLD**; high performance liquid chromatography coupled to a fluorescence detector, **HPLC-UV**; high performance liquid chromatography coupled to ultraviolet detection technology, **IC**; ion chromatography, **MESI**; membrane extraction with a sorbent interface, **MTBE**; methyl tert-butyl ether, **NTD**; needle microextraction trap, **OTT**; denudation trap with film 100 μm thick, **PCB**; polychlorinated biphenyl, **PDMS**; polydimethylsiloxane, **SPDE**; solid-phase dynamic extraction, **SPMD**; semipermeable membrane devices, **SMPE**; solid-phase microextraction*

Appendix D: Instrument calibration curves for the 16 PAHs investigated in the PASE study

Calibration curves for individual PAHs in PAH mix made up in neat hexane (*N*=3)

Calibration curve for naphthalene in neat solvent

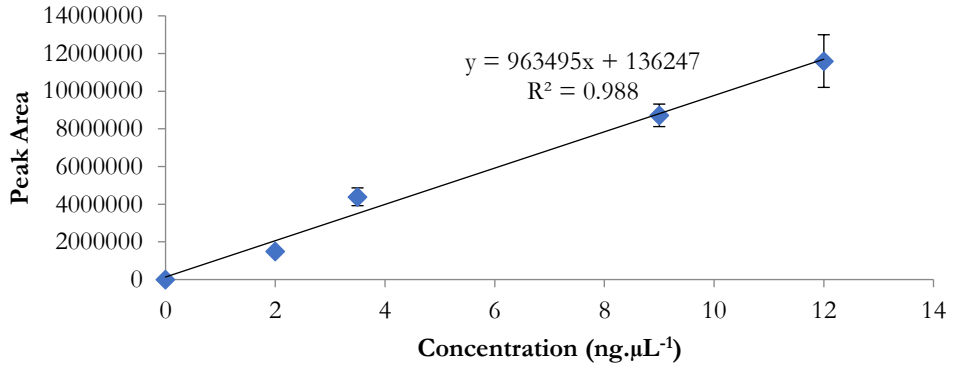

Calibration curve for acenaphthylene in neat solvent

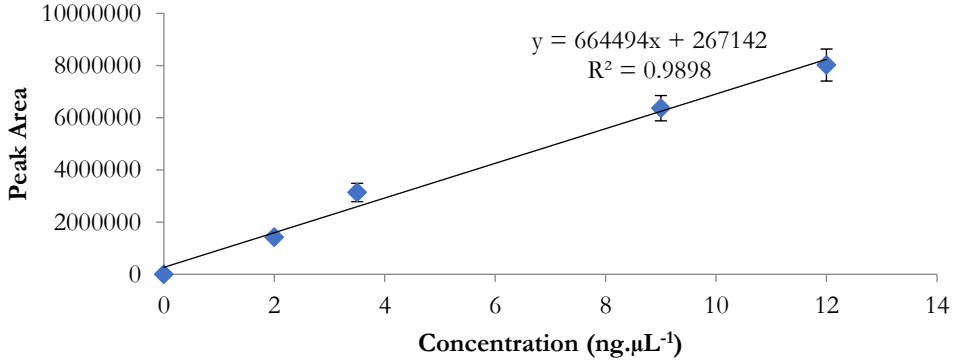

Calibration curve for acenaphthene in neat solvent

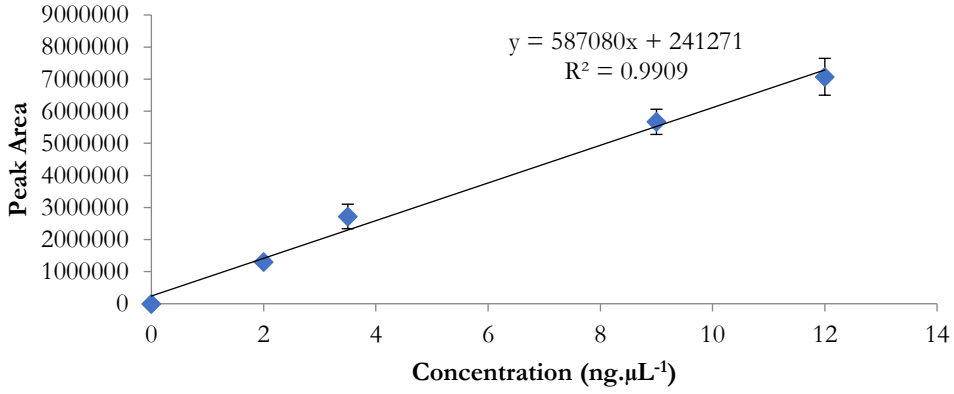

Calibration curve for fluorene in neat solvent

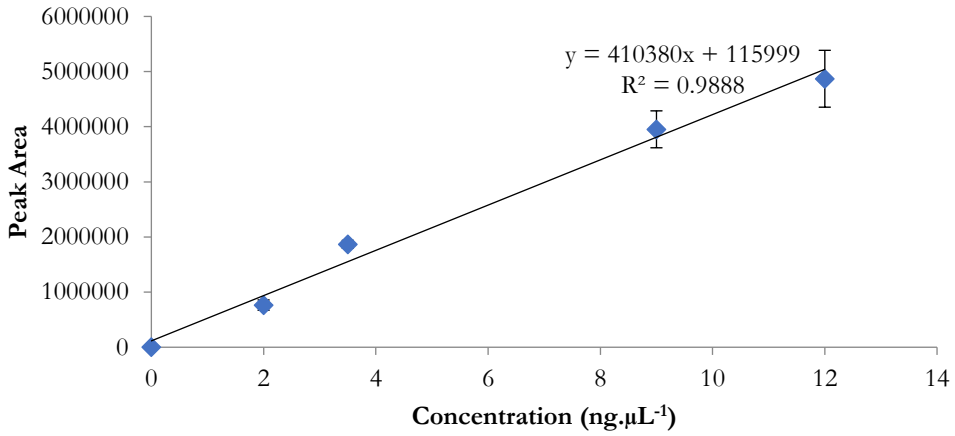

Calibration curve for phenanthrene in neat solvent

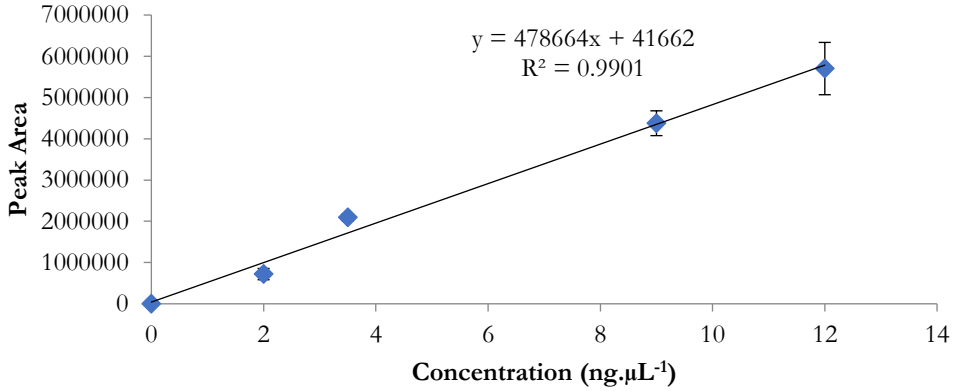

Calibration curve for anthracene in neat solvent

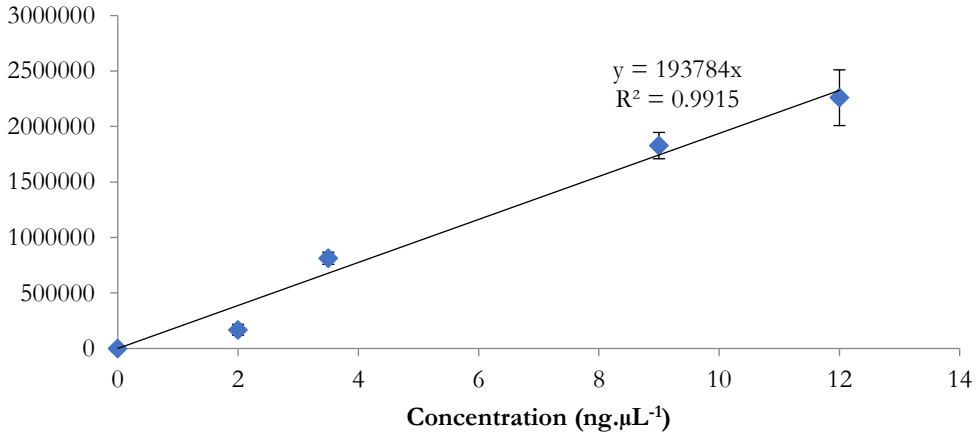

Calibration curve for fluoranthene in neat solvent

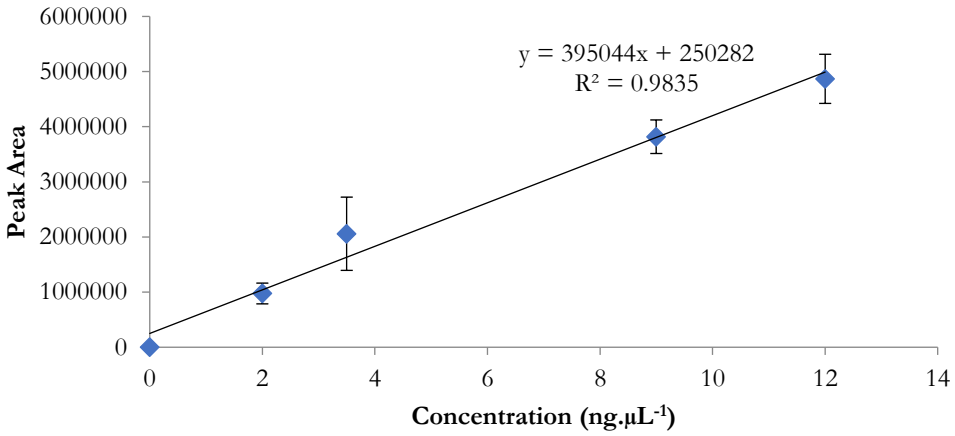

Calibration curve for pyrene in neat solvent

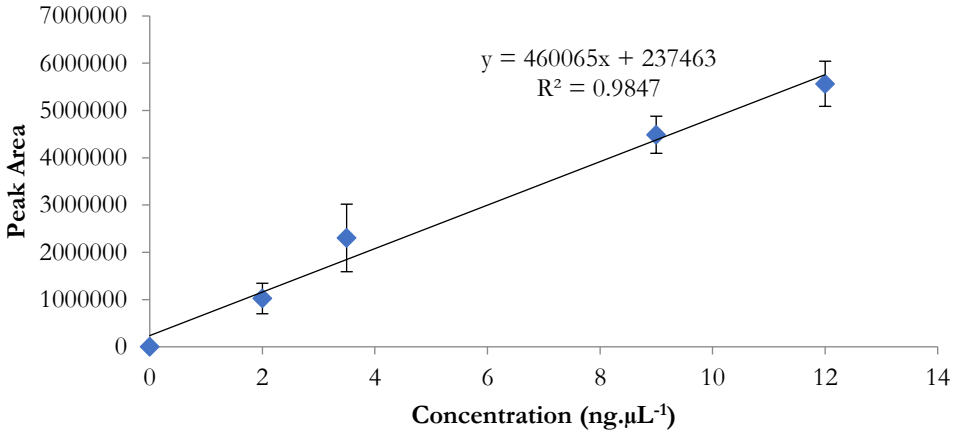

Calibration curve for 2-bromo-naphthalene in neat solvent

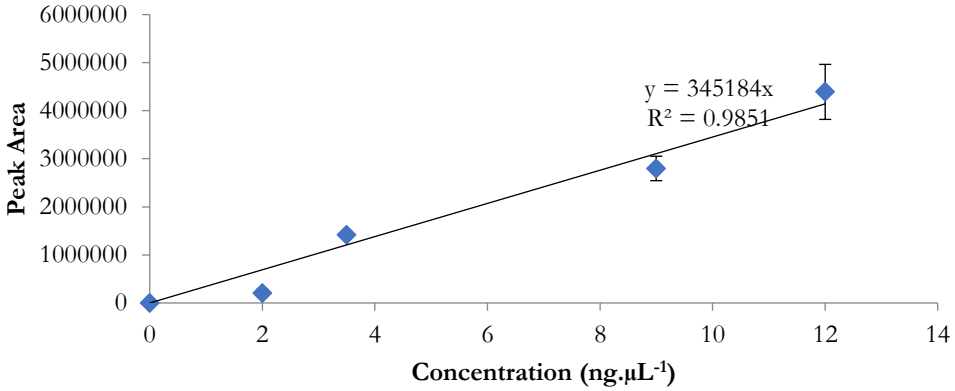

Calibration curve for benz[a]anthracene in neat solvent

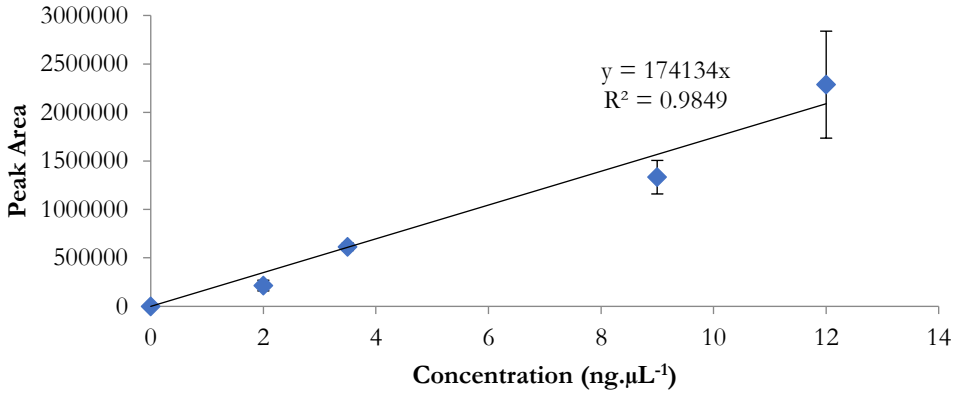

Calibration curve for chrysene in neat solvent

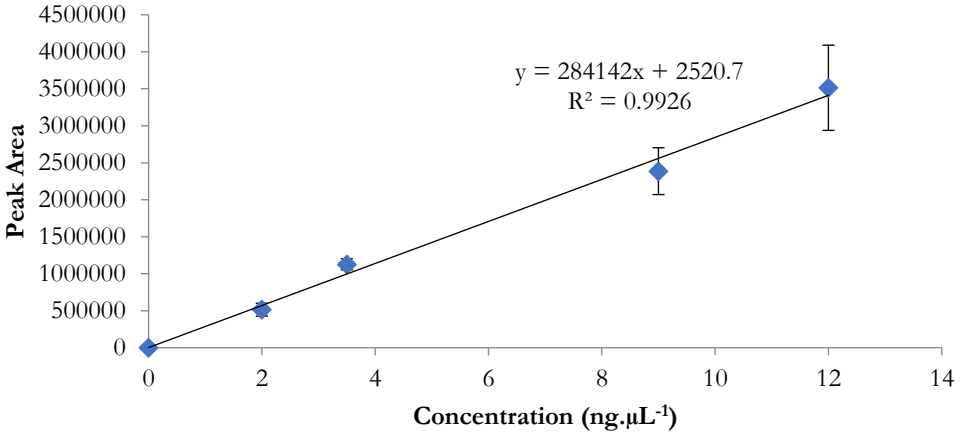

Calibration curve for benzo[b]fluoranthene in neat solvent

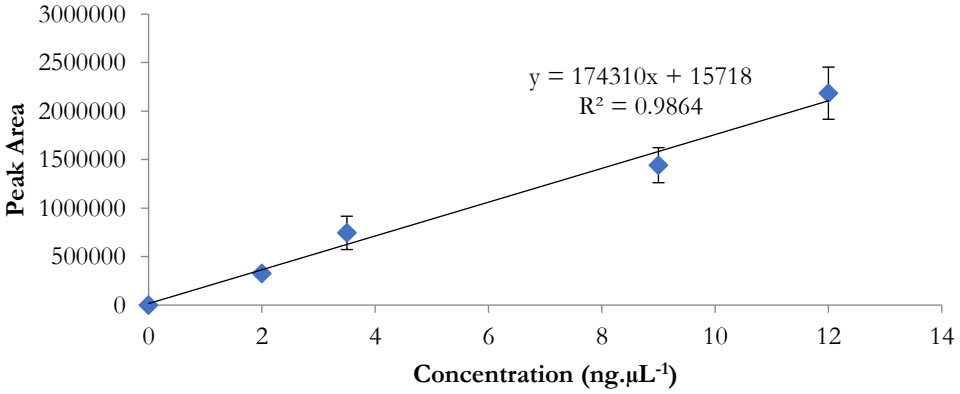

Calibration curve for benzo[a]pyrene in neat solvent

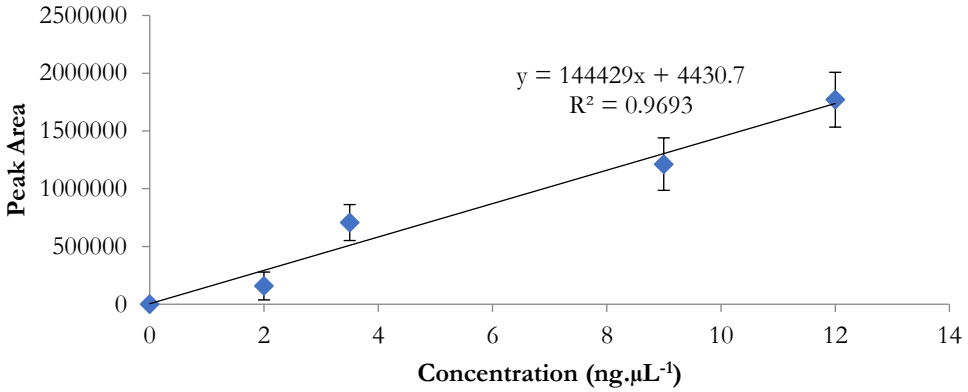

Calibration curve for indeno[1,2,3-cd]pyrene in neat solvent

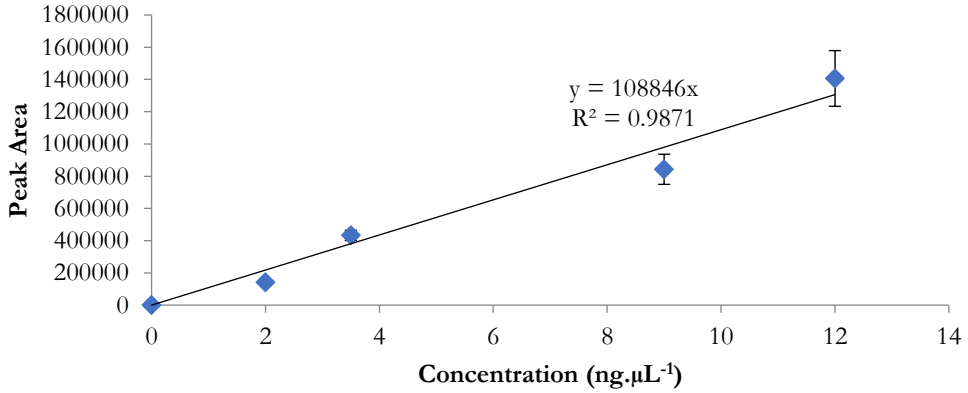

Calibration curve for benzo[ghi]perylene in neat solvent

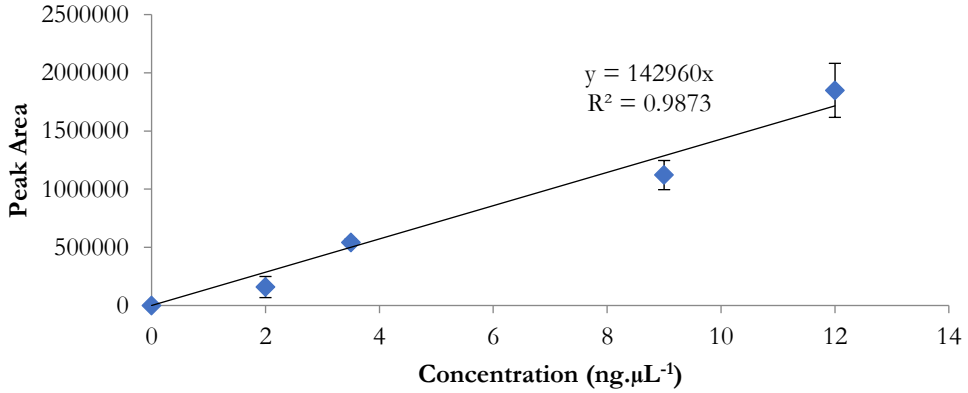

Calibration curve for dibenz[a,h]anthracene in neat solvent

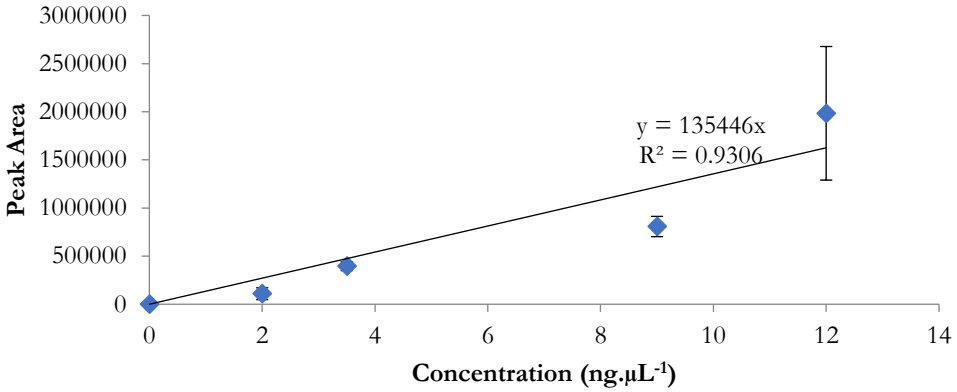

Appendix E: Method calibration curves for the 16 PAHs investigated in the PASE study

Calibration curves for individual PAHs after PASE with a PAH mix spiked onto a GW sampler

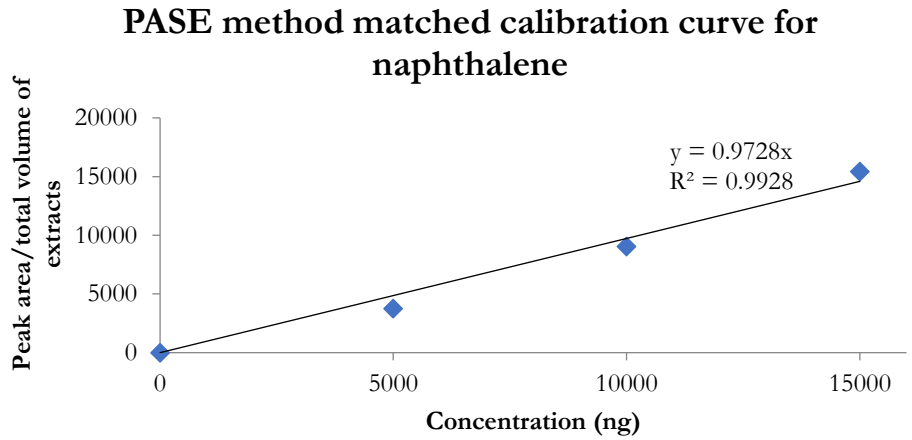

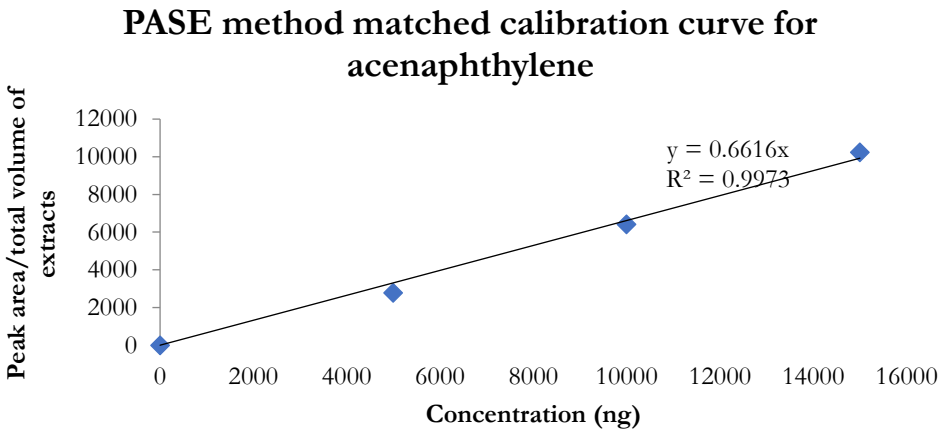

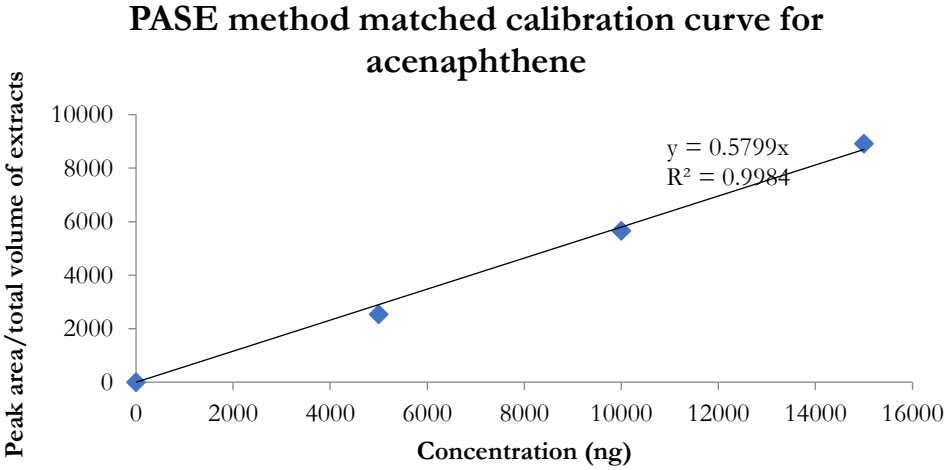

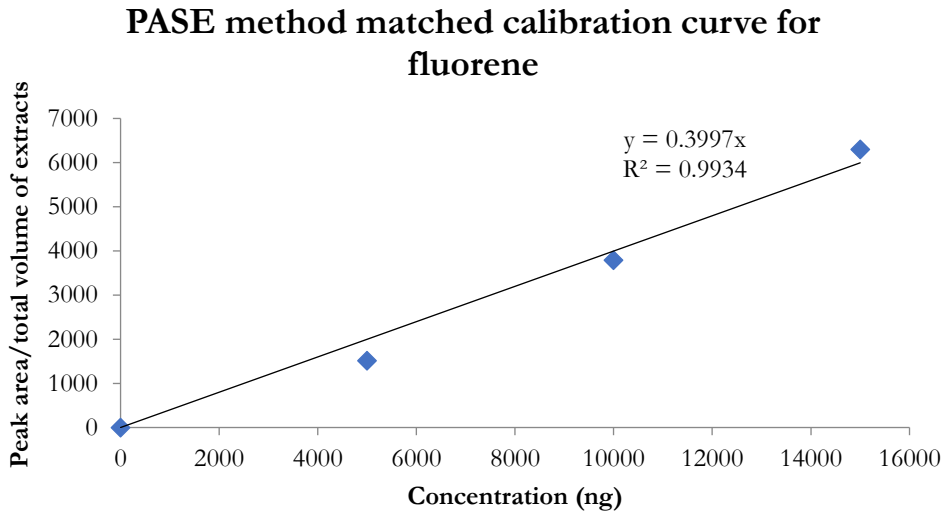

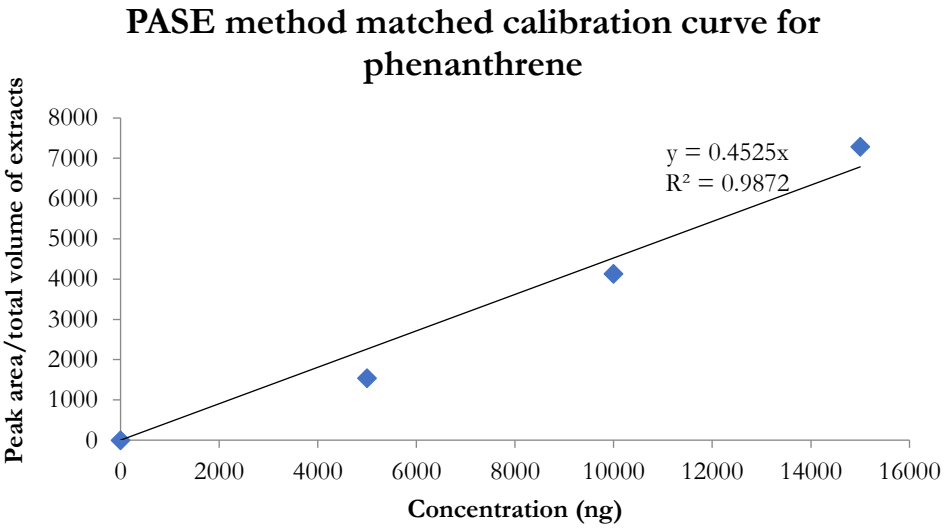

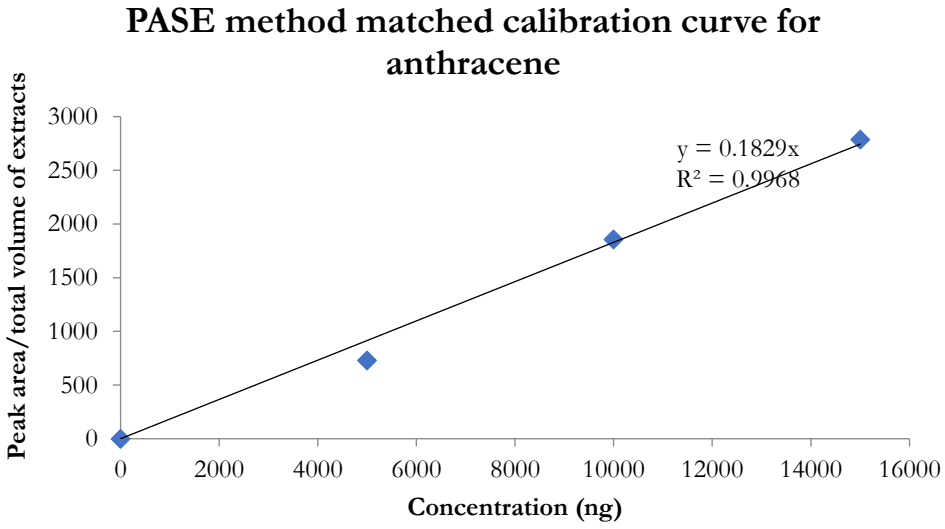

PASE method matched calibration curve for fluoranthene

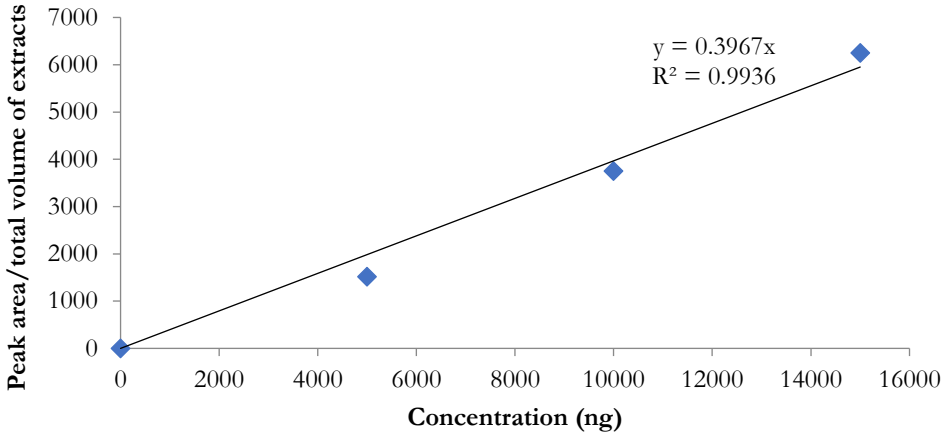

PASE method matched calibration curve for pyrene

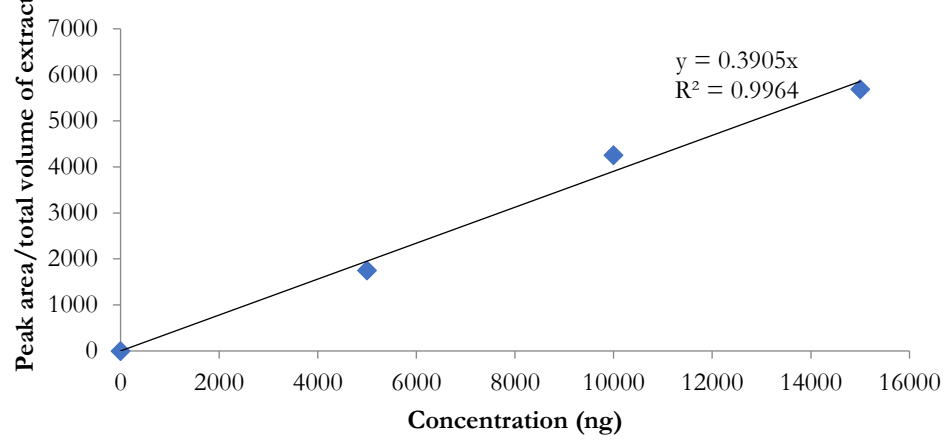

PASE method matched calibration curve for naphthalene, 2-bromo-

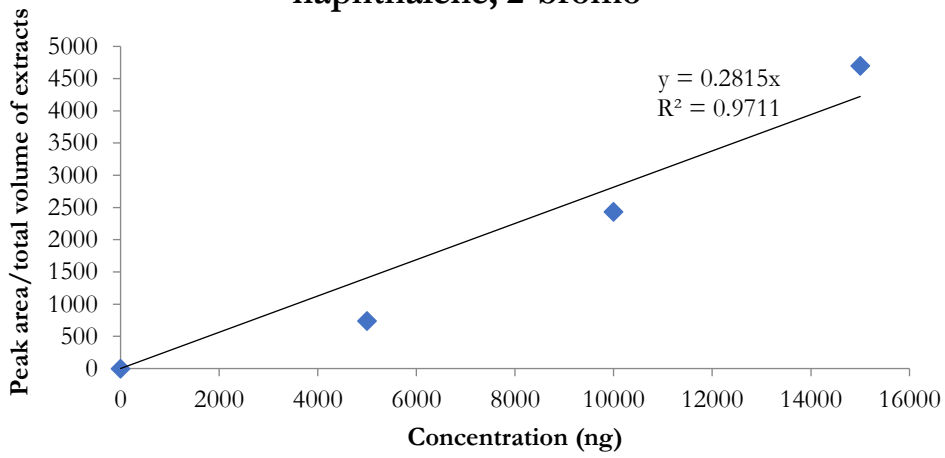

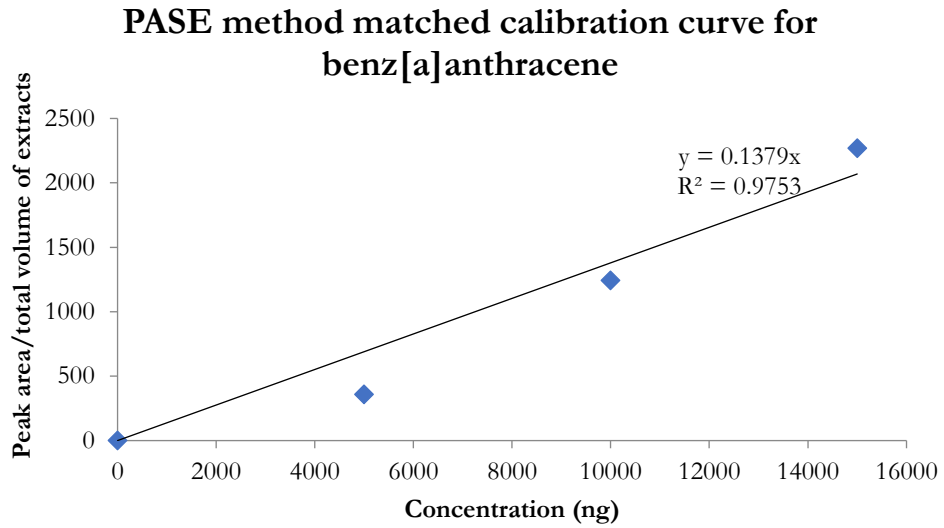

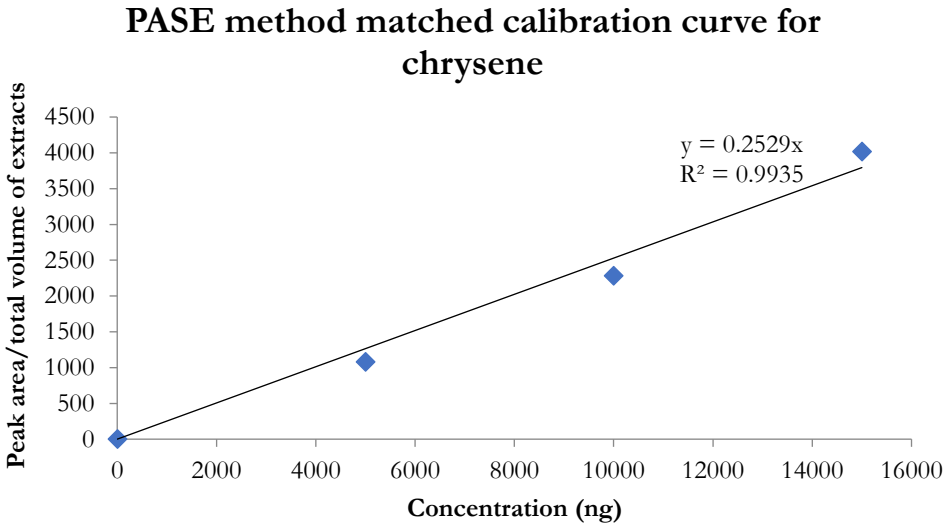

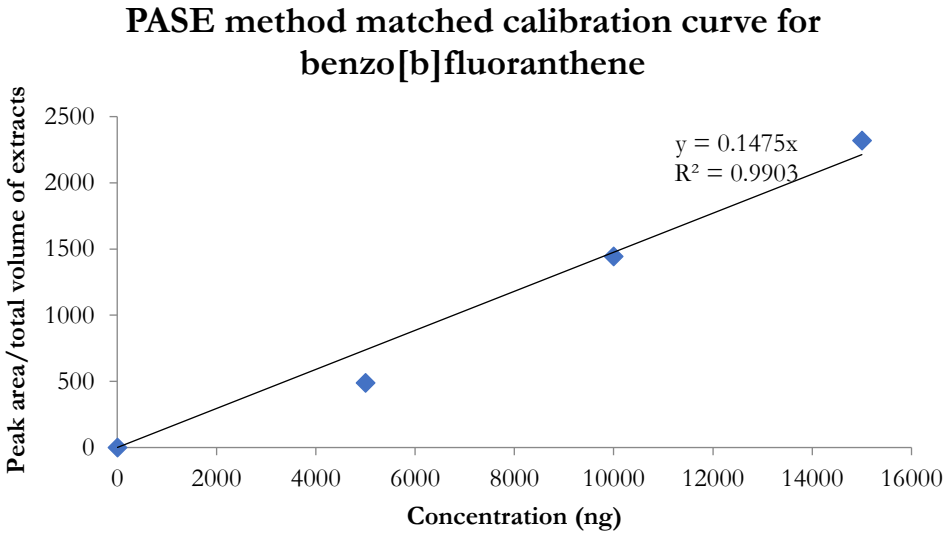

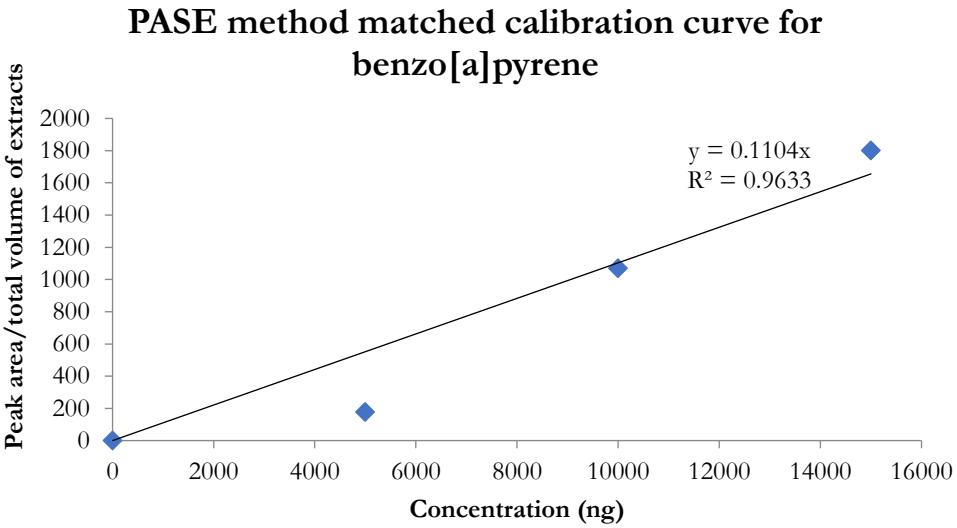

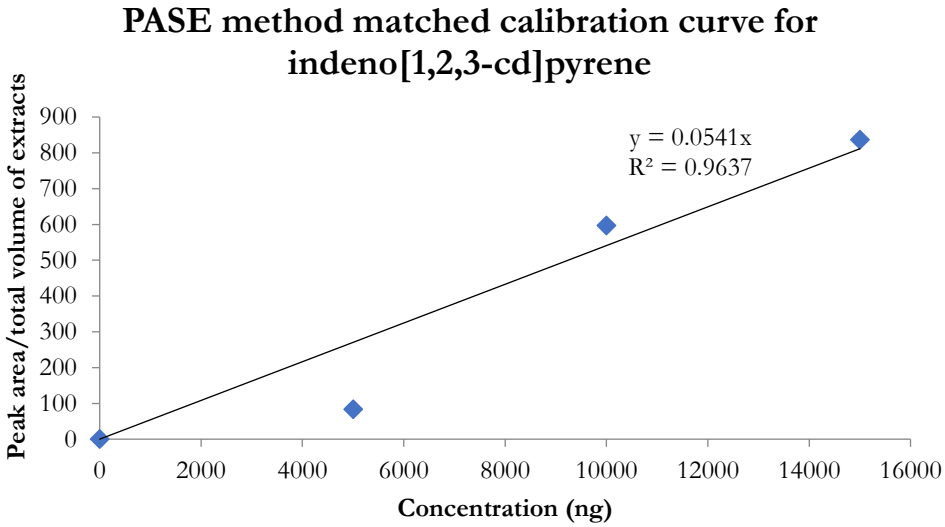

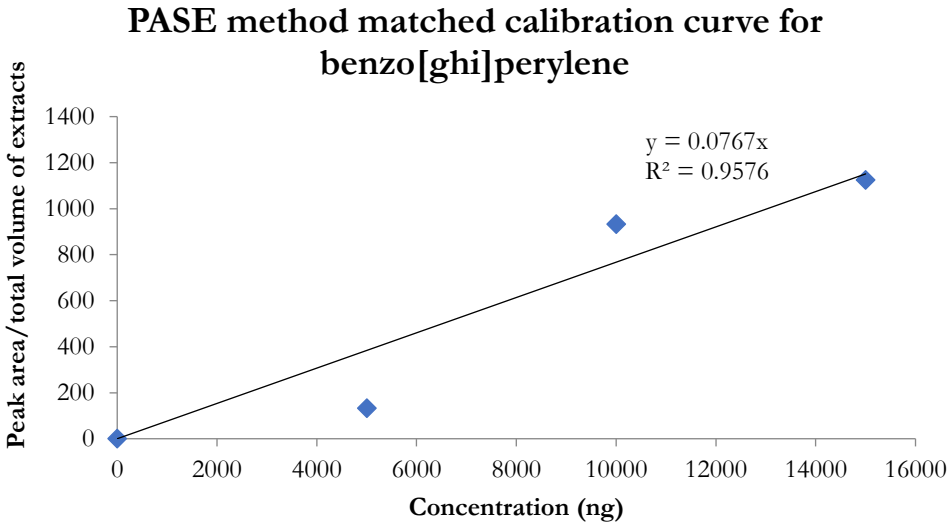

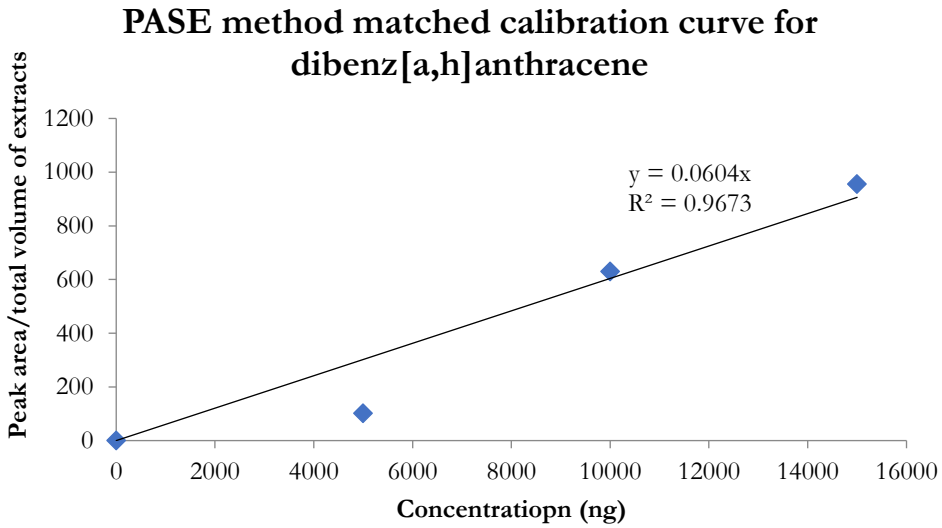

Appendix F: Information relating to the chromatographic tests for tube breakthrough volumes

Table F1: Average retention times (min) used for the calculations of the breakthrough volume for the analytes at isothermal temperatures 25 - 200 °C for the QW sampler. *(-) represent data which is unavailable for a specific analyte at the stated temperature.* (*N*=2, ± SD, (% RSD))

	Average retention times (min) at isothermal temperatures reported with SD. % RSD is reported in brackets underneath each average.								
Temp (°C)	**MeOH**	**Hex**	**Prop**	**Tol**	**But**	**Oct**	**Cycl**	**Dode**	**Hexd**
25	0.51 ± 0.00 (0.11)	0.35 ± 0.01 (1.8)	1.03 ± 0.00 (0.23)	1.11 ± 0.06 (5.6)	4.76 ± 0.15 (3.1)	1.59 ± 0.02 (1.4)	6.74 ± 0.25 (3.7)	-	-
30	0.47 ± 0.05 (11)	0.33 ± 0.00 (1.1)	0.94 ± 0.03 (3.1)	1.02 ± 0.03 (2.5)	3.59 ± 0.18 (5.1)	1.23 ± 0.11 (8.8)	4.55 ± 0.12 (2.7)	-	-
40	0.41 ± 0.00 (0.54)	0.32 ± 0.01 (2.3)	0.53 ± 0.03 (5.9)	0.74 ± 0.03 (3.7)	2.03 ± 0.09 (4.3)	0.84 ± 0.00 (0.16)	2.61 ± 0.10 (3.9)	-	-
50	0.36 ± 0.00 (1.2)	-	0.42 ± 0.02 (3.6)	0.51 ± 0.00 (0.2)	1.25 ± 0.22 (17.2)	0.6 ± 0.02 (3.9)	1.55 ± 0.07 (4.7)	-	-
60	0.36 ± 0.00 (1.1)	-	0.36 ± 0.01 (2.9)	0.44 ± 0.01 (2.7)	0.79 ± 0.04 (5.4)	0.49 ± 0.03 (5.1)	-	-	-
70	0.36 ± 0.00 (0.5)	-	0.35 ± 0.01 (1.6)	-	-	-	0.89 ± 0.01 (1.0)	5.42 ± 0.08 (1.5)	-
80	-	-	-	0.35 ± 0.01 (3.9)	0.48 ± 0.04 (8.9)	0.37 ± 0.02 (4.2)	-	-	-
90	-	-	-	-	-	-	0.51 ± 0.01 (1.3)	2.12 ± 0.03 (1.2)	-
110	-	-	-	-	-	-	-	1.05 ± 0.09 (9.0)	-
120	-	-	-	-	-	-	-	-	5.99 ± 0.14 (2.3)
130	-	-	-	-	-	-	-	0.54 ± 0.00 (0.69)	4.19 ± 0.15 (3.7)
140	-	-	-	-	-	-	-	-	2.79 ± 0.27 (9.8)
150	-	-	-	-	-	-	-	0.41 ± 0.02 (4.1)	-
160	-	-	-	-	-	-	-	-	1.35 ± 0.10 (7.7)
180	-	-	-	-	-	-	-	0.35 ± 0.01 (3.5)	0.76 ± 0.07 (9.8)

200	-	-	-	-	-	-	-	-	0.46 ± 0.00 (1.0)

Abbreviations: ***MeOH****; methanol,* ***Hex****; hexane,* ***Prop****; propanol-2,* ***Tol****; toluene,* ***But****; butan-1-ol,* ***Oct****; octane,* ***Cycl****; cyclohexanone,* ***Dode****; dodecane,* ***Hexd****; hexadecane.*

Table F2: Average retention times used for the calculation of the breakthrough volumes for the analytes at isothermal temperatures ranging from 25 - 190 °C for the GW sampler. *(-) represent data which is unavailable for a specific analyte at the stated temperature. (*N=2, ± SD, (% RSD))

	Average retention times (min) at isothermal temperatures reported with SD. % RSD is reported in brackets underneath each average.								
Temp (°C)	**MeOH**	**Hex**	**Prop**	**Tol**	**But**	**Oct**	**Cycl**	**Dode**	**Hexd**
25	0.82 ± 0.01 (1.0)	0.41 ± 0.01 (1.5)	1.32 ± 0.04 (3.2)	1.39 ± 0.06 (4.0)	5.57 ± 0.05 (0.88)	1.84 ± 0.07 (3.6)	8.02 ± 0.20 (2.5)	-	-
30	0.68 ± 0.01 (0.76)	0.40 ± 0.00 (0.10)	1.09 ± 0.08 (6.9)	1.14 ± 0.01 (0.54)	4.22 ± 0.06 (1.4)	1.47 ± 0.04 (3.0)	6.19 ± 0.4 (6.4)	-	-
35	0.58 ± 0.01 (1.5)	-	0.9 ± 0.03 (3.5)	0.93 ± 0.03 (3.4)	3.16 ± 0.03 (1.0)	1.2 ± 0.00 (0.18)	4.32 ± 0.29 (6.6)	-	-
40	0.52 ± 0.00 (0.52)	0.36 ± 0.01 (2.4)	0.72 ± 0.03 (4.4)	0.79 ± 0.02 (2.3)	2.33 ± 0.00 (0.063)	0.87 ± 0.07 (8.1)	3.3 ± 0.21 (6.3)	-	-
45	0.46 ± 0.00 (0.25)	-	0.66 ± 0.03 (4.1)	0.68 ± 0.00 (0.31)	1.81 ± 0.01 (0.45)	0.8 ± 0.00 (0.25)	2.46 ± 0.08 (3.4)	-	-
50	0.44 ± 0.00 (0.086)	0.36 ± 0.00 (0.030)	0.59 ± 0.02 (4.1)	0.57 ± 0.03 (5.4)	1.44 ± 0.05 (3.6)	0.69 ± 0.02 (2.3)	2.16 ± 0.01 (0.60)	-	-
60	0.43 ± 0.00 (0.37)	-	0.46 ± 0.02 (4.7)	0.48 ± 0.02 (3.9)	0.91 ± 0.06) (6.1)	0.5 ± 0.02 (3.8)	1.45 ± 0.11 (7.6)	-	-
70	0.43 ± 0.00 (0.30)	-	0.42 ± 0.01 (2.0)	0.41 ± 0.01 (3.3)	0.66 ± 0.05 (7.7)	0.43 ± 0.01 (1.2)	1.06 ± 0.01 (0.49)	6.26 ± 0.09 (1.4)	-
80	-	-	-	0.38 ± 0.00 (0.81)	0.49 ± 0.03 (7.0)	0.38 ± 0.01 (3.4)	0.85 ± 0.08 (9.6)	3.83 ± 0.08 (2.0)	-
90	-	-	-	-	-	-	0.64 ± 0.05 (8.4)	2.39 ± 0.06 (2.6)	-
100	-	-	-	-	-	-	-	1.53 ± 0.00 (0.13)	-
110	-	-	-	-	-	-	-	1.06 ± 0.02 (1.9)	-
120	-	-	-	-	-	-	-	0.82 ± 0.03 (3.4)	8.18 ± 0.47 (5.8)
130	-	-	-	-	-	-	-	0.62 ± 0.02 (3.7)	4.71 ± 0.18 (3.9)

140	-	-	-	-	-	-	-	0.49 ± 0.01 (1.0)	3.11 ± 0.1 (3.1)
150	-	-	-	-	-	-	-	-	2.14 ± 0.05 (2.3)
160	-	-	-	-	-	-	-	-	1.49 ± 0.02 (1.0)
170	-	-	-	-	-	-	-	-	1.07 ± 0.01 (0.67)
180	-	-	-	-	-	-	-	-	0.79 ± 0.03 (3.2)
190	-	-	-	-	-	-	-	-	0.62 ± 0.01 (0.87)

Abbreviations: ***MeOH****; methanol,* ***Hex****; hexane,* ***Prop****; propanol-2,* ***Tol****; toluene,* ***But****; butan-1-ol,* ***Oct****; octane,* ***Cycl****; cyclohexanone,* ***Dode****; dodecane,* ***Hexd****; hexadecane.*

Table F3: Average retention times used for the calculation of the breakthrough volume for the analytes at isothermal temperatures 25 - 340 °C for the PDMS sampler. *(-) represent data which is unavailable for a specific analyte at the stated temperature.* (*N*=2, ± SD, (% RSD)).

	Average retention times (min) at isothermal temperatures reported with SD. % RSD is reported in brackets underneath each stated average.								
Temp (°C)	**MeOH**	**Hex**	**Prop**	**Tol**	**But**	**Oct**	**Cycl**	**Dode**	**Hexd**
25	1.61 ± 0.02 (0.99)	9.41 ± 0.07 (0.71)	4.37 ± 0.16 (3.6)	-	-	-	-	-	-
30	1.35 ± 0.01 (0.67)	-	3.57 ± 0.11 (3.0)	-	-	-	-	-	-
35	1.22 ± 0.01 (1.1)	-	-	-	-	-	-	-	-
40	1.03 ± 0.02 (1.5)	5.43 ± 0.03 (0.52)	2.54 ± 0.07 (2.6)	-	-	-	-	-	-
45	0.91 ± 0.00 (0.24)	-	-	-	-	-	-	-	-
50	0.82 ± 0.01 (1.0)	-	1.9 ± 0.02 (1.1)	-	-	-	-	-	-
60	0.72 ± 0.01 (0.80)	3.07 ± 0.05 (1.7)	1.47 ± 0.00 (0.13)	-	-	-	-	-	-
70	0.64 ± 0.01 (1.2)	-	1.21 ± 0.01 (1.9)	-	-	-	-	-	-
80	-	1.96 ± 0.00 (0.23)	-	6.12 ± 0.12 (1.9)	-	-	-	-	-

100	-	1.37 ± 0.00 (0.27)	-	3.64 ± 0.02 (0.50)	1.81 ± 0.06 (3.1)	4.54 ± 0.07 (1.5)	-	-	-
120	-	1.03 ± 0.00 (0.25)	-	2.36 ± 0.01 (0.60)	1.29 ± 0.02 (1.2)	2.83 ± 0.05 (1.7)	4.52 ± 0.06 (1.4)	-	-
140	-	-	-	1.71 ± 0.03 (1.9)	0.98 ± 0.04 (3.6)	1.89 ± 0.02 (0.90)	2.86 ± 0.03 (0.94)	-	-
160	-	-	-	1.31 ± 0.01 (0.62)	0.87 ± 0.04 (4.2)	1.39 ± 0.01 (0.72)	2.06 ± 0.04 (2.1)	7.25 ± 0.06 (0.76)	-
180	-	-	-	1.08 ± 0.03 (2.5)	0.74 ± 0.00 (0.44)	1.08 ± 0.02 (2.0)	1.55 ± 0.01 (0.53)	4.51 ± 0.00 (0.088)	-
200	-	-	-	-	0.68 ± 0.01 (2.0)	0.91 ± 0.02 (2.2)	1.26 ± 0.01 (1.2)	2.94 ± 0.03 (0.92)	-
220	-	-	-	-	-	-	1.04 ± 0.03 (2.6)	2.07 ± 0.02 (0.98)	-
240	-	-	-	-	-	-	-	1.55 ± 0.03 (1.9)	4.49 ± 0.02 (0.38)
260	-	-	-	-	-	-	-	1.25 ± 0.01 (0.48)	3.05 ± 0.03 (0.85)
280	-	-	-	-	-	-	-	-	2.2 ± 0.02 (1.1)
300	-	-	-	-	-	-	-	-	1.66 ± 0.06 (3.6)
320	-	-	-	-	-	-	-	-	1.34 ± 0.01 (0.99)
340	-	-	-	-	-	-	-	-	1.12 ± 0.02 (2.1)

Abbreviations: ***MeOH****; methanol,* ***Hex****; hexane,* ***Prop****; propanol-2,* ***Tol****; toluene,* ***But****; butan-1-ol,* ***Oct****; octane,* ***Cycl****; cyclohexanone,* ***Dode****; dodecane,* ***Hexd****; hexadecane.*

Table F4: Equations determined from the graphs showing the retention volume curves for the lower and higher BP analytes when injected onto a GW, QW and PDMS sampler types in the breakthrough volume set-up at various isothermal temperatures (Figures 4.20 - 4.21).

	Abbreviation	GW	QW	PDMS
Methanol (64.7°C)	MeOH	$y = 69.311e^{-0.014x}$	$y = 47.704e^{-0.007x}$	$y = 66.873e^{-0.02x}$
Hexane (68°C)	Hex	$y = 32.775e^{-0.006x}$	$y = 32.774e^{-0.006x}$	$y = 385.37e^{-0.023x}$
Propanol-2 (82.5°C)	Prop	$y = 155.92e^{-0.025x}$	$y = 146.19e^{-0.025x}$	$y = 231.2e^{-0.029x}$
Toluene (110.6°C)	Tol	$y = 148.8e^{-0.023x}$	$y = 158.73e^{-0.023x}$	$y = 576.36e^{-0.017x}$

Butan-1-ol (117.7°C)	But	$y = 1069.8e^{-0.045x}$	$y = 1016.6e^{-0.043x}$	$y = 113.26e^{-0.009x}$
Octane (125.6°C)	Oct	$y = 226.61e^{-0.029x}$	$y = 212.28e^{-0.026x}$	$y = 553.3e^{-0.016x}$
Cyclohexanone (155.6°C)	Cyclo	$y = 1179.6e^{-0.038x}$	$y = 1132.2e^{-0.038x}$	$y = 598.31e^{-0.014x}$
Dodecane (216.2°C)	Dode	$y = 4870e^{-0.037x}$	$y = 1756.2e^{-0.025x}$	$y = 2983.8e^{-0.018x}$
Hexadecane (286.8°C)	Hexd	$y = 35767e^{-0.036x}$	$y = 22133e^{-0.032x}$	$y = 3207.5e^{-0.014x}$

Table F5: R^2 values for fit of the exponential equations shown in Table H4.

	Abbreviation	GW	QW	PDMS
Methanol (64.7°C)	MeOH	0.7570	0.8170	0.9603
Hexane (68°C)	Hex	0.9422	0.8542	0.9722
Propanol-2 (82.5°C)	Prop	0.9535	0.8753	0.9884
Toluene (110.6°C)	Tol	0.9457	0.9176	0.9734
Butan-1-ol (117.7°C)	But	0.9832	0.9629	0.9430
Octane (125.6°C)	Oct	0.9559	0.9519	0.9728
Cyclohexanone (155.6°C)	Cyclo	0.9727	0.9667	0.9723
Dodecane (216.2°C)	Dode	0.9801	0.8940	0.9817
Hexadecane (286.8°C)	Hexd	0.9872	0.9902	0.9835

Appendix G: Supplementary information regarding the CAST campaign

Table G1: Standards and internal standards used in this study.

Standard	Supplier
Naphthalene	Alfa Aesar
Fluorene	Fluka
Acenaphthene	Fluka
Acenaphthylene	Supelco
Phenanthrene	Alfa Aesar
Anthracene	Fluka
1-Methylnaphthalene	Aldrich
1,2-Dimethylnaphthalene	Alfa Aesar
2-Methylnaphthalene	Supelco
Biphenyl	Supelco
1-Methylfluorene	Aldrich
Fluoranthene	Fluka
Pyrene	Sigma-Aldrich
Benzene	Carl Roth
Toluene	Carl Roth
M-Xylene	Fluka
O-Xylene	Vwr
Ethylbenzene	Alfa Aesar
Benzaldehyde	Sigma Aldrich
Styrene	Fluka
Phenol	Merck
Indene	Aldrich
Indane	Fluka
Alkane Standard Solution C8-C20	Sigma-Aldrich
Benzene D6	Fluka
Toluene D8	Sigma Aldrich
O-Xylene D10	Sigma Aldrich
Naphthalene D8	Sigma Aldrich
Biphenyl D10	Cil - Cambridge Isotope Institute
Acenaphthylene D8	Cil-Cambridge Isotope Laboratories
Acenaphthene D10	Sigma Aldrich
Fluorene D10	Supelco
Phenanthrene D10	Cil-Cambridge Isotope Laboratories
Anthracene D10	Cil - Cambridge Isotope Institute
N-Heptane D16	Sigma Aldrich
N-Dodecane D26	Sigma Aldrich
N-Hexadecane D34	Aldrich

Table G2: CAST target analytes mixture with associated CAS no.s, molecular masses along with associated primary quantification ions as well as their chemical structures.

VOCs				
Compound name	CAS no.	MM ($g.mol^{-1}$)	1°; 2° Q ion	Structure
Benzene	71-43-2	78	78	
Toluene	108-88-3	92	91, 92	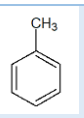
Phenol	108-95-2	94	94	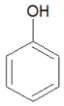
Styrene	100-42-5	104	104, 78	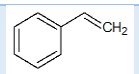
Benzaldehyde	100-52-7	106	77	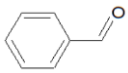
Ethylbenzene	100-41-4	106	91, 106	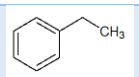
m-Xylene	108-38-3	106	91, 106	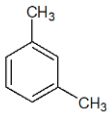
o-Xylene	95-47-6	106	91, 106	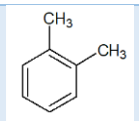
Benzylalcohol	100-51-6	108	79	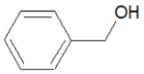
o-Cresol	95-48-7	108	108	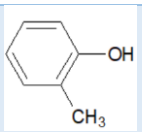
p-Cresol	106-44-5	108	107	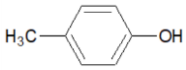
m-Cresol	108-39-4	108	108	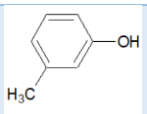
Indene	95-13-6	116	116	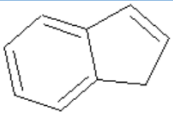

Indane	496-11-7	118	117	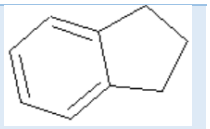
PAHs				
Compound name	CAS no.	MM ($g.mol^{-1}$)	1° Q ion	Structures
Naphthalene	91-20-3	128	128	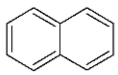
2-methylnaphthalene	91-57-6	142	142	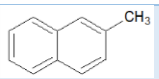
1-methylnaphthalene	90-12-0	142	142	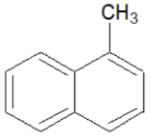
Acenaphthylene	208-96-8	152	152	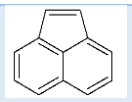
Biphenyl	92-52-4	154	154	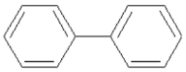
Acenaphthene	83-32-9	154	154	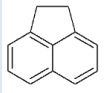
1,2-dimethylnaphthalene	573-98-8	156	156	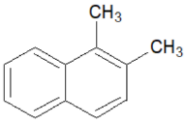
Fluorene	86-73-7	166	166	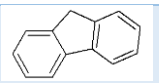
Phenanthrene	85-01-8	178	178	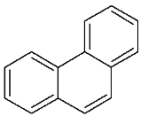
Anthracene	120-12-7	178	178	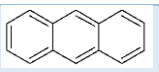
1-methylfluorene	1730-37-6	180	165	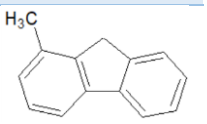
Fluoranthrene	206-44-0	202	202	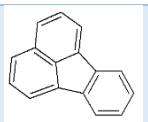
Pyrene	129-00-0	202	202	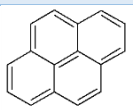
Alkanes				

Compound name	CAS no.	MM (g.mol^{-1})	1° Q ion	Structures
Octane	111-65-9	114	57	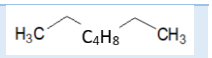
Nonane	111-84-2	128	57	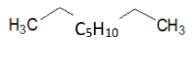
Decane	1224-18-5	142	57	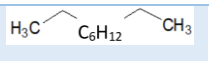
Undecane	1120-21-4	156	57	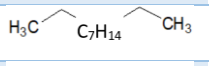
Dodecane	112-40-3	170	57	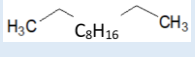
Tridecane	629-50-5	184	57	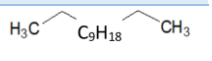
Tetradecane	629-59-4	198	57	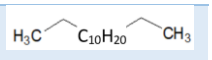
Pentadecane	629-62-9	212	57	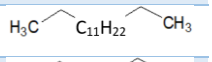
Hexadecane	544-76-3	226	57	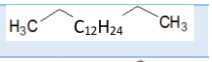
Heptadecane	629-78-7	240	57	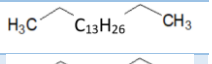
Octadecane	593-45-3	254	57	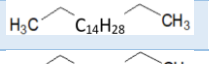
Nonadecane	629-92-5	268	57	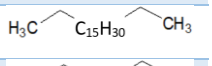
Eicosane	112-95-8	282	57	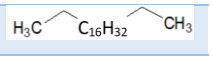

Abbreviations: CAS no*; Chemical Abstracts Service number,* ***MM****; molecular mass,* ***1°****; primary,* ***2°****; secondary,* ***Q****; quantification.*

Table G3: The deuterated IS mixture with which Table C1 target analytes were quantified.

Deuterated IS			
Compound name	CAS no.	MM (g.mol^{-1})/1° Q ion	Structure
n-Heptane-d16	33838-52-7	66	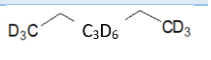
n-Dodecane-d26	16416-30-1	66	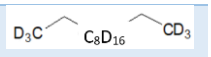
n-Hexadecane-d34	15716-08-2	66	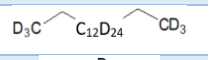
Benzene-d6	1076-43-3	84	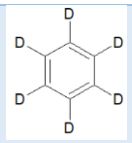
Toluene-d8	2037-26-5	98	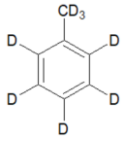
o-Xylene-d10	56004-61-6	98	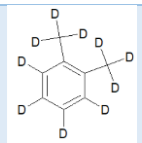

Naphthalene-d8	1146-65-2	136	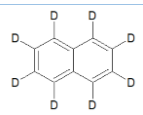
Acenaphthylene-d8	93951-97-4	160	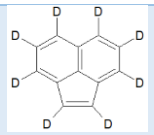
Biphenyl-d10	1486-01-7	164	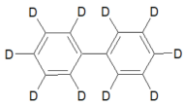
Acenaphthene-d10	15067-26-2	164	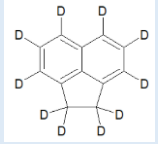
Fluorene-d10	81103-79-9	176	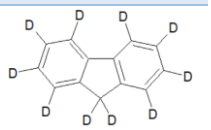
Phenanthrene-d10	1517-22-2	188	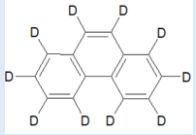
Anthracene-d10	1719-06-8	188	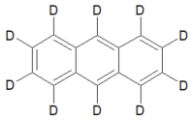

Table G4: Ambient conditions at the start of sampling events for this study

Measurement	Barometric Pressure (hPa)	Wet Bulb (°C)	Dry Bulb (°C)
B0 1	955.5	20.4	26.8
GTL 1	955.8	20.4	26.8
GTL 2	955.9	10.7	27.0
RME 1	956.0	10.7	27.0
RME 2	956.1	9.0	27.7
B0 2	956.2	9.0	27.7
Average	955.9	13.4	27.2
SD	0.2	5.5	0.4
% RSD	0	41	2

Table G5: Mean FTIR results for the sampling events of the undiluted fuel emissions over each 10 min sampling period.

Sample	H_2O (%)	CO_2 (%)	CO (ppm)	O_2 (%)
B0 1	0.58	0.58	9.51	10.30
B0 2	0.57	0.58	9.48	10.30
B0 3	0.65	0.58	9.40	10.20
B0 4	0.66	0.58	9.42	10.20
Mean	**0.62**	**0.58**	**9.45**	**10.25**
SD	**0.05**	**0.00**	**0.05**	**0.06**
% RSD	**7.42**	**0.13**	**0.55**	**0.56**
GTL 1	0.56	0.58	7.89	10.31
GTL 2	0.56	0.58	7.86	10.31
GTL 3	0.66	0.58	7.63	10.50
GTL 4	0.65	0.58	7.65	10.45
Mean	**0.61**	**0.58**	**7.76**	**10.39**
SD	**0.06**	**0.00**	**0.14**	**0.10**
% RSD	**9.10**	**0.21**	**1.77**	**0.94**
RME 1	0.62	0.60	7.25	10.26
RME 2	0.62	0.60	7.30	10.28
RME 3	0.67	0.60	7.32	10.45
RME 4	0.67	0.59	7.64	10.41
Mean	**0.64**	**0.60**	**7.38**	**10.35**
SD	**0.03**	**0.00**	**0.18**	**0.10**
% RSD	**4.79**	**0.63**	**2.43**	**0.93**

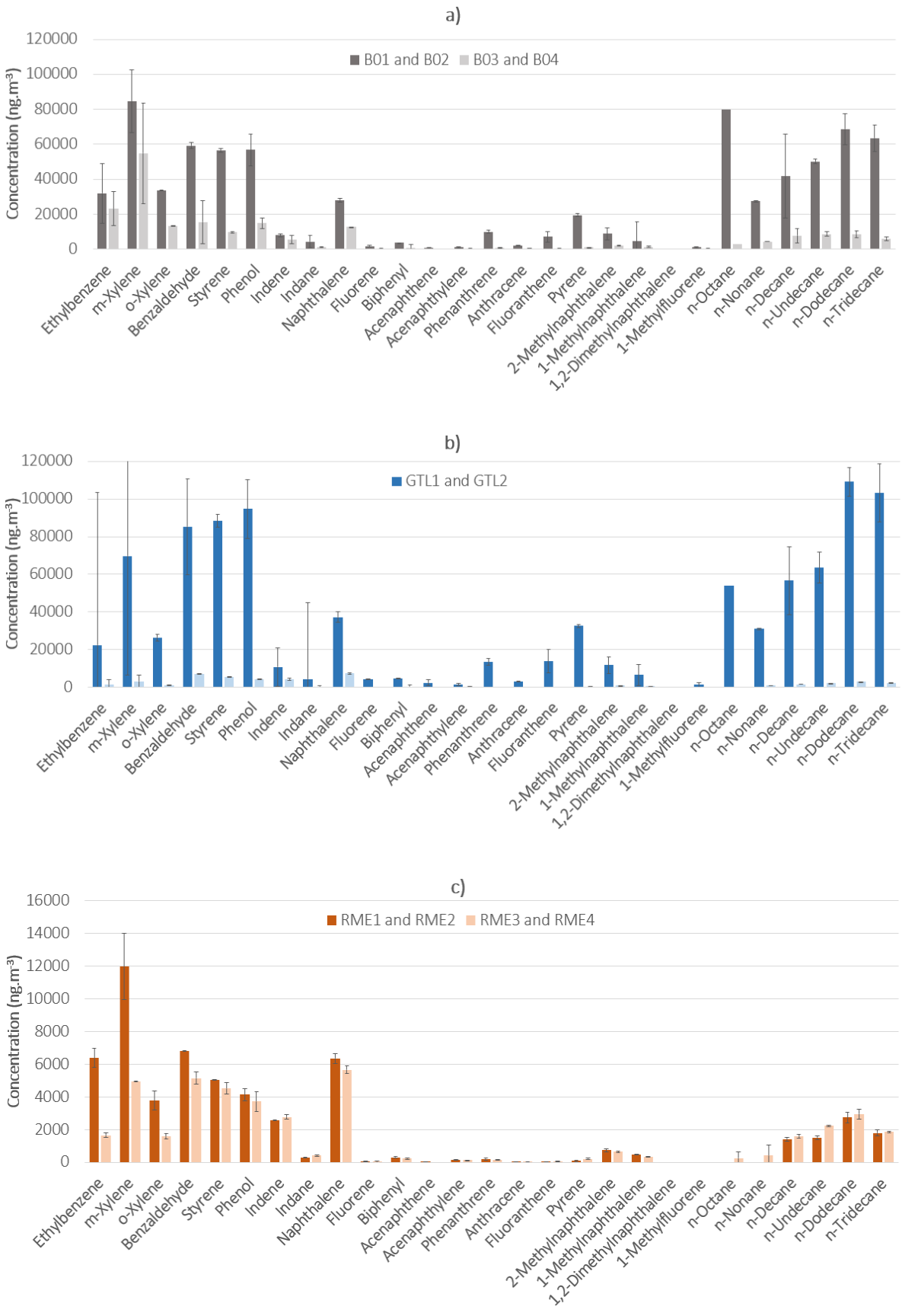

Figure G1: Comparison of sampling event replicates for **a)** B0, **b)** GTL and **c)** RME.

Table G6: Concentrations of target analytes detected upon analysis of blank samplers. *(n.d.) denotes that the specific target analyte was not detected.*

Analyte	Concentration detected (ng)		
	PDMS	GW	Activated charcoal
Benzene	6.72	n.d.	74.95
Toluene	35.60	n.d.	19.25
Ethylbenzene	n.d.	n.d.	n.d.
m-Xylene	n.d.	n.d.	n.d.
o-Xylene	0.01	n.d.	n.d.
Benzaldehyde	n.d.	n.d.	n.d.
Styrene	n.d.	n.d.	n.d.
Phenol	n.d.	n.d.	n.d.
Indene	n.d.	n.d.	n.d.
Indane	n.d.	n.d.	n.d.
Naphthalene	0.07	n.d.	n.d.
Fluorene	n.d.	n.d.	n.d.
Biphenyl	0.01	n.d.	n.d.
Acenaphthene	n.d.	n.d.	n.d.
Acenaphthylene	n.d.	n.d.	n.d.
Phenanthrene	0.01	n.d.	n.d.
Anthracene	0.01	n.d.	n.d.
Fluoranthene	n.d.	n.d.	n.d.
Pyrene	n.d.	n.d.	n.d.
2-Methylnaphthalene	n.d.	n.d.	n.d.
1-Methylnaphthalene	n.d.	n.d.	n.d.
1,2-Dimethylnaphthalene	n.d.	n.d.	n.d.
1-Methylfluorene	n.d.	n.d.	n.d.
n-Octane	n.d.	n.d.	n.d.
n-Nonane	n.d.	n.d.	n.d.
n-Decane	0.01	n.d.	n.d.
n-Undecane	0.01	n.d.	n.d.
n-Dodecane	n.d.	n.d.	n.d.
n-Tridecane	n.d.	n.d.	n.d.
n-Tetradecane	0.05	n.d.	n.d.
n-Pentadecane	0.07	n.d.	n.d.
n-Hexadecane	0.09	n.d.	n.d.
n-Heptadecane	n.d.	n.d.	n.d.
n-Octadecane	n.d.	n.d.	n.d.
n-Nonadecane	n.d.	n.d.	n.d.
n-Eicosane	n.d.	n.d.	n.d.

Table G7: Concentrations of target analytes detected upon thermal desorption of GW samplers after sampling the emissions of CAST combustion of different fuels with associated standard deviations between sampling duplicates. *(n.d.) denotes that the specific target analyte was not detected for a specific analyte/ sampler combination.*

	Average concentrations of target analyte (µg.m^{-3})			% RSD of the duplicate measurements		
Target analytes	**B0**	**GTL**	**RME**	**B0**	**GTL**	**RME**
Benzene	96.63	21.65	26.57	10.09	12.28	5.96
Toluene	773.83	148.24	161.10	3.72	2.33	2.30
Ethylbenzene	23.19	1.36	6.39	0.63	14.06	9.05
m-Xylene	54.90	3.07	11.99	22.43	5.60	16.96
o-Xylene	13.36	1.12	3.79	2.91	8.52	15.63
Benzaldehyde	15.69	6.95	6.82	19.46	1.25	0.33
Styrene	9.78	5.62	5.03	24.03	10.74	0.52
Phenol	15.01	4.38	4.15	0.56	9.58	8.68
Indene	5.53	4.30	2.59	0.02	9.73	0.74
Indane	1.33	0.40	0.31	28.53	9.97	4.56
Naphthalene	12.83	7.40	6.37	13.75	12.64	4.89
Fluorene	0.28	0.07	0.07	61.87	141.11	31.98
Biphenyl	0.85	0.30	0.30	10.94	19.21	15.14
Acenaphthene	0.15	0.06	0.04	141.45	1.59	8.33
Acenaphthylene	0.42	0.23	0.16	84.21	1.13	11.05
Phenanthrene	0.81	0.21	0.22	34.41	0.37	30.69
Anthracene	0.07	0.04	0.01	24.32	63.85	142.59
Fluoranthene	0.44	0.12	0.05	28.34	34.07	7.66
Pyrene	1.18	0.29	0.09	38.74	10.01	29.98
2-Methylnaphthalene	2.06	0.90	0.75	30.84	4.45	12.39
1-Methylnaphthalene	1.46	0.52	0.47	29.26	15.43	4.34
1,2-Dimethylnaphthalene	n.d.	n.d.	n.d.	n.d.	n.d.	n.d.
1-Methylfluorene	n.d.	n.d.	n.d.	n.d.	n.d.	n.d.
n-Octane	2.90	n.d.	n.d.	141.42	n.d.	n.d.
n-Nonane	4.45	n.d.	n.d.	28.04	1.78	n.d.
n-Decane	7.90	1.63	1.43	24.32	1.24	9.17
n-Undecane	8.72	2.24	1.52	13.65	8.92	7.10
n-Dodecane	8.76	3.02	2.75	18.82	2.74	11.17
n-Tridecane	6.06	2.14	1.80	33.12	9.88	10.07
n-Tetradecane	10.74	5.81	4.71	58.44	4.16	16.36
n-Pentadecane	3.62	3.44	3.02	54.29	32.67	0.62

n-Hexadecane	5.22	6.34	4.06	59.61	20.35	23.37
n-Heptadecane	2.16	1.66	1.17	40.45	17.83	26.03
n-Octadecane	2.25	2.10	0.74	50.89	62.41	8.76
n-Nonadecane	2.78	0.91	0.51	76.23	2.11	21.29
n-Eicosane	1.82	0.57	0.30	69.41	8.14	22.08
Total VOCs + SVOCs	1097.16	237.09	259.29			

Table G8: Concentrations of target analytes detected upon thermal desorption of PDMS samplers after sampling the emissions of CAST combustion of different fuels with associated standard deviations between sampling duplicates. *(n.d.) denotes that the specific target analyte was not detected for a specific analyte/sampler combination.*

	Average concentrations of target analyte (µg.m^{-3})			**% RSD of the duplicate measurements**		
Target analytes	**B0**	**GTL**	**RME**	**B0**	**GTL**	**RME**
Benzene	374.65	76.74	71.51	8.72	8.89	7.15
Toluene	774.41	159.30	158.30	0.18	1.61	0.36
Ethylbenzene	7.91	2.07	2.57	18.31	1.64	29.13
m-Xylene	22.07	2.73	5.36	34.95	12.19	30.19
o-Xylene	7.31	1.01	2.38	17.10	38.32	19.83
Benzaldehyde	59.86	27.56	20.25	37.49	9.69	7.30
Styrene	6.53	5.14	3.79	16.97	17.68	11.63
Phenol	54.34	13.28	12.62	6.01	13.91	12.16
Indene	4.28	4.03	3.03	1.99	13.75	7.79
Indane	0.35	0.44	0.25	0.00	5.16	7.45
Naphthalene	13.45	8.96	6.55	23.13	3.17	6.07
Fluorene	0.66	0.09	0.09	61.04	141.31	50.64
Biphenyl	0.80	0.31	0.14	48.49	74.59	4.80
Acenaphthene	0.38	0.12	0.03	80.47	21.37	141.25
Acenaphthylene	0.21	0.31	0.27	141.26	7.57	4.26
Phenanthrene	1.07	0.22	0.21	71.78	76.52	52.34
Anthracene	0.25	n.d.	0.01	64.40	n.d.	142.86
Fluoranthene	0.61	0.05	0.05	5.45	5.17	30.53
Pyrene	0.51	0.16	0.10	119.65	47.45	2.00
2-Methylnaphthalene	3.07	1.11	0.86	75.32	24.08	3.62
1-Methylnaphthalene	2.10	0.78	0.55	32.75	14.58	7.71

1,2-Dimethylnaphthalene	0.38	n.d.	n.d.	141.36	n.d.	n.d.
1-Methylfluorene	n.d.	n.d.	n.d.	n.d.	n.d.	n.d.
n-Octane	n.d.	n.d.	n.d.	n.d.	n.d.	n.d.
n-Nonane	n.d.	n.d.	n.d.	n.d.	n.d.	n.d.
n-Decane	5.73	2.13	1.09	141.43	49.46	0.26
n-Undecane	8.19	3.25	1.52	141.42	38.41	10.44
n-Dodecane	16.44	4.42	3.92	72.83	64.28	66.00
n-Tridecane	16.87	4.56	1.66	97.65	84.11	2.39
n-Tetradecane	520.12	119.29	4.36	139.33	137.22	30.47
n-Pentadecane	150.05	31.72	2.20	131.22	130.84	0.39
n-Hexadecane	1672.63	12.29	9.82	140.53	55.46	96.35
n-Heptadecane	7.50	1.57	0.93	53.58	57.03	28.53
n-Octadecane	10.30	2.13	1.09	46.23	69.11	6.49
n-Nonadecane	18.57	1.16	0.89	26.85	27.60	6.40
n-Eicosane	6.44	1.02	0.64	12.58	33.06	12.86
Total VOCs + SVOCs	3768.03	487.96	317.03			

Table G9a: LODs and LOQs (ng) of target analytes for different samplers, namely PDMS, GW and activated charcoal. PDMS and GW samplers were directly thermally desorbed whilst the activated charcoal extract was first extracted with CS_2 and the extract was injected into the GC port. *(-) denotes that content is unavailable for a specific analyte/sampler combination.*

	Abr.	LOD (ng)			LOQ (ng)		
Target analytes		**PDMS**	**GW**	**Charcoal**	**PDMS**	**GW**	**Charcoal**
Benzene	-	0.03	0.44	0.002	0.09	1.45	0.01
Toluene	-	0.001	0.01	0.002	0.004	0.04	0.01
Ethylbenzene	-	0.02	0.09	0.003	0.06	0.29	0.01
m-Xylene	-	0.05	2.27	0.004	0.15	7.58	0.01
o-Xylene	-	0.07	0.07	0.002	0.22	0.24	0.01
Benzaldehyde	-	0.07	0.13	-	0.22	0.42	-
Styrene	-	0.02	0.13	0.001	0.06	0.43	0.003
Phenol	-	0.04	0.09	0.003	0.14	0.31	0.01
Indene	-	0.05	0.06	-	0.15	0.19	-
Indane	-	0.03	0.06	-	0.11	0.19	-
Naphthalene	Naph	0.004	0.86	0.001	0.01	2.85	0.003
Fluorene	FluE	0.02	0.03	-	0.08	0.11	-

Biphenyl	Biph	0.01	0.01	-	0.04	0.04	-
Acenaphthene	AceE	0.02	0.04	-	0.07	0.13	-
Acenaphthylene	AceY	0.02	0.02	-	0.06	0.08	-
Phenanthrene	Phe	0.01	0.02	-	0.05	0.05	-
Anthracene	Anth	0.02	0.02	-	0.06	0.06	-
Fluoranthene	FluA	0.01	0.02	-	0.03	0.05	-
Pyrene	Pyr	0.01	0.01	-	0.03	0.05	-
2-Methylnaphthalene	2-Mnap	0.03	0.03	-	0.11	0.10	-
1-Methylnaphthalene	1-MNap	0.10	0.58	-	0.33	1.92	-
1,2-Dimethylnaphthalene	1,2-DiMNap	0.001	0.31	-	0.002	1.02	-
1-Methylfluorene	1-MF	0.03	0.05	-	0.10	0.16	-
n-Octane	n-Oct	4.00	3.95	-	13.33	13.16	-
n-Nonane	n-Non	0.79	3.95	-	2.63	13.16	-
n-Decane	n-Dec	0.19	0.63	-	0.62	2.10	-
n-Undecane	n-Und	0.07	0.26	-	0.24	0.87	-
n-Dodecane	n-Dod	0.05	0.07	-	0.17	0.24	-
n-Tridecane	n-Tri	0.06	0.05	-	0.21	0.17	-
n-Tetradecane	n-Tet	0.02	0.04	-	0.06	0.12	-
n-Pentadecane	n-Pent	0.03	0.03	-	0.09	0.12	-
n-Hexadecane	n-Hex	0.04	0.04	-	0.12	0.12	-
n-Heptadecane	n-Hept	0.02	0.03	-	0.07	0.10	-
n-Octadecane	n-OctD	0.03	0.04	-	0.10	0.14	-
n-Nonadecane	n-NonD	0.04	0.04	-	0.13	0.13	-
n-Eicosane	n-Eic	0.05	0.12	-	0.16	0.41	-

Table G9b: LODs and LOQs (ng.m^{-3}) of target analytes for different samplers, namely PDMS, GW and activated charcoal. PDMS and GW samplers were directly thermally desorbed whilst the activated charcoal extract was first extracted with CS_2 and 1 µL of the 3 mL extract was injected into the GC port. *(-) denotes that content is unavailable for a specific analyte/ sampler combination.*

	Abr.	**LOD (µg.m^{-3})**			**LOQ (µg.m^{-3})**		
Target analytes		**PDMS**	**GW**	**Charcoal**	**PDMS**	**GW**	**Charcoal**
Benzene	-	0.01	0.09	0.99	0.02	0.29	3.31

Toluene	-	0.0002	0.002	1.10	0.00	0.01	3.66
Ethylbenzene	-	0.004	0.02	1.78	0.01	0.06	5.94
m-Xylene	-	0.01	0.45	2.26	0.03	1.52	7.55
o-Xylene	-	0.01	0.01	1.49	0.04	0.05	4.95
Benzaldehyde	-	0.01	0.03	-	0.04	0.08	-
Styrene	-	0.003	0.03	0.62	0.01	0.09	2.08
Phenol	-	0.01	0.02	1.50	0.03	0.06	5.01
Indene	-	0.01	0.01	-	0.03	0.04	-
Indane	-	0.01	0.01	-	0.02	0.04	-
Naphthalene	Naph	0.001	0.17	0.48	0.00	0.57	1.59
Fluorene	FluE	0.005	0.01	-	0.02	0.02	-
Biphenyl	Biph	0.002	0.003	-	0.01	0.01	-
Acenaphthene	AceE	0.004	0.01	-	0.01	0.03	-
Acenaphthylene	AceY	0.004	0.005	-	0.01	0.02	-
Phenanthrene	Phe	0.003	0.003	-	0.01	0.01	-
Anthracene	Anth	0.004	0.004	-	0.01	0.01	-
Fluoranthene	FluA	0.002	0.003	-	0.01	0.01	-
Pyrene	Pyr	0.002	0.003	-	0.01	0.01	-
2-Methylnaphthalene	2-Mnap	0.01	0.01	-	0.02	0.02	-
1-Methylnaphthalene	1-MNap	0.02	0.12	-	0.07	0.38	-
1,2-Dimethylnaphthalene	1,2-DiMNap	0.0001	0.06	-	0.00	0.20	-
1-Methylfluorene	1-MF	0.01	0.01	-	0.02	0.03	-
n-Octane	n-Oct	0.80	0.79	-	2.67	2.63	-
n-Nonane	n-Non	0.16	0.79	-	0.53	2.63	-
n-Decane	n-Dec	0.04	0.13	-	0.12	0.42	-
n-Undecane	n-Und	0.01	0.05	-	0.05	0.17	-
n-Dodecane	n-Dod	0.01	0.01	-	0.03	0.05	-
n-Tridecane	n-Tri	0.01	0.01	-	0.04	0.03	-
n-Tetradecane	n-Tet	0.003	0.01	-	0.01	0.02	-
n-Pentadecane	n-Pent	0.01	0.01	-	0.02	0.02	-
n-Hexadecane	n-Hex	0.01	0.01	-	0.02	0.02	-
n-Heptadecane	n-Hept	0.004	0.01	-	0.01	0.02	-
n-Octadecane	n-OctD	0.01	0.01	-	0.02	0.03	-
n-Nonadecane	n-NonD	0.01	0.01	-	0.03	0.03	-
n-Eicosane	n-Eic	0.01	0.02	-	0.03	0.08	-

Appendix H: Calibration curves for the 36 VOCs and SVOCs of interest in the CAST campaign

Section H1: Calibration curves for 36 VOCs and SVOCs thermally desorbed from a GW sampler

D:\TDU\South Africa\CAST\Quan_Graphene_VF-Xms_split10_flow15_V190708.qgm

Calibration

ID#:1 Mass:78.00 Name:Benzene
f(x)=0.006823*x+0.000000
rr2=0.981219

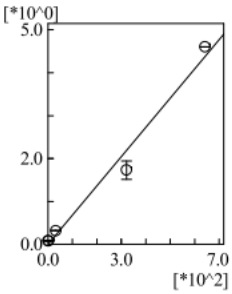

#	Conc. Ratio (ng)	Mean Area Ratio
1	642.103	4.61
2	321.051	1.73
3	32.105	0.32
4	3.211	0.08
5	0.642	0.08

ID#:2 Mass:91.00 Name:Toluene
f(x)=0.005260*x+0.200189
rr2=0.998800

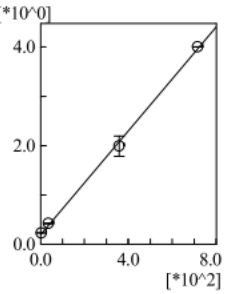

#	Conc. Ratio (ng)	Mean Area Ratio
1	715.183	4.00
2	357.591	1.99
3	35.759	0.42
4	3.576	0.23

ID#:3 Mass:91.00 Name:Ethylbenzene
f(x)=0.007873*x+0.000000
rr2=0.998870

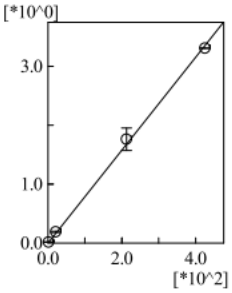

#	Conc. Ratio (ng)	Mean Area Ratio
1	425.481	3.30
2	212.741	1.76
3	21.274	0.19
4	2.127	0.02

ID#:4 Mass:91.00 Name:m-Xylene
f(x)=0.007345*x+0.000000
rr2=0.997759

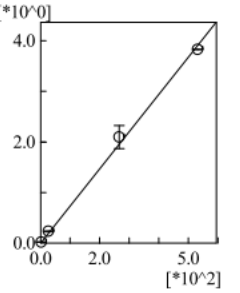

#	Conc. Ratio (ng)	Mean Area Ratio
1	531.238	3.83
2	265.619	2.09
3	26.562	0.23
4	2.656	0.02

ID#:5 Mass:91.00 Name:o-Xylene
f(x)=0.008967*x+0.000000
rr2=0.999958

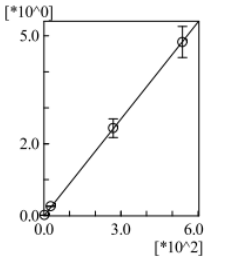

#	Conc. Ratio (ng)	Mean Area Ratio
1	539.213	4.82
2	269.606	2.44
3	26.961	0.27
4	2.696	0.03

ID#:6 Mass:106.00 Name:Benzaldehyde
f(x)=0.004486*x+0.000000
rr2=0.998334

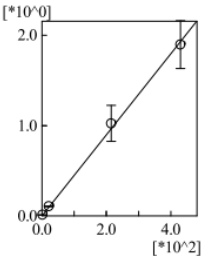

#	Conc. Ratio (ng)	Mean Area Ratio
1	429.614	1.90
2	214.807	1.02
3	21.481	0.11
4	2.148	0.01

ID#:7 Mass:104.00 Name:Styrene
f(x)=0.007127*x+0.000000
rr2=0.999878

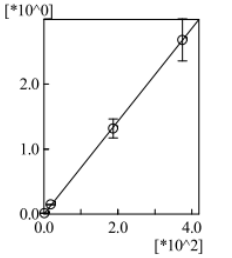

#	Conc. Ratio (ng)	Mean Area Ratio
1	374.260	2.68
2	187.130	1.32
3	18.713	0.15
4	1.871	0.02

ID#:8 Mass:94.00 Name:Phenol
f(x)=0.006741*x+0.000000
rr2=0.999979

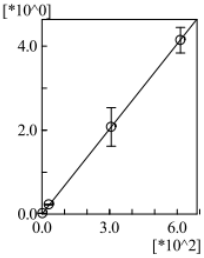

#	Conc. Ratio (ng)	Mean Area Ratio
1	614.666	4.14
2	307.333	2.08
3	30.733	0.23
4	3.073	0.02

ID#:9 Mass:108.00 Name:Benzylalcohol
f(x)=0.000029*x+0.000000
rr2=0.000000

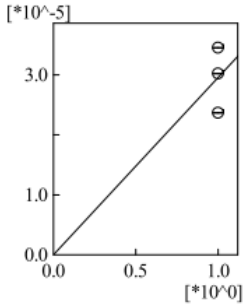

#	Conc. Ratio (ng)	Mean Area Ratio
1	1.000	0.00
2	1.000	0.00
3	1.000	0.00

ID#:10 Mass:108.00 Name:o-Cresol
f(x)=0.000042*x+0.000000
rr2=-1.#IND00

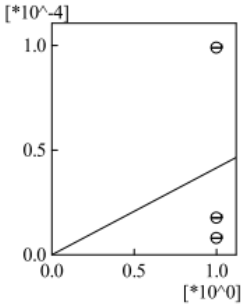

#	Conc. Ratio (ng)	Mean Area Ratio
1	1.000	0.00
2	1.000	0.00
3	1.000	0.00

ID#:11 Mass:108.00 Name:p-Cresol
f(x)=0.000000*x+0.000000
rr2=0.000000

cannot draw

ID#:12 Mass:108.00 Name:m-Cresol
f(x)=0.000026*x+0.000000
rr2=1.000000

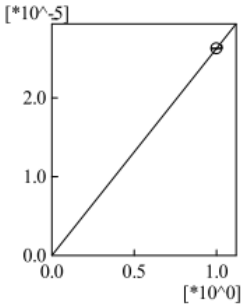

#	Conc. Ratio (ng)	Mean Area Ratio
1	1.000	0.00

ID#:13 Mass:115.00 Name:Indene
f(x)=0.005803*x+0.000000
rr2=0.998950

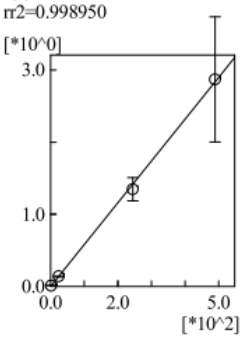

#	Conc. Ratio (ng)	Mean Area Ratio
1	488.788	2.87
2	244.394	1.35
3	24.439	0.14
4	2.444	0.01

ID#:14 Mass:117.00 Name:Indane
f(x)=0.006055*x+0.000000
rr2=1.000000

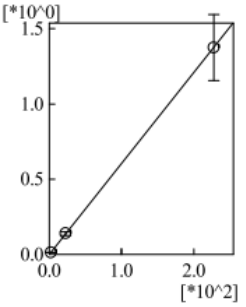

#	Conc. Ratio (ng)	Mean Area Ratio
2	227.220	1.38
3	22.722	0.14
4	2.272	0.02

ID#:15 Mass:128.00 Name:Naphthalene
f(x)=0.013680*x+0.000000
rr2=0.999999

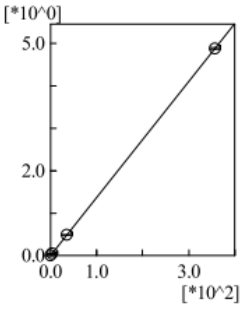

#	Conc. Ratio (ng)	Mean Area Ratio
1	356.400	4.88
2	35.640	0.49
3	3.564	0.05
4	0.356	0.01

ID#:16 Mass:166.00 Name:Fluorene
f(x)=0.039489*x+0.000000
rr2=0.999962

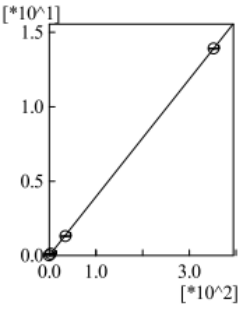

#	Conc. Ratio (ng)	Mean Area Ratio
1	352.000	13.91
2	35.200	1.30
3	3.520	0.13
4	0.352	0.01

ID#:17 Mass:154.00 Name:Biphenyl
f(x)=0.075192*x+0.000000
rr2=0.999998

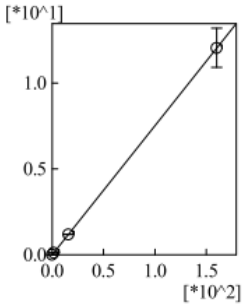

#	Conc. Ratio (ng)	Mean Area Ratio
1	160.000	12.03
2	16.000	1.19
3	1.600	0.13
4	0.160	0.02

ID#:18 Mass:154.00 Name:Acenaphthene
f(x)=0.116073*x+0.000000
rr2=0.999968

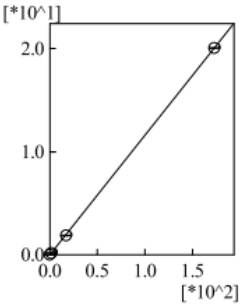

#	Conc. Ratio (ng)	Mean Area Ratio
1	172.900	20.08
2	17.290	1.89
3	1.729	0.19
4	0.173	0.02

ID#:19 Mass:152.00 Name:Acenaphthylene
f(x)=0.045648*x+0.000000
rr2=0.999909

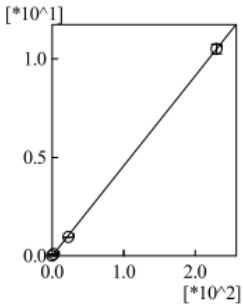

#	Conc. Ratio (ng)	Mean Area Ratio
1	230.000	10.51
2	23.000	0.95
3	2.300	0.10
4	0.230	0.01

ID#:20 Mass:178.00 Name:Phenanthrene
f(x)=0.055204*x+0.000000
rr2=0.999961

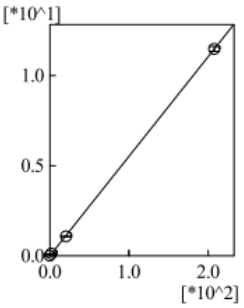

#	Conc. Ratio (ng)	Mean Area Ratio
1	207.760	11.48
2	20.776	1.08
3	2.078	0.12
4	0.208	0.02

ID#:21 Mass:178.00 Name:Anthracene
f(x)=0.067717*x+0.000000
rr2=0.999967

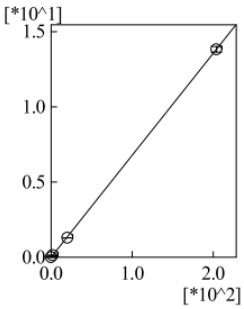

#	Conc. Ratio (ng)	Mean Area Ratio
1	204.000	13.82
2	20.400	1.30
3	2.040	0.13
4	0.204	0.02

ID#:22 Mass:202.00 Name:Fluoranthene
f(x)=0.059326*x+0.000000
rr2=0.999877

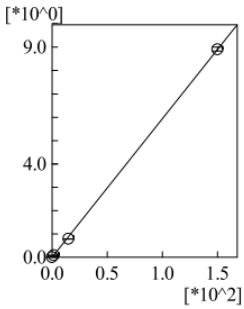

#	Conc. Ratio (ng)	Mean Area Ratio
1	150.024	8.91
2	15.002	0.79
3	1.500	0.08
4	0.150	0.01

ID#:23 Mass:202.00 Name:Pyrene
f(x)=0.066065*x+0.000000
rr2=0.999832

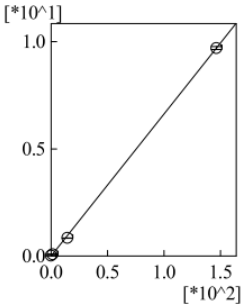

#	Conc. Ratio (ng)	Mean Area Ratio
1	146.520	9.69
2	14.652	0.84
3	1.465	0.09
4	0.147	0.02

ID#:24 Mass:142.00 Name:2-Methylnaphthalene
f(x)=0.007619*x+0.000000
rr2=0.999919

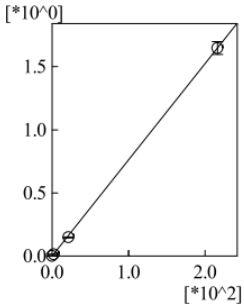

#	Conc. Ratio (ng)	Mean Area Ratio
1	216.000	1.65
2	21.600	0.15
3	2.160	0.01
4	0.216	0.00

ID#:25 Mass:142.00 Name:1-Methylnaphthalene
f(x)=0.009323*x+0.000000
rr2=0.999946

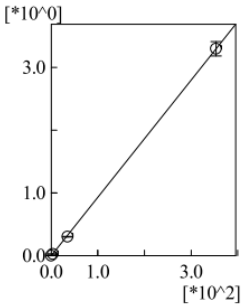

#	Conc. Ratio (ng)	Mean Area Ratio
1	353.400	3.30
2	35.340	0.30
3	3.534	0.03
4	0.353	0.00

ID#:26 Mass:156.00 Name:1,2-Dimethylnaphthalene
f(x)=0.005875*x+0.000000
rr2=0.999897

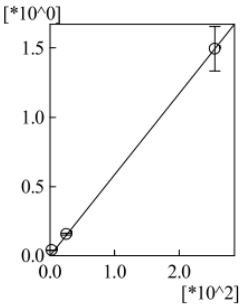

#	Conc. Ratio (ng)	Mean Area Ratio
1	254.800	1.50
2	25.480	0.16
3	2.548	0.04

ID#:27 Mass:165.00 Name:1-Methylfluorene
f(x)=0.038813*x+0.000000
rr2=0.999772

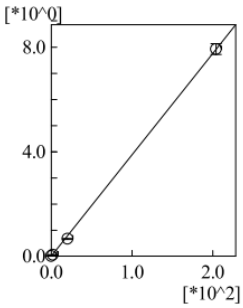

#	Conc. Ratio (ng)	Mean Area Ratio
1	203.840	7.92
2	20.384	0.66
3	2.038	0.06
4	0.204	0.01

ID#:28 Mass:57.00 Name:n-Octane
f(x)=0.007387*x+0.000000
rr2=0.994872

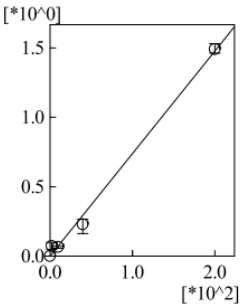

#	Conc. Ratio (ng)	Mean Area Ratio
1	200.000	1.49
2	40.000	0.23
3	10.000	0.07
4	2.000	0.07
5	0.000	0.00

ID#:29 Mass:57.00 Name:n-Nonane
f(x)=0.018455*x+0.000000
rr2=0.999861

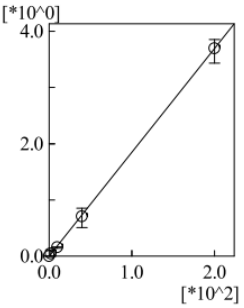

#	Conc. Ratio (ng)	Mean Area Ratio
1	200.000	3.70
2	40.000	0.71
3	10.000	0.16
4	2.000	0.05
5	0.000	0.00

ID#:30 Mass:57.00 Name:n-Decane
f(x)=0.021031*x+0.000000
rr2=0.999967

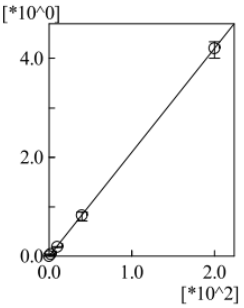

#	Conc. Ratio (ng)	Mean Area Ratio
1	200.000	4.21
2	40.000	0.83
3	10.000	0.19
4	2.000	0.04
5	0.000	0.00

ID#:31 Mass:57.00 Name:n-Undecane
f(x)=0.022665*x+0.000000
rr2=0.999960

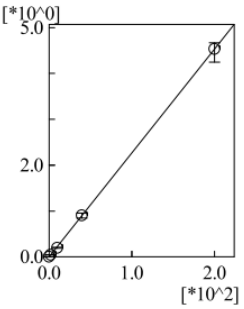

#	Conc. Ratio (ng)	Mean Area Ratio
1	200.000	4.53
2	40.000	0.91
3	10.000	0.20
4	2.000	0.04
5	0.000	0.00

ID#:32 Mass:57.00 Name:n-Dodecane
f(x)=0.023602*x+0.000000
rr2=0.999937

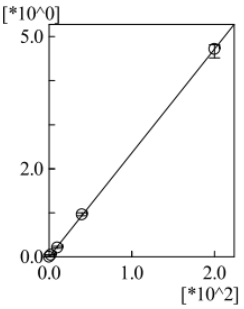

#	Conc. Ratio (ng)	Mean Area Ratio
1	200.000	4.72
2	40.000	0.97
3	10.000	0.21
4	2.000	0.05
5	0.000	0.01

ID#:33 Mass:57.00 Name:n-Tridecane
f(x)=0.023875*x+0.000000
rr2=0.999908

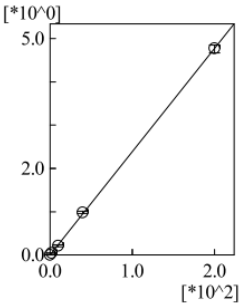

#	Conc. Ratio (ng)	Mean Area Ratio
1	200.000	4.77
2	40.000	0.98
3	10.000	0.21
4	2.000	0.05
5	0.000	0.00

ID#:34 Mass:57.00 Name:n-Tetradecane
f(x)=0.023775*x+0.000000
rr2=0.999904

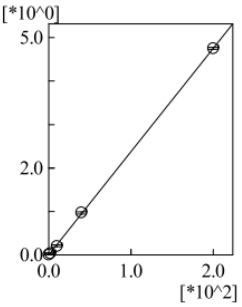

#	Conc. Ratio (ng)	Mean Area Ratio
1	200.000	4.75
2	40.000	0.98
3	10.000	0.21
4	2.000	0.04
5	0.000	0.01

ID#:35 Mass:57.00 Name:n-Pentadecane
f(x)=0.045364*x+0.000000
rr2=0.999919

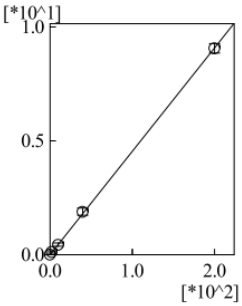

#	Conc. Ratio (ng)	Mean Area Ratio
1	200.000	9.06
2	40.000	1.89
3	10.000	0.44
4	2.000	0.12
5	0.000	0.01

ID#:36 Mass:57.00 Name:n-Hexadecane
f(x)=0.044876*x+0.000000
rr2=0.999885

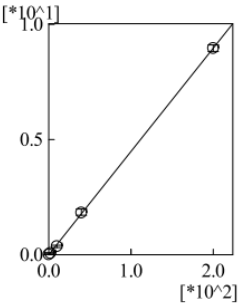

#	Conc. Ratio (ng)	Mean Area Ratio
1	200.000	8.97
2	40.000	1.83
3	10.000	0.37
4	2.000	0.08
5	0.000	0.02

ID#:37 Mass:57.00 Name:n-Heptadecane
f(x)=0.045314*x+0.000000
rr2=0.999915

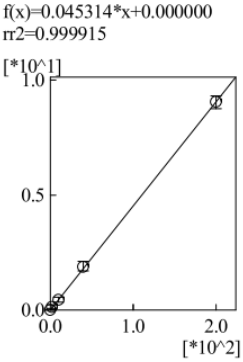

#	Conc. Ratio (ng)	Mean Area Ratio
1	200.000	9.05
2	40.000	1.88
3	10.000	0.43
4	2.000	0.14
5	0.000	0.00

ID#:38 Mass:57.00 Name:n-Octadecane
f(x)=0.044857*x+0.000000
rr2=0.999923

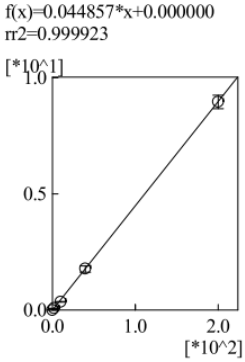

#	Conc. Ratio (ng)	Mean Area Ratio
1	200.000	8.98
2	40.000	1.79
3	10.000	0.36
4	2.000	0.08
5	0.000	0.00

ID#:39 Mass:57.00 Name:n-Nonadecane
f(x)=0.044969*x+0.000000
rr2=0.999883

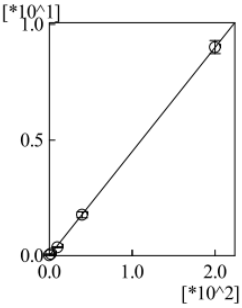

#	Conc. Ratio (ng)	Mean Area Ratio
1	200.000	9.00
2	40.000	1.77
3	10.000	0.36
4	2.000	0.07
5	0.000	0.03

ID#:40 Mass:57.00 Name:n-Eicosane
f(x)=0.038149*x+0.000000
rr2=0.999889

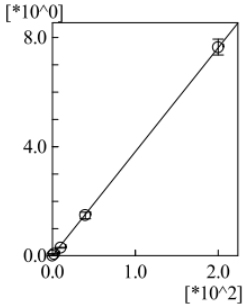

#	Conc. Ratio (ng)	Mean Area Ratio
1	200.000	7.64
2	40.000	1.49
3	10.000	0.30
4	2.000	0.06
5	0.000	0.00

Section H2: Calibration curves for 36 VOCs and SVOCs thermally desorbed from a PDMS sampler

D:\TDU\South Africa\CAST\Quan_VF-Xms_split10_flow15_V190630.qgm

Calibration

ID#:1 Mass:78.00 Name:Benzene
f(x)=0.005689*x+0.000000
rr2=0.999123

#	Conc. Ratio (ng)	Mean Area Ratio
1	642.103	3.69
2	321.051	1.76
3	32.105	0.19

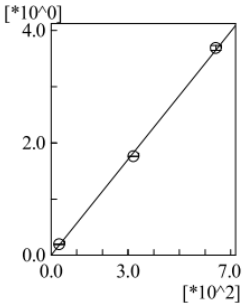

ID#:2 Mass:91.00 Name:Toluene
f(x)=0.005169*x+0.000000
rr2=0.999949

#	Conc. Ratio (ng)	Mean Area Ratio
1	715.183	3.66
2	357.591	1.90
3	35.759	0.37
4	3.576	0.22
5	0.715	0.20

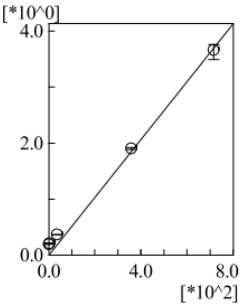

ID#:3 Mass:91.00 Name:Ethylbenzene
f(x)=0.005637*x+0.000000
rr2=0.999321

#	Conc. Ratio (ng)	Mean Area Ratio
1	425.481	2.42
2	212.741	1.15
3	21.274	0.13
4	2.127	0.02
5	0.425	0.01

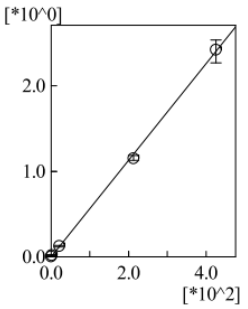

ID#:4 Mass:91.00 Name:m-Xylene
f(x)=0.004547*x+0.000000
rr2=0.999332

#	Conc. Ratio (ng)	Mean Area Ratio
1	531.238	2.44
2	265.619	1.16
3	26.562	0.12
4	2.656	0.01
5	0.531	0.00

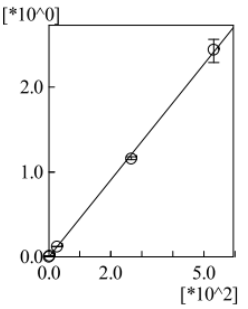

ID#:5 Mass:91.00 Name:o-Xylene
f(x)=0.004579*x+0.000000
rr2=0.999268

#	Conc. Ratio (ng)	Mean Area Ratio
1	539.213	2.50
2	269.606	1.18
3	26.961	0.12
4	2.696	0.01
5	0.539	0.00

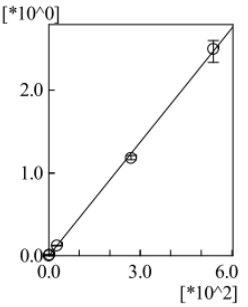

ID#:6 Mass:106.00 Name:Benzaldehyde
f(x)=0.002020*x+0.000000
rr2=0.997993

#	Conc. Ratio (ng)	Mean Area Ratio
1	429.614	0.88
2	214.807	0.40
3	21.481	0.04
4	2.148	0.00
5	0.430	0.00

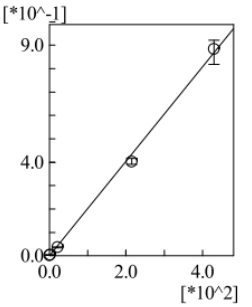

ID#:7 Mass:104.00 Name:Styrene
f(x)=0.003515*x+0.000000
rr2=0.993523

#	Conc. Ratio (ng)	Mean Area Ratio
1	374.260	1.36
2	187.130	0.57
3	18.713	0.06
4	1.871	0.01
5	0.374	0.01

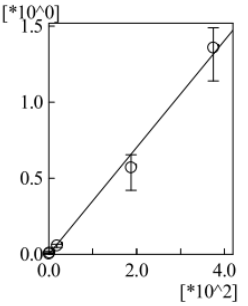

ID#:8 Mass:94.00 Name:Phenol
f(x)=0.003045*x+0.000000
rr2=0.998326

#	Conc. Ratio (ng)	Mean Area Ratio
1	614.666	1.90
2	307.333	0.87
3	30.733	0.08
4	3.073	0.01
5	0.615	0.00

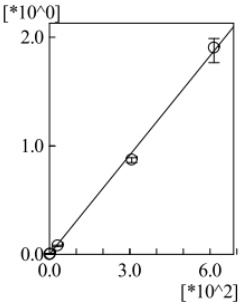

ID#:9 Mass:108.00 Name:Benzylalcohol
f(x)=0.000000*x+0.000000
rr2=0.000000

cannot draw

ID#:10 Mass:108.00 Name:o-Cresol
f(x)=0.000000*x+0.000000
rr2=0.000000

cannot draw

ID#:11 Mass:108.00 Name:p-Cresol
f(x)=0.000000*x+0.000000
rr2=0.000000

cannot draw

ID#:12 Mass:108.00 Name:m-Cresol
f(x)=0.000000*x+0.000000
rr2=0.000000

cannot draw

ID#:13 Mass:115.00 Name:Indene
f(x)=0.007009*x+0.000000
rr2=0.999568

#	Conc. Ratio (ng)	Mean Area Ratio
1	488.788	3.46
2	244.394	1.65
3	24.439	0.16
4	2.444	0.02
5	0.489	0.00

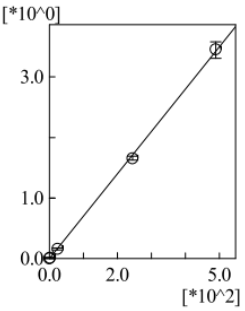

ID#:14 Mass:117.00 Name:Indane
f(x)=0.008253*x+0.000000
rr2=0.999871

#	Conc. Ratio (ng)	Mean Area Ratio
1	454.440	3.77
2	227.220	1.84
3	22.722	0.19
4	2.272	0.02
5	0.454	0.00

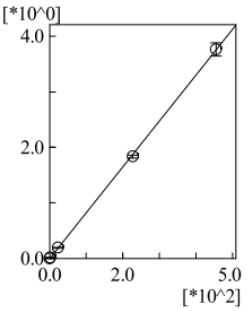

ID#:15 Mass:128.00 Name:Naphthalene
f(x)=0.012694*x+0.000000
rr2=0.999988

#	Conc. Ratio (ng)	Mean Area Ratio
1	356.400	4.52
2	35.640	0.46
3	3.564	0.04
4	0.356	0.01
5	0.071	0.01

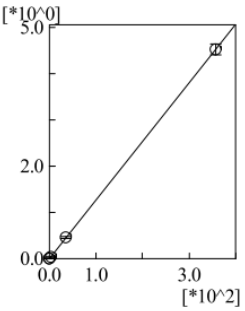

ID#:16 Mass:166.00 Name:Fluorene
f(x)=0.042179*x+0.000000
rr2=0.999922

#	Conc. Ratio (ng)	Mean Area Ratio
1	352.000	14.86
2	35.200	1.36
3	3.520	0.15
4	0.352	0.01
5	0.070	0.00

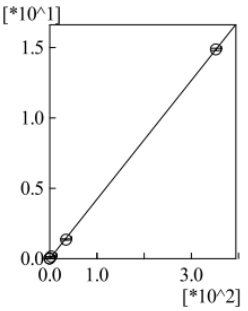

ID#:17 Mass:154.00 Name:Biphenyl
f(x)=0.090853*x+0.000000
rr2=0.999949

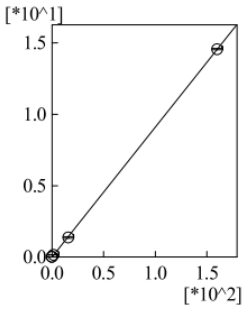

#	Conc. Ratio (ng)	Mean Area Ratio
1	160.000	14.55
2	16.000	1.36
3	1.600	0.15
4	0.160	0.02
5	0.032	0.01

ID#:18 Mass:154.00 Name:Acenaphthene
f(x)=0.122517*x+0.000000
rr2=0.999956

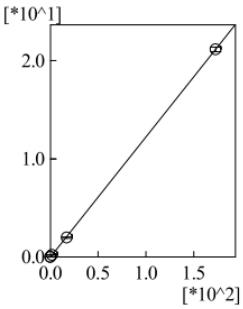

#	Conc. Ratio (ng)	Mean Area Ratio
1	172.900	21.20
2	17.290	1.98
3	1.729	0.22
4	0.173	0.03
5	0.035	0.01

ID#:19 Mass:152.00 Name:Acenaphthylene
f(x)=0.044615*x+0.000000
rr2=0.999947

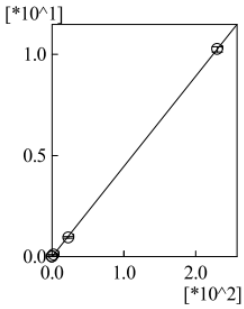

#	Conc. Ratio (ng)	Mean Area Ratio
1	230.000	10.27
2	23.000	0.95
3	2.300	0.10
4	0.230	0.01
5	0.046	0.00

ID#:20 Mass:178.00 Name:Phenanthrene
f(x)=0.054523*x+0.000000
rr2=0.999968

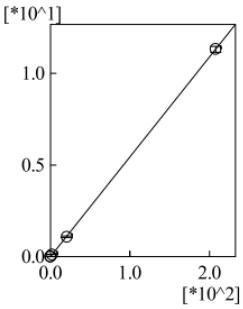

#	Conc. Ratio (ng)	Mean Area Ratio
1	207.760	11.33
2	20.776	1.07
3	2.078	0.12
4	0.208	0.01
5	0.042	0.00

ID#:21 Mass:178.00 Name:Anthracene
f(x)=0.070382*x+0.000000
rr2=0.999933

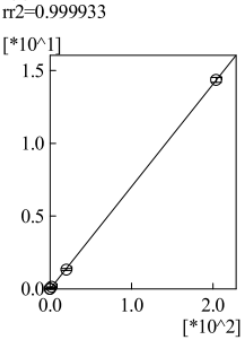

#	Conc. Ratio (ng)	Mean Area Ratio
1	204.000	14.37
2	20.400	1.32
3	2.040	0.14
4	0.204	0.02
5	0.041	0.00

ID#:22 Mass:202.00 Name:Fluoranthene
f(x)=0.059174*x+0.000000
rr2=0.999910

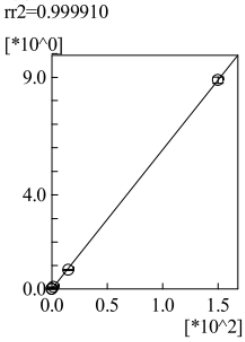

#	Conc. Ratio (ng)	Mean Area Ratio
1	150.024	8.89
2	15.002	0.81
3	1.500	0.09
4	0.150	0.01
5	0.030	0.00

ID#:23 Mass:202.00 Name:Pyrene
f(x)=0.064697*x+0.000000
rr2=0.999913

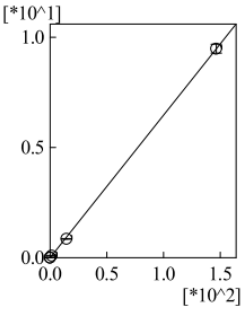

#	Conc. Ratio (ng)	Mean Area Ratio
1	146.520	9.49
2	14.652	0.86
3	1.465	0.10
4	0.147	0.01
5	0.029	0.00

ID#:24 Mass:142.00 Name:2-Methylnaphthalene
f(x)=0.007035*x+0.000000
rr2=0.999909

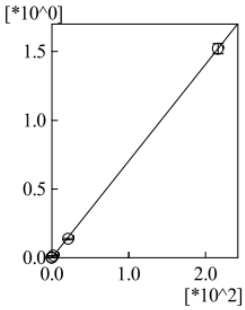

#	Conc. Ratio (ng)	Mean Area Ratio
1	216.000	1.52
2	21.600	0.14
3	2.160	0.01
4	0.216	0.00
5	0.043	0.00

ID#:25 Mass:142.00 Name:1-Methylnaphthalene
f(x)=0.008643*x+0.000000
rr2=0.999962

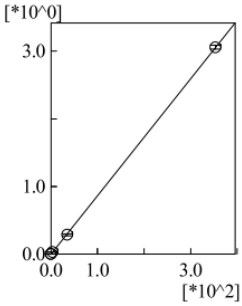

#	Conc. Ratio (ng)	Mean Area Ratio
1	353.400	3.06
2	35.340	0.29
3	3.534	0.03
4	0.353	0.00
5	0.071	0.00

ID#:26 Mass:156.00 Name:1,2-Dimethylnaphthalene
f(x)=0.005113*x+0.000000
rr2=0.999955

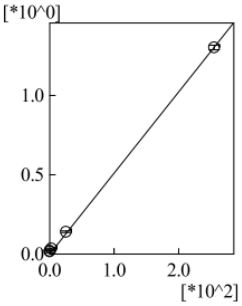

#	Conc. Ratio (ng)	Mean Area Ratio
1	254.800	1.30
2	25.480	0.14
3	2.548	0.04
4	0.255	0.02
5	0.051	0.02

ID#:27 Mass:165.00 Name:1-Methylfluorene
f(x)=0.038827*x+0.000000
rr2=0.999876

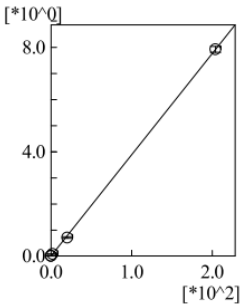

#	Conc. Ratio (ng)	Mean Area Ratio
1	203.840	7.92
2	20.384	0.70
3	2.038	0.08
4	0.204	0.01
5	0.041	0.00

ID#:28 Mass:57.00 Name:n-Octane
f(x)=0.008178*x+0.000000
rr2=0.995932

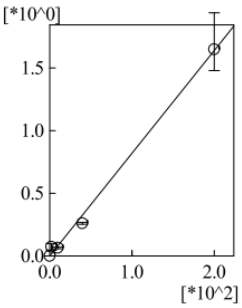

#	Conc. Ratio (ng)	Mean Area Ratio
1	200.000	1.65
2	40.000	0.26
3	10.000	0.07
4	2.000	0.07
5	0.000	0.00

ID#:29 Mass:57.00 Name:n-Nonane
f(x)=0.020185*x+0.000000
rr2=0.999661

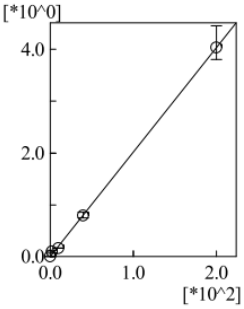

#	Conc. Ratio (ng)	Mean Area Ratio
1	200.000	4.04
2	40.000	0.80
3	10.000	0.17
4	2.000	0.09
5	0.000	0.00

ID#:30 Mass:57.00 Name:n-Decane
f(x)=0.021400*x+0.000000
rr2=0.999885

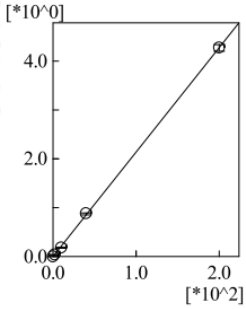

#	Conc. Ratio (ng)	Mean Area Ratio
1	200.000	4.28
2	40.000	0.88
3	10.000	0.18
4	2.000	0.04
5	0.000	0.00

ID#:31 Mass:57.00 Name:n-Undecane
f(x)=0.023164*x+0.000000
rr2=0.999888

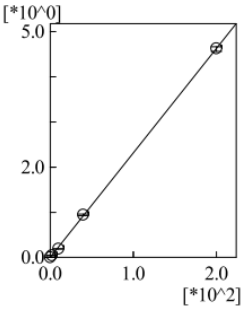

#	Conc. Ratio (ng)	Mean Area Ratio
1	200.000	4.63
2	40.000	0.95
3	10.000	0.19
4	2.000	0.04
5	0.000	0.00

ID#:32 Mass:57.00 Name:n-Dodecane
f(x)=0.023943*x+0.000000
rr2=0.999855

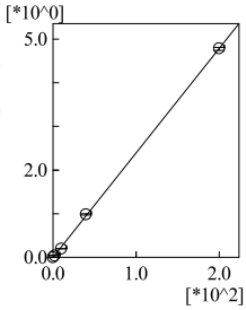

#	Conc. Ratio (ng)	Mean Area Ratio
1	200.000	4.78
2	40.000	0.99
3	10.000	0.20
4	2.000	0.05
5	0.000	0.00

ID#:33 Mass:57.00 Name:n-Tridecane
f(x)=0.024052*x+0.000000
rr2=0.999832

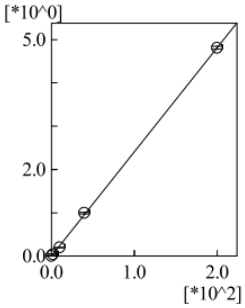

#	Conc. Ratio (ng)	Mean Area Ratio
1	200.000	4.81
2	40.000	0.99
3	10.000	0.20
4	2.000	0.05
5	0.000	0.00

ID#:34 Mass:57.00 Name:n-Tetradecane
f(x)=0.023759*x+0.000000
rr2=0.999845

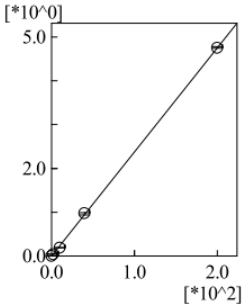

#	Conc. Ratio (ng)	Mean Area Ratio
1	200.000	4.75
2	40.000	0.98
3	10.000	0.19
4	2.000	0.04
5	0.000	0.00

ID#:35 Mass:57.00 Name:n-Pentadecane
f(x)=0.045677*x+0.000000
rr2=0.999724

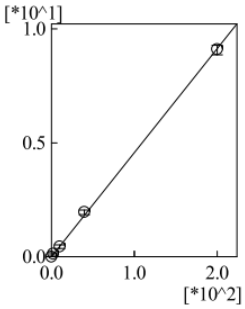

#	Conc. Ratio (ng)	Mean Area Ratio
1	200.000	9.11
2	40.000	1.97
3	10.000	0.45
4	2.000	0.14
5	0.000	0.00

ID#:36 Mass:57.00 Name:n-Hexadecane
f(x)=0.044956*x+0.000000
rr2=0.999711

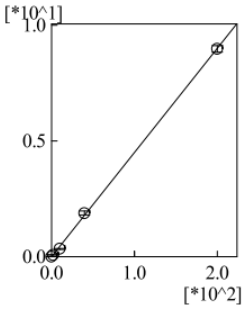

#	Conc. Ratio (ng)	Mean Area Ratio
1	200.000	8.98
2	40.000	1.88
3	10.000	0.35
4	2.000	0.08
5	0.000	0.00

ID#:37 Mass:57.00 Name:n-Heptadecane
f(x)=0.045747*x+0.000000
rr2=0.999664

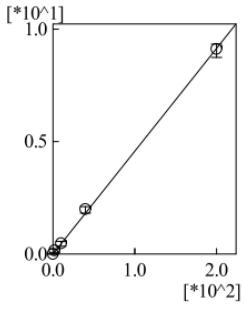

#	Conc. Ratio (ng)	Mean Area Ratio
1	200.000	9.12
2	40.000	1.99
3	10.000	0.47
4	2.000	0.16
5	0.000	0.00

ID#:38 Mass:57.00 Name:n-Octadecane
f(x)=0.045187*x+0.000000
rr2=0.999822

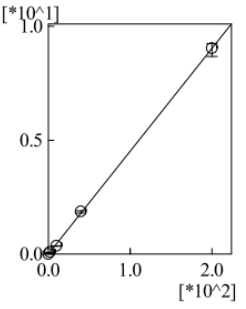

#	Conc. Ratio (ng)	Mean Area Ratio
1	200.000	9.03
2	40.000	1.86
3	10.000	0.36
4	2.000	0.08
5	0.000	0.00

ID#:39 Mass:57.00 Name:n-Nonadecane
f(x)=0.045309*x+0.000000
rr2=0.999827

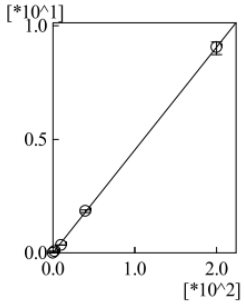

#	Conc. Ratio (ng)	Mean Area Ratio
1	200.000	9.06
2	40.000	1.85
3	10.000	0.35
4	2.000	0.08
5	0.000	0.00

ID#:40 Mass:57.00 Name:n-Eicosane
f(x)=0.038666*x+0.000000
rr2=0.999818

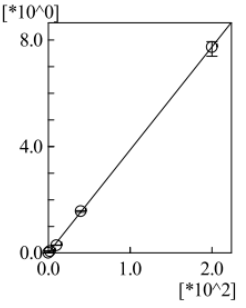

#	Conc. Ratio (ng)	Mean Area Ratio
1	200.000	7.73
2	40.000	1.57
3	10.000	0.29
4	2.000	0.07
5	0.000	0.00

Section H3: Calibration curves for 36 VOCs and SVOCs thermally desorbed from a GW sampler

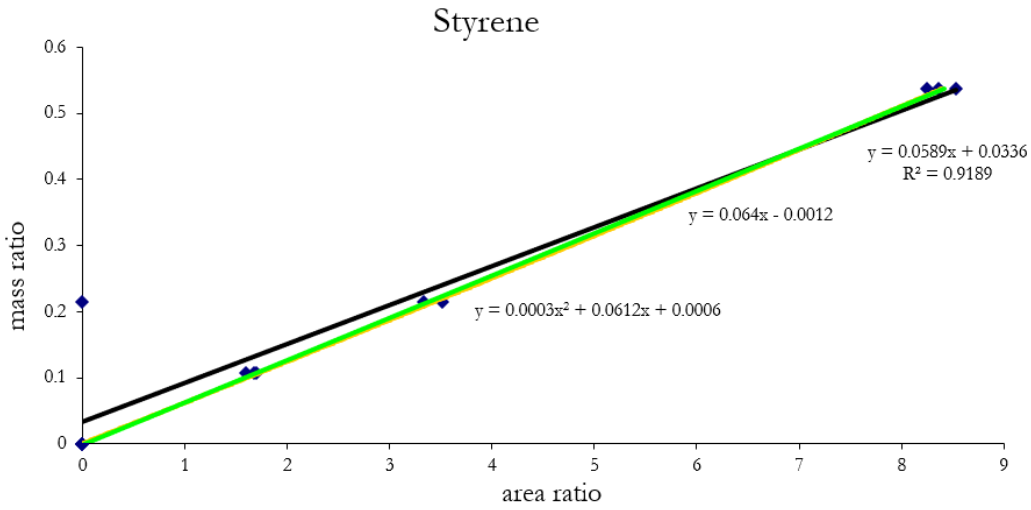

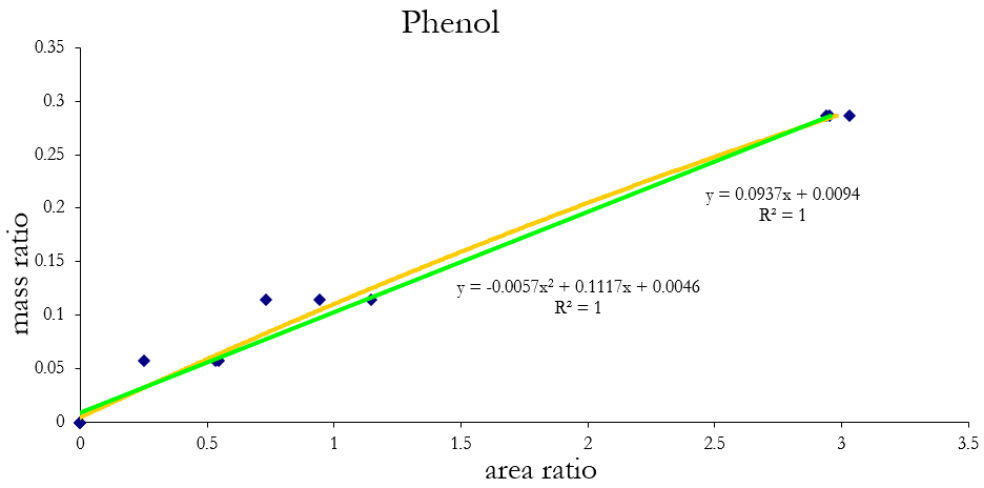

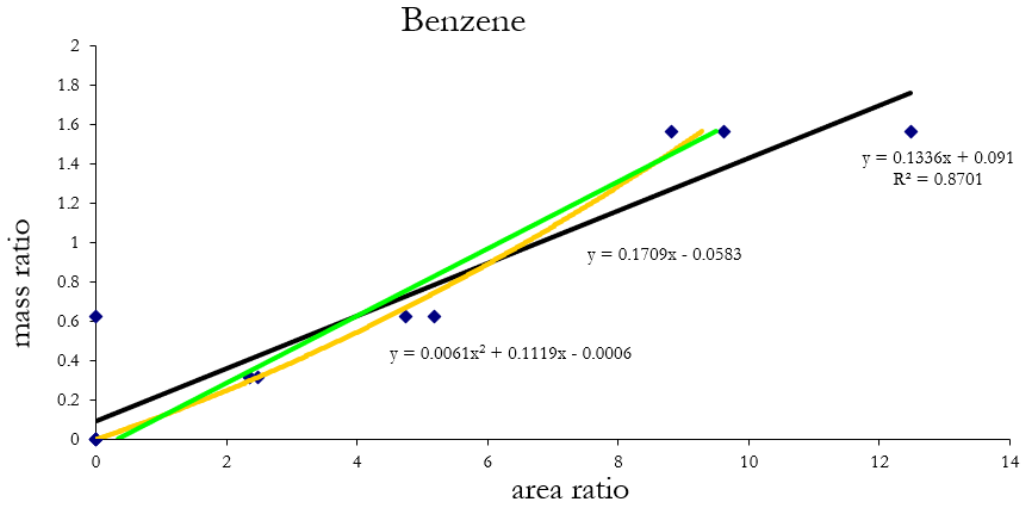

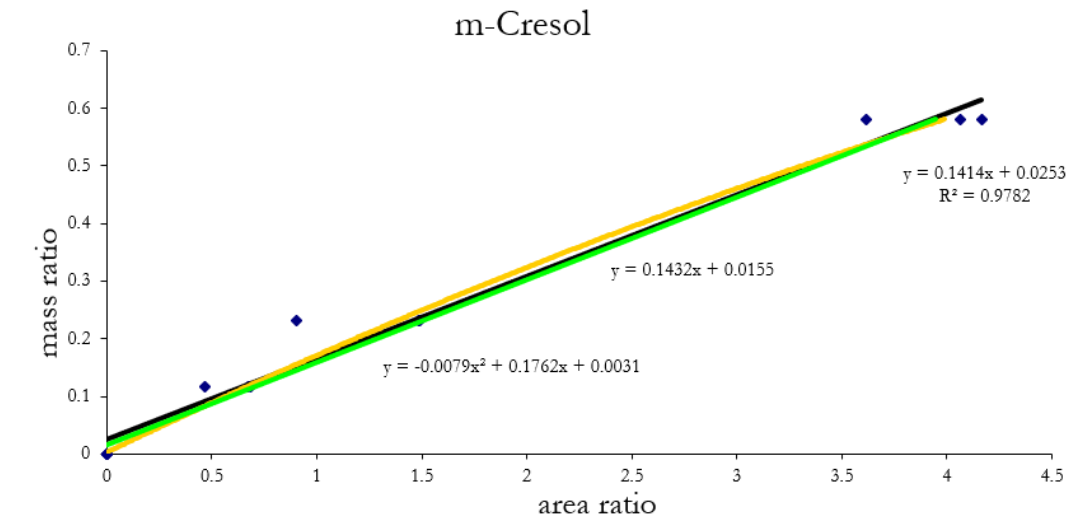

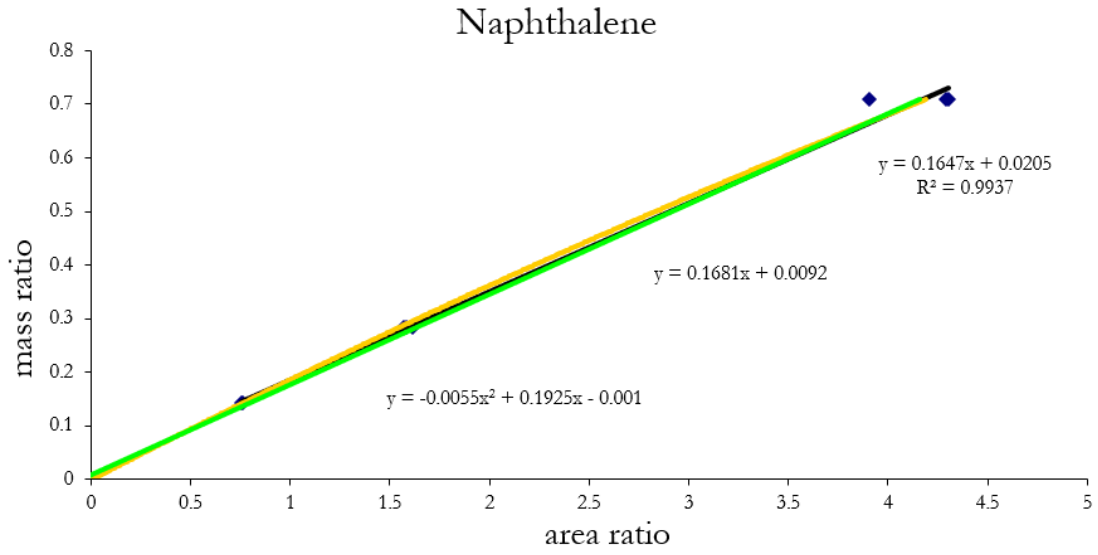

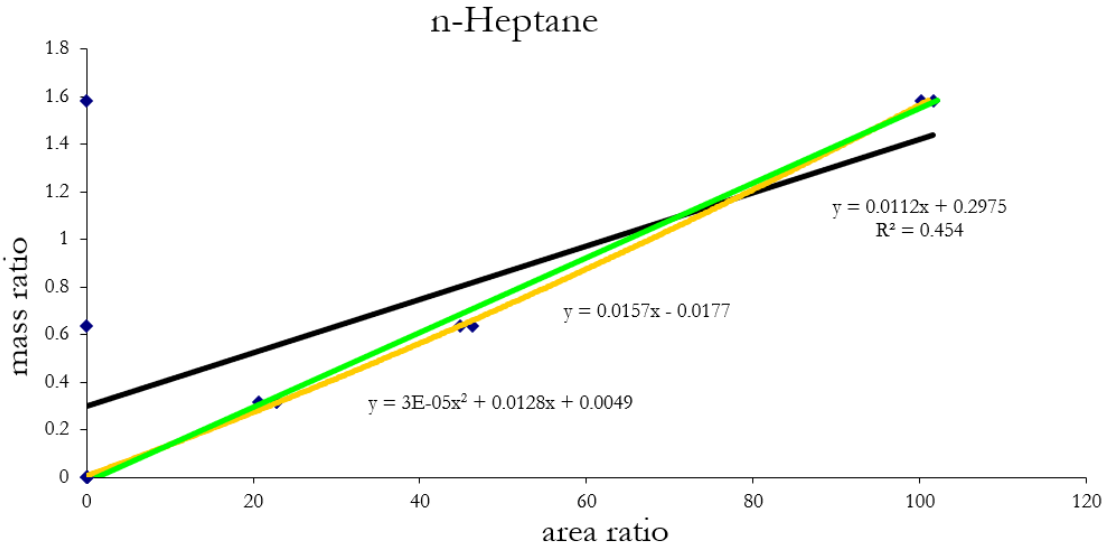

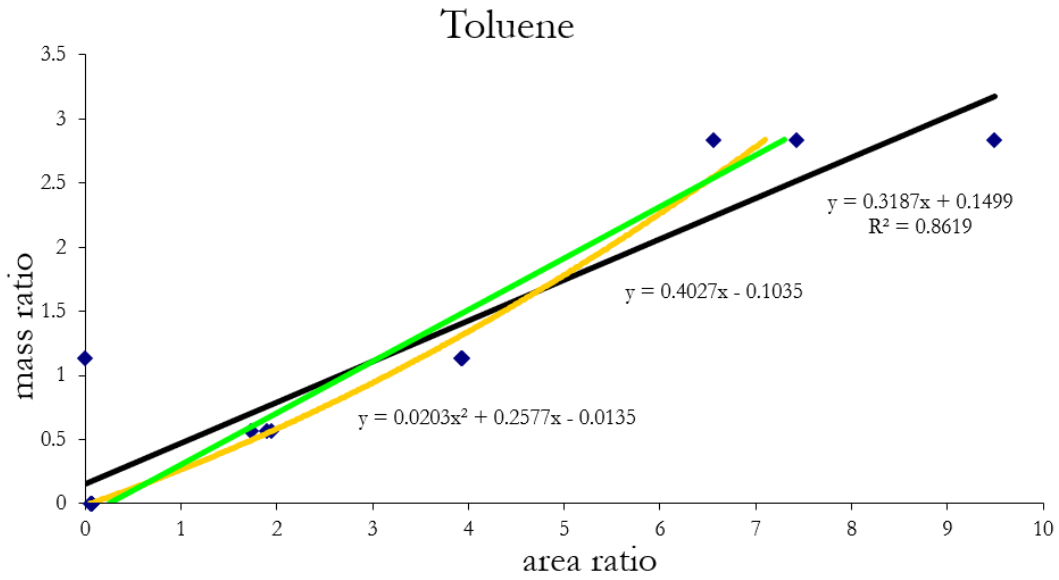

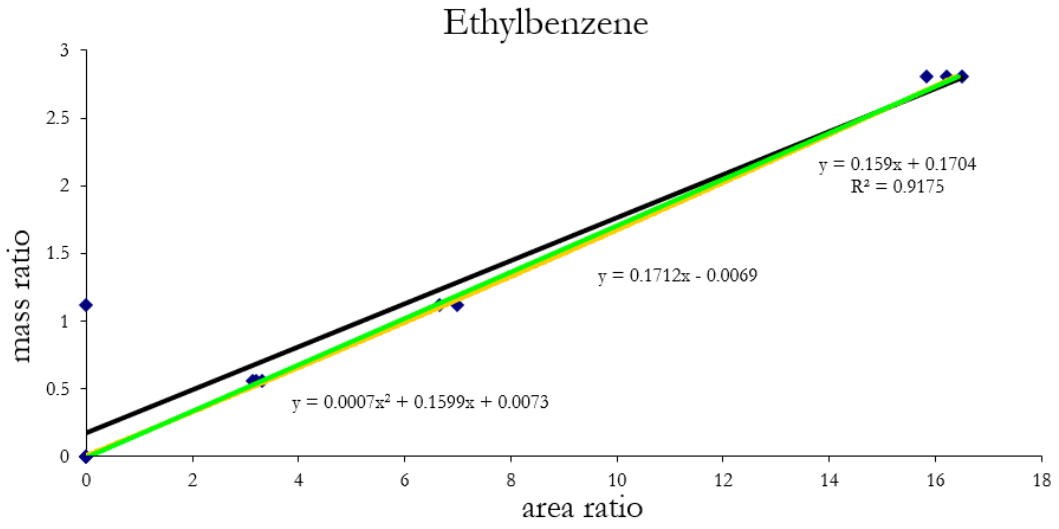

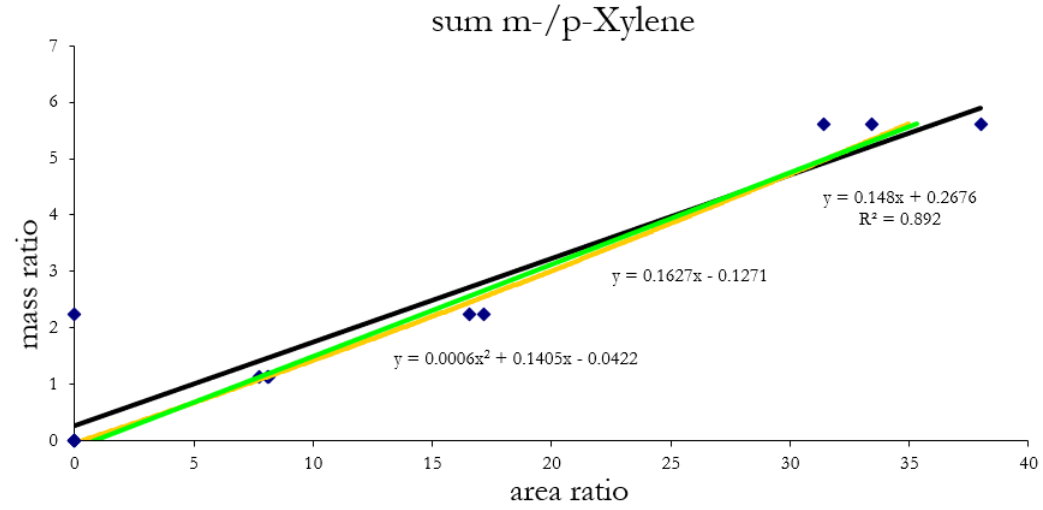

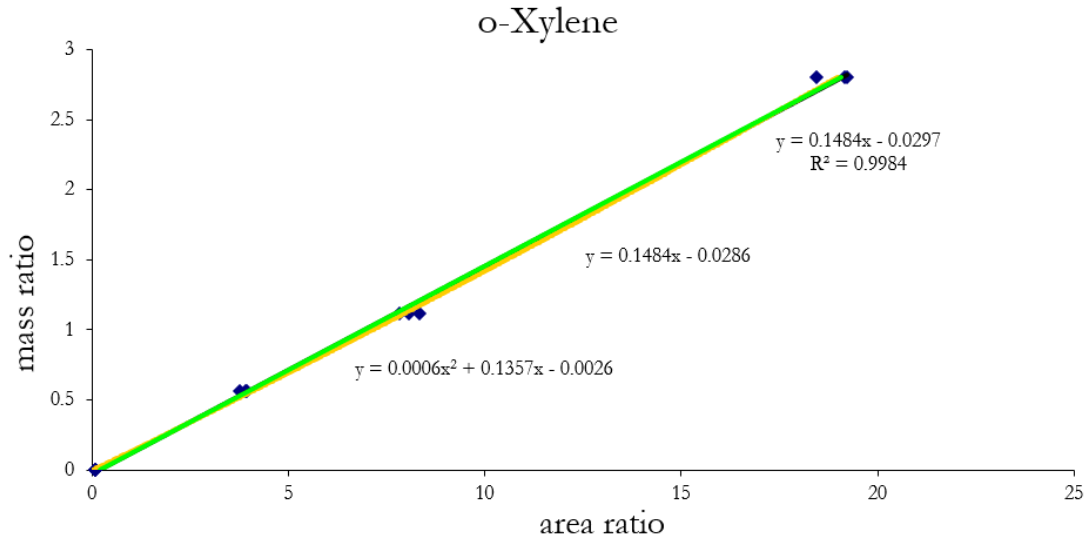

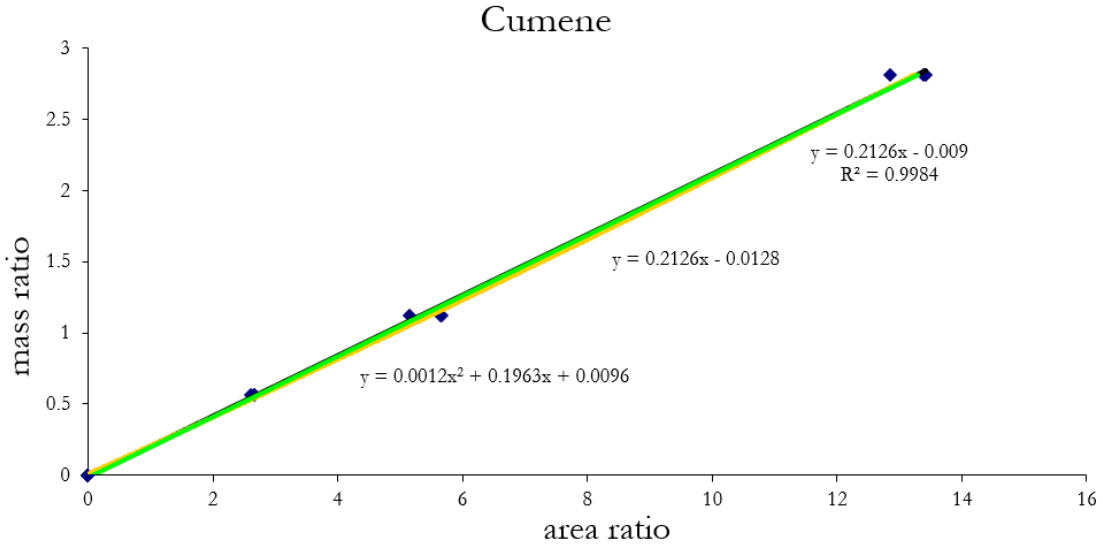

Appendix I: Certificates of analysis

125 Market Street
New Haven, CT 06513
USA

Tel (203)786-5290
Fax (203)786-5287
www.AccuStandard.com

AccuStandard®

CERTIFICATE OF ANALYSIS

Catalog No: M-502-10X
Description: Method 502.2 - Volatile Organic Compounds
Lot: 218101045
Solvent: Methanol
Hazards: *Refer to SDS for complete safety information*

Signal Word: Danger

Date Certified: Oct 8, 2018
Expiration: Oct 8, 2021
Sample Size: 1 mL
Components: 60
Storage Condition: Refrig (0-5 °C)

Included on ISO/IEC 17025 Scope of Accreditation: Yes

Included on ISO 17034 Scope of Accreditation: Yes

Component	CAS #	Purity % (GC/MS)	Prepared Concentration[1] (µg/mL)	Certified Analyte Concentration[2] (µg/mL)
Benzene	71-43-2	99.2	2002	1986
Bromobenzene	108-86-1	100.0	2002	2002
Bromochloromethane	74-97-5	99.1	2005	1987
Bromodichloromethane	75-27-4	99.0	2002	1982
Bromoform	75-25-2	99.2	2000	1984
n-Butylbenzene	104-51-8	99.1	2004	1986
sec-Butylbenzene	135-98-8	100.0	2001	2001
tert-Butylbenzene	98-06-6	99.6	2003	1995
Carbon tetrachloride	56-23-5	100.0	2010	2010
Chlorobenzene	108-90-7	99.6	2004	1996
Chloroform	67-66-3	99.2	2003	1987
2-Chlorotoluene	95-49-8	100.0	2001	2001
4-Chlorotoluene	106-43-4	98.1	2000	1962
Dibromochloromethane	124-48-1	98.4	2002	1970
1,2-Dibromo-3-chloropropane	96-12-8	100.0	2001	2001
1,2-Dibromoethane	106-93-4	100.0	2000	2000
Dibromomethane	74-95-3	99.0	2003	1983
1,2-Dichlorobenzene	95-50-1	98.2	2002	1966
1,3-Dichlorobenzene	541-73-1	98.8	2002	1978
1,4-Dichlorobenzene	106-46-7	100.0	2018	2018
1,1-Dichloroethane	75-34-3	99.8	2001	1997
1,2-Dichloroethane	107-06-2	99.8	2001	1997
1,1-Dichloroethene	75-35-4	99.0	2001	1981
cis-1,2-Dichloroethene	156-59-2	99.0	2001	1981
trans-1,2-Dichloroethene	156-60-5	100.0	2005	2005
1,2-Dichloropropane	78-87-5	99.5	2000	1990
1,3-Dichloropropane	142-28-9	96.7	2070*	2002
2,2-Dichloropropane	594-20-7	99.9	2002	2000
1,1-Dichloropropene	563-58-6	98.5	2001	1971
cis-1,3-Dichloropropene	10061-01-5	100.0	2001	2001
trans-1,3-Dichloropropene	10061-02-6	99.5	2002	1992
Ethylbenzene	100-41-4	99.0	2000	1980
Hexachlorobutadiene	87-68-3	98.0	2002	1962
Isopropylbenzene	98-82-8	100.0	2001	2001
p-Isopropyltoluene	99-87-6	99.4	2002	1990
Dichloromethane	75-09-2	99.9	2003	2001
Naphthalene	91-20-3	98.4	2002	1970
Propylbenzene	103-65-1	100.0	2001	2001
Styrene	100-42-5	100.0	2002	2002
1,1,1,2-Tetrachloroethane	630-20-6	98.9	2001	1979
1,1,2,2-Tetrachloroethane **	79-34-5	98.3	2001	1967
Tetrachloroethene	127-18-4	99.7	2003	1997
Toluene	108-88-3	99.5	2003	1993
1,2,3-Trichlorobenzene	87-61-6	99.7	2000	1994
1,2,4-Trichlorobenzene	120-82-1	99.6	2001	1993
1,1,1-Trichloroethane	71-55-6	100.0	2005	2005
1,1,2-Trichloroethane	79-00-5	98.6	2001	1973

For use in routine laboratory analysis.

AccuStandard is accredited to ISO 17034, ISO/IEC 17025 and certified to ISO 9001:2015

QR-ORG/INO-001
Rev. 5/18

125 Market Street
New Haven, CT 06513
USA

AccuStandard®

Tel (203)786-5290
Fax (203)786-5287
www.AccuStandard.com

CERTIFICATE OF ANALYSIS

Catalog No: M-502-10X
Description: Method 502.2 - Volatile Organic Compounds
Lot: 218101045
Solvent: Methanol

Date Certified: Oct 8, 2018
Expiration: Oct 8, 2021
Sample Size: 1 mL
Components: 60

Component - *continued*	CAS #	Purity % (GC/MS)	Prepared Concentration[1] (µg/mL)	Certified Analyte Concentration[2] (µg/mL)
Trichloroethene	79-01-6	100.0	2001	2001
1,2,3-Trichloropropane	96-18-4	97.5	2054*	2003
1,2,4-Trimethylbenzene	95-63-6	97.5	2051*	2000
1,3,5-Trimethylbenzene	108-67-8	98.1	2001	1963
o-Xylene	95-47-6	99.0	2000	1980
m-Xylene	108-38-3	99.8	2003	1999
p-Xylene	106-42-3	99.9	2001	1999
Bromomethane	74-83-9	99.5	2020	2010
Chloroethane	75-00-3	99.7	2008	2002
Chloromethane	74-87-3	99.5	2008	1998
Dichlorodifluoromethane	75-71-8	99.0	2000	1980
Trichlorofluoromethane	75-69-4	100.0	2000	2000
Vinyl chloride	75-01-4	99.5	2000	1990

* Weight compensated to 100% purity.

** Contains 1.5% Pentachloroethane

A product with a suffix (-1A, -2B, etc. or -01, -02, etc.) on its lot number has had its expiration date extended and is identical to the same lot number without the suffix.

[1] All weights are traceable through NIST, Test No. 684/289871-17

[2] Certified Analyte Concentration = Purity x Prepared Concentration.

The Uncertainty associated with the certified concentration reported on this certificate is ±2.4%. This value is the combined expanded uncertainty and represents an estimated standard deviation equal to the positive square root of the total variation of the uncertainty of components. A normal distribution is assumed and a coverage factor of K=2 is chosen using approximately a 95% confidence level.

Labels and certificates follow U.S. Conventions in reporting numerical values: A comma (,) is used to separate units of one-thousand or greater. A period (.) is used as a decimal place marker.

Certified By: Larry Decker, Organic QC Manager

For use in routine laboratory analysis.

AccuStandard is accredited to ISO 17034, ISO/IEC 17025 and certified to ISO 9001:2015

QR-ORG/INO-001
Rev. 5/18

Certificate of Analysis

QTM PAH MIX 1X1ML,2000UG/ML,DICHLOROMEHTANE

Certified Reference Material

Product ID CRM47930
Lot **LRAC0500**
Expiration Date October 2021
MFG Date October 2018
Storage Conditions Refrigerate
Solvent/Matrix DICHLOROMETHANE

Analyte	*Units*	*Certified Value* [1,4]	*Analytical Value*	*Raw Material Purity,%*	*Raw Material lot*	*Elution order*	*CAS*
NAPHTHALENE	µg/ml	2000 ± 191	2070	99.9	16412TN	1	91-20-3
ACENAPHTHENE	µg/ml	2000 ± 200	2130	99.9	MKCC8329	2	83-32-9
2-BROMONAPHTHALENE	µg/ml	2000 ± 441	2020	99.9	LB94855	3	580-13-2
ACENAPHTHYLENE	µg/ml	2000 ± 196	2080	99.6	LC20622	4	208-96-8
FLUORENE	µg/ml	2000 ± 200	2110	99.4	LC19126	5	86-73-7
PHENANTHRENE	µg/ml	2000 ± 200	2070	99.1	LB92396	6	85-01-8
ANTHRACENE	µg/ml	2000 ± 199	2070	99.9	LC14310	7	120-12-7
FLUORANTHENE	µg/ml	2000 ± 199	2090	98.2	LC08645	8	206-44-0
PYRENE	µg/ml	2000 ± 207	2180	91.6	LB70761	9	129-00-0
BENZO (A) ANTHRACENE	µg/ml	2000 ± 193	2040	99.9	LC19271	10	56-55-3
CHRYSENE	µg/ml	2000 ± 200	2090	99	21L74	11	218-01-9
BENZO (B) FLUORANTHENE	µg/ml	2000 ± 204	2100	99.5	LB95773	12	205-99-2
BENZO (A) PYRENE	µg/ml	2000 ± 194	2040	100	SLBV8459	14	50-32-8
INDENO (1,2,3-CD) PYRENE	µg/ml	2000 ± 198	2080	99.5	ER082107-02	15	193-39-5
DIBENZ (A,H) ANTHRACENE	µg/ml	2000 ± 198	2080	99.7	LC18254	15	53-70-3
BENZO (G,H,I) PERYLENE	µg/ml	2000 ± 195	2050	98.8	LC11626	16	191-24-2

ANAB ACCREDITED REFERENCE MATERIAL PRODUCER
ANAB ACCREDITED TESTING LABORATORY

SIGMA-ALDRICH
2931 Soldier Springs Rd. Laramie, Wyoming 82070 USA
307-742-5452
rictechgroup@sial.com www.sigma-aldrich.com

SIGMA-ALDRICH

3050 Spruce Street, Saint Louis, MO 63103 USA
Email USA: techserv@sial.com Outside USA: eurtechserv@sial.com

Certificate of Analysis

Product Name:	ALKANE STANDARD SOLUTION C_8-C_{20} analytical standard, contains C_8--C_{20}, ~40 mg/L each, in hexane
Product Number:	04070
Batch Number:	BCBS0046V
Brand:	Sigma-Aldrich
CAS Number:	
Formula:	
Formula Weight:	
Quality Release Date:	30 JUN 2016

TEST	SPECIFICATION	RESULT
APPEARANCE (COLOR)	COLORLESS	COLORLESS
APPEARANCE (FORM)	LIQUID	LIQUID
PURITY (GC AREA %)	CONTAINS 13 COMPOUNDS (C8 - C20)	IDENTITY PROOFED, CONTAINS 13 COMPOUNDS (C8 - C20)
DENSITY D20/4	0.659 - 0.661	0.660
REFRACTIVE INDEX N20/D	1.374 - 1.376	1.375

Dr. Claudia Geitner
Manager Quality Control
Buchs, Switzerland

ASG
Analytik-Service
Gesellschaft

ASG Analytik-Service Gesellschaft mbH
Trentiner Ring 30 • 86356 Neusäss • Germany

ASG Analytik-Service Gesellschaft mbH
Trentiner Ring 30
86356 Neusäss

Your reference	:	JBor
Your order id.	:	persönlich
Date of order	:	12.07.2018
Sample receipt	:	12.07.2018
Sender	:	Customer
Start of test period	:	13.07.2018
End of test period	:	20.07.2018
Report date	:	20.07.2018
Page	:	1 of 1

Report No.: 2604998-1

Sample : B0 Wagner - Lieferung vom 11.7.18
Container : glass - bottle 2000 ml
ASG-ID : 2604998_001

Seal No.: -

Parameter	Method	Result	Specification DIN EN 590:2014-04 min.	max.	Unit
Cetane Number (DCN)	DIN EN 15195	56,2	51,0	-	-
Cetane Index	DIN EN ISO 4264	51,8	46,0	-	-
Density (15 °C)	DIN EN ISO 12185	834,4	820	845	kg/m3
PAH content	DIN EN 12916	2,4	-	8,0	% (m/m)
Sulfur content	DIN EN ISO 20884	8,6	-	10	mg/kg
Flash point	DIN EN ISO 2719	62,0	>55	-	°C
Carbon residue (10 % Dist.)	DIN EN ISO 10370	<0,10	-	0,30	% (m/m)
Ash content (775 °C)	DIN EN ISO 6245	0,001	-	0,01	% (m/m)
Water content	DIN EN ISO 12937	28	-	200	mg/kg
Total contamination	DIN EN 12662:2014	<12	-	24	mg/kg
Copper strip corrosion	DIN EN ISO 2160	1	-	1	Korr.Grad
Fatty acid methylester content	DIN EN 14078	<0,1	-	7,0	% (V/V)
Oxidation stability	DIN EN ISO 12205	<1	-	25	g/m3
filterable insolubles		<1	-	-	g/m3
adherent insolubles		<1	-	-	g/m3
Oxidation stability	DIN EN 15751	>48	20	-	h
HFRR (Lubricity at 60 °C)	DIN EN ISO 12156-1	404	-	460	µm
Kin. viscosity (40 °C)	DIN EN ISO 3104	2,608	2,00	4,50	mm2/s
% (V/V) recovery at 250 °C	DIN EN ISO 3405	39,5	-	<65	% (V/V)
% (V/V) recovery at 350 °C		94,2	85	-	% (V/V)
95 % (V/V) recovery		353,4	-	360	°C
CFPP	DIN EN 116	-16	-	*	°C
Manganese (Mn)	DIN EN 16576	<0,5	-	2,0	mg/l
Cloud point	DIN EN 23015	-2	-	-	°C

*requirements: 15.04. - 30.09. max. 0 °C
01.10. - 15.11. max. -10 °C
16.11. - 28.02. max. -20 °C
01.03. - 14.04. max. -10 °C

Ing. Jozef Borovsky (Chemical engineer)

DAkkS Deutsche Akkreditierungsstelle D-PL-11334-01-00

ASG Analytik-Service Gesellschaft mbH
Trentiner Ring 30
86356 Neusäss • Germany

phone +49 (0) 821 450423-0
fax +49 (0) 821 486 2519
e-mail info@asg-analytik.de

General Manager:
Dr. Th. Wilharm, J. Bernath
Amtsgericht Augsburg HRB 12297

ASG Analytik-Service Gesellschaft mbH
Trentiner Ring 30 • 86356 Neusäss • Germany

ASG Analytik-Service Gesellschaft mbH
Trentiner Ring 30
86356 Neusäss

Your reference	:	JBor
Your order id.	:	persönlich
Date of order	:	30.10.2018
Sample receipt	:	30.10.2018
Sender	:	Customer
Start of test period	:	30.10.2018
End of test period	:	07.11.2018
Report date	:	08.11.2018
Page	:	1 of 1

Report No.: 2607823-1

Sample : RME - Lieferung vom 30.10.2018
Container : glass - bottle 1000 ml
ASG-ID : 2607823_001

Seal No.: -

Parameter	Method	Result	Specification DIN EN 14214:2014-06 min.	max.	Unit
Ester content	DIN EN 14103:2015	>99	96,5	-	% (m/m)
Linolenic acid content		9,1	-	12,0	% (m/m)
Density (15 °C)	DIN EN ISO 12185	882,7	860	900	kg/m3
Kin. viscosity (40 °C)	DIN EN ISO 3104	4,442	3,50	5,00	mm2/s
Flash point	DIN EN ISO 2719	171,0	101	-	°C
CFPP	DIN EN 116	-18	-	*	°C
Sulfur content	DIN EN ISO 20884	<5(2,6)	-	10	mg/kg
Cetane Number (DCN)	DIN EN 15195	56,7	51,0	-	-

Sulfated ash (775 °C)	ISO 3987	<0,001	-	0,02	% (m/m)
Water content	DIN EN ISO 12937	152	-	500	mg/kg
Total contamination	DIN EN 12662:1998	<1	-	24	mg/kg
Copper strip corrosion	DIN EN ISO 2160	1	-	1	Korr.Grad
Oxidation stability	DIN EN 14112	10,0	8,0	-	h
Acid value	DIN EN 14104	0,214	-	0,50	mg KOH/g
Iodine value	DIN EN 16300	110,2	-	120	g Iod/100g
Polyunsaturated Methyl Esters	DIN EN 15779/A1	<0,6	-	1,00	% (m/m)
Methanol content	DIN EN 14110	0,03	-	0,20	% (m/m)
Free glycerol content	DIN EN 14105:2011	0,001	-	0,02	% (m/m)
Monoglyceride content		0,51	-	0,70	% (m/m)
Diglyceride content		0,07	-	0,20	% (m/m)
Triglyceride content		0,02	-	0,20	% (m/m)
Total glycerol content		0,142	-	0,25	% (m/m)
Alkali content (Na+K)	DIN EN 14538	<1	-	5,0	mg/kg
Metal Content II (Ca+Mg)		<1	-	5,0	mg/kg
Phosphorous content	DIN EN 14107	<4(<0,5)	-	4,0	mg/kg
Cloud point	DIN EN 23015	-5	-	-	°C

*requirements: 15.04. - 30.09. max. 0 °C
01.10. - 15.11. max. -10 °C
16.11. - 28.02. max. -20 °C
01.03. - 14.04. max. -10 °C

Ing. Jozef Borovsky (Chemical engineer)

ASG Analytik-Service Gesellschaft mbH
Trentiner Ring 30
86356 Neusäss • Germany
phone +49 (0) 821 450423-0
fax +49 (0) 821 486 2519
e-mail info@asg-analytik.de

General Manager:
Dr. Th. Wilharm, J. Bernath
Amtsgericht Augsburg HRB 12297

Appendix J: Journal article

Environmental Technology & Innovation 19 (2020) 100945

Contents lists available at ScienceDirect

Environmental Technology & Innovation

journal homepage: www.elsevier.com/locate/eti

Comparative sampling of gas phase volatile and semi-volatile organic fuel emissions from a combustion aerosol standard system☆

Yvonne C. Mason [a], Genna-Leigh Schoonraad [a], Jürgen Orasche [b], Christoph Bisig [b], Gert Jakobi [b], Ralf Zimmermann [b,c], Patricia B.C. Forbes [a,*]

[a] Department of Chemistry, Faculty of Natural and Agricultural Sciences, University of Pretoria, Lynnwood Road, 0002, South Africa
[b] Comprehensive Molecular Analytics (CMA), Helmholtz Zentrum München, Gmunder Str. 37, 81379 München, Germany
[c] Joint Mass Spectrometry Center, Chair of Analytical Chemistry, University of Rostock, Germany

ARTICLE INFO

Article history:
Received 26 March 2020
Received in revised form 28 May 2020
Accepted 30 May 2020
Available online 1 June 2020

Keywords:
CAST
Graphene wool sampler
PDMS sampler
Diesel combustion
Biodiesel

ABSTRACT

The incomplete combustion of fossil fuels generates hazardous gaseous compounds which have been linked to various adverse environmental and human health effects worldwide. Cleaner alternatives such as gas-to-liquid (GTL) and biofuels such rapeseed oil methyl ester (RME) have therefore been investigated. In this study, a Combustion Aerosol Standard (CAST) was used to generate a diluted, consistent and relatively stable source of fuel emissions from the combustion of diesel, GTL and RME, respectively. Gas phase sampling was carried out by removing particulates using a filter upstream of three different samplers: i) a commercialised activated charcoal sampler; ii) a validated polydimethylsiloxane (PDMS) sampler; and iii) a novel graphene wool (GW) sampler. The latter two were thermally desorbed, whilst the charcoal sampler was solvent extracted. All three samplers were analysed for trace levels of selected volatile organic compounds (VOCs) and semi-volatile organic compounds (SVOCs) by means of gas chromatography–mass spectrometry (GC–MS).

The GW sampler outperformed the PDMS and activated charcoal samplers as the GW sampled the most compounds and had a lower variability in VOC and SVOC (selected polycyclic aromatic hydrocarbon and n-alkane) concentrations sampled, especially in the case of the n-alkanes (average %RSDs of the GW, PDMS and activated charcoal samplers were found to be 23.8%, 43.1% and 52.9%, respectively). The activated charcoal sampler was found to be unsuitable in this study due to the low number of detected compounds, as well as high benzene and toluene backgrounds of the sorbent. Combustion of diesel was found to emit a total VOC and SVOC concentration 4–5 times that of GTL and RME, respectively, based on GW sampler analyses. This study therefore further supports GTL and RME as cleaner fuel alternatives to petroleum derived diesel.

☆ Capsule: A novel graphene wool sampler allowed for the detection of more gaseous VOCs and SVOCs with better reproducibility than other samplers, including standard activated charcoal.

* Corresponding author.
E-mail address: patricia.forbes@up.ac.za (P.B.C. Forbes).

https://doi.org/10.1016/j.eti.2020.100945
2352-1864/

1. Introduction

The detection of hazardous gaseous compounds has become ever more critical as an increasing number of studies link various adverse environmental and human health effects to increasing ambient air pollution (Landrigan et al., 2019; Goldemberg et al., 2018; Yan et al., 2018). Commonly known constituents of air pollution include compounds such as NO_x, SO_x, CO and particulate matter (PM) in addition to volatile organic compounds (VOCs) and semi-volatile organic compounds (SVOCs). Recent literature shows that vehicular emissions are generally reported in terms of the CO, CO_2, NO_x and PM produced (Dagaut et al., 2019; Borillo et al., 2018; He, 2016). There are multiple studies which have focused on the adverse side effects of PM (Bae and Hong, 2018; Gautam et al., 2018; Hime et al., 2018; Chen et al., 2017; Künzli et al., 2005; Peters et al., 1997), which thereby warrants combustion emissions being reported in terms of PM production, however, it is also crucial to be cognisant of gaseous emissions, such as VOCs and SVOCs, as these have also shown to be detrimental to human health (Points, 2019; Mirzaei et al., 2016; Yu and Kim, 2010; Jia et al., 2008; Kawamura et al., 2006). VOCs and SVOCs have been noted to be potentially carcinogenic and may cause the enhancement of respiratory, cardiovascular, infectious and allergic diseases through contact with the skin or through inhalation (Helen et al., 2019; Lerner et al., 2018; Raza et al., 2018; Bernstein et al., 2004; Finlayson-Pitts and Pitts Jr, 1999; Finlayson-Pitts and Pitts, 1997; Hemminki and Pershagen, 1994). It has been noted that a trend towards using biodiesel over petroleum-derived diesel has arisen due to lower reported PM emissions from biodiesel combustion, therefore it is generally considered a cleaner alternative fuel (Damanik et al., 2018; Knothe and Razon, 2017). However, little has been reported on the gaseous organic by-products released by the combustion of these biofuels.

As research into the effects of VOCs and SVOCs has progressed over the years, governing environmental bodies have made it ever more imperative to create a means by which to monitor even lower trace concentrations of these analytes. Currently, VOCs are typically sampled onto retaining media such as commercially available Carbotrap, Carbosieve ™S-III and Tenax® which are either carbon- or polymer-based samplers. SVOCs are commonly sampled onto the same retaining media as the VOCs in addition to retaining media such as multi-channel polydimethylsiloxane (PDMS) traps (Munyeza et al., 2018; Forbes and Rohwer, 2009; Ortner and Rohwer, 1996).

The use of carbon-based air samplers is not a novel concept in the field of environmental analysis, however a novel class of carbon nanostructures, known as graphene, is gaining attention in analytical chemistry due to many of its innately attractive properties. Graphene has been calculated to have an impressive theoretical specific surface area of 2630 m^2 g^{-1} (Züttel et al., 2004) which is far above the 1000 m^2 g^{-1} required of a "strong" sorbent (United States Environmental Protection Agency, 1999). Due to the ultrahigh surface area graphene possesses in combination with its non-polar nature, Schoonraad and Forbes developed a means to synthesise graphene in a way which allows facile use thereof as an adsorbent in an active air sampler, called a graphene wool (GW) sampler, as shown in Figure S1 in the Supplementary Information (Schoonraad and Forbes, 2019a,b; Schoonraad et al., 2020).

A CAST generator, which is based on a laminar propane co-flow diffusion flame, is a useful way to produce stable trace level emissions that mimic the physical and chemical properties which are characteristic of real-world emissions from the combustion of selected fuel sources (Moore et al., 2014). To solve the difficulty of analysing combustion aerosols, which have a tendency to coagulate, particles need to be produced instantaneously in a continuous process with reliable reproducibility (Kasper, 2009) from a regulated aerosol generator. It is from this need that the CAST generator was developed, in which soot particles are formed when the combustion process is quenched with inert "quenching" gas, and its operation has been investigated by various authors (Mueller et al., 2015; Moore et al., 2014). In this study, trace level gas phase emissions which are simultaneously produced from a CAST generator were utilised to evaluate the performance of three different air samplers. Due to the various methods implemented to stabilise the exhaust emissions from the CAST generator, it has been viewed as a stable and repeatable source of PM of a certain size range (Mueller et al., 2015) and therefore the diluted exhaust stream may also be a source of trace levels of organic gas phase combustion emission products.

Here we describe the sampling of gas phase VOCs and SVOCs from a CAST generator utilising a filter upstream of each sampler to capture the PM and thereby only sample the gas phase analytes. The VOCs of interest included benzene, toluene, ethylbenzene and xylenes (BTEX), whilst SVOCs included n-alkane hydrocarbons and polycyclic aromatic hydrocarbons (PAHs). Emissions from each of three different fuel types were sampled from the CAST exhaust in parallel by three different samplers of interest, namely a multichannel PDMS sampler prepared in-house, a commercial activated charcoal sampler, and a novel GW sampler prepared in-house. The activated charcoal sampler was selected due to its use in VOC methods published by the International Organization for Standardization (ISO) and Methods for the Determination of Hazardous Substances (MDHS) (International Organization for Standardization ISO 9487:1991 (E); International Organization for Standardization ISO 16200-1:2001 (E); Methods for the Determination of Hazardous Substances MDHS 96 (2000)). Activated charcoal is also a cheaper alternative to graphitised materials such as Carbotrap®. The CAST system was utilised in this comparison of the performance of the chosen samplers due to the improved stability of emissions the system produces in comparison to real-world emissions, which typically would vary over time which in turn introduces sampling uncertainties. Other gas standard emission generators tend to produce only one compound at a time, and standard gas cylinder mixtures of VOCs cover a very limited range of analytes. The CAST system therefore provides a suitable means to evaluate the performance of the selected samplers, thereby allowing for the determination and evaluation of the strengths and weaknesses of each type of sampler in determining the concentrations of the target organic gas phase analytes at trace levels.

2. Materials and methods

2.1. Reagents and materials

The three fuels that were tested, namely petroleum derived diesel with no added biodiesel (B0), gas-to-liquid (GTL) and rapeseed oil methyl ester (RME) fuels were all purchased from ASG Analytik-Service GmbH, Neusäss, Germany. An ultrasonic bath was utilised to degas each fuel for 30 min prior to use.

Individual stock standards of 36 volatile organic compounds (VOCs) and semi-volatile organic compounds (SVOCs) along with 13 internal standards were purchased from the suppliers listed in Table S1 of the Supplementary Information. Working solutions were prepared by appropriate dilutions of the stock solutions prior to use. For the extraction of analytes from the activated charcoal sampler, anhydrous carbon disulphide (CS_2) (>99% purity) was purchased from Merck, Germany.

2.2. Sampler details

Each of the polydimethylsiloxane (PDMS) traps consisted of twenty-two 55 mm long parallel PDMS tubes (Technical Products, Inc., Georgia, USA) of 0.3 mm i.d. which were housed in a 89 mm long Supelco glass TD tube with an i.d. of 4 mm. Graphene wool (GW) was synthesised in-house as per the optimised conditions described by Schoonraad et al. (2020) using a quartz wool substrate (Acros, Industrial Analytical, South Africa). For the assembly of the GW samplers, approximately 120 mg of GW was weighed out using a calibrated Sartorius Entris analytical balance and then packed into the same glass tubing as the PDMS traps, whilst maintaining a bed length of 60 mm for the GW sampler. The sorbent was held in place by stainless steel screens (Sigma Aldrich, South Africa) which are designed for Gerstel TD tubes of the same i.d.. The traps were then conditioned using a multi-tube conditioner (TC-20 MARKES International, Germany) at 250 °C for 8 h under hydrogen gas flow and were then sealed using Shimadzu stainless steel tube caps. The activated charcoal type BIA tubes were purchased from Dräger, Germany.

2.3. CAST setup

A Combustion Aerosol Standard generator (diesel CAST, Jing mini-CAST 5201D, Switzerland) was operated with propane (99.95%, Linde AG, Germany). The settings were as follows: dilution air (10 L min^{-1}), oxidation air (2.2 L min^{-1}), quenching gas (10 L min^{-1}, fixed), propane fuel (30 mL min^{-1}, fixed) (refer to Mueller et al. (2016) for further details regarding the operation of the CAST). The fuel of choice was supplied to the CAST generator using an inlet from a high-performance liquid chromatography (HPLC) pump at 50 mL min^{-1}. In the viewing window, illustrated by number 4 of Fig. 1, it could be seen that the flame changed from blue to orange once the fuel of interest was added to the propane already combusting in the CAST generator. A photograph of the CAST setup is shown in Figure S2 in the Supplementary Information.

The fuel was introduced to the CAST generator using polytetrafluoroethylene (PTFE) tubing (50 cm) and polyurethane (PU) tubing (5 cm) using a HPLC pump (Kontron, type 420, Germany) and then subsequently, copper tubing was used to connect the HPLC pump to the CAST generator. Antistatic polyurethane hose of 12.0 mm o.d. × 8.0 mm i.d. (Riegler, Germany) was used for all the connections between the CAST and various dilutors, splitters and sampling instrumentation involved in this study. The CAST generated 22 L min^{-1} of undiluted combustion exhaust. From the CAST generator, an exhaust outlet, shown by number 6 in Fig. 1, allowed for the undiluted excess exhaust emissions to be released whilst continuously sampling 0.3 L min^{-1} of this exhaust over the course of the 10 min sampling period for analysis by a flame ionisation detector (FID) (SK-Electronik, GMBH), calibrated with propane (30 ppm) in nitrogen (Linde, Germany), and a Fourier-transform infrared spectroscopy (FT-IR) Gas Analyser (Gasmet, Model: DX4000, Finland). The FID sampled the undiluted CAST exhaust using a 380 °C heated transfer line. Thereafter, 0.3 L min^{-1} (1.5 L min^{-1} for GTL and RME) of the undiluted CAST exhaust was introduced to a porous tube dilutor (Mikro-Glasfaser Filterelement, Type GF-12-57-80E) to which 2.7 L min^{-1} (1.5 L min^{-1} for GTL and RME) of dry air was added to make up a total diluted flow of 3 L min^{-1}. The ejector dilutor then drew the 3 L min^{-1} from the porous dilutor and further diluted the CAST exhaust with laboratory air that was first cleaned by passing through Intersorb Plus (Intersurgical, Sankt Augustin, Germany) to remove CO_2, and then activated charcoal (Carl Roth, Karlsruhe, Germany) and finally through Silicagel (Azelis, Sankt Augustin, Germany) at 27 mL min^{-1}. Any overpressure which may have occurred in the ejector dilutor was released through the outlet shown as number 10 in Fig. 1.

From the ejector dilutor, a custom-built three-way Y-piece stainless steel splitter allowed for the diluted flow of the CAST exhaust to be directed to various sampling instrumentation as well as to the selected samplers. Two of the Y-piece exits lead directly to two sampling stations to which selected samplers were attached and diluted CAST exhaust was drawn through these at 500 mL min^{-1} for 10 min by Gilian® GilAir® Plus Air Sampling Pumps (Sensidyne®, USA).

The second Y-piece was utilised for the measurement of the light absorption properties of the CAST aerosols measured online by means of an Aethalometer® (Magee Scientific, Model AE33-7, Slovenia), which had an optimised diluted flow using a PALAS® VKL 10E dilutor as the Aethalometer® typically required a dilution of 1:10 000 in order to not over saturate the instrument. From the same PALAS® VKL 10E dilutor, the diluted CAST exhaust was additionally measured by a Condensation Particle Counter (CPC, TSI, Model 3022A, USA) and an Electrostatic Classifier (TSI, Model 3082, USA)

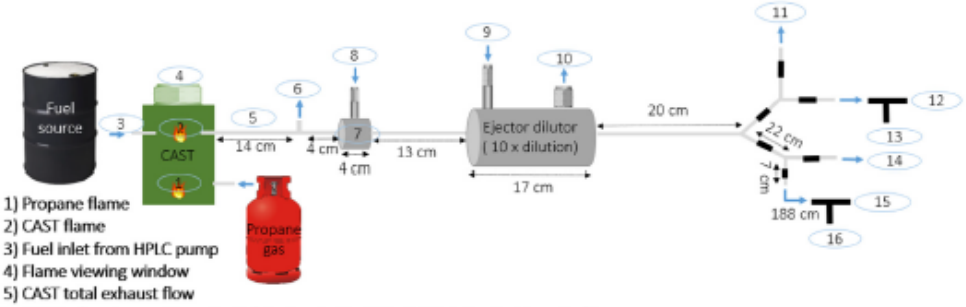

Fig. 1. Schematic diagram of the CAST generator sampling set-up.

connected to a CPC (TSI, Model 3750) in order to determine the stability of the particle number concentration produced from the CAST after changing fuel sources. The particulate matter (PM) measurements were conducted in order to check the stability of the emissions and suitability of the dilution ratios of the different fuels. The combustion of diesel (B0) resulted in higher PM emissions than the other fuels, therefore the emissions required different dilutions for gas phase sampling. The fuel of interest was thus combusted in the CAST generator and the exhaust thereof passed through a porous tube dilutor and an ejector dilutor, in which the dilution flows were adjusted to dilute diesel (B0) emissions by a factor of 100 and to dilute the GTL and RME emissions by a factor of 20.

2.4. Sample collection and extraction

Prior to introducing a new fuel into the CAST generator, the system was cleaned with cotton swabs, Kimtech wipes and a vacuum cleaner. Once cleaned, the selected degassed fuel was introduced into the CAST generator using the HPLC pump and the combustion emissions were monitored by the particle counter and the aethalometer to ensure that the CAST generator was stable and producing a consistent concentration of aerosols. A stainless-steel filter holder assembly was positioned between an empty glass tube upstream and the selected sorbent sampler downstream. The filter holder contained a 13 mm quartz-microfibre disc (Ahlstrom Munksjö, T 293) with a precipitation area diameter of 10 mm. Each sampler was connected to a Gilian® GilAir® Plus Air Sampling Pump (Sensidyne®, USA) using Teflon tubing (Fig. 2), which was operated at 500 mL min^{-1} for 10 min. A photograph of the set-up is shown in Figure S3 in the Supplementary Information.

These sampling pumps were all calibrated for each specific sampler used prior to sampling by means of a Gilibrator 2® (Sensidyne®, USA). This accounted for the individual differing back pressures of the different sampler types. A Kestrel 4500 weather station (Envirocon, South Africa) was used to measure the ambient conditions at the time of the sampling event which are shown in Table S2 of the Supplementary Information. After sampling, PDMS and GW samplers were end-capped and were subsequently wrapped in aluminium foil, sealed in zip lock polyethylene bags and were stored in a freezer at −18 °C until analysis took place within 72 h.

The charcoal tubes were opened with an adjustable ORBO™ Tube Cutter after the sampling event, and the charcoal was emptied into 20 mL amber vials. 3 mL of CS_2 was added, the vials were then sealed and allowed to extract for 12 h in a fume hood at room temperature. Although accredited methods such as the ISO 9487: 1991 (E) state that 500 µL of solvent be used in the extraction of analytes from activated charcoal sorbents, it was found that 3 mL of solvent was required to completely submerse the activated charcoal. After overnight extraction, the extract, with the activated charcoal still in contact with the solvent, was sonicated (Allpax Palsonic, Germany) for 15 min. The supernatant extract was subsequently transferred into a 5 mL amber GC vial and stored in a freezer at −18 °C until batch-wise analysis was conducted within 72 h.

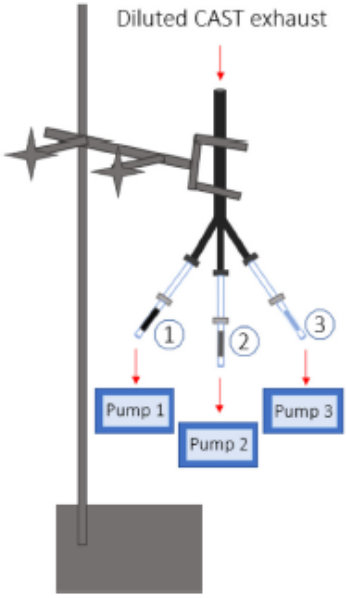

Fig. 2. Schematic of the sampler setup where numbers ①, ② and ③ illustrate the positions of the activated charcoal, GW and PDMS samplers, respectively, during CAST sampling events.

2.5. GC-MS analysis

The PDMS and GW samplers were thermally desorbed using a Thermal Desorption System (TD-20, Shimadzu, Japan) using 60 mL min^{-1} helium from 80 °C to 250 °C for the PDMS and to 280 °C for the GW sampler, both with a hold time of 30 min. The cooled injection system (CIS) method started at 5 °C and ended at 330 °C with a hold time of 30 min. A GC-2010 Plus was coupled to a MS-QP2010 Ultra (both Shimadzu, Japan) and helium was used as carrier gas at a flow rate of 1.6 mL min^{-1}. A split ratio of 10:1 was applied whilst the column used was a VF-XMS 30 m × 0.25 mm i.d. × 0.25 µm d.f. column (Agilent, Netherlands). The GC oven method started with a hold time of 6 min at 60 °C and was ramped to 250 °C at 5 °C min^{-1}. The transfer line temperature was set to 250 °C. The mass spectrometry method was set to scan from m/z 35 to m/z 500 with an electron ionisation energy of 70 eV and an ion source temperature of 230 °C.

The charcoal extracts were injected by a 1 µL hot injection at 280 °C. Helium was used as the carrier gas with a flow rate of 1.5 mL min^{-1}. A split ratio of 1:1 was applied and a SGE BX5 25 m × 0.22 mm i.d. × 0.25 µm d.f. column was used. The oven started with a hold time of 1 min at 40 °C and was ramped to 250 °C at 5 °C min^{-1} and then held for 2 min. The transfer line temperature was set to 270 °C. The mass spectrometry method was the same as for the PDMS and GW sampler analysis.

3. Results and discussion

3.1. FID/FTIR analyses

Since this study occurred over a period of three days, it was of interest to investigate the inter-day CAST generator combustion and emission stability using the flame ionisation detector (FID) and Fourier-transform infrared spectroscopy (FTIR) over the sampling period to determine the reliability of the CAST system for organic gas phase emission sampling. In order to do this, the sampling of the emissions from the CAST generator started with the diesel (B0) fuel type, which was used as a basis for comparison of the other two fuels tested, as petroleum-derived diesel is widely used throughout the world. The experiments then continued onto the gas-to-liquid (GTL) and rapeseed oil methyl ester (RME) fuel types, respectively, and ended with sampling the B0 fuel type as a bracket test to gauge the reproducibility of the CAST emissions between the duplicate measurements sampled over the course of the days over which the sampling took place. In Table 1, each fuel type is allocated numbers 1–4, where 1 and 2 designate the duplicate measurements of the first round of sampling the emissions from each fuel, which were carried out directly after each other, whereas numbers 3 and 4 relate to the duplicate measurements of the second sampling event of the same fuel which were carried out sequentially on a different day.

Table 1
Mean FID results for the sampling events of the undiluted fuel emissions over each 10 min sampling period.

Sampling event	FID (ppm)		
	B0	GTL	RME
1	8.87	7.33	5.60
2	8.75	7.27	5.57
3	7.63	7.09	5.30
4	7.60	7.05	5.49
Mean	8.21	7.19	5.49
SD	0.69	0.14	0.13
%RSD	8.42	1.89	2.46

As can be seen from Table 1, the response of the FID showed higher gas phase organic emissions from each fuel type during the first sampling event as compared to the second sampling event. Although the duplicate sampling events for each fuel type were carried out on different days, no rinsing occurred for intra-fuel sampling events of the GTL and RME fuel types. This could have in turn contributed to the smaller FID measurement difference (i.e. lower %RSD) in the combustion fuel emissions of these fuel types, measured between the duplicate fuel measurements, as compared to B0 which was sampled as a bracket test. Nevertheless, the fuel combustion emissions recorded by the FID, for all of the fuel types, showed that the combustion emissions were significantly different between days, using a statistical t-test at a 95% confidence level. This implies that it is preferable to conduct all tests of a particular fuel type sequentially on one day when using the CAST system, in order to reduce these uncertainties. During the sampling events of each fuel type, additional measurements were taken of the H_2O, CO_2, O_2 percentage and amount of CO (ppm) contained within the combustion emissions from the CAST exhaust. These values were found to not differ significantly during the sampling period (Table S3 in the Supplementary Information).

In order to compare the performance of the samplers, the results from the second sampling events of the B0 and GTL combustion were used, i.e. B0 and GTL 3 and 4 in Table 1, as these results proved to be more reliable from the FID measurements; in that lower %RSDs were recorded. Additionally, it was found that the first round of sampling of the B0 and GTL yielded concentrations that were significantly larger with greater variation than in the second round of sampling as shown in Figure S4 of the Supplementary Information. Since the RME fuel did not contain additives i.e. stabilisers, polymerisation of the combustion products occurred around the flame tip during the second sampling event causing a partial blockage with related potential inconsistencies in results, therefore the duplicates from the first sampling event for that fuel type, i.e. RME 1 and 2 in Table 1, were used for the comparison of the samplers and fuel types.

3.2. Comparison of the compounds detected on each sampler type

The highest number of target analytes were detected from the emissions of diesel (B0), where thermal desorption of the PDMS sampler resulted in the detection of 33 target analytes, whilst 34 were detected upon analysis of the GW sampler. Analysis of the charcoal sampler extracts resulted in the detection of only two of the 36 target analytes in all fuel types sampled; namely benzene and toluene, of which only benzene was above the limit of quantification (LOQ). The low number of analytes detected was likely due to the dilution volume. After analysis of a blank extraction of the activated charcoal sorbent, it was evident that the detected analytes were from the sorbent itself, which contained particularly high levels of benzene. The blank analysis data of the three samplers is shown in Table S4 in the Supplementary Information. Therefore, the comparison of the concentrations of benzene and toluene emitted upon combustion of different fuels is based only on the analysis of the PDMS and GW samplers (as shown in Fig. 3 and detailed in Section 3.4).

There are a number of factors contributing to the lack of analytes detected upon analysis of the activated charcoal sampler extracts as compared to the number of compounds detected upon analysis of the PDMS and GW samplers, as shown in Fig. 3 (also refer to Tables S5 and S6). Firstly, the volume of solvent experimentally determined to be required (3 mL) for the extraction of the activated charcoal may have diluted the sampled analytes to below the limit of detection (LOD) of the analytical method. The charcoal sampler was preliminarily calibrated for only 8 of the 36 target analytes. Further calibration of the remaining 28 target analytes did not occur as no other target compounds other than benzene and toluene were detected upon analysis of the activated charcoal extracts. The LODs for the activated charcoal sampler were calculated to range from 0.48 $\mu g\ m^{-3}$ for naphthalene to 2.26 $\mu g\ m^{-3}$ for m-xylene (Tables S7a and S7b). Comparatively, the LODs for PDMS ranged from 0.0001 $\mu g\ m^{-3}$ for 1,2-dimethylnaphthalene to 0.80 $\mu g\ m^{-3}$ for n-octane, whilst the LODs for GW ranged from 0.002 $\mu g\ m^{-3}$ for toluene to 0.79 $\mu g\ m^{-3}$ for n-octane and n-nonane.

Another reason why the analysis of the activated charcoal extracts could have resulted in the detection of so few compounds is that the activated charcoal may have bound the analytes in an irreversible manner and this, in combination with the low gas phase analyte concentrations which the CAST system produces, could have resulted in the analytes not being detected. The lack of analytes detected occurred even though the activated charcoal was left in CS_2 for 10 h as compared to the recommended extraction time of 30 min (ISO 9487:1991 (E)).

Table 2
The relative advantages and disadvantages of GW, PDMS and charcoal samplers for the sampling of the selected VOCs, PAHs and n-alkanes at trace levels.

	GW sampler	PDMS sampler	Activated charcoal sampler
Advantages	Low background noise		
	Can be reused	Can be reused	Reasonable cost (€3.26 per sampler)
	On average, the lowest standard deviation in recorded duplicate measurements		
	Largest number of compounds detected	A large number of compounds detected	
	Similar analysis time to PDMS	Similar analysis time to GW	
	Can be thermally desorbed therefore requires no solvents in preparation for analysis	Can be thermally desorbed therefore requires no solvents in preparation for analysis	Does not require a lab equipped with a TD system
Disadvantages		Sorbent background (due to siloxanes)	Sorbent background (for toluene and benzene)
	Reasonably costly (€6.88 per sampler)	Most costly (€7.55 per sampler)	Single use
	Lower concentrations of several target analytes reported as compared to PDMS	Larger standard deviation in recorded duplicate measurements as compared to the GW sampler, especially for the n-alkanes	Largest standard deviation in recorded duplicate measurements of benzene
	Requires a lab equipped with thermal desorption system	Requires a lab equipped with a thermal desorption system	Lowest number of compounds detected
			Long extraction time
			Incomplete analyte recovery
			Toxicity of solvent used for extraction i.e. CS_2

As can be seen from Fig. 3(c), the GW sampler was found to be more effective than PDMS in retaining the lighter n-alkanes such as n-octane and n-nonane. However, analysis of the GW sampler generally gave lower concentrations of each target analyte than the PDMS sampler (Fig. 3(a)–(c)). This may be indicative of the GW sampler having a lower breakthrough volume compared to the PDMS sampler however, the true cause is probably due to the thermal desorption parameters being optimised for the PDMS sampler and not for GW desorption. Therefore, the lower concentrations of analytes determined upon analysis of the GW samplers are most likely due to the incomplete thermal desorption of analytes from the GW sampler, which retains analytes more strongly by adsorption rather than by sorption as in the case of PDMS.

3.3. Comparison of the variability between the samplers

As previously stated, the analysis of the PDMS samplers reflected higher concentrations of the target compounds as compared to the GW samplers (Fig. 3). However, the reported concentrations from the analysis of the PDMS samplers showed larger standard deviations as compared to the GW samplers. This could be due to PDMS functioning as a sampler through the action of absorption as opposed to the GW sampler, which functions by adsorbing analytes. Additionally, the structure of the GW sorbent itself, which involves a 2D monolayered structure of one atom thickness, leads to a large number of active sites being open and available for adsorption.

The range of target analytes were dominated by non-polar compounds which would theoretically tend to interact better with the non-polar GW sorbent as compared to the less non-polar PDMS sorbent. The lower standard deviation in the concentrations reported through the analysis of the GW samplers as compared to the analysis of the PDMS samplers is particularly noticeable for the concentrations of the polycyclic aromatic hydrocarbons (PAHs) detected (Fig. 3b) but even more so for the concentrations of n-alkanes detected (Fig. 3c). Therefore, due to the lower degree of uncertainty in concentrations reported upon analysis of the GW sampler and the greater number of compounds detected by the GW sampler as compared to the other two samplers, the GW sampler proved to be the superior sampler as compared to the activated charcoal sampler and the PDMS sampler for the sampling of the selected trace level VOCs, PAHs and n-alkanes in this study. The strengths and weaknesses of the various samplers are summarised in Table 2.

3.4. Effect of the different fuels on the combustion emission profiles

Throughout the sampling period, the ambient temperature differed slightly from 26.8–27.7 °C with a standard deviation of 0.4 whilst the barometric pressure ranged from 955.5–956.2 hPa with a standard deviation of 0.2, as shown in Table S2.

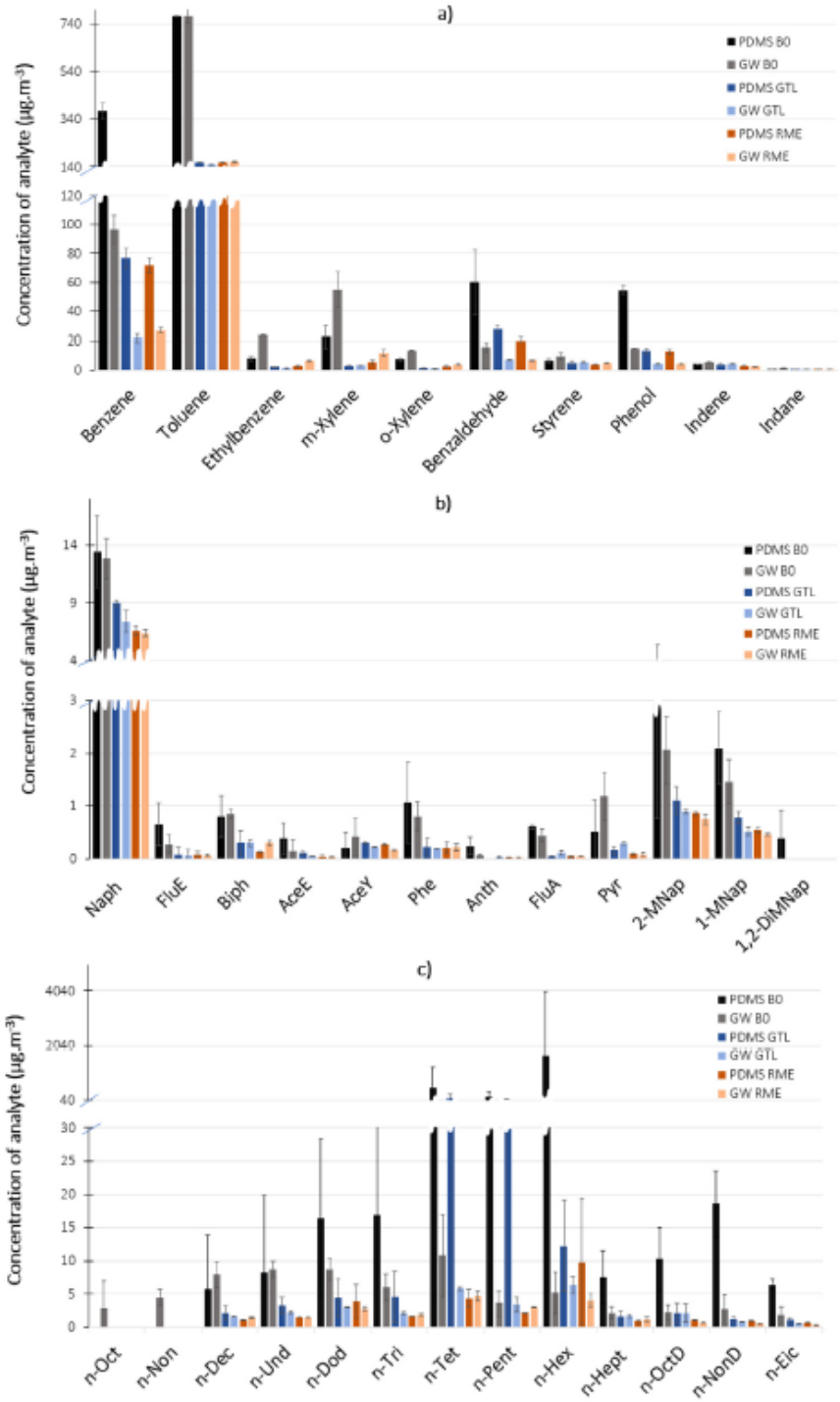

Fig. 3. Detected concentrations of (a) VOCs, (b) PAHs and (c) n-alkanes from the combustion of fuel types B0, GTL and RME sampled from the CAST generator exhaust using PDMS and GW samplers. *The error bars are based on the standard deviation (SD) of duplicate measurements and abbreviations can be found listed in Tables S7a and S7b.*

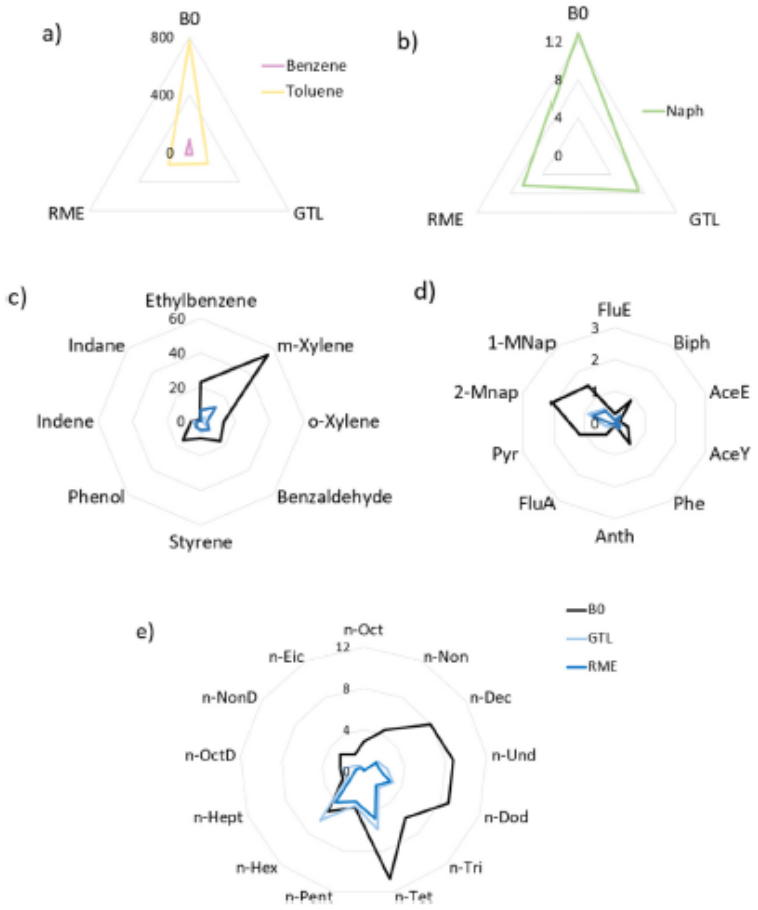

Fig. 4. Relative abundance (μg m^{-3}) of various compounds detected upon analysis of the GW sampler after sampling the gas phase emissions from B0, GTL and RME combustion: (a) benzene and toluene, (b) naphthalene, (c) VOCs, (d) PAHs and (e) n-alkanes.

This showed that the ambient conditions during sampling were fairly consistent and thereby allowed for the comparison of the fuel measurements and the CAST system over the sampling period.

Most of the CAST combustion emission compound profiles for the different fuels tested reflected a similar trend as seen in Fig. 3, when sampled by the PDMS and the GW sampler. Since it has been identified that the PDMS sampler had more variability in the resultant concentrations reported as compared to the GW sampler, the relative concentrations of target analytes within each fuel type emission profile will be discussed in terms of the results reported upon analysis of the GW samplers. Comparing the three fuel types sampled in this study, the combustion of diesel (B0) resulted in higher concentrations of target compounds in most cases, with the exception of the hexadecane in the combustion emissions of gas-to-liquid (GTL) (Fig. 4). As expected, the combustion emissions of rapeseed oil methyl ester (RME) reflected lower concentrations of targeted VOCs and SVOCs as compared to diesel and GTL, with the exception of ethylbenzene and the xylene isomers in the case of GTL (Fig. 4c).

These reported results align with the visual analysis of the filter papers which were placed upstream of the samplers. It can be seen in Fig. 5 that the PM filter from B0 combustion is considerably darker than the filters relating to GTL and RME combustion. The same trend was also observed in the duplicate sampling events conducted with B0 and GTL and RME.

The percent carbon content and total unburned hydrocarbons (THCs) are typically reported in the literature to be the largest in diesel whilst GTL tends to have less, and biodiesels, such as RME, have been reported to have the lowest concentrations (Dagaut et al., 2019; Soriano et al., 2018; Damanik et al., 2018). The measurements are done on %w/w of the fuel before combustion or the measurements of the target molecules are accomplished though the analysis of the PM phase formed after the combustion of the fuel. The compounds present in the different fuels and the relative

Fig. 5. PM filtered from (a) B0, (b) GTL and (c) RME CAST emissions prior to gas phase sampling.

abundancies in terms of engine emissions are also reported. It is important to note that the CAST generator pyrolyses the fuel by means of a diffusion flame therefore the combustion conditions and consequently the emissions, would differ to real-world engine emission scenarios making direct comparisons to other studies difficult.

Furthermore, compounds present in various fuel sources are often reported in terms of total carbon (TC); which is the summation of elemental carbon (EC) and organic carbon (OC) fractions with little detail regarding which specific compounds are present in the OC fraction (Zhou et al., 2019; Atiku et al., 2016; Nyström et al., 2016; Shen et al., 2013). In terms of bettering the fuel source for many forms of machinery in order to reduce emissions which are potentially hazardous to human health, it will be important to determine emission profiles of fuels not only in terms of the particulate matter generated, but also specifically which volatile and semi-volatile organic compounds are being released into the atmosphere, as these can also be detrimental to the environment and to human health, even though they may not be visible.

4. Conclusions

In this study it was found that the commercial activated charcoal sampler was not effective in sampling the trace levels of target analytes produced upon combustion of the fuels tested by the CAST. This could be due to the sample being too dilute and below the LOD due to the volume of the extraction solvent required, as well as the low levels of gas phase VOCs and SVOCs produced by the CAST system, and the small sample volume. In addition to the target analytes being below the LOD for the activated charcoal extracts, the activated charcoal sampler may have irreversibly adsorbed the target analytes. It is also noted that the extraction method for the activated charcoal sampler is time consuming and requires a toxic solvent, and high background concentrations were found for some target analytes. The activated charcoal sampler proved to be the cheapest however, with a once-off use, whilst the PDMS and GW have the advantage of being able to be reconditioned and reused.

The results of the PDMS sampler analysis reflected relatively higher concentrations of the VOC and SVOCs target analytes detected to that of the GW sampler. However, the results from the PDMS sampler analysis also showed a higher variability in the duplicate concentrations reported, particularly for the n-alkanes. The analysis of the GW sampler showed that target analytes were determined with lower uncertainties than with the PDMS sampler and lighter n-alkanes, such as octane and nonane, were detected with the GW sampler but not with the other two samplers. However, the analysis of the GW samplers did reflect lower concentrations of all target analytes sampled as compared to the concentrations reflected by the PDMS sampler. This could indicate that the GW has a lower breakthrough volume than the PDMS sampler or, most likely, that the TD parameters were optimal for the PDMS but resulted in incomplete desorption from the GW sorbent which therefore requires further optimisation such as a higher desorption temperature. Overall, the GW sampler has proven to be superior, as compared to the activated carbon as well as the PDMS sampler in the sampling of the selected trace levels of VOCs, PAHs and n-alkanes in this study. In terms of fuel comparisons, diesel (B0) produced the highest concentration of VOCs and SVOCs upon combustion in the CAST, as compared to rapeseed oil methyl ester (RME) and gas-to-liquid (GTL) fuels.

Regarding the CAST generator itself, it is suggested that one fuel type is used and sampled over a continuous period to definitively establish the reproducibility of the CAST, as significant variation was observed when sampling the fuel emissions on different days, although this variability was compounded by the low levels of target analytes produced by the CAST system. In future comparisons, the final extract volume for the charcoal sampler should be reduced to improve detection limits, especially in light of the low emission levels from the CAST system. It may also be of use to analyse the various fuel types before combustion to determine the aromatic content thereof and compare these to the combustion profiles reported in this study, as well as to compare the samplers using another combustion source which generates higher levels of target VOCs and SVOCs.

CRediT authorship contribution statement

Yvonne C. Mason: Investigation, Formal analysis, Writing - original draft. **Genna-Leigh Schoonraad:** Conceptualization, Investigation. **Jürgen Orasche:** Methodology, Investigation, Formal analysis, Project administration, Writing - review &

editing. **Christoph Bisig:** Methodology, Investigation, Writing - review & editing. **Gert Jakobi:** Methodology, Investigation. **Ralf Zimmermann:** Conceptualization, Resources, Funding acquisition. **Patricia B.C. Forbes:** Conceptualization, Methodology, Investigation, Formal analysis, Writing - review & editing, Supervision, Project administration, Resources, Funding acquisition.

Declaration of competing interest

The authors declare that they have no known competing financial interests or personal relationships that could have appeared to influence the work reported in this paper.

Acknowledgments

Thanks is extended to the Comprehensive Molecular Analytics (CMA) group at Helmholtz Zentrum München for assisting in the sampling campaign as well as the Department of Physics at the University of Pretoria for CVD use. Christoph Bisig would like to acknowledge the support of the Swiss National Science Foundation (grant number P2FRP3_178112). We also thank ASG Analytik-Service for providing the fuels for this campaign.

Funding

Funding provided by the University of Pretoria and the National Research Foundation of South Africa (NRF, grant number 105807) is acknowledged. This work was supported by the German Federal Ministry of Education and Research (BMBF), research contract 01DG17023.

Appendix A. Supplementary data

Supplementary material related to this article can be found online at https://doi.org/10.1016/j.eti.2020.100945.

References

Atiku, F.A., Mitchell, E.J.S., Lea-Langton, A.R., Jones, J.M., Williams, A., Bartle, K.D., 2016. The impact of fuel properties on the composition of soot produced by the combustion of residential solid fuels in a domestic stove. Fuel Process. Technol. 151, 117–125. http://dx.doi.org/10.1016/j.fuproc.2016.05.032.

Bae, S., Hong, Y.-C., 2018. Health effects of particulate matter. J. Korean Med. Assoc. 61 (12), 749–755. http://dx.doi.org/10.5124/jkma.2018.61.12.749.

Bernstein, J.A., Alexis, N., Barnes, C., Bernstein, I.L., Nel, A., Peden, D., Diaz-Sanchez, D., Tarlo, S.M., Williams, P.B., 2004. Health effects of air pollution. J. Allergy Clin. Immunol. 114 (5), 1116–1123. http://dx.doi.org/10.1016/j.jaci.2004.08.030.

Borillo, G.C., Tadano, Y.S., Godoi, A.F.L., Pauliquevis, T., Sarmiento, H., Rempel, D., Yamamoto, C.I., Marchi, M.R.R., Potgieter-Vermaak, s., Godoi, R.H.M., 2018. Polycyclic aromatic hydrocarbons (PAHs) and nitrated analogs associated to particulate matter emission from a Euro V-SCR engine fuelled with diesel/biodiesel blends. Sci. Total Environ. 644, 675–682. http://dx.doi.org/10.1016/j.scitotenv.2018.07.007.

Chen, H., Kwong, J.C., Copes, R., Hystad, P., van Donkelaar, A., Tu, K., Brook, J.R., Goldberg, M.S., Martin, R.V., Murray, B.J., Wilton, A., Kopp, A., Burnett, R.T., 2017. Exposure to ambient air pollution and the incidence of dementia: a population-based cohort study. Environ. Int. 108, 271–277. http://dx.doi.org/10.1016/j.envint.2017.08.020.

Dagaut, P., Bedjanian, Y., Dayma, G., Foucher, F., Grosselin, B., Romanias, M., Shahla, R., 2019. Emission of carbonyl and polyaromatic hydrocarbon pollutants from the combustion of liquid fuels: impact of biofuel blending. J. Eng. Gas Turbines Power 141 (3), 1–8. http://dx.doi.org/10.1115/GT2018-75136.

Damanik, N., Ong, H.C., Tong, C.W., Mahlia, T.M.I., Silitonga, A.S., 2018. A review on the engine performance and exhaust emission characteristics of diesel engines fueled with biodiesel blends. Environ. Sci. Pollut. Res. 25 (16), 15307–15325. http://dx.doi.org/10.1007/s11356-018-2098-8.

Finlayson-Pitts, B.J., Pitts, J.N., 1997. Tropospheric air pollution: ozone, airborne toxics, polycyclic aromatic hydrocarbons, and particles. Science 276 (5315), 1045–1051. http://dx.doi.org/10.1126/science.276.5315.1045.

Finlayson-Pitts, B.J., Pitts Jr, J.N., 1999. Chemistry of the Upper and Lower Atmosphere: Theory, Experiments, and Applications. Elsevier.

Forbes, P.B.C., Rohwer, E.R., 2009. Investigations into a novel method for atmospheric polycyclic aromatic hydrocarbon monitoring. Environ. Pollut. 157 (8–9), 2529–2535. http://dx.doi.org/10.1016/j.envpol.2009.03.004.

Gautam, S., Patra, A.K., Sahu, S.P., Hitch, M., 2018. Particulate matter pollution in opencast coal mining areas: a threat to human health and environment. Int. J. Min. Reclam. Environ. 32 (2), 75–92. http://dx.doi.org/10.1080/17480930.2016.1218110.

Goldemberg, J., Martinez-Gomez, J., Sagar, A., Smith, K.R., 2018. Household air pollution, health, and climate change: cleaning the air. Environ. Res. Lett. 13 (3), 030201. http://dx.doi.org/10.1088/1748-9326/aaa49d.

He, B.-Q., 2016. Advances in emission characteristics of diesel engines using different biodiesel fuels. Renew. Sustain. Energy Rev. 60, 570–586. http://dx.doi.org/10.1016/j.rser.2016.01.093.

Helen, G.S., Liakoni, E., Nardone, N., Addo, N., Jacob, P., Benowitz, N.L., 2019. Comparison of systemic exposure to toxic and/or carcinogenic volatile organic compounds (VOCs) during vaping, smoking, and abstention. Cancer Prev. Res. http://dx.doi.org/10.1158/1940-6207.CAPR-19-0356.

Hemminki, K., Pershagen, G., 1994. Cancer risk of air pollution: epidemiological evidence. Environ. Health Perspect. 102 (4), 187–192. http://dx.doi.org/10.1289/ehp.94102s4187.

Hime, N.J., Marks, G.B., Cowie, C.T., 2018. A comparison of the health effects of ambient particulate matter air pollution from five emission sources. Int. J. Environ. Res. Public Health 15 (6), 1206. http://dx.doi.org/10.3390/ijerph15061206.

International Organization for Standardization, 1991. Workplace air – determination of vaporous aromatic hydrocarbons – charcoal tube/solvent desorption/gas chromatographic method. ISO 9487:1991 (E).

International Organization for Standardization, 2001. Workplace air quality – sampling and analysis of volatile organic compounds by solvent desorption/gas chromatography – Part 1: pumped sampling method. ISO 16200-1:2001 (E).

Jia, C., Batterman, S., Godwin, C., 2008. VOCs in industrial, urban and suburban neighborhoods–Part 2: Factors affecting indoor and outdoor concentrations. Atmos. Environ. 42 (9), 2101–2116. http://dx.doi.org/10.1016/j.atmosenv.2007.11.047.

Kasper, M., 2009. CAST - Combustion aerosol standard: Principle and new applications. [Online] Available at: http://www.sootgenerator.com/documents/Kasper.pdf.
Kawamura, K., Ishiyama, M., Nagatani, N., Hashiba, T., Tamiya, E., 2006. Development of a novel hand-held toluene gas sensor: Possible use in the prevention and control of sick building syndrome. Measurement 39 (6), 490–496. http://dx.doi.org/10.1016/j.measurement.2005.12.014.
Knothe, G., Razon, L.F., 2017. Biodiesel fuels. Prog. Energy Combust. Sci. 58, 36–59. http://dx.doi.org/10.1016/j.pecs.2016.08.001.
Künzli, N., Jerrett, M., Mack, W.J., Beckerman, B., LaBree, L., Gilliland, F., Thomas, D., Peters, J., Hodis, H.N., 2005. Ambient air pollution and atherosclerosis in Los Angeles. Environ. Health Perspect. 113 (2), 201–206. http://dx.doi.org/10.1289/ehp.7523.
Landrigan, P.J., Fuller, R., Fisher, S., Suk, W.A., Sly, P., Chiles, T.C., Bose-O'Reilly, S., 2019. Pollution and children's health. Sci. Total Environ. 650, 2389–2394. http://dx.doi.org/10.1016/j.scitotenv.2018.09.375.
Lerner, J.E.C., de los Angeles Gutierrez, M., Mellado, D., Giuliani, D., Massolo, L., Sanchez, E.Y., Porta, A., 2018. Characterization and cancer risk assessment of VOCs in home and school environments in gran La Plata, Argentina. Environ. Sci. Pollut. Res. 25 (10), 10039–10048. http://dx.doi.org/10.1007/s1135.
Methods for the Determination of Hazardous Substances, 2000. Volatile Organic Compounds in Air (4). Laboratory method using pumped solid sorbent tubes, solvent desorption and gas chromatography. MDHS 96.
Mirzaei, A., Leonardi, S.G., Neri, G., 2016. Detection of hazardous volatile organic compounds (VOCs) by metal oxide nanostructures-based gas sensors: A review. Ceram. Int. 42 (14), 15119–15141. http://dx.doi.org/10.1016/j.ceramint.2016.06.145.
Moore, R.H., Ziemba, L.D., Dutcher, D., Beyersdorf, A.J., Chan, K., Crumeyrolle, S., Raymond, T.M., Thornhill, K.L., Winstead, E.L., Anderson, B.E., 2014. Mapping the operation of the miniature combustion aerosol standard (Mini-CAST) soot generator. Aerosol Sci. Technol. 48 (5), 467–479. http://dx.doi.org/10.1080/02786826.2014.890694.
Mueller, L., Jakobi, G., Orasche, J., Karg, E., Sklorz, M., Abbaszade, G., Weggler, B., Jing, L., Schnelle-Kreis, J., Zimmermann, R., 2015. Online determination of polycyclic aromatic hydrocarbon formation from a flame soot generator. Anal. Bioanal. Chem. 407 (20), 5911–5922. http://dx.doi.org/10.1007/s0021.
Mueller, L., Schnelle-Kreis, J., Jakobi, G., Orasche, J., Jing, L., Canonaco, F., Prevot, A.S.H., Zimmermann, R., 2016. Combustion process apportionment of carbonaceous particulate emission from a diesel fuel burner. J. Aerosol Sci. 100, 61–72. http://dx.doi.org/10.1016/j.jaerosci.2016.06.003.
Munyeza, C.F., Dikale, O., Rohwer, E.R., Forbes, P.B.C., 2018. Development and optimization of a plunger assisted solvent extraction method for polycyclic aromatic hydrocarbons sampled onto multi-channel silicone rubber traps. J. Chromatogr. A 1555, 20–29. http://dx.doi.org/10.1016/j.chroma.2018.04.053.
Nyström, R., Sadiktsis, I., Ahmed, T.M., Westerholm, R., Koegler, J.H., Blomberg, A., Sandström, T., Boman, C., 2016. Physical and chemical properties of RME biodiesel exhaust particles without engine modifications. Fuel 186, 261–269. http://dx.doi.org/10.1016/j.fuel.2016.08.062.
Ortner, E.K., Rohwer, E.R., 1996. Trace analysis of semi-volatile organic air pollutants using thick film silicone rubber traps with capillary gas chromatography. J. High Resolut. Chromatogr. 19 (6), 339–344. http://dx.doi.org/10.1002/jhrc.1240190607.
Peters, A., Döring, A., Wichmann, H.-E., Koenig, W., 1997. Increased plasma viscosity during an air pollution episode: a link to mortality? Lancet 349 (9065), 1582–1587. http://dx.doi.org/10.1016/S0140-6736(97)01211-7.
Points, J., 2019. Global VOC standards to address a volatile global problem: Dr. Ehrenstrofer.
Raza, N., Hashemi, B., Kim, K.-H., Lee, S.-H., Deep, A., 2018. Aromatic hydrocarbons in air, water, and soil: Sampling and pretreatment techniques. TRAC Trends Anal. Chem. 103, 56–73. http://dx.doi.org/10.1016/j.trac.2018.03.012.
Schoonraad, G.-L., Forbes, P.B.C., 2019a. System and method for manufacturing graphene wool, SA provisional patent application 2019/00675. filed on 1 February 2019.
Schoonraad, G.-L., Forbes, P.B.C., 2019b. Air pollutant trap, SA provisional patent application 2019/00674. filed on 1 February 2019.
Schoonraad, G.-L., Madito, M.J., Manyala, N., Forbes, P.B.C., 2020. Synthesis and optimisation of a novel graphene wool material by atmospheric pressure chemical vapour deposition. J. Mater. Sci. 55, 545–564. http://dx.doi.org/10.1007/s10853-019-03948-0.
Shen, G., Xue, M., Wei, S., Chen, Y., Zhao, Q., Li, B., Wu, H., Tao, S., 2013. Influence of fuel moisture, charge size, feeding rate and air ventilation conditions on the emissions of PM, OC, EC, parent PAHs, and their derivatives from residential wood combustion. J. Environ. Sci. 25 (9), 1808–1816. http://dx.doi.org/10.1016/S1001-0742(12)60258-7.
Soriano, J.A., García-Contreras, R., Leiva-Candia, D., Soto, F., 2018. Influence on performance and emissions of an automotive diesel engine fueled with biodiesel and paraffinic fuels: GTL and biojet fuel farnesane. Energy Fuels 32 (4), 5125–5133. http://dx.doi.org/10.1021/acs.energyfuels.7b03779.
United States Environmental Protection Agency, 1999. Compendium method TO-17 determination of volatile organic compounds in ambient air using active sampling onto sorbent tubes. [Online] Available at: https://www3.epa.gov/ttnamti1/files/ambient/airtox/to-17r.pdf.
Yan, B., Liu, S., Zhao, B., Li, X., Fu, Q., Jiang, G., 2018. China's fight for clean air and human health. Environ. Sci. Technol. 52, 8063–8064. http://dx.doi.org/10.1021/acs.est.8b03137.
Yu, C.W.F., Kim, J.T., 2010. Building pathology, investigation of sick buildings–VOC emissions. Indoor Built Environ. 19 (1), 30–39. http://dx.doi.org/10.1177/1420326X09358799.
Zhou, S., Zhou, J., Zhu, Y., 2019. Chemical composition and size distribution of particulate matters from marine diesel engines with different fuel oils. Fuel 235, 972–983. http://dx.doi.org/10.1016/j.fuel.2018.08.080.
Züttel, A., Sudan, P., Mauron, P., Wenger, P., 2004. Model for the hydrogen adsorption on carbon nanostructures. Appl. Phys. A 78 (7), 941–946. http://dx.doi.org/10.1007/s00339-003-2412-1.

Comparative sampling of gas phase volatile and semi-volatile organic fuel emissions from a combustion aerosol standard system

Yvonne C. Mason[a], Genna-Leigh Schoonraad[a], Jürgen Orasche[b], Christoph Bisig[b], Gert Jakobi[b], Ralf Zimmermann[b,c], Patricia B.C. Forbes[a]

[a] Department of Chemistry, Faculty of Natural and Agricultural Sciences, University of Pretoria, Lynnwood Road, 0002, South Africa
[b] Comprehensive Molecular Analytics (CMA), Helmholtz Zentrum München, Gmunder Str. 37, 81379 München, Germany
[c] Joint Mass Spectrometry Center, Chair of Analytical Chemistry, University of Rostock, Germany

Supplementary Information

Figure S1: Graphene wool sampler showing the GW of 60 mm bed length housed in a glass tube with glass end caps held in place by Teflon sleeves. ***Source:*** *Adapted from (Schoonraad and Forbes, 2019b).*

Figure S2: Photograph of the CAST generator sampling set-up.

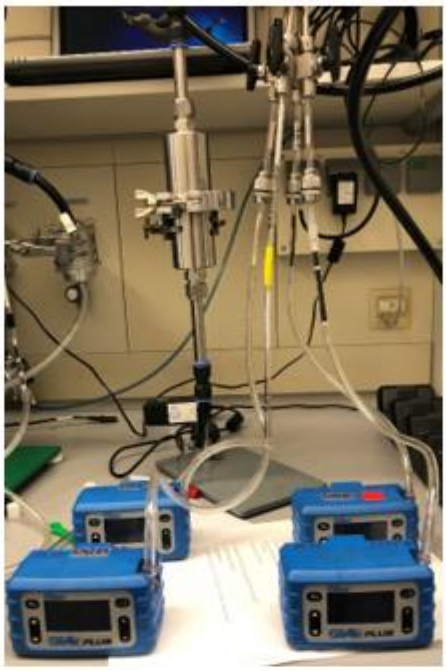

Figure S3: Photograph of the sampler setup for the activated charcoal, GW and PDMS samplers, respectively, during CAST sampling events. *Note: The fourth sampling point was for another experiment and is not reported on here.*

Table S1: Standards and internal standards used in this study.

Standard	Supplier
Naphthalene	Alfa Aesar
Fluorene	Fluka
Acenaphthene	Fluka
Acenaphthylene	Supelco
Phenanthrene	Alfa Aesar
Anthracene	Fluka
1-Methylnaphthalene	Aldrich
1,2-Dimethylnaphthalene	Alfa Aesar
2-Methylnaphthalene	Supelco
Biphenyl	Supelco
1-Methylfluorene	Aldrich
Fluoranthene	Fluka
Pyrene	Sigma-Aldrich
Benzene	Carl Roth
Toluene	Carl Roth
M-Xylene	Fluka
O-Xylene	Vwr
Ethylbenzene	Alfa Aesar

Benzaldehyde	Sigma Aldrich
Styrene	Fluka
Phenol	Merck
Indene	Aldrich
Indane	Fluka
Alkane Standard Solution C8-C20	Sigma-Aldrich
Benzene D6	Fluka
Toluene D8	Sigma Aldrich
O-Xylene D10	Sigma Aldrich
Naphthalene D8	Sigma Aldrich
Biphenyl D10	Cil - Cambridge Isotope Institute
Acenaphthylene D8	Cil-Cambridge Isotope Laboratories
Acenaphthene D10	Sigma Aldrich
Fluorene D10	Supelco
Phenanthrene D10	Cil-Cambridge Isotope Laboratories
Anthracene D10	Cil - Cambridge Isotope Institute
N-Heptane D16	Sigma Aldrich
N-Dodecane D26	Sigma Aldrich
N-Hexadecane D34	Aldrich

Table S2: Ambient conditions at the start of sampling events for this study

Measurement	Barometric Pressure (hPa)	Wet Bulb (°C)	Dry Bulb (°C)
B0 1	955.5	20.4	26.8
GTL 1	955.8	20.4	26.8
GTL 2	955.9	10.7	27.0
RME 1	956.0	10.7	27.0
RME 2	956.1	9.0	27.7
B0 2	956.2	9.0	27.7

Table S3: Mean FTIR results for the sampling events of the undiluted fuel emissions over each 10 min sampling period.

Sample	H_2O (%)	CO_2 (%)	CO (ppm)	O_2 (%)
B0 1	0.58	0.58	9.51	10.30
B0 2	0.57	0.58	9.48	10.30
B0 3	0.65	0.58	9.40	10.20
B0 4	0.66	0.58	9.42	10.20
Mean	0.62	0.58	9.45	10.25
SD	0.05	0.00	0.05	0.06
%RSD	7.42	0.13	0.55	0.56

GTL 1	0.56	0.58	7.89	10.31
GTL 2	0.56	0.58	7.86	10.31
GTL 3	0.66	0.58	7.63	10.50
GTL 4	0.65	0.58	7.65	10.45
Mean	0.61	0.58	7.76	10.39
SD	0.06	0.00	0.14	0.10
%RSD	9.10	0.21	1.77	0.94
RME 1	0.62	0.60	7.25	10.26
RME 2	0.62	0.60	7.30	10.28
RME 3	0.67	0.60	7.32	10.45
RME 4	0.67	0.59	7.64	10.41
Mean	0.64	0.60	7.38	10.35
SD	0.03	0.00	0.18	0.10
%RSD	4.79	0.63	2.43	0.93

a)

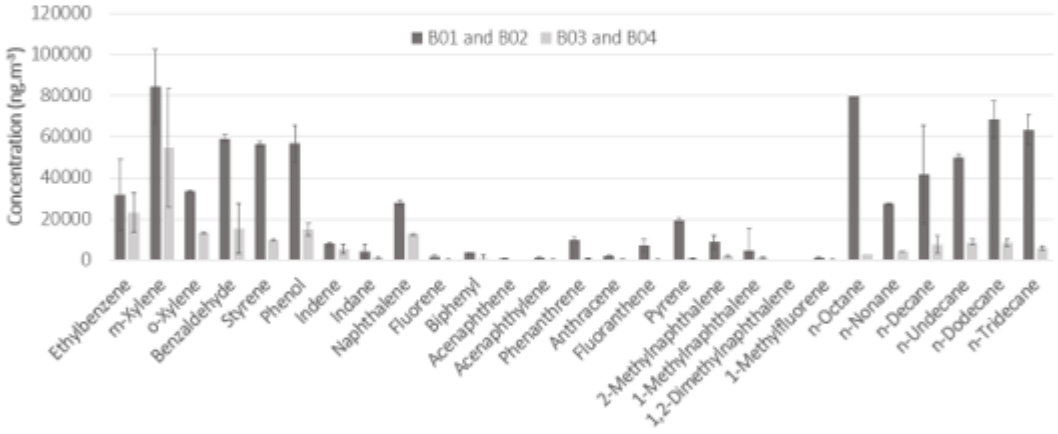

b)

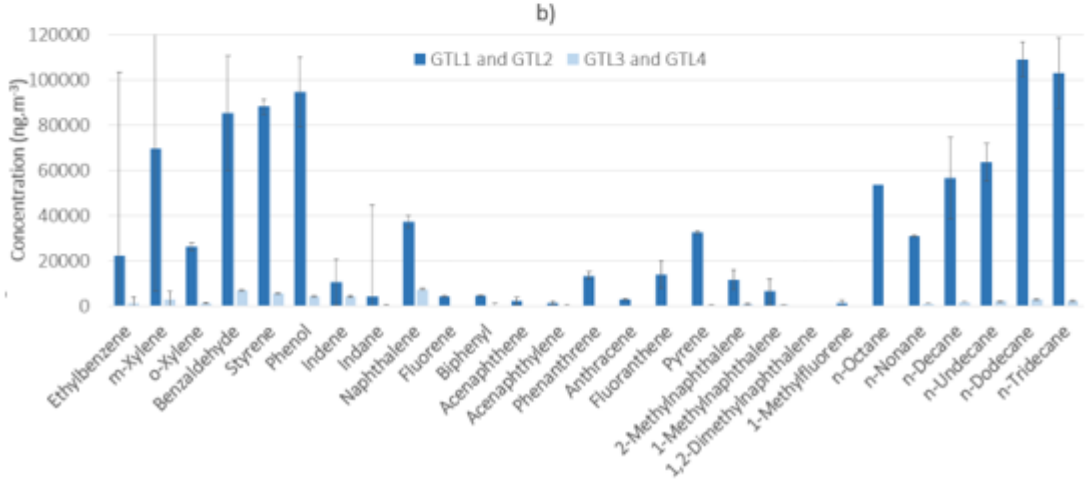

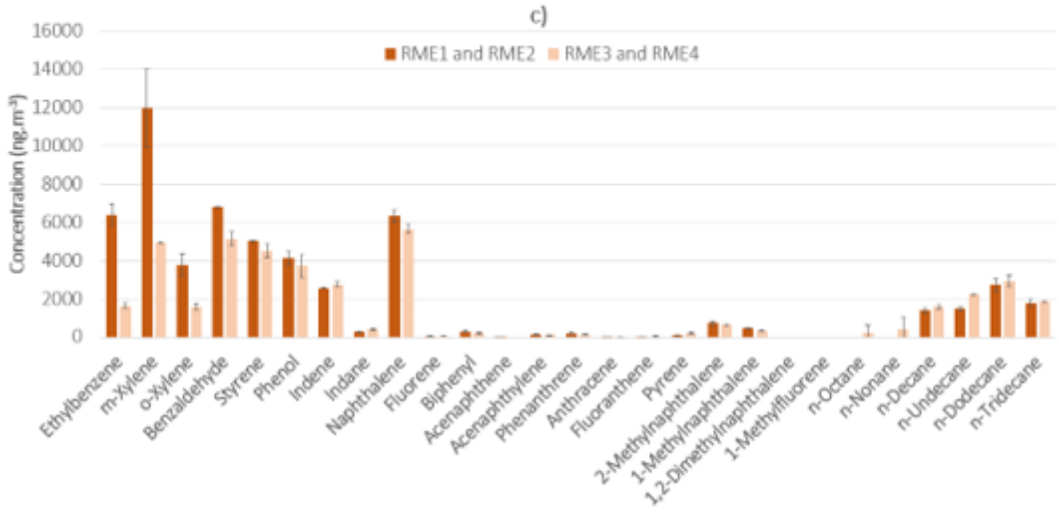

Figure S4: Comparison of sampling event replicates for B0 a), GTL b) and RME c)

Table S4: Concentrations of target analytes detected upon analysis of blank samplers. *(n.d.) denotes that the specific target analyte was not detected.*

Analyte	Concentration detected (ng)		
	PDMS	GW	Activated charcoal
Benzene	6.72	n.d.	74.95
Toluene	35.60	n.d.	19.25
Ethylbenzene	n.d.	n.d.	n.d.
m-Xylene	n.d.	n.d.	n.d.
o-Xylene	0.01	n.d.	n.d.
Benzaldehyde	n.d.	n.d.	n.d.
Styrene	n.d.	n.d.	n.d.
Phenol	n.d.	n.d.	n.d.
Indene	n.d.	n.d.	n.d.
Indane	n.d.	n.d.	n.d.
Naphthalene	0.07	n.d.	n.d.
Fluorene	n.d.	n.d.	n.d.
Biphenyl	0.01	n.d.	n.d.
Acenaphthene	n.d.	n.d.	n.d.
Acenaphthylene	n.d.	n.d.	n.d.
Phenanthrene	0.01	n.d.	n.d.
Anthracene	0.01	n.d.	n.d.
Fluoranthene	n.d.	n.d.	n.d.
Pyrene	n.d.	n.d.	n.d.
2-Methylnaphthalene	n.d.	n.d.	n.d.
1-Methylnaphthalene	n.d.	n.d.	n.d.
1,2-Dimethylnaphthalene	n.d.	n.d.	n.d.
1-Methylfluorene	n.d.	n.d.	n.d.
n-Octane	n.d.	n.d.	n.d.

n-Nonane	n.d.	n.d.	n.d.
n-Decane	0.01	n.d.	n.d.
n-Undecane	0.01	n.d.	n.d.
n-Dodecane	n.d.	n.d.	n.d.
n-Tridecane	n.d.	n.d.	n.d.
n-Tetradecane	0.05	n.d.	n.d.
n-Pentadecane	0.07	n.d.	n.d.
n-Hexadecane	0.09	n.d.	n.d.
n-Heptadecane	n.d.	n.d.	n.d.
n-Octadecane	n.d.	n.d.	n.d.
n-Nonadecane	n.d.	n.d.	n.d.
n-Eicosane	n.d.	n.d.	n.d.

Table S5: Concentrations of target analytes detected upon thermal desorption of GW samplers after sampling the emissions of CAST combustion of different fuels with associated standard deviations between sampling duplicates. *(n.d.) denotes that the specific target analyte was not detected for a specific analyte/sampler combination.*

	Average concentrations of target analyte ($\mu g.m^{-3}$)			%RSD of the duplicate measurements		
Target analytes	**B0**	**GTL**	**RME**	**B0**	**GTL**	**RME**
Benzene	96.63	21.65	26.57	10.09	12.28	5.96
Toluene	773.83	148.24	161.10	3.72	2.33	2.30
Ethylbenzene	23.19	1.36	6.39	0.63	14.06	9.05
m-Xylene	54.90	3.07	11.99	22.43	5.60	16.96
o-Xylene	13.36	1.12	3.79	2.91	8.52	15.63
Benzaldehyde	15.69	6.95	6.82	19.46	1.25	0.33
Styrene	9.78	5.62	5.03	24.03	10.74	0.52
Phenol	15.01	4.38	4.15	0.56	9.58	8.68
Indene	5.53	4.30	2.59	0.02	9.73	0.74
Indane	1.33	0.40	0.31	28.53	9.97	4.56
Naphthalene	12.83	7.40	6.37	13.75	12.64	4.89
Fluorene	0.28	0.07	0.07	61.87	141.11	31.98
Biphenyl	0.85	0.30	0.30	10.94	19.21	15.14
Acenaphthene	0.15	0.06	0.04	141.45	1.59	8.33
Acenaphthylene	0.42	0.23	0.16	84.21	1.13	11.05

Phenanthrene	0.81	0.21	0.22	34.41	0.37	30.69
Anthracene	0.07	0.04	0.01	24.32	63.85	142.59
Fluoranthene	0.44	0.12	0.05	28.34	34.07	7.66
Pyrene	1.18	0.29	0.09	38.74	10.01	29.98
2-Methylnaphthalene	2.06	0.90	0.75	30.84	4.45	12.39
1-Methylnaphthalene	1.46	0.52	0.47	29.26	15.43	4.34
1,2-Dimethylnaphthalene	n.d.	n.d.	n.d.	n.d.	n.d.	n.d.
1-Methylfluorene	n.d.	n.d.	n.d.	n.d.	n.d.	n.d.
n-Octane	2.90	n.d.	n.d.	141.42	n.d.	n.d.
n-Nonane	4.45	n.d.	n.d.	28.04	1.78	n.d.
n-Decane	7.90	1.63	1.43	24.32	1.24	9.17
n-Undecane	8.72	2.24	1.52	13.65	8.92	7.10
n-Dodecane	8.76	3.02	2.75	18.82	2.74	11.17
n-Tridecane	6.06	2.14	1.80	33.12	9.88	10.07
n-Tetradecane	10.74	5.81	4.71	58.44	4.16	16.36
n-Pentadecane	3.62	3.44	3.02	54.29	32.67	0.62
n-Hexadecane	5.22	6.34	4.06	59.61	20.35	23.37
n-Heptadecane	2.16	1.66	1.17	40.45	17.83	26.03
n-Octadecane	2.25	2.10	0.74	50.89	62.41	8.76
n-Nonadecane	2.78	0.91	0.51	76.23	2.11	21.29
n-Eicosane	1.82	0.57	0.30	69.41	8.14	22.08
Total VOCs + SVOCs	1097.16	237.09	259.29			

Table S6: Concentrations of target analytes detected upon thermal desorption of PDMS samplers after sampling the emissions of CAST combustion of different fuels with associated standard deviations between sampling duplicates. *(n.d.) denotes that the specific target analyte was not detected for a specific analyte/sampler combination.*

	Average concentrations of target analyte ($\mu g.m^{-3}$)			%RSD of the duplicate measurements		
Target analytes	**B0**	**GTL**	**RME**	**B0**	**GTL**	**RME**

Benzene	374.65	76.74	71.51	8.72	8.89	7.15
Toluene	774.41	159.30	158.30	0.18	1.61	0.36
Ethylbenzene	7.91	2.07	2.57	18.31	1.64	29.13
m-Xylene	22.07	2.73	5.36	34.95	12.19	30.19
o-Xylene	7.31	1.01	2.38	17.10	38.32	19.83
Benzaldehyde	59.86	27.56	20.25	37.49	9.69	7.30
Styrene	6.53	5.14	3.79	16.97	17.68	11.63
Phenol	54.34	13.28	12.62	6.01	13.91	12.16
Indene	4.28	4.03	3.03	1.99	13.75	7.79
Indane	0.35	0.44	0.25	0.00	5.16	7.45
Naphthalene	13.45	8.96	6.55	23.13	3.17	6.07
Fluorene	0.66	0.09	0.09	61.04	141.31	50.64
Biphenyl	0.80	0.31	0.14	48.49	74.59	4.80
Acenaphthene	0.38	0.12	0.03	80.47	21.37	141.25
Acenaphthylene	0.21	0.31	0.27	141.26	7.57	4.26
Phenanthrene	1.07	0.22	0.21	71.78	76.52	52.34
Anthracene	0.25	n.d.	0.01	64.40	n.d.	142.86
Fluoranthene	0.61	0.05	0.05	5.45	5.17	30.53
Pyrene	0.51	0.16	0.10	119.65	47.45	2.00
2-Methylnaphthalene	3.07	1.11	0.86	75.32	24.08	3.62
1-Methylnaphthalene	2.10	0.78	0.55	32.75	14.58	7.71
1,2-Dimethylnaphthalene	0.38	n.d.	n.d.	141.36	n.d.	n.d.
1-Methylfluorene	n.d.	n.d.	n.d.	n.d.	n.d.	n.d.
n-Octane	n.d.	n.d.	n.d.	n.d.	n.d.	n.d.
n-Nonane	n.d.	n.d.	n.d.	n.d.	n.d.	n.d.
n-Decane	5.73	2.13	1.09	141.43	49.46	0.26
n-Undecane	8.19	3.25	1.52	141.42	38.41	10.44
n-Dodecane	16.44	4.42	3.92	72.83	64.28	66.00
n-Tridecane	16.87	4.56	1.66	97.65	84.11	2.39
n-Tetradecane	520.12	119.29	4.36	139.33	137.22	30.47
n-Pentadecane	150.05	31.72	2.20	131.22	130.84	0.39

n-Hexadecane	1672.63	12.29	9.82	140.53	55.46	96.35
n-Heptadecane	7.50	1.57	0.93	53.58	57.03	28.53
n-Octadecane	10.30	2.13	1.09	46.23	69.11	6.49
n-Nonadecane	18.57	1.16	0.89	26.85	27.60	6.40
n-Eicosane	6.44	1.02	0.64	12.58	33.06	12.86
Total VOCs + SVOCs	3768.03	487.96	317.03			

Table S7a: LODs and LOQs (ng) of target analytes for different samplers, namely PDMS, GW and activated charcoal. PDMS and GW samplers were directly thermally desorbed whilst the activated charcoal extract was first extracted with CS_2 and the extract was injected into the GC port. *(-) denotes that content is unavailable for a specific analyte/sampler combination.*

	Abr.	LOD (ng)			LOQ (ng)		
Target analytes		**PDMS**	**GW**	**Charcoal**	**PDMS**	**GW**	**Charcoal**
Benzene	-	0.03	0.44	0.002	0.09	1.45	0.01
Toluene	-	0.001	0.01	0.002	0.004	0.04	0.01
Ethylbenzene	-	0.02	0.09	0.003	0.06	0.29	0.01
m-Xylene	-	0.05	2.27	0.004	0.15	7.58	0.01
o-Xylene	-	0.07	0.07	0.002	0.22	0.24	0.01
Benzaldehyde	-	0.07	0.13	-	0.22	0.42	-
Styrene	-	0.02	0.13	0.001	0.06	0.43	0.003
Phenol	-	0.04	0.09	0.003	0.14	0.31	0.01
Indene	-	0.05	0.06	-	0.15	0.19	-
Indane	-	0.03	0.06	-	0.11	0.19	-
Naphthalene	Naph	0.004	0.86	0.001	0.01	2.85	0.003
Fluorene	FluE	0.02	0.03	-	0.08	0.11	-
Biphenyl	Biph	0.01	0.01	-	0.04	0.04	-
Acenaphthene	AceE	0.02	0.04	-	0.07	0.13	-
Acenaphthylene	AceY	0.02	0.02	-	0.06	0.08	-
Phenanthrene	Phe	0.01	0.02	-	0.05	0.05	-
Anthracene	Anth	0.02	0.02	-	0.06	0.06	-
Fluoranthene	FluA	0.01	0.02	-	0.03	0.05	-

Pyrene	Pyr	0.01	0.01	-	0.03	0.05	-
2-Methylnaphthalene	2-Mnap	0.03	0.03	-	0.11	0.10	-
1-Methylnaphthalene	1-MNap	0.10	0.58	-	0.33	1.92	-
1,2-Dimethylnaphthalene	1,2-DiMNap	0.001	0.31	-	0.002	1.02	-
1-Methylfluorene	1-MF	0.03	0.05	-	0.10	0.16	-
n-Octane	n-Oct	4.00	3.95	-	13.33	13.16	-
n-Nonane	n-Non	0.79	3.95	-	2.63	13.16	-
n-Decane	n-Dec	0.19	0.63	-	0.62	2.10	-
n-Undecane	n-Und	0.07	0.26	-	0.24	0.87	-
n-Dodecane	n-Dod	0.05	0.07	-	0.17	0.24	-
n-Tridecane	n-Tri	0.06	0.05	-	0.21	0.17	-
n-Tetradecane	n-Tet	0.02	0.04	-	0.06	0.12	-
n-Pentadecane	n-Pent	0.03	0.03	-	0.09	0.12	-
n-Hexadecane	n-Hex	0.04	0.04	-	0.12	0.12	-
n-Heptadecane	n-Hept	0.02	0.03	-	0.07	0.10	-
n-Octadecane	n-OctD	0.03	0.04	-	0.10	0.14	-
n-Nonadecane	n-NonD	0.04	0.04	-	0.13	0.13	-
n-Eicosane	n-Eic	0.05	0.12	-	0.16	0.41	-

Table S7b: LODs and LOQs ($ng.m^{-3}$) of target analytes for different samplers, namely PDMS, GW and activated charcoal. PDMS and GW samplers were directly thermally desorbed whilst the activated charcoal extract was first extracted with CS_2 and 1 µL of the 3 mL extract was injected into the GC port. *(-) denotes that content is unavailable for a specific analyte/sampler combination.*

	Abr.	LOD ($\mu g.m^{-3}$)			LOQ ($\mu g.m^{-3}$)		
Target analytes		**PDMS**	**GW**	**Charcoal**	**PDMS**	**GW**	**Charcoal**
Benzene	-	0.01	0.09	0.99	0.02	0.29	3.31

Toluene	-	0.0002	0.002	1.10	0.00	0.01	3.66
Ethylbenzene	-	0.004	0.02	1.78	0.01	0.06	5.94
m-Xylene	-	0.01	0.45	2.26	0.03	1.52	7.55
o-Xylene	-	0.01	0.01	1.49	0.04	0.05	4.95
Benzaldehyde	-	0.01	0.03	-	0.04	0.08	-
Styrene	-	0.003	0.03	0.62	0.01	0.09	2.08
Phenol	-	0.01	0.02	1.50	0.03	0.06	5.01
Indene	-	0.01	0.01	-	0.03	0.04	-
Indane	-	0.01	0.01	-	0.02	0.04	-
Naphthalene	Naph	0.001	0.17	0.48	0.00	0.57	1.59
Fluorene	FluE	0.005	0.01	-	0.02	0.02	-
Biphenyl	Biph	0.002	0.003	-	0.01	0.01	-
Acenaphthene	AceE	0.004	0.01	-	0.01	0.03	-
Acenaphthylene	AceY	0.004	0.005	-	0.01	0.02	-
Phenanthrene	Phe	0.003	0.003	-	0.01	0.01	-
Anthracene	Anth	0.004	0.004	-	0.01	0.01	-
Fluoranthene	FluA	0.002	0.003	-	0.01	0.01	-
Pyrene	Pyr	0.002	0.003	-	0.01	0.01	-
2-Methylnaphthalene	2-Mnap	0.01	0.01	-	0.02	0.02	-
1-Methylnaphthalene	1-MNap	0.02	0.12	-	0.07	0.38	-
1,2-Dimethylnaphthalene	1,2-DiMNap	0.0001	0.06	-	0.00	0.20	-
1-Methylfluorene	1-MF	0.01	0.01	-	0.02	0.03	-
n-Octane	n-Oct	0.80	0.79	-	2.67	2.63	-
n-Nonane	n-Non	0.16	0.79	-	0.53	2.63	-
n-Decane	n-Dec	0.04	0.13	-	0.12	0.42	-
n-Undecane	n-Und	0.01	0.05	-	0.05	0.17	-
n-Dodecane	n-Dod	0.01	0.01	-	0.03	0.05	-
n-Tridecane	n-Tri	0.01	0.01	-	0.04	0.03	-
n-Tetradecane	n-Tet	0.003	0.01	-	0.01	0.02	-
n-Pentadecane	n-Pent	0.01	0.01	-	0.02	0.02	-
n-Hexadecane	n-Hex	0.01	0.01	-	0.02	0.02	-

n-Heptadecane	n-Hept	0.004	0.01	-	0.01	0.02	-
n-Octadecane	n-OctD	0.01	0.01	-	0.02	0.03	-
n-Nonadecane	n-NonD	0.01	0.01	-	0.03	0.03	-
n-Eicosane	n-Eic	0.01	0.02	-	0.03	0.08	-

Appendix K: References relating to the Appendices

ACGIH. **2012**. ACGIH® threshold limit values (TLVs®) and biological exposure indices (BEIs®). [Online] Available at: https://www.nsc.org/Portals/0/Documents/facultyportal/Documents/fih-6e-appendix-b.pdf

Alonso, M., Godayol, A., Antico, E., and Sanchez, J.M. **2011**. Needle microextraction trap for on-site analysis of airborne volatile compounds at ultra-trace levels in gaseous samples. *Journal of separation science*, 34, 2705-2711.

ATSDR. **2010**. Regulations, advisories and guidelines. [Online] Available at: https://www.atsdr.cdc.gov/toxprofiles/tp199-c8.pdf

Baltussen, E., Boer, A.D, Sandra, p., Janssen, H.G., and Cramers, C. **1999**. Monitoring of nicotine in air using sorptive enrichment on polydimethylsiloxane and TD-CGC-NPD. *Chromatographia*, 49, 520-524.

Baltussen, E., Janssen, H.G., Sandra, P., and Cramers, C. **2005**. A new method for sorptive enrichment of gaseous samples: application in air analysis and natural gas characterization. *Journal of High Resolution Chromatography*, 20, 385-393.

Campos, V.P., Oliveira, A.S., Cruz, L.P.S., Borges, J., and Tavares, T.M. **2010**. Optimization of parameters of sampling and determination of reduced sulfur compounds using cryogenic capture and gas chromatography in tropical urban atmosphere. *Microchemical Journal*, 96(2), 283-289.

Chang, C.C., Lo, S.J., Lo, J.G., and Wang, J.L. **2003**. Analysis of methyl tert-butyl ether in the atmosphere and implications as an exclusive indicator of automobile exhaust. *Atmospheric Environment*, 37(34), 4747-4755.

Czaplicka, M., and K. Klejnowski. **2002**. Determination of volatile organic compounds in ambient air: comparison of methods. *Journal of chromatography A*, 976(1-2), 369-376.

Dudek, M., Kloskowski, A., Wolska, L., Pilarczyk, M., and Namieśnik, J. **2002**. Using different types of capillary chromatographic columns as denudation traps: a comparison of sorption properties. *Journal of chromatography A*, 977(1), 115-123.

Es-haghi, A., Baghernejad, M., and Bagheri, H. **2012**. In situ solid-phase microextraction and post on-fiber derivatization combined with gas chromatography–mass spectrometry for determination of phenol in occupational air. *Analytica Chimica Acta*, 742, 17-21.

Gorlo, D., Zygmunt, B., Dudek, M., Jaszek, A., Pilarczyk, M., and Namieśnik, J. **1999**. Application of solid-phase microextraction to monitoring indoor air quality. *Fresenius' Journal of Analytical Chemistry*, 363, 696-699.

Hsieh, L.L., Chang, C.C., Sree, U., and Lo, J.G. **2006**. Determination of volatile organic compounds in indoor air of buildings in nuclear power plants, Taiwan. *Water, Air, and Soil Pollution*, 170, 107-121.

Huang, G., Hou, J., and Zhou, X. **2009**. A measurement method for atmospheric ammonia and primary amines based on aqueous sampling, OPA derivatization and HPLC analysis. *Environmental Science & Technology*, 43, 5851-5856.

Isetun, S., Nilsson, U., and Colmsjö, A. **2004**. Evaluation of solid-phase microextraction with PDMS for air sampling of gaseous organophosphate flame-retardants and plasticizers. *Analytical and Bioanalytical Chemistry*, 380, 319-324.

Jia, C., Batterman, S., and Godwin, C. **2008a**. VOCs in industrial, urban and suburban neighborhoods, Part 2: factors affecting indoor and outdoor concentrations. *Atmospheric Environment*, 42(9), 2101-2116.

2008b. VOCs in industrial, urban and suburban neighborhoods, Part 1: Indoor and outdoor concentrations, variation, and risk drivers. *Atmospheric Environment*, 42(9), 2083-2100.

Kawahara, J., Horikoshi, R., Yamaguchi, T., Kumagai, K., and Yanagisawa, Y. **2005**. Air pollution and young children's inhalation exposure to organophosphorus pesticide in an agricultural community in Japan. *Environment International*, 31(8), 1123-1132.

Komazaki, Y., Hiratsuka, M., Narita, Y., Tanaka, S., and Fujita, T. **1999**. The development of an automated continuous measurement system for the monitoring of HCHO and CH3CHO in the atmosphere by using an annular diffusion scrubber coupled to HPLC. *Fresenius' Journal of Analytical Chemistry*, 363, 686-695.

Krol, S., Zabiegala, B., and Namiesnik, J. **2012**. Measurement of benzene concentration in urban air using passive sampling. *Analytical and Bioanalytical Chemistry*, 403, 1067-1082.

Król, S., Namieśnik, J., and Zabiegała, B. **2014**. α-Pinene, 3-carene and d-limonene in indoor air of Polish apartments: the impact on air quality and human exposure. *Science of The Total Environment*, 468, 985-995.

Liu, X., Pawliszyn, R., Wang, L., and Pawliszyn, J. **2004**. On-site monitoring of biogenic emissions from Eucalyptus dunnii leaves using membrane extraction with sorbent interface combined with a portable gas chromatograph system. *Analyst*, 129, 55-62.

Molbase. **2015**. Bromobenzene. [Online] Available at: http://www.molbase.com/en/msds_108-86-1-moldata-27695.html.

NIOSH. **2018a**. 1,2-Dibromo-3-chloropropane. [Online] Available at: https://www.cdc.gov/niosh/npg/npgd0184.html.

2018b. 1,2-Dibromoethane. [Online] Available at: https://www.cdc.gov/niosh/npg/npgd0270.html.

2018c. 1,2,4-Trimethylbenzene. [Online] Available at: https://www.cdc.gov/niosh/npg/npgd0638.html.

2018d. '1,3-Dichloropropene. [Online] Available at: https://www.cdc.gov/niosh/npg/npgd0199.html

2018e. '1,3,5-Trimethylbenzene. [Online] Available at: https://www.cdc.gov/niosh/npg/npgd0639.html.

2018f. 'Ethylene dibromide. [Online] Available at: https://www.cdc.gov/niosh/npg/npgd0270.html.

NOISH. **2018**. Coal tar pitch volatiles. [Online] Available at: https://www.cdc.gov/niosh/npg/npgd0145.html.

Nollet, L.M.L., and Lambropoulou, D.A. **2017**. Chromatographic Analysis of the Environment : Mass Spectrometry Based Approaches. *Chromatographic Science Series*. 4th Edition.

Oikawa, D., Takeuchi, W., Murata, S., Takahashi, K., and Sekine, Y. **2012**. Measurement of concentrations of thioglycolic acid, dithiodiglycolic acid and ammonia in indoor air of a beauty salon. *Journal of Occupational Health*, 54(5), 370-375.

PubChem. **2018a**. 'Acenaphthylene', Accessed 8 April. https://pubchem.ncbi.nlm.nih.gov/compound/acenaphthylene.

2018b. Anthracene. [Online] Available at: https://pubchem.ncbi.nlm.nih.gov/compound/8418.

2018c. Benz[a]anthracene. [Online] Available at: https://pubchem.ncbi.nlm.nih.gov/compound/5954.

2018d. Benzo[ghi]perylene. [Online] Available at: https://pubchem.ncbi.nlm.nih.gov/compound/9117.

2018e. benzo[k]fluoranthene. [Online] Available at: https://pubchem.ncbi.nlm.nih.gov/compound/9158#section=Exposure-Control-and-Personal-Protection.

2018f. dibenz[a,h]anthracene. [Online] Available at: https://pubchem.ncbi.nlm.nih.gov/compound/5889#section=Exposure-Control-and-Personal-Protection.

2018g. Fluoranthene. [Online] Available at: https://pubchem.ncbi.nlm.nih.gov/compound/9154.
2018h. Fluorene. [Online] Available at: https://pubchem.ncbi.nlm.nih.gov/compound/6853.
2018i. Indeno[1,2,3-cd]pyrene[Online] Available at: https://pubchem.ncbi.nlm.nih.gov/compound/9131.

Ramirez, N., Cuadras, A., Rovira, E., Borrull, F., and Marce, R.M. **2010**. Comparative study of solvent extraction and thermal desorption methods for determining a wide range of volatile organic compounds in ambient air. *Talanta*, 82(2), 719-727.

Regueiro, J., Garcia-Jares, C., Llompart, M., Lamas, J.P., and Cela, R. **2009**. Development of a method based on sorbent trapping followed by solid-phase microextraction for the determination of synthetic musks in indoor air. *Journal of Chromatography A*, 1216(14), 2805-2815.

Söderström, H.S., and Bergqvist, P.A. **2004**. Passive air sampling using semipermeable membrane devices at different wind-speeds in situ calibrated by performance reference compounds. *Environmental Science & Technology*, 38(18), 4828-4834.

Toxnet. **2008**. Dichlorobenzene. [Online] Available at: https://toxnet.nlm.nih.gov/cgi-bin/sis/search/a?dbs+hsdb:@term+@DOCNO+6372.

Ueta, I., Mizuguchi, A., Fujimura, K., Kawakubo, S., and Saito, Y. **2012**. Novel sample preparation technique with needle-type micro-extraction device for volatile organic compounds in indoor air samples. *Analytica Chimica Acta*, 746, 77-83.

Van Durme, J., Demeestere, K., Dewulf, J., Ronsse, F., Braeckman, L., Pieters, J., and Van Langenhove, H. **2007**. Accelerated solid-phase dynamic extraction of toluene from air. *Journal of Chromatography A*, 1175(2), 145-153.

Wang, J.L., Chang, C.C., and Lee, K.Z. **2012**. In-line sampling with gas chromatography–mass spectrometry to monitor ambient volatile organic compounds. *Journal of Chromatography A*, 1248, 161-168.